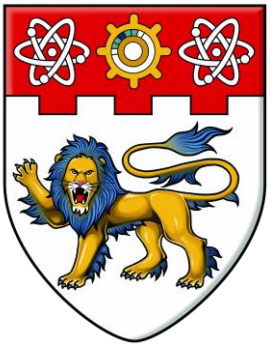

NANYANG TECHNOLOGICAL UNIVERSITY

MECHANICS OF HYDROGELS - A MODELING AND SIMULATION APPROACH

WILLIAM TOH
SCHOOL OF MECHANICAL AND AEROSPACE ENGINEERING

2016

MECHANICS OF HYDROGELS – A MODELING AND SIMULATION APPROACH W. TOH 2016

MECHANICS OF HYDROGELS - A MODELING AND SIMULATION APPROACH

WILLIAM TOH

School of Mechanical and Aerospace Engineering

A thesis submitted to the Nanyang Technological University in partial fulfilment of the requirement for the degree of Doctor of Philosophy

2016

Acknowledgements

The publication of this thesis would not have been possible without the help and support from many people. First and foremost, I would like to express my deepest gratitude to my academic supervisors, A/P Ng Teng Yong and Prof. Liu Zishun. The tremendous amounts of trust that they empower me to carry out independent research and advice in times when I reach plateaus have given me the confidence to overcome the numerous milestones in the past four years.

Next, my sincere gratitude to my family: my dad Kem-Peng, mum Jenny, brother Jason and sister-in-law Diana for the unwavering care and concern. My dearest girlfriend Yu Ting, for the love, understanding and the help in proofreading this thesis. Many thanks to everyone in Team RR2: Chun Kiat, Ken Tay, Jian Hao, Kuan Thai, Kok Hon and Martin, for the countless tea-break sessions and friendship fostered over the past years from undergraduate studies all the way to completing our PhDs together. Also to all my friends beyond the boundaries of this PhD community, a big thank you for making my life more interesting.

In addition, I would like to thank Mr. Ding Zhiwei from the Institute of High Performance Computing (A*STAR) for the many fruitful discussions in several of our collaborations. Furthermore, to all staff in NTU and IHPC who have rendered their assistance in making this thesis a reality, especially Dr. Pei Qingxiang from IHPC and Mdm. Tan-Yeo Lay Foon from NTU, who are always patient in explaining all matters related to administrative procedures in the respective institutions.

Finally, I would like to acknowledge the Nanyang President's Graduate Scholarship for the financial support over the duration of the scholarship, and the Graduate Studies Office for the opportunities provided in nominating me for the attendance in the inaugural Global Young Scientists' Summit 2013, and the TU-Delft IDEA League summer school.

Abstract

Constituting of chemically cross-linked polymers, hydrogels are an interesting class of materials that are able to undergo significantly large deformation through the imbibement of solvent. These large deformations can also be triggered by external stimuli through appropriate change of constituents. In this thesis, the mechanical, thermodynamic and kinetic properties of various environmentally sensitive hydrogels were modeled and analyzed to study the different interesting phenomena exhibited, namely the phase transition and instability during swelling.

The thesis begins the study with investigation of the kinetics of neutral, temperature-sensitive, as well as pH-sensitive hydrogels. The swelling kinetics of these hydrogels were shown to closely resemble heat transfer laws, and finite element procedures on Abaqus were thus developed to simulate transient swelling behavior exploiting the close similarity in differential form between swelling kinetics and heat transfer laws. The finite element procedure was verified by comparisons with both analytical solutions and available experimental data. Several numerical examples of transient swelling behavior of hydrogels, including inhomogeneous free swelling of a cube, constrained swelling of a gel blanket, three-dimensional swelling of a gel block, and interactions with hard and soft surfaces, were subsequently investigated.

Next, the phenomena of phase transition and large deformation of temperature-sensitive, photo-thermo-sensitive and magneto-thermo-sensitive hydrogels were investigated. This was done by considering the chemical thermodynamics of the gels in equil4ibrium with external loads and environmental stimuli. Constitutive equations were derived and the material models were implemented on Abaqus using both UHYPER and UMAT subroutines. It was shown that the phase transition temperature of a temperature sensitive hydrogel could be altered by the addition of foreign particles, and also through the variation of strength of external stimuli. Several numerical

examples highlighting interesting phenomena, such as phase transition and phase co-existence, and potential applications in microfluidic devices were subsequently studied.

Lastly, this thesis examines the instabilities induced when a gel swells. Various cases of buckling, including buckling of a thin annulus, bifurcation of a gel layer with periodic hole array, transient surface wrinkling during swelling were studied. The analysis was carried out using finite element models developed in the earlier studies and also through linear perturbation analysis for the case of surface wrinkling.

Table of Contents

List of symbols

$\mathcal{A}$	Affinity of photochemical reaction
A_0	Coefficient for Flory-interaction parameter for PNIPAM
A_1	Coefficient for Flory-interaction parameter for PNIPAM
AH	Acid with conjugate base A^-
A^-	Conjugate base of acid AH
$\mathbf{A}$	Coefficient matrix in state space analysis
B_{mag}	Magnetic field strength
$\overline{B}$	Normalized magnetic field strength
B_0	Coefficient for Flory-interaction parameter for PNIPAM
B_1	Coefficient for Flory-interaction parameter for PNIPAM
B_i	Body force on elemental volume
c^s	Solvent concentration in current state
c^{H^+}	H^+ concentration within *pH*-sensitive gel in current state
c^+	Counter-ion concentration within *pH*-sensitive gel in current state
c^-	Co-ion concentration within *pH*-sensitive gel in current state
$\tilde{c}^{H^+}$	H^+ concentration in external solution in current state
$\tilde{c}^+$	Counter-ion concentration in external solution in current state
$\tilde{c}^-$	Co-ion concentration in external solution in current state
c_p	Specific heat capacity
c_p^{gel}	Specific heat capacity of gel
c_p^p	Specific heat capacity of polymer
c_p^s	Specific heat capacity of solvent
c_v^{gel}	Volumetric heat capacity of gel
$c_v^{polymer}$	Volumetric heat capacity of polymer

c_v^w	Volumetric heat capacity of water
C^s	Solvent concentration in reference state
C^m	Magnetic spin concentration in reference state
C^p	Photo-chemical reaction concentration in reference state
C_{ijkl}	Tangent modulus tensor
dv	Elemental volume in current state
dV	Elemental volume in reference state
ds	Elemental surface area in current state
dS	Elemental surface area in reference state
D	Coefficient of diffusion
D_e	Thermal conductivity from experimental data
$D_{\exp}$	Diffusion coefficient used in linear theory
$\mathbf{D}$	State transition matrix for a single homogeneous layer of gel in state space solution
E_p	Energy released in photo-excitation
f	Frequency of monochromatic light
f^{Cu}	Photo-sensitive nano-particle volume fraction in polymer network
f^m	Magnetic particles volume fraction in polymer network
F_{iK} or $\mathbf{F}$	Deformation gradient
$\mathbf{F}_0$	Initial free swelling deformation gradient
$\mathbf{F}'$	Deformation gradient relative to $\mathbf{F}_0$
$\tilde{\mathbf{F}}$	Deformation gradient after linear perturbation
H	Thickness of gel blanket
H^+	Hydrogen ion
H_{iK} or $\mathbf{H}$	Transpose of inverse of deformation gradient

I_0	Light intensity
I_1	First invariant of deformation gradient
$\overline{I}_1$	Deviatoric invariant of deformation gradient
j_i	Diffusion flux in current state
j_i^s	Diffusion flux due to solvent in current state
$j_i^{H^+}$	Diffusion flux due to hydrogen ion in current state
j_i^+	Diffusion flux due to counter-ion in current state
j_i^-	Diffusion flux due to co-ion in current state
J_K	Diffusion flux in reference state
J	Third invariant of deformation gradient
k_B	Boltzmann constant
$\mathbf{K}$	State transition matrix for entire gel in state space solution
L	Characteristic length of diffusion
m^{gel}	Mass of gel
M	Magnetization
n_i	Normal vector of elemental surface area in current state
N_K	Normal vector of elemental surface area in reference state
N	Number of polymeric chains per unit reference volume
$\boldsymbol{P}$	Mechanical load applied to a gel
q_i	Heat flux
r	Internal heat generation
s_{iK}	Nominal stress
s_1, s_2, s_3	Principal nominal stress
S_0	Surface enclosing hydrogel in reference state
t	Time

$\bar{t}$	Non-dimensionalized time
T	Temperature
T_0	Initial temperature
T_1	Magnitude of incremental stress Δs_{12}
T_{22}	Magnitude of incremental stress Δs_{22}
T_{amb}	Ambient temperature
T_i	Traction on elemental surface
u_A	Displacement at point A
u_B	Displacement at point B
u_C	Displacement at point C
u_D	Displacement at point D
u_E	Displacement at point E
$\dot{U}$	Material time derivative of thermal energy
U_1	Magnitude of incremental displacement Δu_1
U_2	Magnitude of incremental displacement Δu_2
V_0	Volume of hydrogel in reference state
W	Free energy in a gel
$\hat{W}$	Free energy function after Legendre Transformation
W_{net}	Free energy of stretching
W_{mix}	Free energy of mixing
W_{ion}	Free energy of ionization
W_{dis}	Free energy of dissociation
W_{pho}	Free energy of photochemical reactions
W_{mag}	Free energy of magnetization

x_i or $\mathbf{x}$	Coordinates in current state
X_K or $\mathbf{X}$	Coordinates in reference state
α	Proportionality constant
$\alpha^{polymer}$	Coefficient of thermal expansion of polymer
α^{w}	Coefficient of thermal expansion of water
α^{Cu}	Coefficient of thermal expansion of copper
χ	Flory interaction parameter of mixing
χ_0 ,	Flory interaction parameter for temperature sensitive hydrogel
χ_1	Flory interaction parameter for temperature sensitive hydrogel
$\chi_{0,new}$	Flory interaction parameter for temperature sensitive hydrogel, corrected for addition of nano-particles.
$\chi_{1,new}$	Flory interaction parameter for temperature sensitive hydrogel, corrected for addition of nano-particles.
δ_{ij}	Kronecker delta function
δl	Incremental distance moved by external load P
δx_i	Incremental coordinates
δA	Surface area of incremental hydrogel element
δC^p	Incremental change in photochemical reaction concentration
δC^s	Incremental change in solvent concentration
δF_{iK}	Incremental change in deformation gradient
δN^p	Incremental change in number of photochemical reactions
δN^s	Incremental change in number of solvent molecules
δV	Volume of incremental hydrogel
δW	Change in free energy
δU	Change in virtual potential energy
δW_{ext}	Change in virtual external work

δW_{int}	Change in virtual internal work
Δu_i	Incremental displacement in linear perturbation
$\Delta u_{i,k}$	Partial derivative of incremental displacement in linear perturbation
ε	$\Delta u_{1,1} + \Delta u_{2,2}$
ε_{ijk}	Alternating tensor
ϕ	Polymer volume fraction
$\hbar$	Planck constant
κ	Coefficient of thermal conductivity
κ^p	Coefficient of thermal conductivity of polymer
κ^s	Coefficient of thermal conductivity of solvent
λ_0	Initial isotropic stretch under free swelling in initial chemical potential
λ_0^*	Average value of initial and final stretch ratio in 1D swelling
λ_1 , λ_2 , λ_3	Principal stretches
λ_∞	Final stretch ratio in 1D swelling
λ_i	Stretch ratio of the i^{th} layer in state-space analysis
μ^B	Chemical potential of magnetic field
μ^p	Chemical potential of photochemical reactions
μ^s	Chemical potential of external solvent
$\bar{\mu}^s$	Normalized chemical potential
$\bar{\mu}_0^s$	Initial chemical potential
ν	Volume of a solvent molecule
ω	Wave number of surface instability
$\prod$	Lagrange multiplier
θ	pH value

ρ	Material density
ρ^{gel}	Material density of gel
ρ^{p}	Material density of polymer network
ρ^{s}	Material density of solvent
σ_{ij}	Cauchy stress
$\sigma_1, \sigma_2, \sigma_3$	Principal Cauchy stress
$\bar{\sigma}_1$, $\bar{\sigma}_2$, $\bar{\sigma}_3$	Normalized principal Cauchy stress
$\bar{\sigma}$	Sum of normalized principal Cauchy stresses
τ	Correction factor in Flory interaction parameter for addition of light-absorbing nano-particles
ξ	Shorthand for long expressions
ζ	Characteristic time of diffusion

List of figures

List of tables

1. Introduction

1.1. Literature review

1.1.1. Introduction

Being biocompatible, hydrogels have been a popular material of choice for many applications. Driven by humans' vanity, one of the earliest applications of hydrogels is the contact lens, which Wichterle and Lim (1960) proposed as a superior alternative to plastics. Consisting of sparse crosslinks in the hydrophilic polymer network, gels are able to imbibe and retain water up to 99% of their volume, causing them to swell to many times their initial volume (Deligkaris et al., 2010; Huglin, 1989; Kishida and Ikada, 2001; Oguz, 2007; Silva Nykanen et al., 2011), as seen in Figure 1-1.

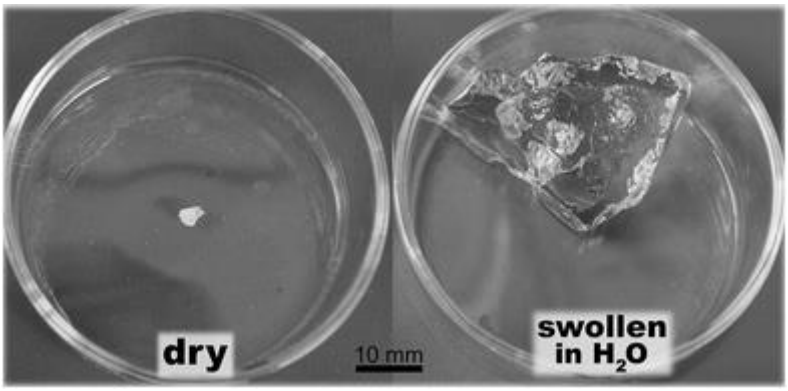

Figure 1-1: A piece of hydrogel swollen to 871 times its dry volume. Reproduced from Silva Nykanen et al. (2011)

Other than the absorption of solvent, as in the case of a neutral hydrogel, the deformation of hydrogels can also be triggered by different environmental stimuli through the incorporation of different monomers or constituent particles. The types of environmental stimuli that can trigger deformation in hydrogels are extensive, some examples of the stimuli include, but not limited to, *pH* value, temperature, electric, light, pressure, specific-ion, bio-chemical, chemical (Aguilar et al., 2007; Chatterjee et al., 2003; Deligkaris et al., 2010; Jeong and

Gutowska, 2002; Li and Kong, 2007; Meng and Hu, 2010; Qiu and Park, 2001). The large deformation triggered by these external stimuli proves to be a useful tool for implementation of smart devices. These environmentally sensitive gels are also termed 'smart hydrogels'. With more research into smart hydrogels, the potential applications involving hydrogels have grown phenomenally to include areas such as contact lens, sensors (Bashir et al., 2002; Sheppard Jr et al., 1995; Zhang et al., 2004), flow control devices (Baldi et al., 2002; Harmon et al., 2003b; Johnson et al., 2004; Lai et al., 2007; Satarkar et al., 2009; Sugiura et al., 2007), controlled drug release (Chu, 2003; Elvira et al., 2004; Gupta et al., 2002; Jeong et al., 2006; Liu et al., 2006; Siepmann et al., 1999), artificial muscles (Bassil et al., 2008; Bassil et al., 2011; Mirfakhrai et al., 2007), micro total analysis systems (van der Linden et al., 2003) and actuators (Bassik et al., 2010; Hoffmann et al., 1999; Kim et al., 2011; Kwon et al., 2010; Wang et al., 2013a)

Due to the vast diversity in applications, researchers have been spurred to develop theories to describe and understand the swelling behavior of hydrogels. In this thesis, we review some of the recent works aligned with the direction of providing a better understanding of gel behaviors. The chapter is organized as follows: Section 1.1.2 provides some theories on the equilibrium swelling of a gel; Section 1.1.3 covers the kinetics of swelling; Section 1.1.4 talks about the efforts in developing modeling and simulation tools; Section 1.1.5 investigates the intriguing phenomenon of swelling induced instabilities.

1.1.2. Equilibrium swelling theories

1.1.2.1. *Free energy functions*

In the thermodynamic treatment of hydrogels, Flory and Rehner (1943) first suggested that the Helmholtz free energy of a polymer network in an aqueous solution can be written as the additive decomposition of the free energy of elastic stretch of the polymer network and the free energy of mixing when the polymer network interacts with a solution.

The free energy of elastic network stretch considers solely the stretch of the polymer network and is akin to the stretch of a rubber. Anand (1996), Arruda and Boyce (1993), Flory and Rehner Flory and Rehner (1943), Lopez-Pamies (2010), Marckmann and Verron (2006), Mooney (1940), Rivlin and Saunders (1951), Valanis and Landel (1967) have suggested various forms of free energy function describing large deformation in solids.

The form derived by Flory and Rehner (1943) is based on Gaussian statistics and is one of the most commonly used form in the modeling of hydrogels (Bouklas and Huang, 2012; Cai and Suo, 2011; Hong et al., 2009a; Hong et al., 2010; Kang and Huang, 2010c; Marcombe et al., 2010; Zhang et al., 2009). However, the derivation of this model based on Gaussian statistical methods has been commented to show lack of consideration for the limited extensibility in polymer networks. As such, non-Gaussian statistical models such as those derived by Anand (1996) and Arruda and Boyce (1993) have been used alternatively (Chester, 2012; Chester and Anand, 2010, 2011; Chester et al., 2014).

In contrast with the free energy of stretch, the free energy of mixing does not involve as much controversy, as most hydrogel models are associated with the model developed by Flory (1942) and Huggins (1941). A parameter in the free energy of mixing is χ, which is commonly referred to as the Flory interaction parameter. χ is a dimensionless measure of the enthalpy of mixing in the range of $0 < \chi < 1.2$. A lower χ is associated with higher swelling ratios.

It has been shown that under mechanical constrains, the concentration of solvent within a swollen gel is inhomogeneous in equilibrium (Hong et al., 2009a; Pritchard and Terentjev, 2013; Zhao et al., 2008). Baek and Pence (2011) studied the effects of loss of saturation on the deformation of a gel in equilibrium.

In temperature sensitive hydrogels, Huggins (1964) decomposed the interaction parameter into enthalpic and entropic components, which are dependent on temperature and polymer concentration. Various experimental fittings on temperature sensitive hydrogels have been performed to obtain parameters specific to different monomers (Afroze et al., 2000; Caykara et al., 2006; Erman and Flory, 1986; Hassan and Durning, 1999; Kojima et al., 2013; Oliveira et al., 2004; Shimizu et al., 2003; Shirota et al., 1998), which have been adopted in various thermodynamic theories for temperature sensitive hydrogel models (Birgersson et al., 2008; Cai and Suo, 2011; Ding et al., 2013; Hino and Prausnitz, 1998; Li et al., 2005b; Li et al., 2005c).

In polyelectrolyte gels, Ricka and Tanaka (1984), Brannon-Peppas and Peppas (1991), Hong et al. (2010), Marcombe et al. (2010) and Yan et al. (2014) have created equilibrium models by assuming that in addition to the free energy of network stretch and mixing, the free energy of polyelectrolyte gels also consists of the free energy of ionization and free energy of dissociation.

1.1.3. Kinetic theory for gel swelling

Whilst the use of Flory-Rehner model has been widely adopted for the study of gel swelling, there lies a less than unified theory for the study of gel swelling kinetics, as some theories consider the polymer network and fluid to be distinct phases for the robustness. Some theories treat the polymer-fluid interaction as a single phase by coupling the diffusion of solvent with the large deformation of the network, simplifying the development process of numerical simulation methods used to predict the response of hydrogels.

The deformation gradient is often based on a multiplicative decomposition of elastic and swelling parts (Boyce and Arruda, 2001; Chester and Anand, 2010; Duda et al., 2010). However, Hong et al. (2008) noted that in the long time scale, the elastic part of deformation may be taken to be an instantaneous

process and taken to be unity in the modeling of migration of solvent molecules into the gel.

1.1.3.1. *Neutral gel*

The earliest theories of gel swelling were based on considering the polymer network and solvent as two separate phases, deriving equations of motions based on Newton's second law (Tanaka et al., 1973) by including the effects of friction, relative velocity and viscosity between the different phases. Tanaka and Fillmore (1979) later developed a kinetic model based on the longitudinal bulk modulus and friction coefficient between the two phases.

With assumption of negligible shear modulus, the Tanaka-Fillmore model was able to come up with accurate predictions for spherical gels. However, Peters and Candau (1986) showed that the Tanaka-Fillmore model could only satisfactorily describe gel swelling kinetics and could not be generalized for non-spherical gels. By including effects of shear modulus, Peters and Candau (1988) was able to describe kinetics for cylindrical gels.

For a generalization to gels of arbitrary shapes, Li and Tanaka (1990) proposed a separation of the swelling process into a two-step process, consisting of an initial diffusion, followed by a shear relaxation which minimizes shear energy built up during the diffusion process. With this approach, the authors were able to provide analytical solutions for two limiting cases, a long cylindrical gel and a large disc gel.

Doi and Onuki (1992) proposed a coupling relation between stress and gel composition by using phenomenological hydrodynamic relations, treating the gel as a two-fluid model. Using the stress-diffusion coupling model, Yamaue and Doi developed analytical solutions for the one-dimensional swelling dynamics of polymer gels under various external constraints (Yamaue and Doi, 2004a; Yamaue and Doi, 2004b; Yamaue and Doi, 2005). Using the theory of

mixtures, Calderer et al. (2008) developed a model for the dynamics of polymer gels to compare the derivation method, assumptions and resulting equations.

Later, Doi (2009) described the swelling dynamics of a polymer gel by treating the equilibrium swelling of the gel to be similar to the swelling of the polymer network, and derived the dynamic equations based on Lagrangian mechanics, where time evolution is based on velocities of the polymer network and solvent molecules.

A thermodynamic continuum treatment of the material allows for consideration of the gel and solvent as a single entity, as opposed to the multi-phase approach.

Durning and Morman (1993) proposed a continuum approach to overcome the shortcomings of the hydrodynamic models proposed in the multi-phase approach by treating the gel as a single phase. Thereafter, Baek and Srinivasa (2004), Hong et al. (2008), Duda et al. (2010) and Chester and Anand (2010) have developed mono-phase theories which couple diffusion and large deformation, paving the way for future works in the continuum mechanics studies of hydrogel swelling.

The method of Lagrange multiplier is commonly used to impose constrains on the constitutive theories. For the case of polymeric gels, the Lagrange multiplier is analogous to osmotic pressure of the solvent. Cai and Suo (2012) and Li et al. (2012b) has investigated this osmotic pressure as equations of state of a gel.

Making use of the coupled diffusion-deformation theory, Yoon et al. (2010) developed a linearized poro-elastic swelling kinetic theory to characterize material properties such as the modulus, Poisson's ratio and permeability of a gel swelling within the regime of linear poro-elasticity. Bouklas and Huang

(2012) compared the linear and non-linear theories and showed the linear theory to be consistent within the linear portion of swelling.

1.1.3.2. *Temperature sensitive gel*

As compared with neutral gels, there is much less literature focusing on the swelling kinetics of temperature sensitive hydrogels. This might be due to the overshadowing study on the effects on temperature on the equilibrium state phase transition phenomenon.

Colombo et al. (1996) and Grassi et al. (1999) modeled the kinetics of a temperature sensitive as a combination of Fickian and relaxation mechanisms. Comparing several experimental results, Okajima et al. (2002) observed that the swelling of a temperature sensitive gel fits an exponential trend.

Birgersson et al. (2008) developed a multi-phase theory for the transient response of a temperature sensitive hydrogel by considering conservation laws for the polymer and fluid phase separately using the mixture theory. Analysis took place in a non-dimensional framework to elucidate important characteristics as well as simplify governing equations.

By considering entropy imbalance, Chester and Anand (2011) extended the coupled theory for fluid permeation in elastomeric materials (Chester and Anand, 2010) to account for thermal response in temperature-sensitive hydrogels.

1.1.3.3. *Polyelectrolyte gel*

Kinetic theory of polyelectrolyte gels (*pH* gels) are mostly assumed to follow the Nernst-Planck equation of ion diffusion kinetics (Helfferich and Plesset, 1958). Other than kinetic laws, the distribution of ions within the gel is also dependent on ionic interactions, following the Poisson-Nernst-Planck equation.

Chu et al. (1995) incorporated diffusion-mechanical relaxation into swelling kinetics of pH-sensitive gels. De et al. developed several kinetic models for pH-sensitive gels, with assumptions of Donnan Theory (De et al., 2002) and a chemo-electro-mechanical model restricting the Donnan Theory to within the Debye length (De and Aluru, 2004).

1.1.4. Simulation of hydrogel behaviors

1.1.4.1. *Finite element method*

With development of the mono-phase theories, finite element simulation of hydrogel swelling has been expedited, in particular with the use of finite element software Abaqus for its versatility in defining material models through user-defined subroutines.

Subroutines used for equilibrium swelling include UHYPER and UMAT. UHYPER models the equilibrium swelling of a gel through definition of the free energy function and its derivatives whereas UMAT defines material properties through the tangent modulus tensor and Cauchy stress. Requiring only the free energy function, UHYPER is a popular choice due to the ease of implementation. On the other hand, UMAT requires a more thorough derivation and is more robust in the sense that it is able to model materials with anisotropic initial conditions.

(Hong et al., 2009a), Marcombe et al. (2010) and Ding et al. (2013) have developed UHYPER subroutines for temperature sensitive, neutral and pH-sensitive hydrogels respectively while Kang and Huang (2010c) has developed UMAT subroutine for neutral gels.

The finite element model for swelling kinetics of gels requires the use of the UEL subroutine, which requires a lengthy derivation for the tangent modulus, Cauchy stress and discretization. Zhang et al. (2009), (Chester and

Anand, 2011), Chester (2012) and Chester et al. (2014) have developed the UEL subroutines for neutral and temperature sensitive hydrogels.

Owing to the powerful multiphysics coupling mechanism present, COMSOL is a popular software of choice for simulation of heavily coupled physical material models. With COMSOL, Lucantonio et al. (2013) simulated transient swelling kinetics of polymeric gels, Wang and Hong (2012) and Li et al. (2013b) studied visco-elastic polymer gels and Birgersson et al. (2008) studied temperature sensitive gels.

Wallmersperger et al. (2011a, b) developed a chemo-electro-mechanical finite element model to solve for the equilibrium swelling of pH-sensitive gels, taking into account effects of various ions and their interactions.

1.1.4.2. *Meshless methods*

Other than the finite element method, meshless methods are frequently used in the simulation of hydrogels. Much work on the multiphysical modeling and meshless Hermite-Cloud simulation of polyelectrolyte gels had been done by Li and Lam et al., including multi-effect-coupling electric stimulus (MECe) models to simulate the response of electric-sensitive hydrogels (Chen et al., 2005; Lam et al., 2006; Li, 2009; Li et al., 2003, 2006, 2007a; Li et al., 2007c, d; Li et al., 2004b; Luo et al., 2007); multi-effect-coupling pH-stimulus (MECpH) model for the swelling behavior of pH-sensitive hydrogels (Li et al., 2005a; Li and Yew, 2009; Li et al., 2004a; Li et al., 2009; Li et al., 2005d; Ng et al., 2010); multi-effect-coupling pH-electric-stimuli (MECpHe) model, simulating response of a dual electric-pH-sensitive hydrogel (Li et al., 2007b; Luo et al., 2008); and a multi-effect-coupling ionic-strength-stimulus (MECis) model for ionic strength sensitive hydrogels (Lai and Li, 2010, 2011; Li and Lai, 2011). In addition to the Hermite-Cloud meshless method, a strong-form meshless random differential quadrature (RDQ) method was developed for the simulation

of two dimensional deformation of pH-sensitive hydrogels (Li and Mulay, 2011).

1.1.4.3. *Other simulation methods*

Molecular dynamics simulations have also been used for the equilibrium state swelling properties of hydrogels. (Tamai et al., 1996) performed molecular dynamics simulations to study the distributions and dynamics of hydrogen-bonds, diffusion of water, and the orientational relaxation of water. Kenkare et al. (2000) studied the equilibrium swelling of neutral hydrogels using a combined discontinuous molecular dynamics and Monte Carlo technique, considering each monomer and solvent molecule as hard spheres. Quesada-Perez et al. (2012) applied coarse grained molecular dynamics, using a truncated Leonard-Jones potential for interaction between particles and a hydrophobic interaction potential, simulating the steady state swelling behavior of gels due to temperature and pH changes.

1.1.5. Mechanical instabilities

Mechanical instabilities, such as wrinkling, creasing, buckling and bifurcation are commonly observed phenomenon in hydrogels.

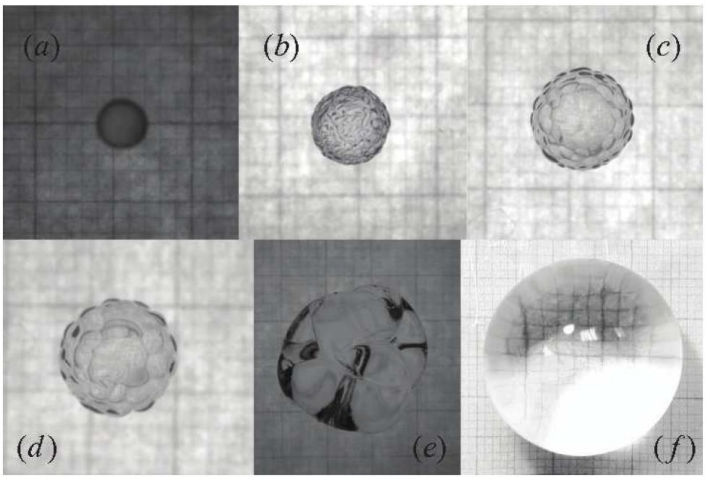

Figure 1-2: Surface instability in transient swelling. Wrinkle size increase with time as gel becomes increasingly swollen. Reproduced from Peixinho and Mukhopadhyay (2013)

Tanaka et al. (1987), Tanaka et al. (1992), Ji and Ding (2002), Guvendiren et al. (2010a), Barros et al. (2012) and Peixinho and Mukhopadhyay (2013) reported the formation and transient growth of surface wrinkles that form when a dry hydrogel was hydrated. Figure 1-2 shows an example of this instability.

Matsuo and Tanaka (1992), Tokita et al. (2000) and Ji and Ding (2001) discussed the formation of bubbled patterns when a gel shrinks. It was observed that under different shrinking ratios, gel rods evolve into various bubbled or bamboo patterns, as seen in Figure 1-3.

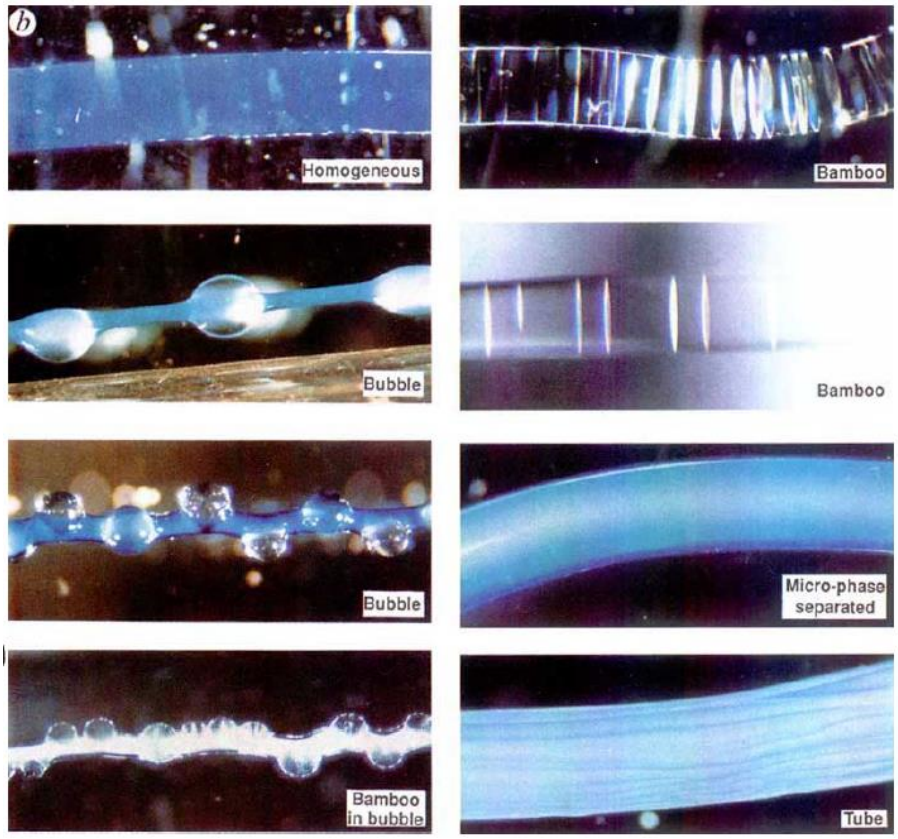

Figure 1-3: Patterns in a shrinking gel. reproduced from Matsuo and Tanaka (1992)

Guvendiren et al. (2010b; 2009) studied the surface pattern formation of gels with depth-wise gradient crosslinking. It was found that by varying the

depth-wise crosslink density, the surface patterns that appear can be varied, as seen in Figure 1-4.

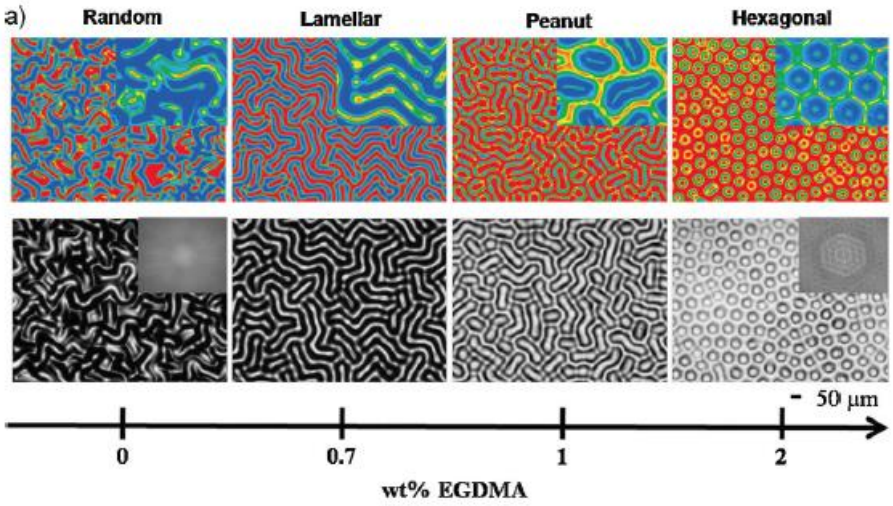

Figure 1-4: Surface patterns that appear when crosslink density is varied. Reproduced from Guvendiren et al. (2009)

DuPont Jr et al. (2010) investigated the transient evolution of wrinkles in gel strips, with experimental results showing that local surface wrinkles will first appear, before subsequently transiting into bulk buckling of the entire gel, as shown in Figure 1-5. Mora and Boudaoud (2006) and Lee et al. (2012) investigated the relationship between geometry and bulk buckling modes of swelling gels. It was shown that the wrinkle mode shapes are largely dependent on the initial geometry of the gel rather than material properties.

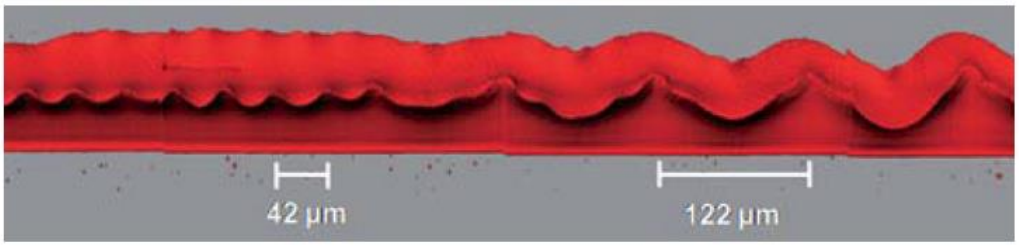

Figure 1-5: Evolution of surface wrinkles into bulk wrinkles. Reproduced from DuPont Jr et al. (2010)

Sultan and Boudaoud (2008) and Cao and Hutchinson (2012) studied the instability present in bilayer structures, shown in Figure 1-6. Ohzono and Shimomura (2004) and Breid and Crosby (2011) further investigated the dependence of wrinkle morphology on strain and stress respectively. The bilayer structure is very popular with theoretical analyses due to its availability of analytical solutions as an approximation to various structures (e.g. (Wu et al., 2013)).

Figure 1-6: Buckling of a gel film attached to a compliant substrate. Reproduced from Sultan and Boudaoud (2008)

Mullin et al. (2007) and Zhang et al. (2008) reported that in a polymeric film with regular perforations, it is possible to obtain ordered two-dimensional patterns through the gel's instability mechanism. The pattern transformation for a square lattice of perforations is shown in Figure 1-7.

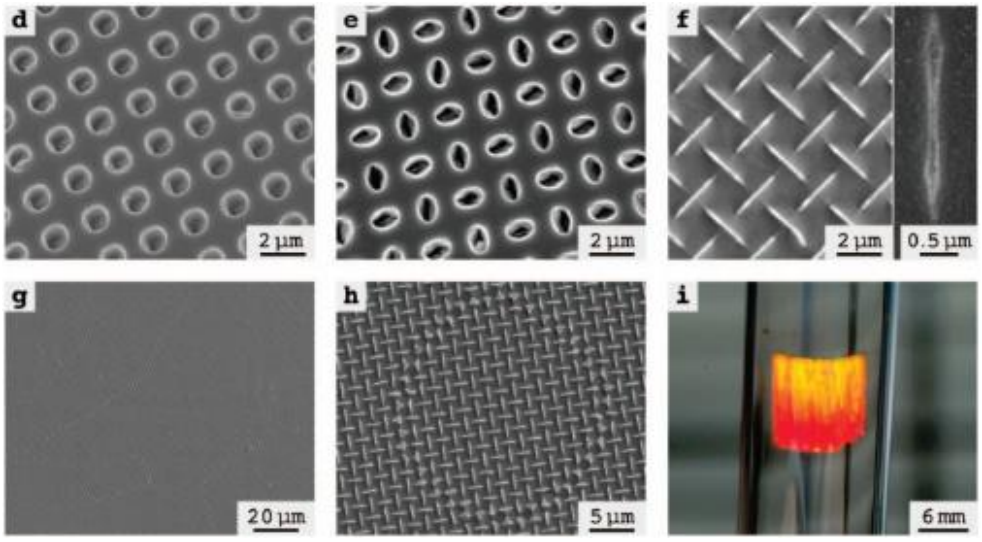

Figure 1-7: Pattern transformation in a square array of periodic holes in a gel film. Reproduced from Zhang et al. (2008)

These mechanical instabilities, initially deemed to be undesirable, have recently become subjects of interest to utilize the instability into useful applications, such as tunable adhesion, micro-patterning, particle sorting, microfluidics, micro-fabrication and actuation (Chen and Yang, 2012; Chen and Yin, 2010; Hu et al., 1998; Kim et al., 2010; Kwon et al., 2010; Yang et al., 2010; Yin et al., 2009).

These exciting potential applications have spurred many theoretical analyses of instability in gels in several broad areas, including bilayer structures consisting of gel films and/ or substrates (Cai et al., 2011; Huang and Suo, 2002a, b; Huang et al., 2004; Jia and Ben Amar, 2013; Kang and Huang, 2010a; Kang and Huang, 2010b; Liu et al., 2010; Liu et al., 2011; Wu et al., 2013); wrinkling of thick gel layers with uniform material properties (Ben Amar and Ciarletta, 2010; Hong et al., 2009b; Trujillo et al., 2008; Weiss et al., 2013; Xiao et al., 2012); surface wrinkling of thick gel layers with non-uniform depth-wise crosslink densities (Wu et al., 2013), bulk buckling of geometrically constrained thin gels (Lee et al., 2012; Li et al., 2013a; Liu et al., 2010; Zhang et al., 2014); buckling of spherical structures (Fogle et al., 2013; Komura et al., 2005; Li et al., 2011b; Yin et al., 2008); and pattern formation in gel films with periodic hole arrays (Okumura et al., 2015; Okumura et al., 2014).

The two main modes of instabilities are wrinkling and creasing, and it can be seen for different geometries, one mode takes precedence over the other although both modes are possible. Wong et al. (2010), Jin et al. (2011) and Jin et al. (2014); Wong et al. (2010) investigated the critical conditions for the onset of each type of instability.

With the development of Abaqus finite element subroutines, the instability of gels has been used to explain phenomena commonly seen in nature, such as biological growth, which is analogous to swelling of hydrogels. Liu et al. (2013) studied the growth in plants, Li et al. (2011a) studied the formation of mucosa,

Cao et al. (2012) studied the wrinkling in skins and Dervaux and Ben Amar (2011) studied the formation of tumors.

1.2. Research objectives

This thesis aims to address several issues which is found to be lacking in current literature. Firstly, this thesis sets out to develop suitable tools using finite element method to simulate and predict the transient swelling process of a gel. Making use of coupled temperature-displacement elements used for thermo-mechanical analysis, we aim to develop finite element models for the swelling kinetics of neutral, temperature sensitive and pH-sensitive hydrogels. It is hoped that through this work, the rigorous work of developing lengthy special-purposed elements subroutines can be simplified. These finite element models will be compared with experimental data, and then utilized to simulate various common cases which may be experienced by hydrogels.

Secondly, this thesis aims to develop a more thorough understanding of the phase transition phenomenon that most hydrogels experience. This will be done viz a variational approach, by considering the work done by various mechanical and chemical loads on a responsive hydrogel. The effects of various types of environmental stimuli, in particular to changes in temperature, light irradiation and exposure to an external magnetic field, and how they affect the phase transition of a gel will be studied in depth. In addition, the material properties will be implemented using finite element method to predict the behavior of responsive gels in reaction to external stimuli. The finite element implementation will be done using two different subroutines, UMAT and UHYPER due to the pros and cons that are inherent each subroutine.

Thirdly, the instability of a gel during swelling will also be studied in depth, using linear perturbation analysis and the finite element models developed in the earlier chapters. Several cases of swelling induced instabilities will be studied to provide a better understanding of the seemingly complex

phenomenon. It is hoped that these studies will aid in better harnessing of instabilities for potential applications rather than as undesirable traits.

1.3. Main contributions of present study

This PhD work has made contributions in several areas. Firstly, this thesis proposed and developed a novel method to create finite element models for the simulation of transient swelling kinetics of neutral, temperature-sensitive and *pH*-sensitive hydrogels. This method greatly reduces the amount of rigor required in developing a UEL subroutine in Abaqus, and also increases the flexibility in using various element types for simulation.

Secondly, the thesis proposed equilibrium swelling theories for the large inhomogeneous deformation of stimuli responsive hydrogels, which includes temperature-sensitive, photo-thermo-sensitive and magneto-thermo-sensitive hydrogels. In accordance with the proposed theories, finite element models were also developed and implemented to facilitate the study of large deformation of hydrogels in various potential applications. The finite element models were implemented using both UHYPER and UMAT subroutines.

Thirdly, based on the finite element models developed, this thesis investigated various types of deformation induced instabilities in gels, including surface wrinkling, bulk buckling and pattern transformation, using the finite element models developed in earlier Chapters. In addition, a state-space method was developed to provide semi-analytical solutions to the growth of surface wrinkles in transient swelling of neutral hydrogels.

1.4. Thesis Outline

The structure of this thesis is arranged as follows: Chapter 2 discusses and develops simulation models to describe the transient swelling behaviors of neutral hydrogels, temperature sensitive hydrogels and pH-sensitive hydrogels. Chapter 3 studies the mechanics and thermodynamics of inhomogeneous

deformation of hydrogels in equilibrium. The model developed was used to study potential applications of temperature and photo-thermal sensitive hydrogels, and also the phase transition phenomenon that a gel experiences in the course of swelling. Chapter 4 studies swelling induced instabilities using linear perturbation analysis for the case of one-dimensional swelling, and finite element simulation for three-dimensional cases of swell-induced instabilities. Chapter 5 concludes the thesis by giving a summary of the work presented herein. Chapter 6 presents an outlook on the future work that may be explored in the area of mechanics of hydrogels. Finally, a list of publications that arose from the research work related to this thesis is given after the list of references.

2. Deformation kinetics of hydrogels

When a cross-linked polymer network imbibes a large amount of solvent, the entropy that is associated from the mixing of the polymer and solvent will result in a swollen state, more commonly known as a gel. The cross-linking of polymers can allow for reversible deformation. Depending on its constituents, a gel is able to deform under the influence of various external stimuli, such as temperature, *pH*-value and light. This unique property of polymeric gels provides tremendous potential for applications in diverse areas, such as biomimetic devices, drug delivery, flow control and sensors (Bashir et al., 2002; Deligkaris et al., 2010; Elvira et al., 2004; Huglin, 1989; Jeong et al., 2005; Kishida and Ikada, 2001; Li and Kong, 2007; Richter et al., 2008).

The mechanics of the gel deformation is dependent on the elastic deformation of strong chemical cross-links and the viscous deformation due to the diffusion of solvents across the material boundary. Early studies on the mechanics of gel swelling (Li and Tanaka, 1990; Peters and Candau, 1988) involved decomposing the material into the two individual phases for independent analyses, which limits the analysis of such materials to simple geometries, such as spheres (Tanaka and Fillmore, 1979), long cylinders (Li and Tanaka, 1990; Peters and Candau, 1988) and large disks (Li and Tanaka, 1990; Peters and Candau, 1988).

In the past, the theory of such multi-phasic gel materials was not favorable for mainstream numerical methods such as the finite element method (FEM), although early works exist for multi-phasic models. As such, finite element analysis of large deformation in these gel materials was limited to rubber hyperelasticity, such as the Arruda-Boyce, Ogden and Mooney-Rivlin models (Marckmann and Verron, 2006). The introduction of continuum theories, treating the different phases of deformation as a single phase, (Chester and Anand, 2010; Duda et al., 2010; Hong et al., 2008) improved the feasibility of FEM implementation for polymeric gels materials. Following the philosophy of

this approach, Hong et al. (Hong et al., 2009a) developed a hyperelastic model for the large deformation of polymeric gels via the UHYPER subroutine in the Abaqus solver. Subsequently, the coupled theory was extended to environmentally sensitive hydrogels, such as *pH*-sensitive gels (Marcombe et al., 2010) and temperature-sensitive gels (Cai and Suo, 2011; Chester and Anand, 2011). While material models for these models exist, they are limited to the equilibrium state whereby the chemical potential is homogenous throughout the gel. Despite the formulation of a user-defined element for the simulation of gel kinetics (Zhang et al., 2009), it is to the author's best knowledge that the transient swelling kinetics was not implemented in a robust manner.

In this Chapter, we attempt to utilize FEM to simulate the swelling kinetics of hydrogels by drawing an analogy between the diffusion of solvent molecules and conduction heat transfer within solids. Although this is similar to another recent work, which also uses the diffusion-heat transfer analogy, we present a method which directly defines thermal properties, as opposed to the definition of the governing equation and its derivatives. This analogy greatly simplifies the procedure for developing full material models by making use of the coupled temperature-displacement elements which can be found in the Abaqus element library.

In addition to this work providing a valuable tool to researchers for the study of gel kinetic deformation in the various applications of soft matter, we also hope to inspire works to adopt this simplified approach, and in particular, works on kinetic studies of diffusion driven mechanisms.

2.1. Neutral hydrogels

The work in this section examines the dynamics of non-linear large deformation of neutral polymeric gels. The kinetics of gel deformation was carried out by combining the knowledge from existing hyperelastic theory for gels and kinetic laws for diffusion of small molecules. As finite element models for the transient swelling process is not available in commercial finite element software, we developed a customized finite element model/methodology which can be used to simulate the transient swelling process of hydrogels. The method was developed based on the similarities between diffusion and heat transfer laws, and by determining the equivalent thermal properties for gel kinetics. Several numerical examples were investigated to explore the capabilities of the present finite element model. Some of the simulation results were compared with available experimental data, and these comparisons show good degrees of similarities.

2.1.1. Theory of neutral hydrogels

2.1.1.1. *Kinematics of deformation*

In the presence of external forces and/or solvent with a different chemical potential, a polymer network will undergo deformation. We define the undeformed state as the reference state and the deformed state as the current state, as shown in Figure 2-1.

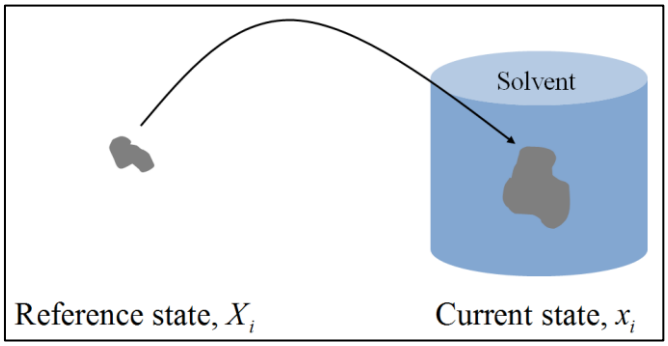

Figure 2-1: A dry polymeric gel in the reference state is placed in contact with a solvent of constant chemical potential and deforms into the current state

From the theory of continuum mechanics, the state of deformation is characterized by the deformation gradient, which is defined as

$$F_{iK}\left(\mathbf{X},t\right)=\frac{\partial x_i\left(\mathbf{X},t\right)}{\partial X_K}\ . \tag{2.1}$$

The deformation gradient F_{iK} describes the state of deformation by finding the partial derivative of the current state x_i with respect to the reference state X_K at any time *t*.

2.1.1.2. *Thermodynamics of deformation*

Adopting the outline of thermodynamics of deformation of gel by Hong et al. (2009a), we will derive the framework for the hyperelastic theory for large deformation of gels in equilibrium under a mechanical load and in contact with a solvent.

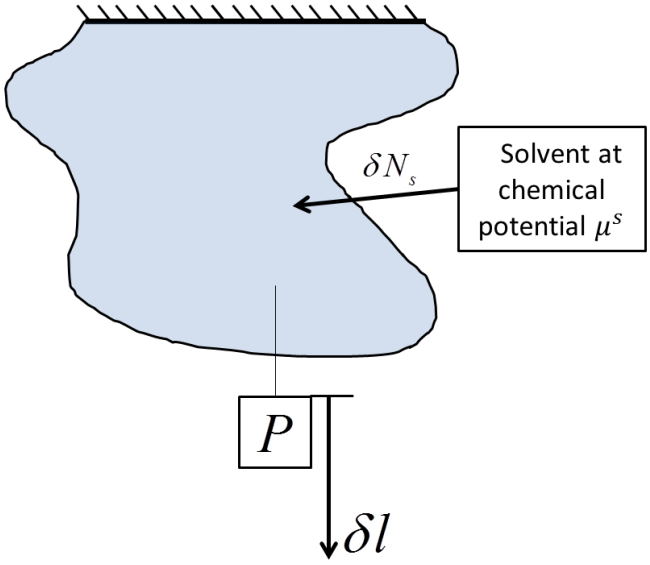

Figure 2-2: A hydrogel domain subjected to external weight *P* and exposed to an external solvent of fixed chemical potential μ^s.

Referring to Figure 2-2, when a gel is deformed, there is work done due to external forces and solvent action. In the equilibrium state, the total work done must be equal to the change in free energy present in the gel. For the elemental volume, defining the deformation as $\delta x_i(\mathbf{X})$, defining the concentration of solvent within the elemental volume as $C^s(\mathbf{X})$, chemical potential as μ^s, body force as $B_i(\mathbf{X})$ and traction as $T_i(\mathbf{X})$, the work done on the gel equals to the sum of $\mu^s \delta C^s \delta V$, $B_i \delta x_i \delta V$ and $T_i \delta x_i \delta A$.

In this equilibrium state, the free energy in the unit element is defined by $\delta W(\mathbf{F}, C^s)$. Integrating over the entire volume of gel, we arrive at the integral equation

$$\int \delta W dV = \int B_i \delta x_i dV + \int T_i \delta x_i dA + \mu^s \int \delta C^s dV \,. \tag{2.2}$$

In addition, the dependence of free energy on $\mathbf{F}$ and C^s means that a small change in W is defined as

$$\delta W = \frac{\partial W(F_{iK}, C^s)}{\partial F_{iK}} \delta F_{iK} + \frac{\partial W(F_{iK}, C^s)}{\partial C^s} \delta C^s \,. \tag{2.3}$$

From the principle of virtual work for elastic bodies (Kelly, 2008), where change in virtual potential energy equals external virtual work done, we write

$$\delta U = \delta W_{ext} \,. \tag{2.4}$$

Defining s_{iK} as nominal stress, which is related to the true stress σ_{ij} by $\sigma_{ij} = s_{iK} F_{jK} / \det \mathbf{F}$, the virtual potential energy change and external virtual works can be written as

$$\delta U = -\delta W_{\text{int}} = -\left[-\int s_{iK} \frac{\partial}{\partial X_K} (\delta x_i) dV \right] = \int s_{iK} \delta F_{iK} dV \,. \tag{2.5}$$

$$\delta W_{ext} = \int T_i \delta x_i dA + \int B_i \delta x_i dV \,. \tag{2.6}$$

Substituting equations (2.5) and (2.6) into equation (2.4), we obtain

$$\int s_{iK} \delta F_{iK} dV = \int T_i \delta x_i dA + \int B_i \delta x_i dV \,. \tag{2.7}$$

Substituting equations (2.3) and (2.7) into equation (2.2) and re-arranging, we obtain the conservative form as

$$\int \left(\frac{\partial W\left(F_{iK}, C^s\right)}{\partial F_{iK}} - s_{iK} \right) \delta F_{iK} dV + \int \left(\frac{\partial W\left(F_{iK}, C^s\right)}{\partial C^s} - \mu^s \right) \delta C^s dV = 0 \,. \tag{2.8}$$

Since integration is carried out for arbitrary changes δF_{iK} and δC^s, the bracketed terms in the integrands must be equal to zero, therefore the nominal stress and chemical potential are defined as

$$s_{iK} = \frac{\partial W\left(F_{iK}, C^s\right)}{\partial F_{iK}}, \tag{2.9}$$

$$\mu = \frac{\partial W\left(F_{iK}, C^s\right)}{\partial C} \,. \tag{2.10}$$

2.1.1.3. *Flory Free energy function*

The swelling of a polymeric gel depends on two factors: the deformation of the polymer network and the mixing of solvent molecules into the network. Flory and Rehner (1943) assumed the free energy function $W\left(\mathbf{F}, C^s\right)$ of a

polymeric gel to be an additive decomposition of the free energy function of network stretch, $W_{net}\left(\mathbf{F}\right)$, and mixing $W_{mix}\left(C^s\right)$.

$$W\left(\mathbf{F},C^s\right)=W_{net}\left(\mathbf{F}\right)+W_{mix}\left(C^s\right). \tag{2.11}$$

2.1.1.4. *Specialization of free energy density function*

Works by Flory (1942; 1953) and Huggins (1941) have developed explicit forms of the free energy functions, which are widely adopted by recent works in the modeling of hydrogels. However, the expressions for the mixing free energy adopted by Hong et al. (2009a; 2008) exhibited a slight difference with the expression adopted by Cai and Suo (2011) and Kang and Huang (2010c). Kang and Huang (2010c) also noted that this difference in expressions of the mixing free energy function has no significant effect on swelling deformation. In this thesis, the expression adopted by Cai and Suo (2011) is employed. Writing in principal stretches such that $\mathbf{F}=diag\left(\lambda_1,\lambda_2,\lambda_3\right)$, the free energy functions are defined as

$$\left.\begin{aligned} W_{net}\left(\mathbf{F}\right)&=\frac{1}{2}Nk_BT\left(\lambda_1^2+\lambda_2^2+\lambda_3^2-3-2\ln\left(\lambda_1\lambda_2\lambda_3\right)\right)\\ W_{mix}\left(C^s\right)&=-\frac{k_BT}{\nu}\left[\nu^sC^s\ln\left(\frac{1+\nu^sC^s}{\nu^sC^s}\right)+\frac{\chi\nu^sC^s}{1+\nu^sC^s}\right] \end{aligned}\right\} \tag{2.12}$$

where λ_1, λ_2, λ_3 denote the stretch in the principal directions; N is the number of polymer chains per unit dry polymer volume; k_B the Boltzmann constant; T the temperature; ν the volume of a solvent molecule; C^s the concentration of solvent and χ a dimensionless measure of mixing enthalpy, known as the Flory-interaction parameter.

2.1.1.5. *Molecular incompressibility constraint*

One essential assumption is that of molecular incompressibility, which requires that both polymer network and solvent molecules do not undergo any volumetric change during the swelling process. This assumption is expressed as

$$1+\nu^s C^s = \det(\mathbf{F}) = \lambda_1\lambda_2\lambda_3 \tag{2.13}$$

Equations (2.9) and (2.10) were derived without the incompressibility constraint. By imposing equation (2.13) as a constraint through a Lagrangian multiplier $\Pi(\mathbf{X},t)$ in the free energy function, equations (2.9) and (2.10) are transformed into

$$s_{iK} = \frac{\partial W\left(F_{iK}, C^s\right)}{\partial F_{iK}} - \Pi H_{iK} \det \mathbf{F} \tag{2.14}$$

$$\mu = \frac{\partial W\left(F_{iK}, C^s\right)}{\partial C^s} + \Pi \nu \tag{2.15}$$

Where H_{iK} is the transpose of the inverse of deformation gradient.

In hydrogels, an important parameter is the chemical potential, which measures the change in entropy when the concentration of solvent molecules changes. The explicit expression for chemical potential is required for the finite element implementation, and this section provides a derivation of the expression for μ^s.

Using the Flory-Rehner free energy function, the principal nominal stresses s_1, s_2, s_3 and chemical potential μ^s are specialized to

$$\left.\begin{aligned} s_1 &= Nk_BT\left(\lambda_1 - \lambda_1^{-1}\right) - \Pi\lambda_2\lambda_3 \\ s_2 &= Nk_BT\left(\lambda_2 - \lambda_2^{-1}\right) - \Pi\lambda_1\lambda_3 \\ s_3 &= Nk_BT\left(\lambda_3 - \lambda_3^{-1}\right) - \Pi\lambda_1\lambda_2 \end{aligned}\right\} \tag{2.16}$$

$$\mu^s = k_B T\left[\ln\left(\frac{\nu C^s}{1+\nu C^s}\right)+\frac{1}{1+\nu C^s}+\frac{\chi}{\left(1+\nu C^s\right)^2}\right]+\Pi\nu \tag{2.17}$$

respectively. Equations (2.15) to (2.17) are derived by Hong et al. (2008).

Using the relations $J\sigma_{ij} = s_{iK}F_{jK}$ and $J = \det(\mathbf{F})$, we obtain

$$\left.\begin{aligned}\sigma_1 &= Nk_BT\left(\lambda_1^2-1\right)-\Pi J\\ \sigma_2 &= Nk_BT\left(\lambda_2^2-1\right)-\Pi J\\ \sigma_3 &= Nk_BT\left(\lambda_3^2-1\right)-\Pi J\end{aligned}\right\} \tag{2.18}$$

$$\mu^s = kT\left[\ln\left(\frac{J-1}{J}\right)+\frac{1}{J}+\frac{\chi}{J^2}\right]+\Pi\nu \tag{2.19}$$

Combining equations (2.18) and (2.19) to eliminate Π, we arrive at

$$\bar{\mu}^s = \left[\ln\left(\frac{J-1}{J}\right)+\frac{1}{J}+\frac{\chi}{J^2}\right]+N\nu\left(\frac{\bar{I}_1 J^{2/3}-3}{3J}\right)-\frac{\left(\bar{\sigma}_1+\bar{\sigma}_2+\bar{\sigma}_3\right)}{3} \tag{2.20}$$

where σ_1, σ_2 and σ_3 are the principal true stresses, $\bar{I}_1 = \left(\lambda_1^2+\lambda_2^2+\lambda_3^2\right)J^{-2/3}$ the deviatoric invariant. The overbars represent non-dimensionalized quantities, i.e. $\bar{\mu}^s = \mu^s/k_BT$ and $\bar{\sigma}_i = \sigma_i/\left(k_BT/\nu\right)$.

2.1.1.6. *Equivalence to a hyperelastic solid*

In this section, we show that the boundary value problem of a deforming polymeric gel can be reduced into the form of a hyperelastic solid, which may be implemented into Abaqus via the use of the user-subroutine UHYPER.

Introducing another free energy function through a Legendre transformation,

$$\hat{W}\left(\mathbf{F},\mu^s\right)=W\left(\mathbf{F},C^s\right)-\mu^s C^s \tag{2.21}$$

We convert the equations (2.2), (2.9) and (2.10) into the following respective equations

$$\int \delta\hat{W}dV=\int B_i\delta x_i dV+\int T_i\delta x_i dA \tag{2.22}$$

$$s_{iK}=\frac{\partial\hat{W}\left(F_{iK},\mu^s\right)}{\partial F_{iK}} \tag{2.23}$$

$$C^s=-\frac{\partial\hat{W}\left(F_{iK},\mu^s\right)}{\partial\mu^s} \tag{2.24}$$

The transformed equilibrium integral equation (2.22) now takes the form of the equilibrium equation of a hyperelastic solid. Combining equations (2.11), (2.13), (2.14) and (2.21), we arrive at the free energy function.

$$\begin{aligned}W\left(\mathbf{F},\mu^s\right)=&\frac{1}{2}Nk_BT\left(I_1-3-2\ln\left(J\right)\right)\\&-\frac{k_BT}{\nu}\left[\left(J-1\right)\ln\left(\frac{J}{J-1}\right)+\frac{\chi\left(J-1\right)}{J}\right]-\frac{\mu^s}{\nu}\left(J-1\right)\end{aligned} \tag{2.25}$$

Equation (2.25) defines the free energy of the polymeric gel as a hyperelastic material which defines the state of deformation through the independent variables I_1, J and μ^s .

2.1.1.7. *Transient swelling kinetics*

The swelling kinetics of a polymeric gel is due to the migration of solvent molecules within and across the material boundary. The chemical potential form of Fick's first law is used to represent the chemical potential driven flow

of solvent molecules (Feynman et al., 1963; Hong et al., 2008; Zhang et al., 2009). Writing in the current frame, the diffusion flux is given by

$$j_i = -\frac{c^s D}{k_B T}\frac{\partial \mu^s}{\partial x_i} = -cD\frac{\partial \bar{\mu}^s}{\partial x_i} \tag{2.26}$$

where the coefficients, $c^s = C^s / J$ represents current solvent concentration and D represents diffusion coefficient.

Equation (2.26) describes the state of steady state diffusion. For transient diffusion, the governing equation for diffusion is obtained by the assumption of conservation of solvent molecules, i.e. no chemical reaction takes place so that there is neither creation nor destruction of molecules. In the reference state, the governing equation is written as

$$\frac{\partial C^s(\mathbf{X},t)}{\partial t} + \frac{\partial J_K(\mathbf{X},t)}{\partial X_K} = 0 \tag{2.27}$$

Converting it into the current state, invoking the incompressibility constraint and integrating throughout, we obtain the weak form as

$$\int_V \frac{1}{\det(\mathbf{F})}\frac{\partial J}{\partial t}dv + \int_S v\, j_i n_i ds = 0 \tag{2.28}$$

Applying the chain rule on equation (2.20) through the assumption of $J = f\left(\bar{\mu}^s, \bar{I}_1, \bar{\sigma}\right)$, we write the material time rate of J as

$$\frac{\partial J}{\partial t} = \frac{\partial J}{\partial \bar{\mu}^s}\frac{\partial \bar{\mu}^s}{\partial t} + \frac{\partial J}{\partial \bar{I}_1}\frac{\partial \bar{I}_1}{\partial t} + \frac{\partial J}{\partial \bar{\sigma}}\frac{\partial \bar{\sigma}}{\partial t} \tag{2.29}$$

where $\bar{\sigma} = \bar{\sigma}_1 + \bar{\sigma}_2 + \bar{\sigma}_3$, and the partial derivatives of J are defined as

$$\left.\begin{aligned} \frac{\partial J}{\partial \bar{\mu}^s} &= \xi \\ \frac{\partial J}{\partial \bar{I}_1} &= -\frac{N\nu}{3J}\xi \\ \frac{\partial J}{\partial \bar{\sigma}} &= \frac{1}{3}\xi \end{aligned}\right\} \tag{2.30}$$

where $\xi = \dfrac{9J^3\left(J-1\right)}{9J-18\chi\left(J-1\right)-N\nu\left(9-\bar{I}_1 J^{2/3}\right)\left(J^2-J\right)}$.

Combining equations (2.28) and (2.29), the governing equation can be expressed as

$$\int \frac{1}{\det\left(\mathbf{F}\right)}\frac{\partial J}{\partial \bar{\mu}}\frac{\partial \bar{\mu}}{\partial t}dv + \int \nu j_i n_i ds = -\int \frac{1}{\det\left(\mathbf{F}\right)}\left(\frac{\partial J}{\partial \bar{I}_1}\frac{\partial \bar{I}_1}{\partial t} + \frac{\partial J}{\partial \bar{\sigma}}\frac{\partial \bar{\sigma}}{\partial t}\right)dv \tag{2.31}$$

2.1.2. Numerical procedure for neutral hydrogel kinetics

We assume local equilibrium at all material points within the volume, and subsequently describe the equilibrium condition by applying the hyperelastic gel theory developed in Section 2.1.1. The use of this hyperelastic gel theory allows for the study of large deformations in polymeric gels subjected to inhomogeneous swelling caused by external mechanical loads.

2.1.2.1. *Heat conduction-diffusion analogy*

In heat transfer within solids, the temperature gradient forms a driving potential which transfers energy around the body through heat conduction. Fourier's Law of heat conduction states that the heat flux is proportional to the temperature gradient (Bergman et al., 2011; Kakac and Yener, 1985), and can be expressed as

$$q_i = -\kappa\frac{\partial T}{\partial x_i} \tag{2.32}$$

The transient heat conduction process is described by the heat conduction equation. In the formulation for the heat transfer elements, the integral form of the heat conduction equation used takes the following form (Simulia, 2010),

$$\int \rho \frac{dU}{dt} dv + \int q_i n_i ds = \int r dv \tag{2.33}$$

Where ρ is the density, *dU/dt* the material time rate of internal thermal energy, *q* the heat flux and *r* the internal heat generation.

By representing chemical potential using temperature, we can see a similarity between the governing equations of diffusion and heat transfer. This implies that the transient swelling kinetics takes the same form as transient heat conduction and that thermal conduction elements can be used to describe the transient swelling kinetics of polymeric gels.

For the kinetics of solvent migration, we make use of the similarity between heat conduction and mass diffusion. Therefore, instead of reformulating an entirely new user-defined element for this purpose, we are able to make use of the inbuilt coupled temperature-displacement analysis in Abaqus. This analogy greatly reduces the amount of time taken for the finite element formulation of gel swelling kinetics. We rewrite equations (2.26), (2.31), (2.32) and (2.33) in Table 2-1 for the reader's convenience.

Table 2-1: Governing equations of gel swelling kinetics and heat transfer

	Flux	Governing equation
Gel Diffusion	$j_i = -c^s D \frac{\partial \bar{\mu}^s}{\partial x_i}$	$\int \frac{1}{\det(\mathbf{F})} \frac{\partial J}{\partial \bar{\mu}} \frac{\partial \bar{\mu}^s}{\partial t} dv + \int \nu j_i ds = -\int \frac{1}{\det(\mathbf{F})} \left(\frac{\partial J}{\partial \bar{I}_1} \frac{\partial \bar{I}_1}{\partial t} + \frac{\partial J}{\partial \bar{\sigma}} \frac{\partial \bar{\sigma}}{\partial t} \right) dV$
Heat transfer	$q_i = -\kappa \frac{\partial T}{\partial x_i}$	$\int \rho \frac{dU}{dT} \frac{dT}{dt} dv + \int q_i n_i ds = \int r dv$

For a fully coupled temperature-displacement analysis, the thermal properties required are density, conductivity and specific heat. Using the subroutine USDFLD, we can directly define these properties as functions of the stretch invariants, as shown from equations (2.34) to (2.37). In addition, a change in $\bar{I}_1$ means a change in volume of the network, thus resulting in a change in the number solvent molecules present in the network. Similarly, a change in the stresses present would facilitate the migration of solvent molecules into the network. Therefore, the effects of $\bar{I}_1$ and $\bar{\sigma}$ can be likened to a source of solvent molecules, analogous to a heat source present in internal heat generation in heat transfer. This internal heat generation is introduced through subroutine HETVAL, through the definition of equation (2.38). Thereafter, the use of thermally-coupled elements will account for mass diffusion within the material.

Comparing the equations presented in Table 1, we set the equivalent thermal properties to be

$$\rho \equiv \frac{1}{\det(\mathbf{F})} = \frac{1}{J} \tag{2.34}$$

$$\mathrm{c}_p \equiv \frac{\partial J}{\partial \bar{\mu}^s} \tag{2.35}$$

$$T \equiv \bar{\mu}^s \tag{2.36}$$

$$\kappa \equiv \nu c^s D = \left(\frac{J-1}{J} \right) D \tag{2.37}$$

$$
\begin{aligned}
r &\equiv -\nu \frac{1}{\det(\mathbf{F})}\left(\frac{\partial C^s}{\partial \bar{I}_1}\frac{\partial \bar{I}}{\partial t}+\frac{\partial C^s}{\partial \bar{\sigma}}\frac{\partial \bar{\sigma}}{\partial t}\right) \\
&\approx -\nu \frac{1}{\det(\mathbf{F})}\left(\frac{\partial C^s}{\partial \bar{I}_1}\frac{\Delta \bar{I}_1}{\Delta t}+\frac{\partial C^s}{\partial \bar{\sigma}}\frac{\Delta \bar{\sigma}}{\Delta t}\right)
\end{aligned}
\tag{2.38}
$$

where the partial derivatives of J are found in equation (2.30). In the quantification of the term in equation (2.38), we approximate the time derivatives of $\bar{I}_1$ and $\bar{\sigma}$ the terms through finite differencing of each term. The terms $\Delta\bar{I}_1$ and $\Delta\bar{\sigma}$ are obtained from the difference of results between the current and previous increments, and Δt is the time increment in the current increment.

Although stemming from the same heat transfer analogy, the finite element implementation differs greatly with that of Duan et al. (2013), where the governing equation (2.28) was directly implemented. Instead, we transform equation (2.28) into equation (2.31) before implementation. This transformation has resulted in two additional terms, which arose due to the incompressibility constraint. Therefore the effects of incompressibility on swelling kinetics can also be investigated.

It should be noted that the main function of this heat transfer analogy is simply a numerical means for obtaining the chemical potential distribution within the gel. This chemical potential distribution, together with the hyperelastic gel theory, would then determine the stress, displacement and solvent concentration within the gel.

In the imposition of chemical potential boundary condition, numerical errors will arise when there is an instantaneous increase in chemical potential due to excessive distortion in surface elements. To circumvent this problem, instead of imposing the boundary condition as an instantaneous increase, the chemical potential is imposed as a linear ramp over a very short duration, which

is an insignificant percentage of the characteristic time of diffusion L^2/D. Through this manner of boundary condition imposition, we will be able to obtain virtually-instantaneous increases in chemical potential with no computational errors.

To show the dependence of swelling kinetics on the diffusion coefficient, we normalize time with the Fourier number $\zeta = L^2/D$ and lengths with characteristic length L.

2.1.3. Numerical examples for neutral hydrogel kinetics

In the examples that ensue, the material properties of $D = 8.0\times10^{-10}$ $\mathrm{m^2 s^{-1}}$, $\chi = 0.1$ and $N\nu = 0.001$ are used. These values are representative of most polymeric gels (Hong et al., 2008) but do not correspond to any specific polymer. To generalize the trends which are exhibited, non-dimensionalization is carried out. For a length scale of *L*, time is represented by $\bar{t} = t/\zeta$, and lengths are represented by $\bar{x} = x/L$.

2.1.3.1. *One-dimensional constrained swelling – verification of numerical model*

Here, the accuracy of the present kinetic model is evaluated through the case of a one-dimensional swelling of a hydrogel. This case is an idealization of the swelling of a thin gel bounded to a rigid substrate, as shown in Figure 2-3. The present simulation results are then compared against the experimental data reported by Yoon et al. (2010).

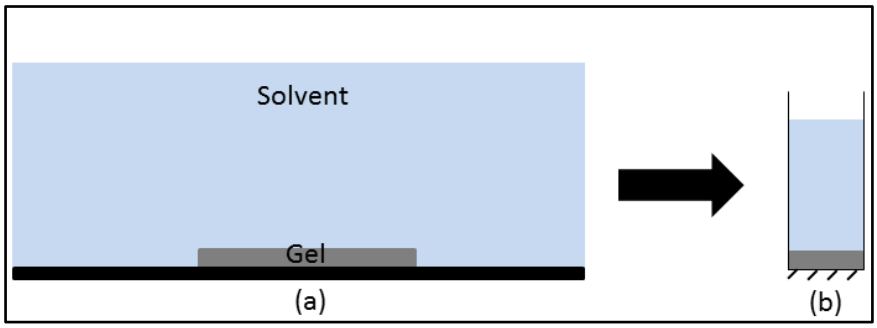

Figure 2-3: (a) Thin gel bounded to rigid substrate exposed to solvent; (b) 1D idealization which assumes solvent only contact gel from the top.

Prior to using the finite element model, we first performed a mesh convergence test for verification of the numerical model. Using one-dimensional constrained swelling, we simulated the process using 1, 5, 20, 100, 200, 500 and 1000 C3D8T elements, some of which are shown in Figure 2-4. Simulation times were in the range of a few minutes to an hour, depending on the size of the mesh.

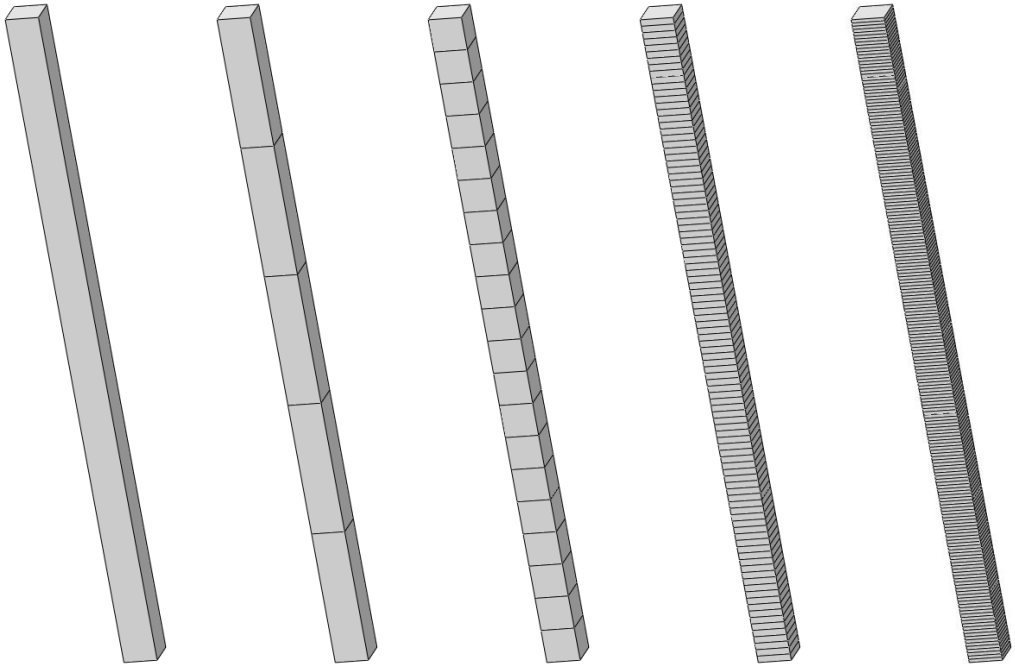

Figure 2-4: Meshes of model used in the one-dimensional constrained swelling for convergence test, consisting of (a) 1 element, (b) 5 elements, (c) 20 elements, (d) 100 elements and (e) 200 elements.

The boundary conditions included fixed bottom surface, symmetric boundary conditions on the lateral faces and a temperature boundary condition of $\bar{\mu}^s = 0$ at the top surface.

We compared the swelling ratio of the top surface at non-dimensionalized times of $\bar{t} = 5,\ 50$ and 200. Figure 2-5 shows the results for the mesh convergence test. We observe that as the number of elements increase to 200 or more, the values of the swelling ratio at the top surface of the gel will reach a constant value. This verifies that there is mesh convergence in the finite element model.

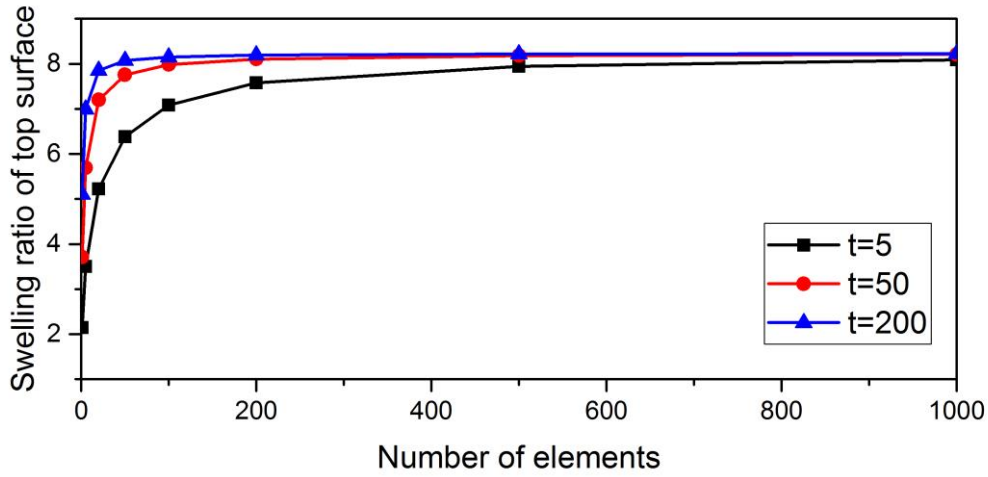

Figure 2-5: Mesh convergence test results for one-dimensional constrained swelling using 1, 5, 20, 100, 200, 500 and 1000 elements.

After the convergence tests, the finite element results were then verified with analytical solutions for correctness of the coding, as well as for theoretical soundness of the formulation.

Analytical solutions for the case of one-dimensional constrained swelling can be obtained by solving the non-linear diffusion equation

$$\lambda_0^2 \frac{\partial \lambda_2}{\partial t} = D \frac{\partial}{\partial X_2}\left(\xi \frac{\partial \lambda_2}{\partial X_2} \right) \tag{2.39}$$

where $\xi(\lambda_2) = \frac{1}{\lambda_0^2 \lambda_2^4} - \frac{2\chi\left(\lambda_0^2 \lambda_2 - 1\right)}{\lambda_0^4 \lambda_2^5} + N\nu \frac{\left(\lambda_0^2 \lambda_2 - 1\right)\left(\lambda_2^2 + 1\right)}{\lambda_0^2 \lambda_2^4}$.

Equation (2.39) has been solved by Bouklas and Huang (2012) using finite difference method. In solving this equation, we had adopted the finite difference scheme outlined in the reference. The interested reader may refer to the original reference for the detailed solution steps. Figure 2-6 show solutions generated by both the finite difference method and finite element method for comparison. 1000 elements were used in the finite element simulation, which took about 1 hour of simulation time. We observed that there is excellent agreement between both methods.

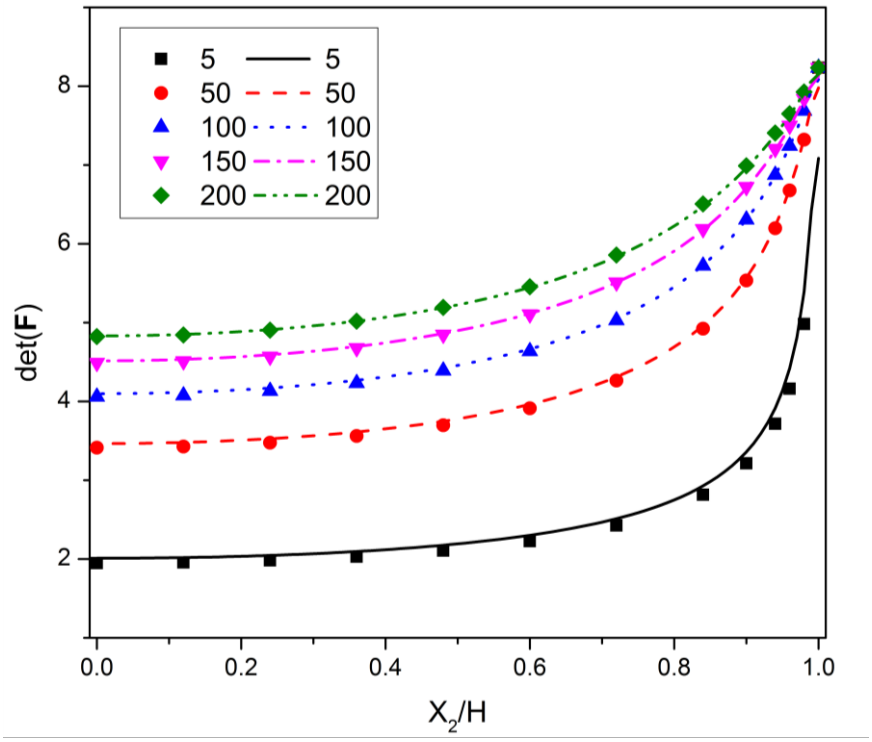

Figure 2-6: Comparison of FEM results (line) with finite difference results (dot) for the swelling ratio of a gel with the parameters $N\nu = 0.001$, $\chi = 0.1$ and $\bar{\mu}_0^s = -1$ for various normalized times.

We had adopted similar conditions outlined in Yoon et al. (2010) for our simulation. The gel, with material properties $N\nu = 0.01$ and $\chi = 0.46$, initially

at a chemical potential of $\bar{\mu}_0^s = -10$, was exposed to a chemical potential of $\bar{\mu}^s = 0$ at the top of the layer. From the boundary conditions, the isotropic stress-free pre-stretch of the gel, calculated using equation (2.20), is $\lambda_0 = 1.0000035$. The final stretch ratio of the gel was calculated by solving the equation

$$\ln\left(\frac{\lambda_0^2\lambda_\infty - 1}{\lambda_0^2\lambda_\infty}\right) + \frac{1}{\lambda_0^2\lambda_\infty} + \frac{\chi}{\left(\lambda_0^2\lambda_\infty\right)^2} + \frac{N\nu}{\lambda_0^2}\left(\lambda_\infty - \frac{1}{\lambda_\infty}\right) = 0, \tag{2.40}$$

giving a final stretch ratio of $\lambda_\infty = 1.804056$ and a net stretch of about 1.8 times the initial thickness. The transient response of the thickness was then reported. With different thicknesses for the specimens used in the experiment, non-dimensionalization was performed to show the trends that were present in the swelling of the gels.

Noting that there is a difference in definition of the diffusion flux, the diffusion coefficient $D_{\text{exp}} = 1.5\times10^{-11}\ \text{m}^2\text{s}^{-1}$ has to be adjusted to fit the non-linear theory used in the finite element model. Bouklas and Huang (2012) compared the linear poro-elastic theory and non-linear theory, and determined that the adjustment of *D* is to be through a scale of $\xi\left(\lambda_0^*\right)$, i.e.

$$D = \frac{D_{\text{exp}}}{\xi\left(\lambda_0^*\right)} \tag{2.41}$$

where $\lambda_0^* = \frac{\lambda_0 + \lambda_\infty}{2}$, $\xi\left(\lambda_0^*\right) = \frac{1}{\lambda_0^2\lambda_0^{*4}} - \frac{2\chi\left(\lambda_0^2\lambda_0^* - 1\right)}{\lambda_0^4\lambda_0^{*5}} + N\nu\frac{\left(\lambda_0^2\lambda_0^* - 1\right)\left(\lambda_0^{*2} + 1\right)}{\lambda_0^2\lambda_0^{*4}}$.

Equation (2.41) gives a value of $D = 6.87\times10^{-11}\ \text{m}^2\text{s}^{-1}$, which is used in the normalization of experimental data presented by Yoon et al. (2010). Normalized simulation and experimental results were plotted and presented in

Figure 2-7. The simulation results were in good agreement with the experimental results in the initial swelling phase, although the simulation results showed a slower swelling rate in the subsequent times. This observation is due to the non-linearity of the kinetic theory, as opposed to the linear poro-elastic theory, which the experimental results might be fortuitously fitted to, as commented by Bouklas and Huang (2012).

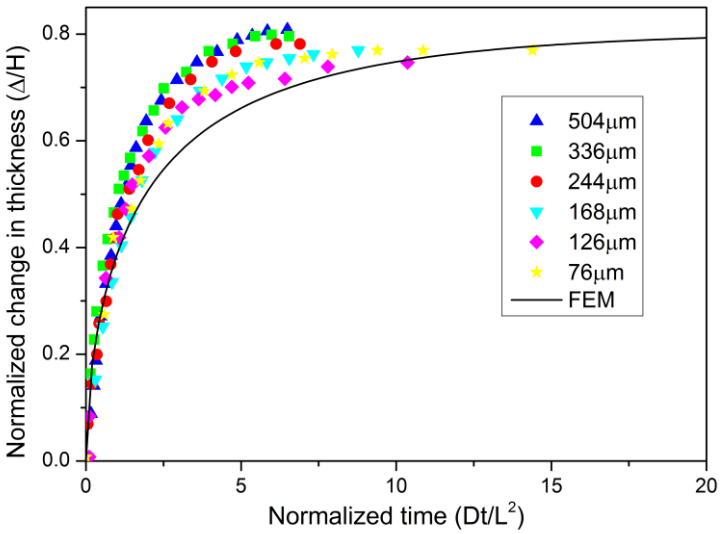

Figure 2-7: Comparison of simulation results with experimental results of Yoon et al. (2010). Solid line represents simulation results, while discrete points represent experimental data with different gel thicknesses.

2.1.3.2. *Free swelling of a cubic gel*

It is easy but erroneous to comprehend and visualize that a cube under swelling will swell homogenously in all directions during the transition from initial to equilibrium states, i.e. the cube will remain cubic during the swelling process. However, this is not the case as the corners of the cube possess higher solvent concentration as compared to the faces of the cube. This would translate into the scenario whereby swelling is more prominent at the corners of the cube as compared to the faces of the cube during the transition process. As time progresses, the cube will eventually reach a state of homogenous chemical potential, thus giving rise to a perfect cube at the end of the swelling process.

This example describes a cube initially in equilibrium at $\bar{\mu}_0^s = -1$, but immersed in a solvent of $\bar{\mu}^s = 0$ at $\bar{t} = 0$. The transient process of the cube swelling at various normalized times is shown in Figure 2-8.

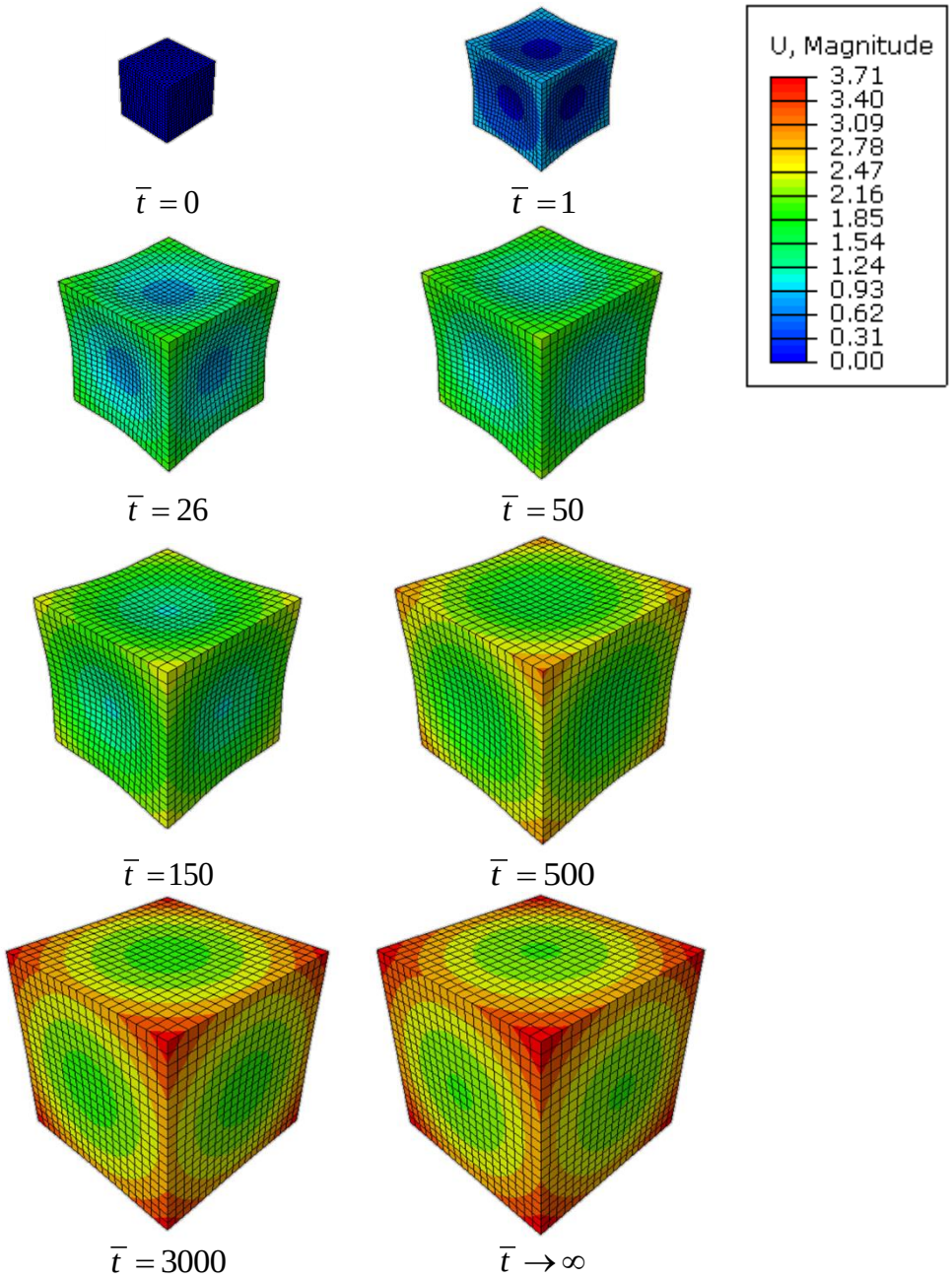

Figure 2-8: Displacement contour plot for the non-dimensionalized free swelling cubic gel at various times. The plots follow the same scale to show the large deformation present.

In this model, 10×10×10 C3D8T elements and 1331 nodes were used. The total computation took about 3 hours. Due to symmetry, only one eighth of the cube was simulated. The node, which represents the centre of the cube, was fixed and the cut faces perpendicular to *x*,y,z-axes had XSYM, YSYM and? ZSYM boundary conditions. The other 3 faces were subjected to a temperature boundary condition of $\bar{\mu}^s = 0$.

Figure 2-9 shows the variation of λ_1 at three points (illustrated in inset) on the *y*-*z* surface of two geometrically similar cubes with different characteristic lengths and diffusion coefficients.

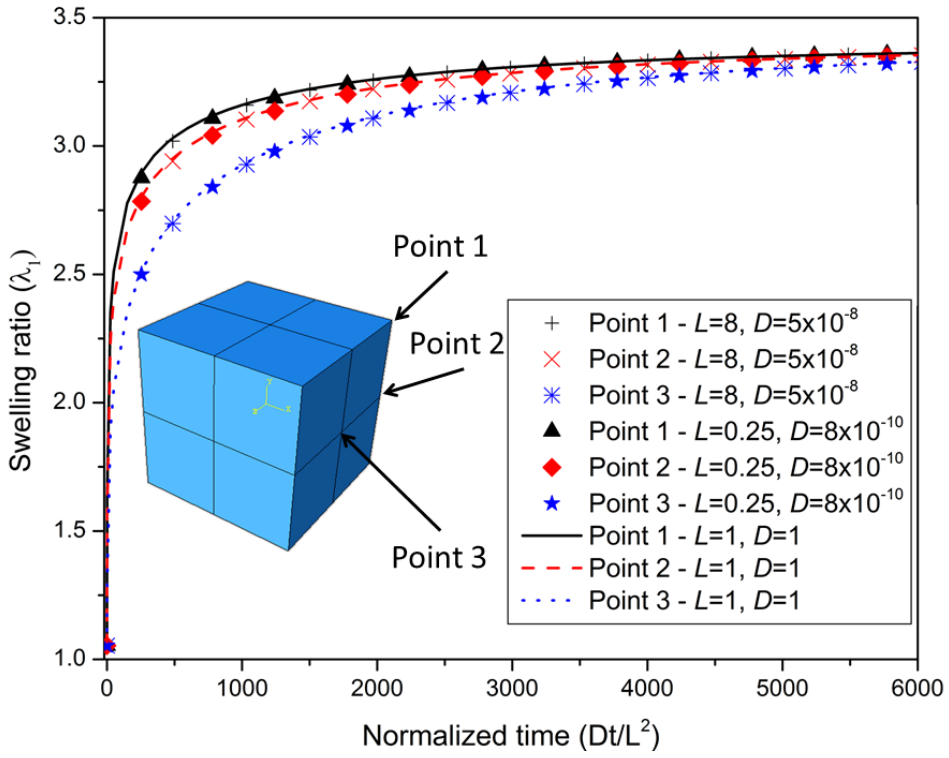

Figure 2-9: Time variation of swelling ratio. Discrete points are for a cube with $L = 0.25$ m , $D = 8.0\times10^{-10}$ $\mathrm{m^2 s^{-1}}$ and $L = 8$ m , $D = 5.0\times10^{-8}$ $\mathrm{m^2 s^{-1}}$. Lines are for the normalized dimensions of $L = 1$ m , $D = 1.0$ $\mathrm{m^2 s^{-1}}$. Inset shows the three selected points for the non-dimensional study. These points possess the same equilibrium stretch ratio in the *x*-direction but different swelling rates

It was evident that while the initial rates of swelling of the points were different, the eventual uniform distribution of chemical potential within the cube would lead to uniform swelling at all points. The long term equilibrium swelling ratio computed was also coherent with analytical solutions for equilibrium swelling conditions presented by Hong et al. (2009a). This verified that the end state of this transient analysis approaches theoretical equilibrium conditions.

In addition, from the overlapping of the two sets of data, we could see the dependence on diffusion coefficient and the square of the characteristic length. This observation shows the usefulness of non-dimensionalization when modeling at a very small scale, as it allows the user to work at a larger length scale. It also facilitates the comparison of specimens of different dimensions as will be seen in the succeeding section.

2.1.3.3. *Three dimensional constrained swelling*

In practical applications of polymeric gels, the gel will be restricted at some points in order to secure it in place. The bondage of parts of the gel structure results in inhomogeneous swelling subjected to external forces. This section demonstrates the capability of this finite element model to simulate the kinetics of inhomogeneous swelling of gels in various cases.

In this example, we attempt to qualitatively compare the present simulation results with the experimental observations of Achilleos et al. (2000). The base of a rectangular block of gel of dimensions 0.44cm×1cm×1cm is rigidly fixed and the remaining sides exposed to a constant chemical potential.

The experimental data of Achilleos et al. (2000) and corresponding present simulation results are presented in Figure 2-10 and Figure 2-11 respectively. We take the characteristic length to be the ratio of volume to wetted surface area, which gives $L = 1.13\times10^{-3}$ m.

It could be observed that while the edge profiles were not exactly the same, there was a similarity in the shapes and polymer concentration distribution and the discrepancies may be attributed to imperfections in the experimental setup. The polymer concentration distribution contour plots showed similar distribution patterns and gel shapes. The study of kinetics of constrained swelling is useful for diverse applications of gels. For example, in the modeling of fluid-structure interaction present in microfluidic valves (Zhang et al., 2012).

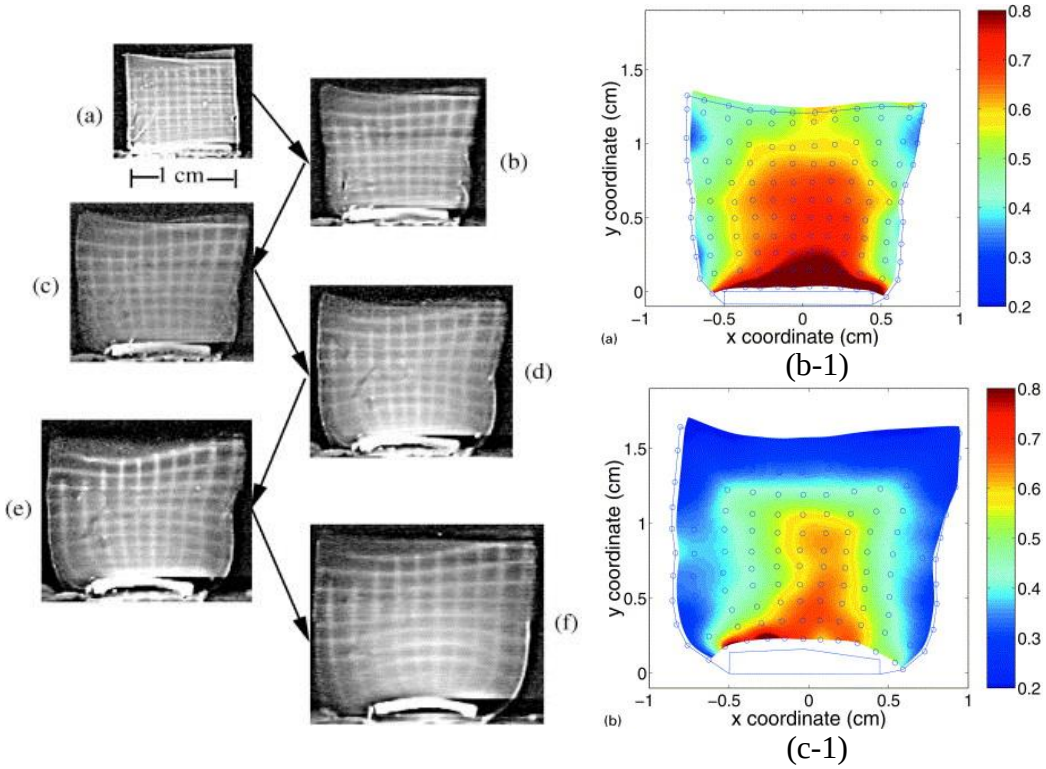

Figure 2-10: (a)-(f) shapes of cross-section of gel at t=0, 1.25h, 2.25h, 6h, 8.5h and 24h. (b-1) and (c-1) show the polymer concentrations at t=1.25h and 2.25h. Reprinted with permission (Achilleos et al., 2000).

Due to symmetry, a half model was used. The mid-plane was assigned symmetrical boundary condition and the bottom of the gel was fixed. In this simulation, the model consisted of 1980 C3D8T elements, corresponding to 5488 nodes. Simulation time was about 2 hours.

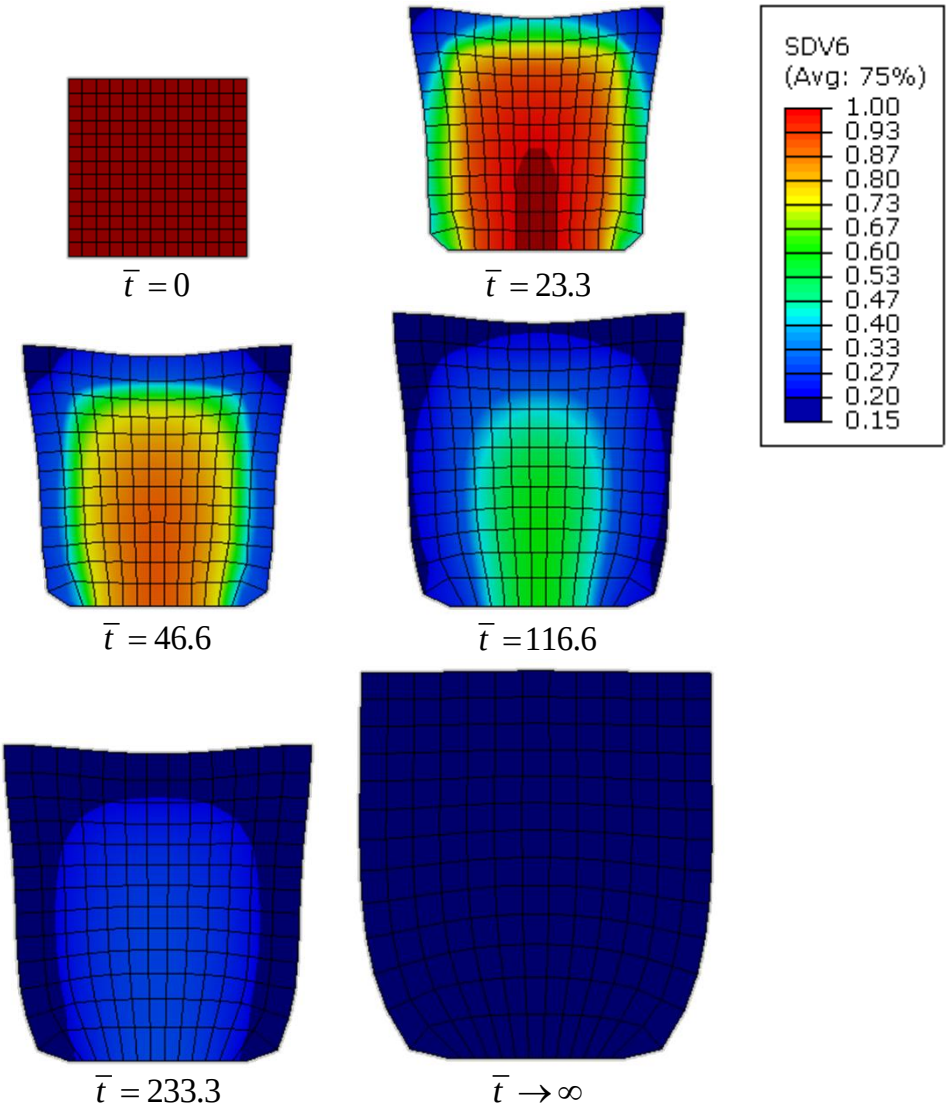

Figure 2-11: Simulation results at various times. The contour plots show polymer concentration of the gel at the mid-plane.

2.1.3.4. *Bending of a free swelling gel sheet*

When a gel sheet is exposed to solvent from one side and allowed to swell freely, there will be large amounts of curling present in the transverse direction of the beam. This phenomena was experimentally explored by Holmes et al. (2011). This curling action of the gel beam is similar to the curling of a piece of paper immersed in water, which was investigated by Reyssat and Mahadevan (2011).

The finite element model was created to simulate a gel sheet of length 20 and thickness 1. Plane strain condition was assumed as we were interested in the lateral deformation of the sheet. Due to symmetry, we modelled half the length of the sheet together with symmetrical boundary conditions. The model contained 1000 C3D8T elements and 2222 nodes. Simulation time was about 1 hour. The bottom part of the line of symmetry was fixed. The gel was given an initial isotropic stretch of $\lambda_0 = 3$ at chemical potential $\bar{\mu}_0^s = -0.00026982$ .At time $\bar{t} = 0$, a uniform surface chemical potential of $\bar{\mu}^s = 0$ was applied on the top surface. Figure 2-12 shows the initial and boundary conditions for the simulation.

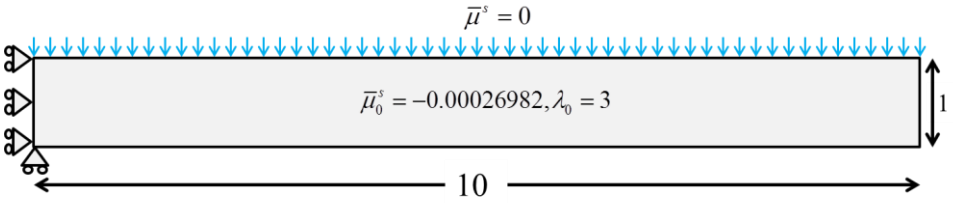

Figure 2-12: Boundary conditions for simulation of bending of a gel beam

The large amount of deformation present in this phenomenon provided a good demonstration of the finite element model's capability to simulate the highly non-linear nature of gel swelling. Figure 2-13 shows the deformation of the gel during various times of the swelling process.

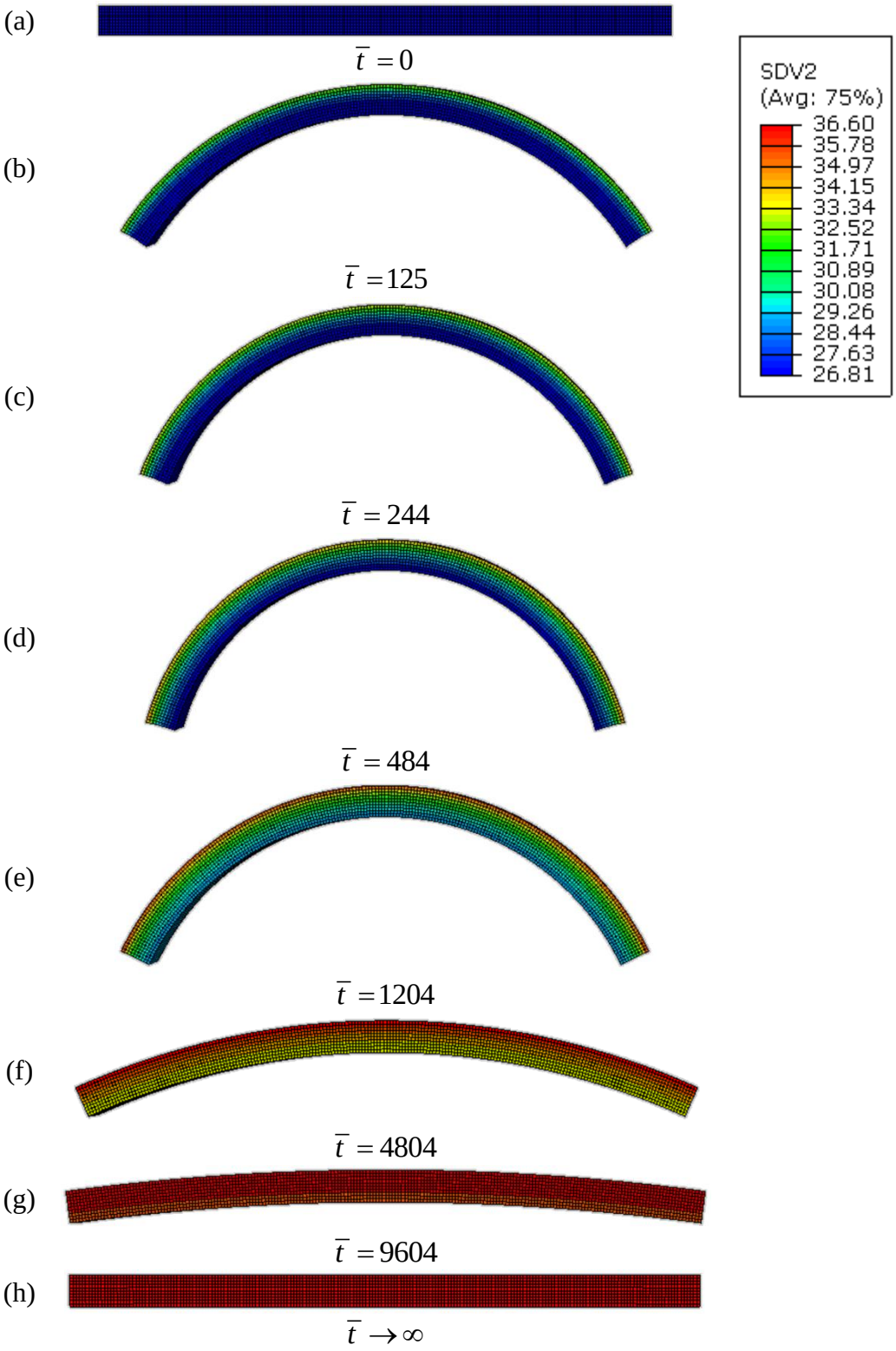

Figure 2-13: Contour plot of swelling ratio of the bending gel beam at various normalized times.

2.2. Temperature sensitive hydrogels

Extending our work in Section 2.1, we develop a finite element model for the swelling kinetics of temperature sensitive hydrogels. The simulation of temperature sensitive hydrogels is not as straightforward as in neutral gels due to the additional loading parameter required: temperature. Therefore, as a simplification, we make a reasonable assumption that the heat transfer process is much faster than the diffusion process when the gel is exposed to a solvent with different temperature. We will prove the appropriateness of this assumption through numerical simulations.

2.2.1. Theory of temperature sensitive hydrogels

2.2.1.1. *Free energy function*

Following the inhomogeneous theory for a temperature sensitive hydrogel by Ding et al. (2013), we write the free energy function of a temperature sensitive hydrogel as

$$W\left(\mathbf{F},C^s,T\right)=W_{net}\left(\mathbf{F}\right)+W_{mix}\left(C^s,T\right) \tag{2.42}$$

where $W_{net}=\frac{1}{2}Nk_BT\left[F_{iK}F_{iK}-3-2\ln\left(\det\mathbf{F}\right)\right]$ is the free energy of network stretch and $W_{mix}=k_BT\left(C^s\ln\frac{\nu C^s}{1+\nu C^s}+\frac{\chi C^s}{1+\nu C^s}\right)$ the free energy of mixing between polymer and solvent. The free energy functions of a temperature sensitive hydrogel is the same as that of a neutral gel, with the exception that the Flory interaction parameter, χ, is no longer a constant. The interaction parameter is given by

$$\chi\left(\phi,T\right)=\chi_0+\chi_1\phi \tag{2.43}$$

where χ_0 and χ_1 are temperature dependent parameters which are specific to the monomer type. Afroze et al. (2000) performed experimental fittings for poly(N-isopropylamide) and obtained that

$$\left.\begin{aligned}\chi_0 &= A_0 + B_0 T \\ \chi_1 &= A_1 + B_1 T\end{aligned}\right\} \tag{2.44}$$

with the values of A_0, B_0, A_1 and B_1 given in Table 2-2.

Table 2-2: Flory-interaction parameters for PNIPAM

Parameter	Value
A_0	−12.947
A_1	17.92
B_0	0.04496 K^{-1}
B_1	−0.0569 K^{-1}

As with the neutral hydrogel, we invoke the molecular incompressibility constraint discussed in Section 2.1.1.4. With the molecular incompressibility constraint, the stress in the gel is given by

$$\frac{\nu\sigma_{ij}}{k_B T} = \frac{N\nu}{J}(F_{ik}F_{ik} - \delta_{ij}) + \left[\ln\left(\frac{J-1}{J}\right) + \frac{1}{J} + \frac{\chi_0 - \chi_1}{J^2} + \frac{2\chi_1}{J^3} - \frac{\mu^s}{k_B T}\right]\delta_{ij} \tag{2.45}$$

Equation (2.45) relates the true stress to the deformation gradient. Rewriting it, a general expression for the chemical potential for water molecules within the gel is obtained as

$$\mu^s = \frac{Nk_B T\nu}{3J}(I_1 - 3) + k_B T\left[\ln\left(\frac{J-1}{J}\right) + \frac{1}{J} + \frac{\chi_0 - \chi_1}{J^2} + \frac{2\chi_1}{J^3}\right] - \frac{(\sigma_1 + \sigma_2 + \sigma_3)\nu}{3}$$

(2.46)

where $I_1 = F_{ik}F_{ik}$ is the first invariant of the deformation gradient.

2.2.1.2. *Swelling kinetics of a temperature sensitive hydrogel*

The swelling kinetics of a temperature consists of two processes, namely heat transfer within the gel as the exterior is exposed to a different temperature, and diffusion of solvent molecules within the gel as the gel is being hydrated or dehydrated.

In practical considerations, it is a reasonable assumption to treat the heat transfer process as an instantaneous one in the presence of the diffusion process, as the heat transfer is usually much faster as compared to the mass diffusion process (Chester, 2011). In this case, the swelling kinetic of gel structure may be regarded as the migration of solvent molecules within and across the material boundary isothermally. Figure 2-14 gives an illustration of this approximation. The dynamic deformation process (1) generally refers to a process from state *A* to state *C*, where both the temperature and chemical potential of the solution changes. As heat transfer is a much faster process as compared to mass diffusion, we can approximate the above process by two steps: process (2) is the heat transfer process, which is assumed to be instantaneous when compared with process (3), which is the mass diffusion process. A virtual intermediate state *B* is defined to be the state where process (2) has finished while process (3) has not started. In this state, the temperature in the gel is homogenous and equal to the temperature of the surroundings. The chemical potential is also homogenous but different from the surrounding solutions. The exact value of chemical potential may be calculated by equation (2.45). As mentioned earlier, since process (2) is much faster and the gel material does not undergo much deformation, we only model process (3) as an approximation to process (1).

During the mass diffusion process, the flux relates to the gradient of chemical potential by the following equation (Hong et al., 2008)

$$j_i = -\frac{c^s D}{k_B T}\frac{\partial \mu^s}{\partial x_i} = -c^s D\frac{\partial \bar{\mu}^s}{\partial x_i} \tag{2.47}$$

where $c^s = C^s / J$ is the current density, D is the diffusion coefficient and $\bar{\mu}^s = \mu^s / k_B T$ is the non-dimensional representation of the chemical potential.

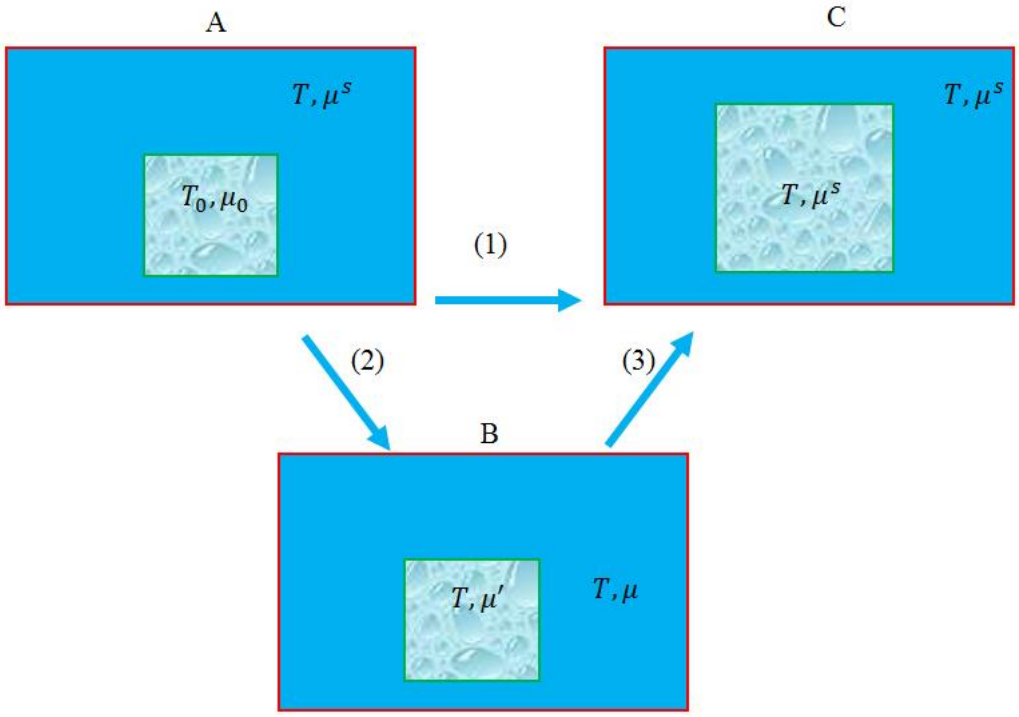

Figure 2-14: The swelling of a temperature sensitive hydrogel (1) is taken to be a two step process consisting of heat transfer (2), followed by mass diffusion (3).

The conservation of the mass may be written as:

$$\int \frac{1}{J}\frac{dC^s}{dt}dv + \int j_i n_i ds = 0 \tag{2.48}$$

By using the incompressibility condition given by equation (2.13), the above equation may be rewritten as:

$$\int \frac{1}{J}\frac{dJ}{dt}dv + \int j_i n_i ds = 0 \tag{2.49}$$

An expression for $\frac{dJ}{dt}$ is needed to implement equation (2.49). To obtain an expression for it, we rewrite equation (2.46) in a non-dimensional form as

$$\bar{\mu}^s = \frac{N\nu}{3J}(\bar{I}_1 J^{\frac{2}{3}} - 3) + \left[\ln\left(\frac{J-1}{J}\right) + \frac{1}{J} + \frac{\chi_0 - \chi_1}{J^2} + \frac{2\chi_1}{J^3}\right] - \frac{\bar{\sigma}_1 + \bar{\sigma}_2 + \bar{\sigma}_3}{3} \tag{2.50}$$

where $\bar{\mu}^s = \mu^s / k_B T$, $\bar{\sigma}_i = \sigma_i / (k_B T/\nu)$, $\bar{I}_1 = I_1 J^{-\frac{2}{3}}$ is the deviatoric invariant.

Using the chain rule, and assume $J = f(\bar{I}_1, \bar{\sigma}, \bar{\mu}^s)$ in equation (2.50), $\frac{dJ}{dt}$ is written as:

$$\frac{dJ}{dt} = \frac{\partial J}{\partial \bar{\mu}^s}\frac{d\bar{\mu}^s}{dt} + \frac{\partial J}{\partial \bar{I}_1}\frac{d\bar{I}_1}{dt} + \frac{\partial J}{\partial \bar{\sigma}}\frac{d\bar{\sigma}}{dt} \tag{2.51}$$

where $\bar{\sigma} = \bar{\sigma}_1 + \bar{\sigma}_2 + \bar{\sigma}_3$.

By combining equations (2.48) and (2.51), the governing equation may be rewritten as:

$$\int \frac{1}{J}\frac{\partial J}{\partial \bar{\mu}}\frac{d\bar{\mu}}{dt}dv + \int \nu j_i n_i ds = \int \frac{1}{J}\left(\frac{\partial J}{\partial \bar{I}_1}\frac{d\bar{I}_1}{dt} + \frac{\partial J}{\partial \bar{\sigma}}\frac{d\bar{\sigma}}{dt}\right)dv \tag{2.52}$$

2.2.2. Numerical procedure for temperature sensitive hydrogel kinetics

Making use of the heat transfer-diffusion analogy elaborated in Section 2.1.2.1, we implement the finite element model of the temperature sensitive gel using the following equivalent terms,

$$\rho \equiv \frac{1}{J} \tag{2.53}$$

$$c_p \equiv \frac{\partial J}{\partial \bar{\mu}^s} \tag{2.54}$$

$$T \equiv \bar{\mu}^s \tag{2.55}$$

$$\kappa \equiv \frac{(J-1)}{J} D \tag{2.56}$$

$$r \equiv -\frac{1}{J}\left(\frac{\partial J}{\partial \bar{I}_1} \frac{d\bar{I}_1}{dt} + \frac{\partial J}{\partial \bar{\sigma}} \frac{d\bar{\sigma}}{dt} \right) \tag{2.57}$$

where the partial derivatives given in Equation (2.57) are derived to be

$$\left.\begin{aligned} \frac{\partial J}{\partial \bar{\mu}^s} &= \xi \\ \frac{\partial J}{\partial \bar{I}_1} &= -\frac{1}{3} J^{-\frac{1}{3}} N v \xi \\ \frac{\partial J}{\partial \bar{\sigma}} &= \frac{1}{3}\xi \end{aligned}\right\} \tag{2.58}$$

where ξ is used as a short-hand for the long expression given by

$$\xi = \frac{9J^4(J-1)}{N v \bar{I}(1-J)J^{\frac{8}{3}} + 9NvJ^3 + 9[(1-Nv) + 2(\chi_1 - \chi_0)]J^2 + 18(\chi_0 - 4\chi_1)J + 54\chi_1}.$$

Now, every term is expressed in terms of the quantities that are accessible as field variables in Abaqus. To implement the method in Abaqus, we have

adopted the UHYPER for temperature-sensitive gel to govern the mechanical behavior, and we can easily define the heat capacity, conductivity and density as functions of stretch invariants using subroutine USDFLD. The heat source term given by equation (2.57) is defined through subroutine HETVAL. With the concurrent use of the three subroutines, the kinetics of gel deformation can be studied in Abaqus using a fully coupled temperature-displacement analysis.

2.2.3. Numerical examples for temperature sensitive hydrogel kinetics

Prior to the numerical simulations to be performed in the subsequent Sections, mesh convergence tests were carried out. The convergence tests made use of the same setup as the convergence test used in Section 2.1.3.1, i.e. one-dimensional constrained swelling with number of elements ranging from 1 to 1000.

2.2.3.1. *Swelling of a gel disk – comparison with experimental results*

To verify the correctness of our model, we compared the simulation results with the available experiment measurements reported by Zhuang et al. (2000). In the experiments, the gel was cut into disks with thickness of 2 mm and diameter 1 cm. The results were reported using mass swelling ratio. Using physical parameter reported in the literature (Bae et al., 1989; Bird et al., 2007; Prokop et al.; Schwaiger and Köhler, 2013; Wagner and Pruß, 2002), we converted the mass swelling ratio to volume swelling ratio. The physical properties for the polymer and solvent phases are summarized in Table 2-3. Since the values for *Nv* and *D* were not given in the references, we perform fitting to obtain these values. Table 2-4 summarizes the parameter values for gels with different composition. We had chosen the isotropic state with initial stretch 1.0001 as the dry state to avoid singularity of the free energy function when $J = 1$. It could be observed that different Sodium Acrylate contents could

result in different polymer chains density (Nv) and diffusion coefficient (D). Figure 2-15 shows good agreement between experimental results and simulation results.

Table 2-3: Physical properties of gel materials

	Density $\left(\mathrm{kgm^{-3}}\right)$	Heat Capacity $\left(\mathrm{Jkg^{-1}K^{-1}}\right)$	Thermal conductivity $\left(\mathrm{Wm^{-1}K^{-1}}\right)$
Network	1.2×10^{3}	2×10^{4}	2
Solvent	1×10^{3}	4.2×10^{3}	$-1.05\times10^{-5}T^{2}+7.98\times10^{-3}T-8.38\times10^{-1}$

Table 2-4: Physical parameters for gel with different composite. NIPA and SA stands for N-isopropylacrylamide and sodium acrylate respectively

No.	NIPA:SA	Nv	$D\left(\mathrm{m^{2}s^{-1}}\right)$
B07	90:10	0.003	7×10^{-8}
B03	98:2	0.01	1.2×10^{-8}

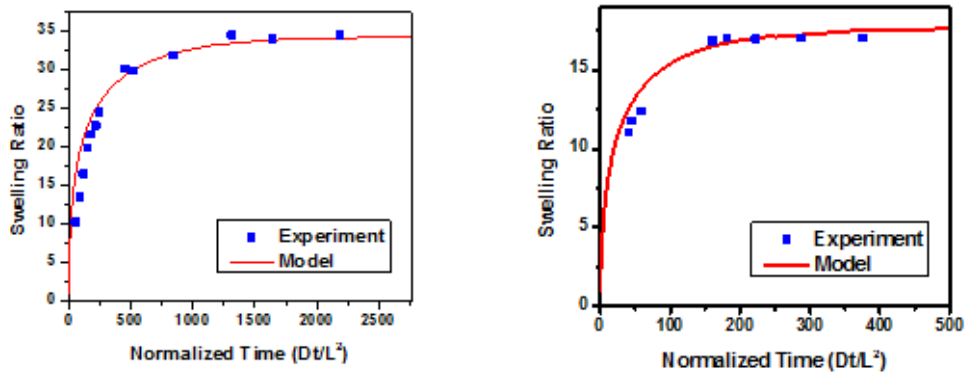

(a) (b)

Figure 2-15: Comparison of simulation results with experimental results (Zhuang et al., 2000). (a) Swelling ratio as a function of time for sample No. B07, $Nv=0.003$, $D=7\times10^{-8}\ \mathrm{m^{2}s^{-1}}$ (b) Swelling ratio as a function of time for sample No. B03, $Nv=0.01$, $D=1.2\times10^{-8}\ \mathrm{m^{2}s^{-1}}$. The simulation model is a cylinder with a diameter of 1cm and thickness 2mm and dry gels are put into water at 297K.

2.2.3.2. *Free swelling cube - verification of assumption*

In Section 2.3.1.1, we have assumed that heat transfer is a much faster process than mass diffusion. We will now verify this assumption. The total time for heat transfer can be obtained by treating mass diffusion as an instantaneous process. We assume that the transfer of heat energy is due to conduction of heat in both the polymer network as well as solvent molecules. We assume deformation to be temperature driven as the gel is pre-swollen to a state of homogenous chemical potential. Heat conduction equation is given by equations (2.32) and (2.33).

We assume the conductivity to be a mixture of conductivities of both components. The thermal conductivities of the polymer network and solvent are assumed to be isotropic, with conductivity of solvent taken to be dependent on temperature as shown in Table 2-3. The density and heat capacity of the mixture can be derived from conservation of mass and incompressibility constraint. The conductivity, density and specific heat capacity are expressed as

$$\kappa = \phi\kappa^{p} + (1-\phi)\kappa^{s} \tag{2.59}$$

$$\rho^{gel} = \frac{\rho^{p} + \rho^{s}(J-1)}{J} \tag{2.60}$$

$$c_{p}^{gel} = \frac{c_{p}^{p} + c_{p}^{s}(J-1)}{J} \tag{2.61}$$

where the superscripts p and s represent polymer network and solvent molecules respectively, and their values are given in Table 2-1.

The deformation process was simulated as a heat transfer process with the concurrent use of UHYPER and USDFLD. The simulation used the same process as the above two methods. We considered the process where a cubic gel of unit length was immersed in water which was undergoing a temperature drop

from 303K to 283K. Using the method proposed in section 2.2.1.2, this process was equivalent to a process where the normalized chemical potential increased from -0.17 to 0, which corresponded to a swell from initial stretch 2.200 to a final stretch of 3.137. The isotropic stress-free stretches were calculated using equation (2.62), given by

$$\frac{Nk_BT_0}{\lambda_1^{\,2}\lambda_0}(\lambda_1^{\,2}-1)+\frac{k_BT_0}{\nu}\left[\ln\left(\frac{\lambda_1^{\,2}\lambda_0-1}{\lambda_1^{\,2}\lambda_0}\right)+\frac{1}{\lambda_1^{\,2}\lambda_0}+\frac{\chi_0-\chi_1}{\left(\lambda_1^{\,2}\lambda_0\right)^2}+\frac{2\chi_1}{\left(\lambda_1^{\,2}\lambda_0\right)^3}\right]-\frac{\mu^s}{\nu}=0 \tag{2.62}$$

Similar to the model in Section 2.1.3.2, $10\times10\times10$ C3D8T elements and 1331 nodes were used and the total computation time taken was about 3 hours. Due to symmetry, only one eighth of the cube was simulated, with the node representing the centre of the cube fixed, the cut faces perpendicular to *x*,y,z-axes having XSYM, YSYM AND ZSYM boundary conditions. The other 3 faces were subjected to a temperature boundary condition of $\bar{\mu}^s=0$.

Static analysis assumes that the gel will remain homogenous during the swelling process, which is not the case. To see how exactly the gel was deforming, several representative states had been selected as shown in Figure 2-16 and Figure 2-17. It was observed that the corner part of the gel materials would be the first to deform because of its relatively larger contact surface with the solution. We had chosen a non-dimensional time $\bar{t}=t/\zeta$, where $\zeta=L^2/D$ is the characteristic time, D the diffusion coefficient given in Table 2-4 and L the length of the cube for method 1. A non-dimensional time $\bar{t}=0.144\times tD_e/L^2=t/\zeta$ was chosen for method 2, where $D_e=k^p/\left(c_p^p\rho^p\right)$. This equality can be easily verified with the physical properties provided in Table 2-3 and Table 2-4.

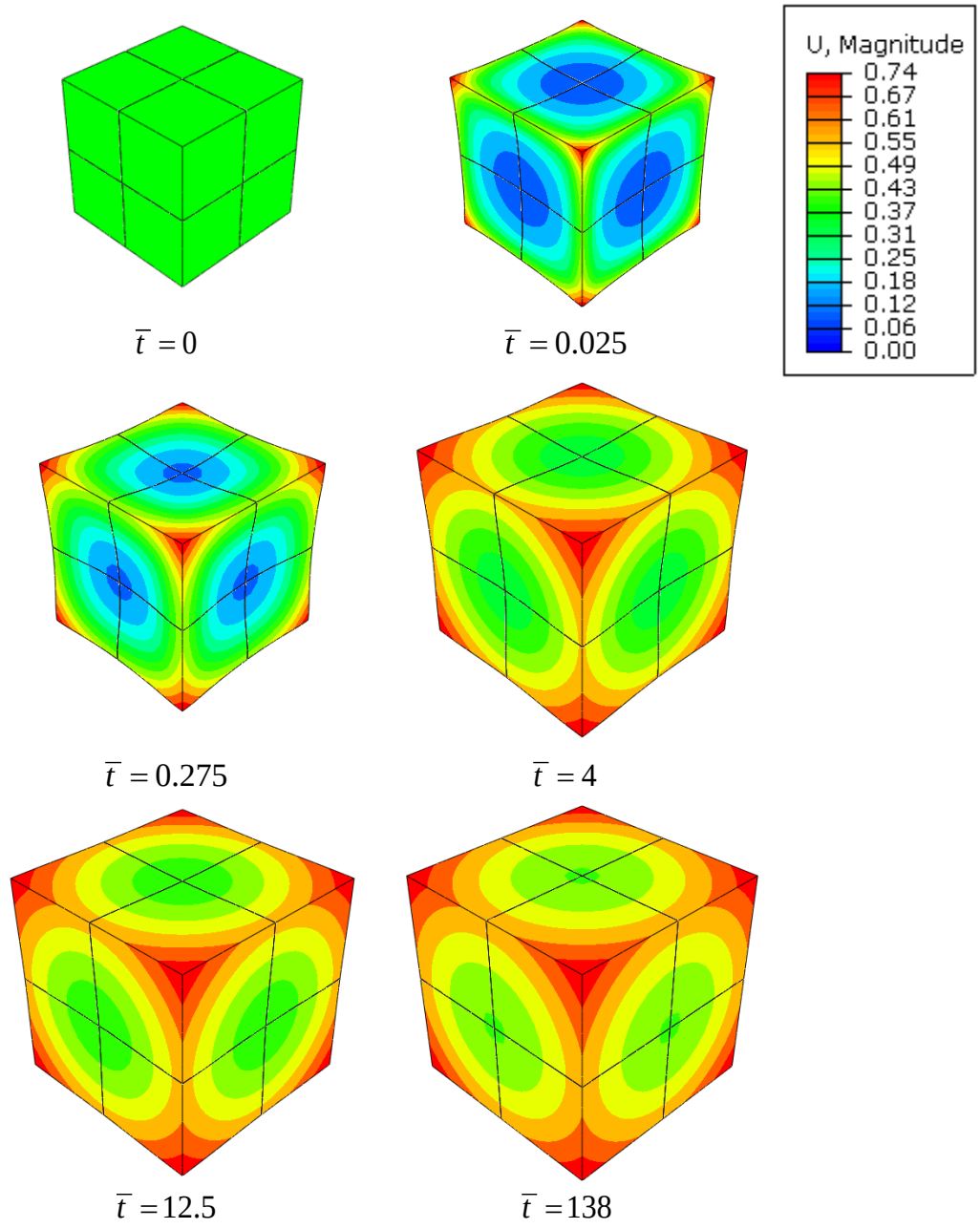

Figure 2-16: Displacement contour plots for non-dimensioned free swelling cubic under method 1 gel at various times. The plots follow the same scale so as to show the large deformation process. In this method, heat transfer is treated as an instantaneous process.

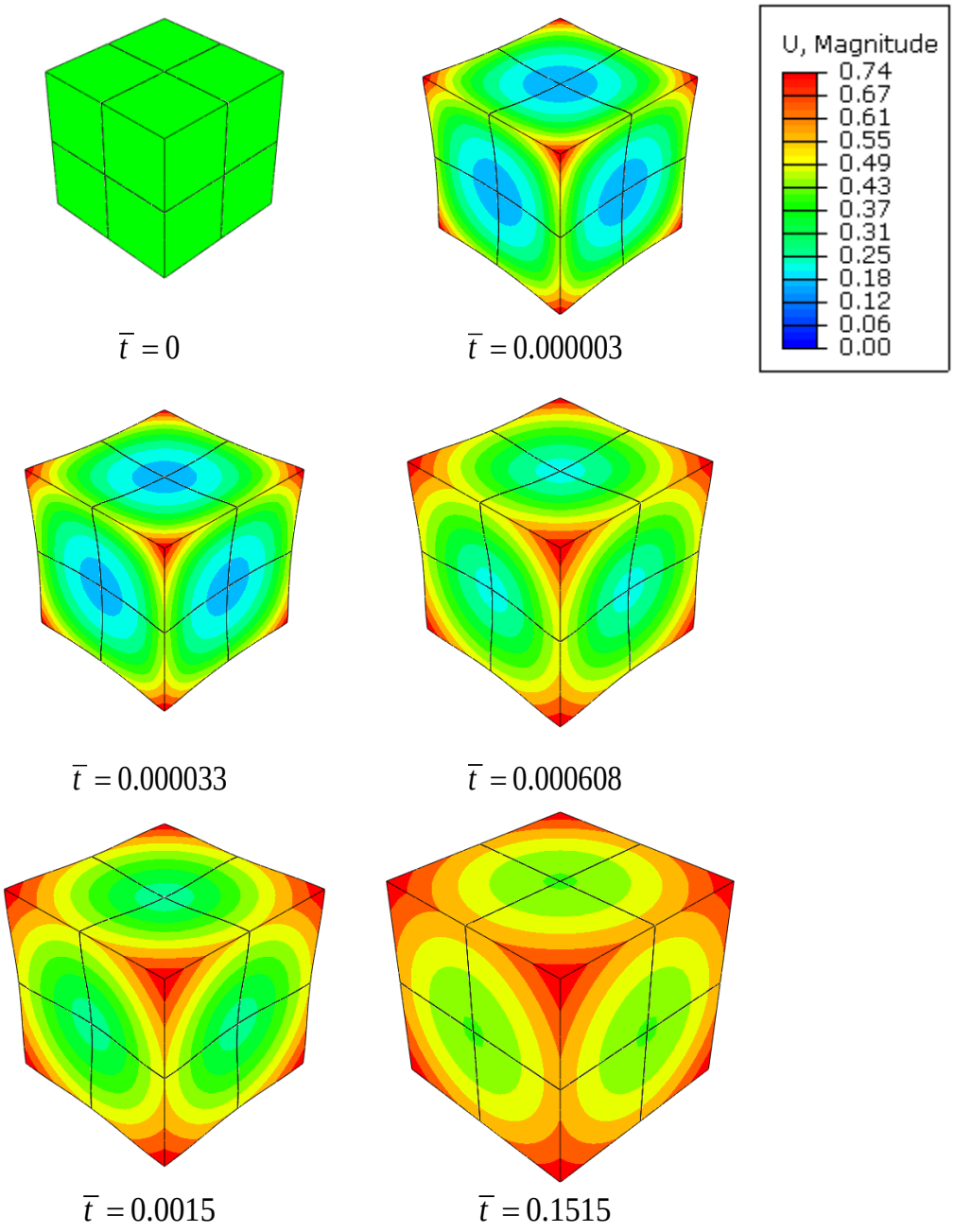

Figure 2-17: Displacement contour plots for non-dimensioned free swelling cubic gel at various times. The plots follow the same scale so as to show the large deformation process. In this method, mass diffusion is treated as an instantaneous process

To have a better idea of the fact that different parts of the gel deform at various rates, four points were chosen for further studies. Consider an eighth of a cube, as highlighted in red, with points *A*, *B*, *C* and *D* as shown in Figure 2-18.

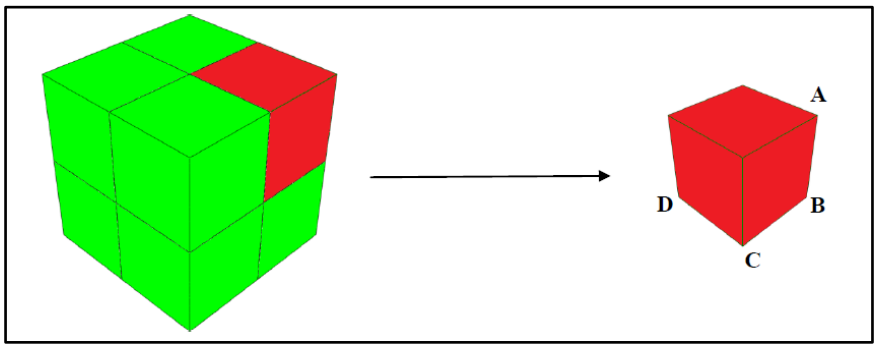

Figure 2-18: Schematic illustrations of the four chosen points

The change of stretches at points *A*, *B*, *C*, *D* with respect to time are plotted in Figure 2-19.

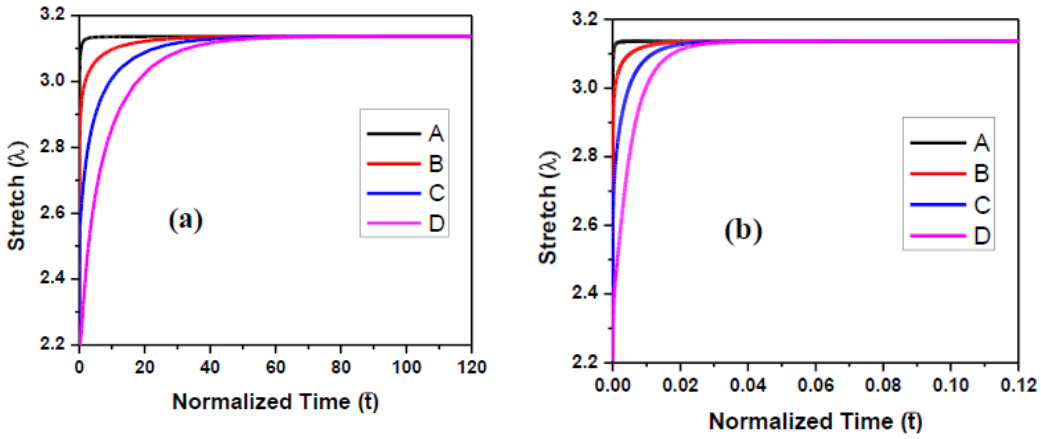

Figure 2-19: Stretches at the four chosen points as a function of time. (a) Method 1: treating heat transfer as an instantaneous process. (b) Method (2): treating diffusion as an instantaneous process

For both methods, it was evident that while the initial rates of swelling were different, the eventual uniform distribution of chemical potential and temperature would lead to homogenous swelling at all points. And the long term equilibrium stretch was consistent with the analytical solution calculated by equation (2.62). This verified that the final state of the transient analysis

would approach the theoretical equilibrium state. At the center of the cube, the time it would take to reach the long equilibrium stretch was expected to be the total time taken for the swelling process. It was observed that the total swelling time using method 1 (assuming heat transfer was instantaneous) was about 100 and 0.06 for method 2(assuming diffusion was instantaneous). The total diffusion time was about three orders slower than that of the heat transfer process. This showed that mass diffusion process is a much slower process as compared to heat transfer, thus verifying our assumption.

2.3. *pH*-sensitive hydrogels

Polymeric gels can undergo large deformation when subjected to an external solution of varying *pH*-values. It is imperative to understand the deformation process of pH-sensitive hydrogels for the effective application of this attractive material in the biomedical and microfluidic fields. In the modeling process of this multi-phase material, the finite element modeling is a useful tool for the development of future applications. It allows developers to test a wide variety of material responses in a cost-effective and efficient manner and reduces the need to conduct extensive laboratory experiments. Although a finite element user-defined material model is available for the equilibrium state, the transient response of the *pH*-sensitive gel has not been effectively modeled. Based on the work in Sections 2.1and 2.2, the transient swelling process of *pH*-sensitive hydrogel is being studied and a finite element model is further developed to simulate the transient phenomena. Some benchmark examples will be investigated to demonstrate the model's capabilities to simulate non-linear deformation kinetics present in several applications of *pH*-sensitive hydrogels.

In this section, we will study the transient swelling mechanism of a *pH*-sensitive hydrogel and extend the diffusion-heat transfer analogy developed in Section 2.1 to present a simulation model for predicting the dynamic response of a *pH*-sensitive hydrogel over time.

2.3.1. Theory of *pH*-sensitive gel

2.3.1.1. *Free energy function of a pH-sensitive gel*

Following the theory of constrained swelling of a *pH*-sensitive hydrogel developed by Marcombe et al. (2010), the total free energy of the *pH*-sensitive gel is assumed to be the sum of four free energies

$$W = W_{net} + W_{mix} + W_{ion} + W_{dis} \tag{2.63}$$

where the individual free energies are: the free energy due to mechanical stretching of polymer network, W_{net}; the free energy due to mixing of solvent and polymer network, W_{mix}; the free energy due to mixing of ions with polymer network, W_{ion}; and the free energy due to dissociation of acidic groups within the polymer network, W_{dis}.

As with the formulation of neutral and temperature sensitive hydrogels, we assume molecular incompressibility. For a *pH*-sensitive hydrogel, the assumption of molecular incompressibility consists of the volumes from the hydrogen ions $\left(H^+\right)$, co-ions $\left(-\right)$ and counter-ions, in addition to the volume of solvent molecules within neutral and temperature sensitive hydrogels. However, we assume that the volumes of the ions are insignificant compared to the solvent molecules and thus have no contribution towards the volume of the gel. This assumption is represented by the familiar equation

$$1+\nu C^s = \det \mathbf{F} \tag{2.64}$$

For implementation of the equilibrium swelling theory within Abaqus, a Legendre transformation was performed to reduce the thermodynamic equilibrium equation of the gel into the form as assumed by a hyperelastic solid.

The nominal stress s_{iK} that is present in the gel is the partial derivative of the Legendre transformed free energy function with respect to the deformation gradient, and is expressed explicitly as a function of crosslink density, N; temperature in the unit of energy, $k_B T$; internal and external ion concentrations, c^α and $\tilde{c}^\alpha$ respectively, where α represents the hydrogen ions H^+, co-ions $\left(-\right)$ and counter-ions $\left(+\right)$; and the Flory interaction parameter, χ. Using the

relationship between Cauchy stress and nominal stress, $\sigma_{ij} = s_{iK}F_{jK}/\det\mathbf{F}$, we obtain the Cauchy stress as

$$\sigma_{ij} = \frac{Nk_BT}{J}\left(F_{iK}F_{iK} - \delta_{ij}\right) - \left(\Pi_{sol} + \Pi_{ion}\right)\delta_{ij} \tag{2.65}$$

where $\Pi_{ion} = kT\left(c^{H^+} + c^+ + c^- - \tilde{c}^{H^+} - \tilde{c}^+ - \tilde{c}^-\right)$, $\Pi_{sol} = -\frac{kT}{v^s}\left[\ln\left(\frac{J-1}{J}\right) + \frac{1}{J} + \frac{\chi}{J^2}\right]$ and δ_{ij} represents the Kronecker delta function.

2.3.1.2. *Swelling kinetics of a pH-sensitive hydrogel*

The swelling kinetics of a polymeric gel is due to the migration of the ions and solvent molecules within and across the material boundary. Assuming the ion concentration to be significantly lower than the solvent concentration, the swelling of the gel can be taken to be purely driven by the migration of solvent molecules, i.e.

$$j_i = j_i^s + j_i^{H^+} + j_i^+ + j_i^- \approx j_i^s \tag{2.66}$$

where j_i denotes total diffusion flux; $j_i^{H^+}$ the diffusion flux of H^+ ions; j_i^+ the diffusion flux of counter-ions; j_i^- the diffusion flux of co-ions; and j_i^s the diffusion flux of solvent molecules. We assume that the migration of solvent molecules follows the chemical potential form of Fick's Law, which may be written in the form

$$\begin{aligned} j_i &= -\frac{c^s D}{k_B T}\frac{\partial \mu^s}{\partial x_i} \\ &= -\left[\left(\frac{J-1}{J}\right)D\frac{\partial \bar{\mu}^s}{\partial \theta}\right]\frac{\partial \theta}{\partial x_i} \end{aligned} \tag{2.67}$$

where $c^s = C^s/J$ represents the current solvent concentration; D represents the diffusion coefficient and θ represents *pH* of the gel.

The chemical potential of the solvent molecules, μ^s, is equivalent to an osmotic pressure which is expressed in the form

$$\mu^s = -k_B T \nu^s \left(\tilde{c}^{H^+} + \tilde{c}^{+} + \tilde{c}^{-} \right) \tag{2.68}$$

Combining equations (2.65) to (2.68) and making the flux to be proportional to the *pH*-gradient, the diffusion flux is then written in the form

$$j_i = -\left[-2\left(\frac{J-1}{J} \right) D \frac{\partial \left(\nu \bar{c}^{H^+} \right)}{\partial \theta} \right] \frac{\partial \theta}{\partial x_i} \tag{2.69}$$

Equation (2.69) describes the state of steady state diffusion. The time dependent governing equation for diffusion is obtained by the assumption of conservation of ions and solvent molecules. In the current state, without any internal ion/solvent source, the governing equation is written as

$$\int \frac{1}{\det \mathbf{F}} \frac{\partial \left(\nu C^s \right)}{\partial t} dv + \int \nu \, j_i ds = 0 \tag{2.70}$$

where νC^s is the sum of volume of all particles in the gel.

2.3.2. Numerical procedure for *pH*-sensitive hydrogel kinetics

Using the heat transfer-diffusion analogy elaborated in Section 2.1.2, we implemented the finite element model in a similar fashion, the equivalent material properties are derived as shown.

$$\rho = \frac{1}{J} \tag{2.71}$$

$$c_p = \left(\frac{\partial J}{\partial \nu \overline{c_H}} + \frac{\partial J}{\partial \nu c_H} \frac{\partial \nu c_H}{\partial \nu \overline{c_H}} \right) \Bigg/ \left(1 - \frac{\partial J}{\partial \nu c_H} \frac{\partial \nu c_H}{\partial J'} \right) \tag{2.72}$$

$$\begin{aligned} r &= \left(\frac{\partial J}{\partial \overline{\sigma}} \frac{d\overline{\sigma}}{dt} + \frac{\partial J}{\partial I} \frac{dI}{dt} \right) \Bigg/ \left(J \left(\frac{\partial J}{\partial c_H} \frac{\partial c_H}{\partial J'} - 1 \right) \right) \\ &\approx \left(\frac{\partial J}{\partial \overline{\sigma}} \frac{\Delta\overline{\sigma}}{\Delta t} + \frac{\partial J}{\partial I} \frac{\Delta I}{\Delta t} \right) \Bigg/ \left(J \left(\frac{\partial J}{\partial c_H} \frac{\partial c_H}{\partial J'} - 1 \right) \right) \end{aligned} \tag{2.73}$$

$$k = D \left(2\nu c + \frac{\partial c_H}{\partial \overline{c_H}} + \frac{\partial c_+}{\partial \overline{c_H}} + \frac{\partial c_-}{\partial \overline{c_H}} \right) \tag{2.74}$$

where the partial derivatives are defined in equations (2.75) to (2.84).

$$\frac{\partial J}{\partial \overline{\sigma}} = \frac{1}{3\xi_1} \tag{2.75}$$

$$\frac{\partial J}{\partial \overline{I}} = -\frac{N\nu}{3} \frac{J^{-1/3}}{\xi_1} \tag{2.76}$$

$$\frac{\partial J}{\partial \nu \overline{c_H}} = \frac{1}{\xi_1} \left(-\frac{\nu \overline{c_+} \nu c_H}{\left(\nu \overline{c_H} \right)^2} + \frac{2\nu \overline{c_H} + \nu \overline{c_+}}{\nu c_H} - 2 \right) \tag{2.77}$$

$$\frac{\partial J}{\partial \nu \overline{c_+}} = \frac{1}{\xi_1} \left(\frac{\nu c_H}{\nu \overline{c_H}} + \frac{\nu \overline{c_H}}{\nu c_H} - 2 \right) \tag{2.78}$$

$$\frac{\partial J}{\partial \nu c_H} = \frac{1}{\xi_1} \left(1 + \frac{\nu \overline{c_+}}{\nu \overline{c_H}} - \frac{\nu \overline{c_-} \nu \overline{c_H}}{\left(\nu c_H \right)^2} \right) \tag{2.79}$$

$$\frac{\partial \alpha}{\partial \nu \overline{c_H}} = \left[-\frac{1}{\left(J - 1 \right)^2} + \frac{1}{J^2} + \frac{2}{J^3} + \frac{6\chi}{J^4} + N\nu \left(\frac{-2}{J^3} + \frac{4}{27} \overline{I}_1 J^{-4/3} \right) \right] \frac{\partial J}{\partial \nu \overline{c_H}} \tag{2.80}$$

$$\frac{\partial \nu c_H}{\partial J'} = -\frac{NK\nu f / J'^2}{\xi_2} \tag{2.81}$$

$$\frac{\partial \nu c_H}{\partial \overline{\nu c_H}} = \frac{1}{\xi_2}\left[\frac{\overline{\nu c_+}\left(\nu c_H\right)^3}{\left(\overline{\nu c_H}\right)^2} + \left(2\overline{\nu c_H} + \overline{\nu c_+}\right)\left(\nu c_H + NK\nu\right)\right] \tag{2.82}$$

$$\frac{\partial \nu c_+}{\partial \overline{\nu c_H}} = \frac{\partial \nu c_H}{\partial \overline{\nu c_H}}\frac{\overline{\nu c_+}}{\overline{\nu c_H}} - \frac{\nu c_H \overline{\nu c_+}}{\left(\overline{\nu c_H}\right)^2} \tag{2.83}$$

$$\frac{\partial \nu c_-}{\partial \overline{\nu c_H}} = -\frac{\partial \nu c_H}{\partial \overline{\nu c_H}}\frac{\overline{\nu c_H}\,\overline{\nu c_-}}{\left(\nu c_H\right)^2} + \frac{2\overline{\nu c_H} + \overline{\nu c_+}}{\nu c_H} \tag{2.84}$$

where the terms ξ_1 and ξ_2 are $\xi_1 = \left[\frac{1}{J-1} - \frac{1}{J} - \frac{1}{J^2} - \frac{2\chi}{J^3} + N\nu\left(-\frac{\bar{I}_1}{9J^{4/3}} + \frac{1}{J^2}\right)\right]$,

$$\xi_2 = \left[3\left(\nu c_H\right)^2\left(1 + \frac{\overline{\nu c_+}}{\overline{\nu c_H}}\right) + 2\nu c_H NK\nu\left(1 + \frac{\overline{\nu c_+}}{\overline{\nu c_H}}\right) - \left(\frac{NK\nu f}{J'} + \left(\overline{\nu c_H}\right)^2 + \overline{\nu c_H}\,\overline{\nu c_+}\right)\right].$$

2.3.3. Numerical examples for *pH*-sensitive hydrogel kinetics

With recent developments in utilizing *pH*-sensitive hydrogels, there exists a need to simulate and predict how the gel would respond in actual operations. The following two examples attempt to simulate transient gel swelling behavior in two typical applications of *pH*-sensitive gels, which include a microfluidic device and a bi-layer cantilever beam.

2.3.3.1. *Gel pillar in flow control*

One application of hydrogels is in the area of microfluidics (Moore et al., 2000), where fluid flow is controlled by the volumetric change of the gel, as swelling in the gel would cause restriction in the fluid passage. At a certain

point, the swelling gel will come into contact with the wall of the valve, thus stopping flow through the valve completely.

Current studies on simulating *pH*-sensitive gel microfluidic valves are focused on the equilibrium state of inhomogeneous swelling of the gel (He et al., 2012; Zhang et al., 2012), and thus do not consider how the gel changes with the evolution of time during the entire process of swelling.

Using the material model developed in this work, we were able to simulate this transient swelling process and observe how the gel deforms as well as visualize the stress distribution upon contact with a hard surface.

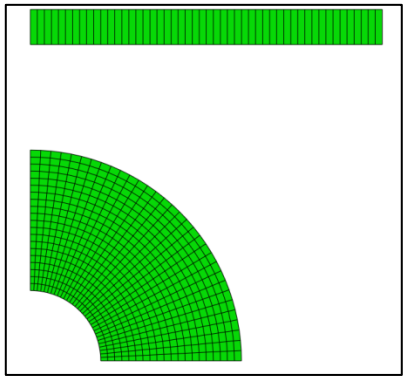

Figure 2-20: Reduced 2d plane strain model

The simulation considered a cylindrical gel pillar in close proximity with a pair of flat parallel valve walls. To reduce the simulation time, several geometrical simplifications were made to the model. Firstly, we assumed a large aspect ratio (L/D) and reduced the 3D model into a 2D plane strain model (Figure 2-20). Secondly, due to mirror symmetry in the cross sectional view of the model, a quarter model was sufficient to represent the entire structure. Parameters used were an outer radius of 0.3 mm, inner radius of 0.1 mm, and a diffusion coefficient of $D = 8\times10^{-10}\ \mathrm{m^2 s^{-1}}$. 640 4-node bilinear displacement and temperature plane strain elements (CPE4T) were used to mesh the cylindrical portion while 50 4-node bilinear plane strain elements

(CPE4) were used to mesh the rigid valve wall. The gel, initially at *pH*=3, was fixed at the inner surface and exposed to a *pH* value of 6 on the outer surface.

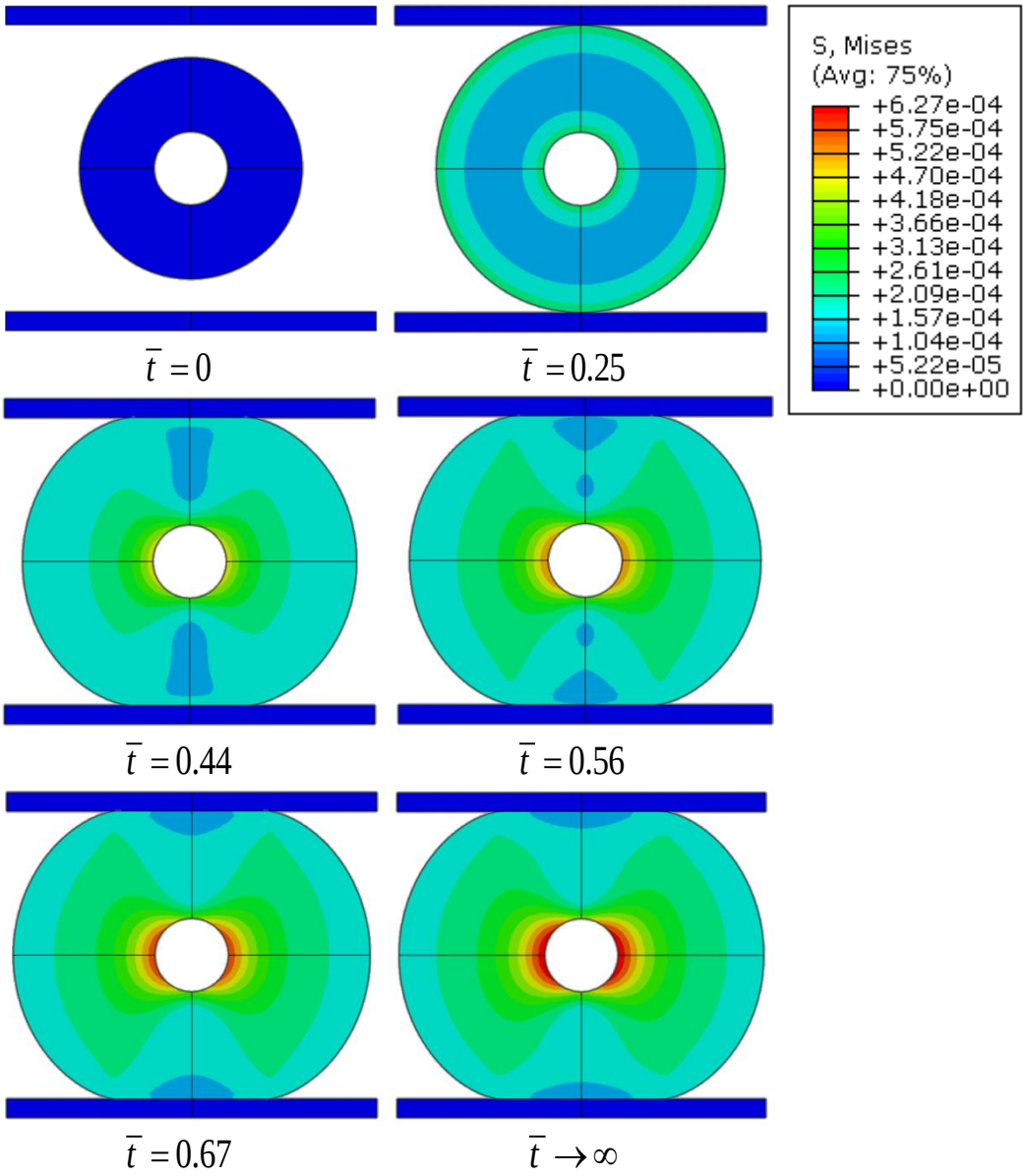

Figure 2-21: Mises stress distribution of the gel at various non-dimensionalized times

With the kinetics model, we were able to predict stress distributions of the gel at various stages of the swelling and thus prevent gel material failure. Figure 2-21 shows the stress distribution of the gel at various non-dimensionalized

times $\bar{t}$, where L is the characteristic length of the gel, which is essentially the outer diameter.

2.3.3.2. *Bi-layer cantilever beam*

In applications for sensing, a hydrogel is often bounded to a substrate which does not swell in the presence of an external solvent. When exposed to the external stimuli, the hydrogel will undergo deformation and the mismatch in swelling ratios of the gel and substrate will result in differential swelling. This differential swelling is useful in sensor applications by measuring the extent of bending in the structure (Bashir et al., 2002; Kwon et al., 2010).

In this example, we explored a *pH*-sensor with a simple geometry of two equally sized strips, one made of *pH*-sensitive gel and the other an elastic substrate, both fixed at one end of the structure. 1000 4-node bilinear displacement and temperature plane strain CPE4T elements were used to mesh the gel while 1000 4-node bilinear plane strain elements (CPE4) were used to mesh the elastic substrate. The initial condition of the gel was set to be at $pH = 5$ as this allowed both swelling and deswelling of the gel. When exposed to an acidic solvent of $pH = 2$, the gel would deswell and the structure would bend towards the direction of the side of the gel. Conversely, when exposed to an alkaline solvent of $pH = 8$, the gel would swell and the structure would bend towards the direction of the side of the substrate. It is this ability to bend in both directions and to different extents that makes the structure useful for actuation and sensing. Figure 2-22 shows the deformation of the bi-layer cantilever beam.

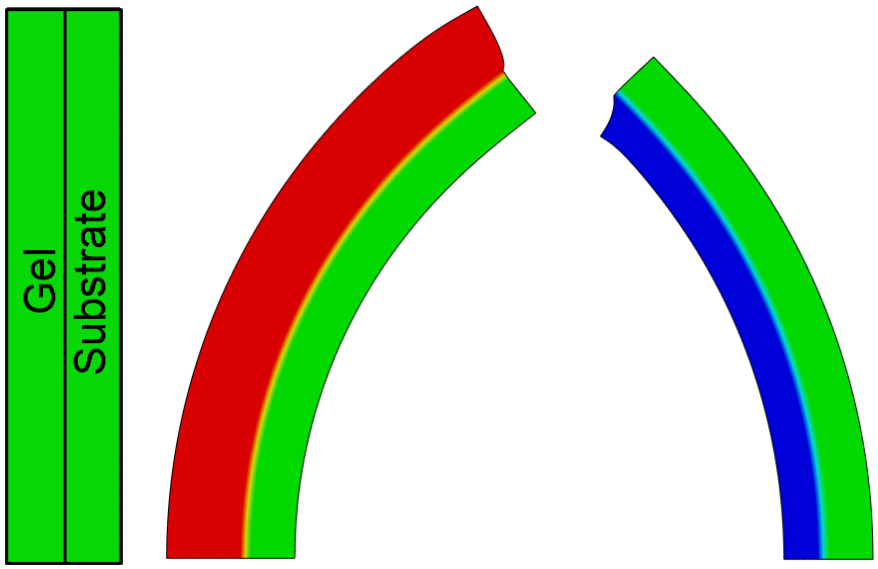

(a) (b) (c)

Figure 2-22: (a) beam originally in equilibrium at *pH*=5, (b) beam exposed to solvent of *pH*=8, (c) beam exposed to solvent of *pH*=2

The graphs in Figure 2-23 show the change in lateral displacement of the corner nodes in which deflection occurs. It is interesting to note that the swelling process takes a much longer time than the deswelling process. Thus, the swelling process will take a much longer time to reach equilibrium position.

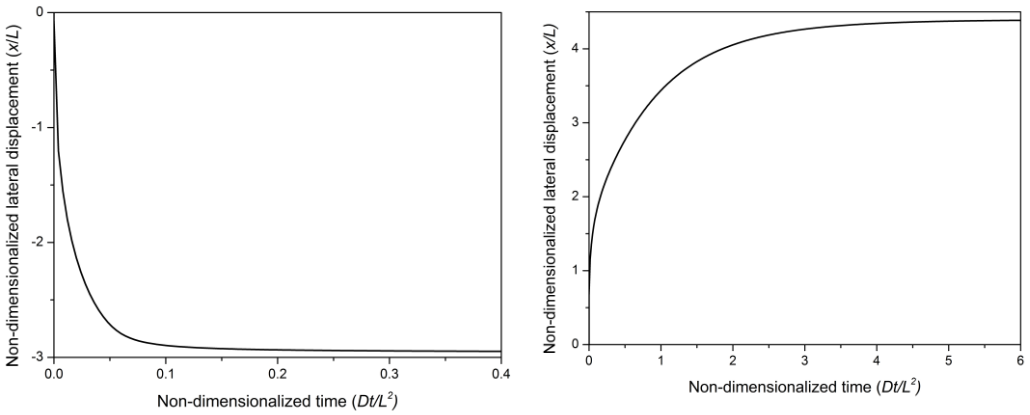

(a) (b)

Figure 2-23: Lateral displacement of top right node for changes in *pH* from (a) 5 to 8, (b) 5 to 2.

2.4. Concluding remarks

The transient swelling kinetics of hydrogels was investigated in this chapter. A novel method of simulating swelling kinetics through finite element software Abaqus was introduced. Implementation of this method exploited the similarity between governing equations of heat transfer and diffusion kinetics and made use of readily available coupled temperature-displacement elements offered by Abaqus. Non-linear hyperelastic gel theory was used together with coupled temperature-displacement analysis to study the transient swelling response of polymeric gels by representing chemical potential as a temperature field. Equivalent terms for making the thermal-diffusion analogy were derived by comparison of the governing equations. This analogy is useful not just for polymeric gels, but can also be applied to other diffusion driven mechanical processes. The model had been implemented for simulation of neutral, temperature-sensitive and *pH*-sensitive hydrogels.

In neutral gels, we had studied the inhomogeneous nature of the swelling process through several numerical examples, including a free swelling cube, one-dimensional constrained swelling and rectangular block attached to a rigid substrate. Non-dimensionalization had allowed for the upscaling or downscaling of the modeling subject, thus reducing possible numerical errors.

The deformation kinetics of temperature-sensitive hydrogel was more complicated compared with normal polymeric gels as it involved heat transfer process in addition to chains stretching and diffusion of solvent molecules. This had restricted us from directly simulating the transient behavior by utilizing the analogy between heat transfer and diffusion. However, the assumption that heat transfer is a much faster process as compared to diffusion, such that heat transfer could be treated as an instantaneous process, had greatly simplified the problem. Using the available physical parameters, we had validated this assumption. Several numerical examples including surface

creasing, bifurcation and buckling of swelling gels were presented to illustrate the applications of our methods in explaining experimental observations.

The heat transfer-diffusion analogy method was further extended to study the transient swelling response of *pH*-sensitive hydrogels by representing *pH*-value as a temperature field. The kinetics of *pH*-sensitive gel swelling was investigated with numerical examples of a gel cylinder in contact with a hard surface and a bi-layer cantilever beam.

Using this method of implementation, we had greatly reduced the efforts required for development of finite element models, eliminating the need for discretization of constitutive equations into forms required for various element types. In fact, this method offers much more versatility as compared to simulation models developed using user-defined elements. This is as the subroutine developed using this method can be readily adapted for any element types, such as 2D or 3D elements, without any need to perform additional discretizations for different element types. With this analogical finite element model, we hope to provide more insight on the transient swelling phenomena using earlier established models in an easy-to-implement model.

Lastly, it is to be noted that the method proposed in this Section was to allow for the reduction of time and effort required to develop a fully working material model for the simulation of gel swelling kinetics. Therefore, although the finite element method was used, there is no need for a formal finite element formulation, which is a necessary component if the UEL subroutine were to be employed instead. However, a formulation for the finite element procedure has been included in the Appendix for completeness. Interested readers may also refer to literature works involving UEL subroutine, as mentioned in Section 1.1.4.1.

3. Inhomogeneous deformation of responsive hydrogels

In this chapter, we will investigate the mechanics of large deformation of temperature-sensitive hydrogels, photo-thermal sensitive hydrogels and magneto-thermal sensitive hydrogels. The phase transition and their dependence on environmental factors will be investigated through the development of continuum thermodynamic equilibrium theories. Finite element models using subroutines UHYPER and UMAT of Abaqus will be developed based on governing equations and specialized free energy functions to simulate behavior of these gels.

The governing equations and equilibrium conditions of an isothermal process under arbitrary mechanical and chemical conditions will be derived via a variational approach. After adopting an explicit free energy density function, we will derive and discuss the constitutive equations and chemical potential of solvent molecular within the gel. Based on the theory, numerical procedures for the finite element simulation of several types of hydrogels will also be developed. Numerical examples will then be presented to exhibit the capability of the numerical procedures.

3.1. Temperature sensitive hydrogel

The temperature sensitive hydrogel is a very common gel material and it has been widely studied in literature. In this section, we formulate a field theory for the inhomogeneous large deformation of temperature sensitive hydrogels.

3.1.1. Equilibrium swelling theory of temperature sensitive hydrogels

We adopt a variational approach in deriving the governing equations and equilibrium conditions when a gel undergoes isothermal inhomogeneous large deformation. A similar variational approach was proposed by Kang and Huang (Kang and Huang, 2010c) for neutral hydrogels.

Consider a hydrogel body (reference state) of volume V_0 enclosed by a surface S_0 as shown in Figure 3-1. When the hydrogel is immersed in a solvent of chemical potential μ^s, solvent molecules can enter or leave the polymeric gel across the surface S. In the system, the gel is subject to a body force b_i and surface traction t_i. In addition, the surface S may be mechanically constrained or chemically isolated from the solvent. As with earlier sections, we defined the state of deformation using the deformation gradient $\mathbf{F}$.

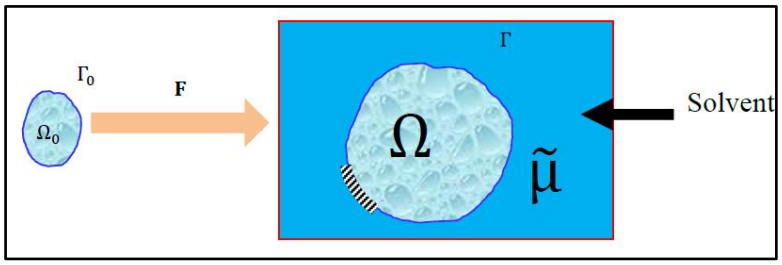

Figure 3-1: A dry polymeric gel in reference state is placed in contact with a solvent and deforms into the current state.

To obtain the equilibrium condition, consider an infinitesimal process. In a short time δt, the displacement field in the reference coordinate is denoted by

$\delta\mathbf{x}(\mathbf{X})$ and the work done δW_{ext} by the environment in the reference coordinates is expressed as:

$$\delta W_{ext} = \int B_i \delta x_i dV + \int T_i \delta x_i dS + \int \mu^s \delta C^s dV \tag{3.1}$$

where C^s is the nominal concentration of the solvent molecular, dV , dS are the differential volume and area in the reference coordinate.

Assume a general form of the nominal free energy density function $W(\mathbf{F}, C^s)$ at a certain temperature. The variation of energy of the hydrogel, δU is

$$\delta U = \int \delta W dV = \int \frac{\partial W}{\partial F_{iK}} \delta F_{iK} dV + \int \frac{\partial W}{\partial C^s} \delta C^s dV \tag{3.2}$$

Using integrating by parts to evaluate the first term, we get

$$\delta U = \int \frac{\partial}{\partial X_K} (\frac{\partial W}{\partial F_{iK}} \delta x_i) dV - \int \frac{\partial}{\partial X_K} (\frac{\partial W}{\partial F_{iK}}) \delta x_i dV + \int \frac{\partial W}{\partial C} \delta C dV \tag{3.3}$$

Applying divergence theorem to the first term of equation (3.3), we get

$$\delta U = \int \frac{\partial W}{\partial F_{iK}} N_K \delta x_i dS - \int \frac{\partial}{\partial X_K} (\frac{\partial W}{\partial F_{iK}}) \delta x_i dV + \int \frac{\partial W}{\partial C} \delta C dV \tag{3.4}$$

The principle of virtual work requires that

$$\delta U = \delta W_{ext} \tag{3.5}$$

Substituting equations (3.1) and (3.4) into equation (3.5) yields

$$\int \left(\frac{\partial W}{\partial F_{iK}} N_K - T_i \right) \delta x_i dS - \int \left(\frac{\partial}{\partial X_K} \frac{\partial W}{\partial F_{iK}} + B_i \right) \delta x_i dV + \int \left(\frac{\partial W}{\partial C} - \mu^s \right) \delta C^s dV = 0 \tag{3.6}$$

Equation (3.6) holds for arbitrary changes δx_i and δC^s and so the quantity in each pair of parentheses vanishes. Thus we get the following equilibrium conditions

$$\frac{\partial}{\partial X_K}\frac{\partial W}{\partial F_{iK}} + B_i = 0 \text{ in } V_0 \tag{3.7}$$

$$\frac{\partial W}{\partial C^s} - \mu^s = 0 \quad \text{in } V_0 \tag{3.8}$$

$$\frac{\partial W}{\partial F_{iK}} N_K - T_i = 0 \text{ on } S_0 \tag{3.9}$$

The nominal stress s_{iK} may be defined as the work conjugate of the deformation gradient, i.e.

$$s_{iK} = \frac{\partial W}{\partial F_{iK}} \tag{3.10}$$

In such case, equations (3.7) and (3.9) can be interpreted as the conditions for mechanical equilibrium. It can be observed from equation (3.8) that the chemical potential of solvent molecular inside gel μ^s can be defined as the work conjugate of the solvent concentration, i.e.

$$\mu^s = \frac{\partial W}{\partial C^s} \tag{3.11}$$

Equation (3.11) stipulates that the chemical potential of solvent with the gel is homogenous and equal to the chemical potential of the external solvent during the equilibrium state.

3.1.1.1. *Free Energy Model*

Based on the work of Cai and Suo (2011), the field theory of temperature-sensitive hydrogels has been formulated further. Since the crosslink density is typically very low, we assumed that the crosslink density negligibly affects the interaction between the monomers and the solvent molecules. Hence the Helmholtz Free energy of the hydrogel was considered to be contributed from the stretching of the network and the mixing of the polymer and the solvent independently. Tthe free energy density of gel could thus be written as:

$$W = W_{net}(\mathbf{F}) + W_{mix}(C^s, T) \tag{3.12}$$

where W_{net} is the energy due to the stretching of network and W_{mix} is the energy due to the mixing of the polymers and the solvent.

We imposed the molecular incompressibility constraint (Section 2.1.1.4) in the gel and enforced this constraint by adding a Lagrange multiplier term $\Pi\left[1 + vC^s - \det(\mathbf{F})\right]$ to the free energy density function. Thus the free energy density W has the form:

$$W = W_{net}(\mathbf{F}) + W_{mix}(C^s, T) + \Pi\left[1 + vC^s - \det(\mathbf{F})\right] \tag{3.13}$$

A general expression for Π can be obtained by substituting equation (3.13) into equation (3.11), giving

$$\Pi = \frac{1}{v}\left(\mu - \frac{\partial W_{mix}}{\partial C^s}\right) \tag{3.14}$$

The expression obtained here is consistent with the work of Hong et al. (2009a), Cai and Suo (2012) and Li et al. (2012b).

3.1.1.2. *Specialization of free energy function*

As with Section 2.2.1.1, we take the free energy due to the stretching of a network of polymer

$$W_{net}(\mathbf{F}) = \frac{1}{2} N k_B T \left[F_{ik} F_{ik} - 3 - 2\ln(\det \mathbf{F}) \right] \tag{3.15}$$

and free energy of mixing of the long polymer with the solvent to be

$$W_{mix}(C^s, T) = k_B T \left[C \ln\left(\frac{\nu C^s}{1+\nu C^s} \right) + \frac{\chi C^s}{1+\nu C^s} \right] \tag{3.16}$$

with the parameter χ given by

$$\chi(T, \phi) = \chi_0 + \chi_1 \phi \tag{3.17}$$

where $\chi_0 = A_0 + B_0 T$, $\chi_1 = A_1 + B_1 T$ and $\phi = 1 \Big/ \left(1+\nu C^s\right)$, ϕ is the volume fraction of the polymer in the hydrogel. The values of A_0 , B_0 , A_1 and B_1 vary for different monomers.

For a temperature-sensitive gel, the exact form of Π can be obtained by substituting equation (3.16) into equation (3.14) to give

$$\Pi = \frac{k_B T}{\nu} \left[\frac{\mu}{k_B T} - \ln\left(\frac{\nu C^s}{1+\nu C^s} \right) - \frac{1}{1+\nu C^s} - \frac{\chi_0}{\left(1+\nu C^s\right)^2} - \frac{\left(1-\nu C^s\right)\chi_1}{\left(1+\nu C^s\right)^3} \right] \tag{3.18}$$

Invoking the incompressibility constraint, given in equation (2.13), to eliminate C^s , equation (3.18) is converted to

$$\Pi = \frac{k_B T}{\nu} \left[\frac{\mu}{k_B T} - \ln\left(\frac{J-1}{J} \right) - \frac{1}{J} - \frac{\chi_0 - \chi_1}{J^2} - \frac{2\chi_1}{J^3} \right] \tag{3.19}$$

where $J = \det(\mathbf{F})$ is the swelling ratio of the gel.

The nominal stress is obtained by substituting equation (3.13) into (3.10) to give

$$s_{ik} = \frac{\partial W_{net}}{\partial F_{ik}} - \Pi J H_{ik} = N k_B T (F_{ik} - H_{ik}) - \Pi J H_{ik} \tag{3.20}$$

Note that we have used the mathematical relation $\partial J / \partial F_{ik} = J H_{ik}$ in order to derive equation (3.20), where $\mathbf{H}$ is the transpose of $\mathbf{F}^{-1}$.

The true stress can be obtained through the relation

$$J \sigma_{ij} = s_{ik} F_{jk} \tag{3.21}$$

By substituting equation (3.20) into equation (3.21), we obtain

$$\sigma_{ij} = \frac{N k_B T}{J} (F_{ik} F_{jk} - \delta_{ij}) - \Pi \delta_{ij} \tag{3.22}$$

By substituting equation (3.19) into equation (3.22), the true stress is expressed as,

$$\sigma_{ij} = \frac{N k_B T}{J} (F_{ik} F_{jk} - \delta_{ij}) + \frac{k_B T}{\nu} \left[\ln\left(\frac{J-1}{J} \right) + \frac{1}{J} + \frac{\chi_0 - \chi_1}{J^2} + \frac{2\chi_1}{J^3} - \frac{\mu^s}{\nu} \right] \delta_{ij} \tag{3.23}$$

Equation (3.23) relates the true stress to the deformation gradient. Rewriting equation (3.23), a general expression for the chemical potential for water molecules inside gel is obtained as

$$\mu^s = \frac{N k_B T \nu}{3J} (I_1 - 3) + k_B T \left[\ln\left(\frac{J-1}{J} \right) + \frac{1}{J} + \frac{\chi_0 - \chi_1}{J^2} + \frac{2\chi_1}{J^3} \right] - \frac{(\sigma_1 + \sigma_2 + \sigma_3)\nu}{3} \tag{3.24}$$

where $I_1 = F_{ik} F_{ik}$ is the invariant of the deformation gradient.

3.1.2. Numerical procedure for equilibrium swelling of temperature sensitive hydrogels

It can be seen from equation (3.15) that when $J=1$, the free energy density is singular. This singularity could be remedied by choosing any reference state with $J>1$ (Hong et al., 2009a). In our previous study on temperature-sensitive hydrogels (Ding et al., 2013), an isotropic swelling state is chosen as the initial state. As a result, it cannot be used to study the deformation with an anisotropic initial state. In the present study, we chose an initial state with a deformation gradient in the form of:

$$\mathbf{F_0}=\begin{bmatrix}\lambda_{0,1} & 0 & 0\\ 0 & \lambda_{0,2} & 0\\ 0 & 0 & \lambda_{0,3}\end{bmatrix} \tag{3.25}$$

Let $\mathbf{F}'$ be the deformation gradient relative to the chosen reference state, then the deformation gradient $\mathbf{F}$ is given as follows:

$$\mathbf{F}=\mathbf{F}'\mathbf{F_0} \tag{3.26}$$

In present study, we used commercial software Abaqus subroutines to implement our derivation. There are two options offered by Abaqus to specify the nonlinear constitutive behavior of a hydrogel as user-defined materials, i.e. subroutines UHYPER and UMAT. The former (UHYPER) has been successfully implemented (Ding et al., 2013). However, UHYPER has a restriction - the initial state has to be isotropic, i.e. the initial stretch of the gel in all 3 directions must be equal, $\lambda_{1,0}=\lambda_{2,0}=\lambda_{3,0}=\lambda_0$. This is because UHYPER calculations are based on the invariants of the deformation gradient (i.e. I_1, I_2 and J) rather than actual components of the deformation gradient. This may pose problems in specific cases where the gel is not initially isotropic, such as the case when the gel is given a pre-stretch in 1 of the directions. To circumvent this limitation, we implemented our current FEM using UMAT. Since the true

stress had been derived explicitly in equation (3.23),we only need to derive the fourth order tangent modulus tensor **C**. The tangent modulus can be defined through the variation in the Kirchhoff stress

$$\delta(J\sigma_{ij}) = JC_{ijkl}\delta D_{kl} + J(\sigma_{kj}\delta W_{ik} - \sigma_{ik}\delta W_{kj}) \tag{3.27}$$

where the tensor $\delta\mathbf{D}$ and $\delta\mathbf{W}$ are the virtual rate of deformation and virtual spin tensor respectively, defined as:

$$\delta\mathbf{D} = sym(\delta\mathbf{F} \bullet \mathbf{F}^{-1}) \tag{3.28}$$

$$\delta\mathbf{W} = asym(\delta\mathbf{F} \bullet \mathbf{F}^{-1}) \tag{3.29}$$

By using equation (3.23), the variation of the Kirchhoff stress is calculated as follows

$$\delta(J\sigma_{ij}) = Nk_BT\left\{\frac{\delta_{ij}}{N\nu}\xi + \frac{2}{3}J^{-\frac{1}{3}}\delta J + J^{\frac{2}{3}}\delta\tilde{B}_{ij}\right\} \tag{3.30}$$

where $\xi = -\frac{\mu^s}{k_BT} + \frac{1}{J-1} + \ln\left(\frac{J-1}{J}\right) - \frac{4(A_1 + B_1T)}{J^3} + \frac{(A_0 - A_1) + (B_0 - B_1)T}{J^2}$.

It can be shown mathematically that

$$\delta J = J\delta D_{kk} \tag{3.31}$$

$$\delta\tilde{B}_{ij} = T_{ijkl}(\delta D_{kl} - \frac{\delta_{kl}}{3}\delta D_{kk}) + \tilde{B}_{kj}\delta W_{ik} - \tilde{B}_{ik}\delta W_{kj} \tag{3.32}$$

where the fourth order tensor **T** is defined as,

$$T_{ijkl} = \frac{1}{2}\left(\tilde{B}_{jl}\delta_{ik} + \tilde{B}_{ik}\delta_{jl} + \tilde{B}_{jk}\delta_{il} + \tilde{B}_{il}\delta_{jl}\right) \tag{3.33}$$

By substituting equations (3.31) and (3.32) into equation (3.30), an explicit expression for the tangent modulus tensor at the current state is obtained as:

$$C_{ijkl} = Nk_BT\left[J^{-\frac{1}{3}}T_{ijkl} + \frac{\xi}{N\nu}\delta_{ij}\delta_{kl} \right] \tag{3.34}$$

Using Equation (3.23) and Equation (3.34) for the true stress and tangent modulus respectively, a user subroutine was coded in the format of the UMAT in Abaqus.

The free energy density function introduces five material parameters namely, A_0, A_1, B_0, B_1 and $N\nu$, where $N\nu$ is a dimensionless measure of the polymer crosslink density in the dry network. The values of A_0, A_1, B_0 and B_1 depend on the type of monomer. The values of these parameters for poly(N-isopropyl acrylamide) (PNIPAM) are readily provided by Afroze et al. (2000) in Table 2-2.

We had adopted the above properties of PNIPAM gels and set $N\nu$=0.01 in the examples presented herein. To fully define the material in the subroutine, we would also need to provide the initial temperature T_0 the initial chemical potential of the external solution μ_0^s and the corresponding swelling ratios λ_1, λ_2, λ_3 in x, y, z directions respectively. As an equilibrium state, these values need to satisfy Equation (3.23).

3.1.3. Numerical Examples for equilibrium swelling of temperature sensitive hydrogels

To verify the correctness of the developed finite element method and highlight the advantage of UMAT over UHYPER, several numerical examples are provided in this section. It has to be noted that for the numerical examples presented henceforth, it is possible to use a single element to simulate the

swelling of the gel due to homogeneity, as noted by Hong et al. (2009a). Therefore no mesh convergence tests were conducted.

3.1.3.1. *Free Swelling*

The analytical solution may be obtained by searching the value of J at which the free energy functions is minimized at a certain temperature T. It can also be derived analytically. In the free swelling process, the chemical potential for water molecules given by equation (3.24) may be simplified as

$$\mu^s = \frac{Nk_BT\nu}{J}(J^{\frac{2}{3}} - 1) + k_BT\left[\ln\left(\frac{J-1}{J}\right) + \frac{1}{J} + \frac{\chi_0 - \chi_1}{J^2} + \frac{2\chi_1}{J^3}\right] \qquad (3.35)$$

By using the equilibrium conditions given by equation (3.23) and the fact that the chemical potential of water $\mu^s = 0$, the analytical solution may be written as:

$$\frac{NkT\nu}{3J}(J^{\frac{2}{3}} - 3) + kT\left[\ln\left(\frac{J-1}{J}\right) + \frac{1}{J} + \frac{\chi_0 - \chi_1}{J^2} + \frac{2\chi_1}{J^3}\right] = 0 \qquad (3.36)$$

The numerical solutions obtained using UHYPER and UMAT are also plotted as shown in Figure 3-2. In this problem we had chosen a value $N\nu = 0.01$. For verification purpose, the experimental data collected by (Oh et al., 1998) is also plotted. As shown in the figure, the numerical results using UMAT were in good agreement with the analytical solutions, the numerical results using UHYPER and the experimental data. It should be noted that for a discontinuous phase transition, FEM is unable to overcome the turning points. To obtain both parts of the phase transition curve, we employed the method proposed by Ding et al. (2013), which is to start simulation from both ends, which terminate at points A and B.

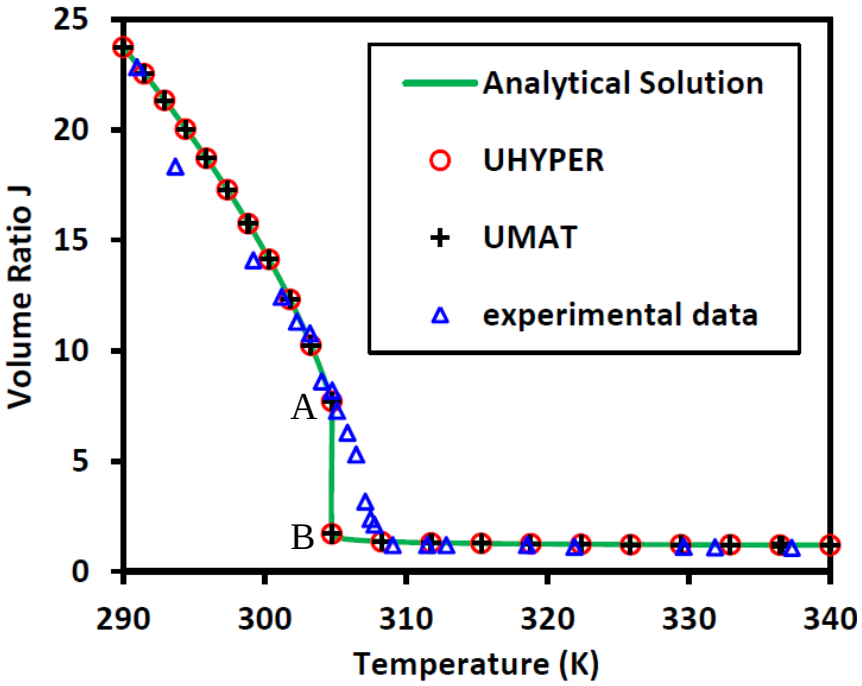

Figure 3-2: Volume of free-swelling hydrogel as a function of temperature. The triangles represent experimental results presented in (Oh et al., 1998)

3.1.3.2. *Uniaxial Constraint*

Deformation under a uniaxial constraint means that the swelling gel is fixed vertically and free to swell in the other two directions. In this case, the lateral stretches are the same, while the longitudinal stretch in the third direction is constant. i.e. $\lambda_1 = \lambda_2 = \lambda$, $\lambda_3 = \lambda_0$. Thus $J = \lambda^2 \lambda_0$ and $I = 2J/\lambda_0 + {\lambda_0}^2$.

To illustrate the constraints of UHYPER, we considered two cases i.e. $\lambda_0 = 1$ and $\lambda_0 = 2$. Uniaxial constrained swelling induces stress in the longitudinal direction, while lateral stresses are zero. Using equation (3.24), and the condition $\sigma_1 = \sigma_2 = 0$, the parameter to define the initial state needs to satisfy the following equation.

$$\frac{Nk_BT_0}{{\lambda_1}^2\lambda_0}({\lambda_1}^2 - 1) + \frac{k_BT_0}{\nu}\xi - \frac{\mu^s}{\nu} = 0 \tag{3.37}$$

where $\xi = \ln\left(\frac{\lambda_1^2\lambda_0 - 1}{\lambda_1^2\lambda_0}\right) + \frac{1}{\lambda_1^2\lambda_0} + \frac{\chi_0 - \chi_1}{\left(\lambda_1^2\lambda_0\right)^2} + \frac{2\chi_1}{\left(\lambda_1^2\lambda_0\right)^3}$.

The analytical solution may also be derived by using the fact that the chemical potential of water $\mu^s = 0$,

$$\frac{N\nu}{\lambda_1^2\lambda_0}(\lambda_1^2 - 1) + \xi = 0 \tag{3.38}$$

Alternatively, the analytical solution could also be obtained by searching the value of J at which the global minimum of the free energy functions is achieved at a certain temperature T. The numerical calculations obtained using UHYPER and UMAT are also plotted in Figure 3-3 together with the analytical solution. As seen from Figure 3-3(a), UHYPER is only applicable to the process below the phase transition temperature in the case $\lambda_0 = 2$ and is not applicable at all for the case $\lambda_0 = 1$. As mentioned previously, this is due to the fact that the reference state for UHYPER has to be isotropic swelling. When $\lambda_0 = 1$ is fixed, the corresponding isotropic swelling state is the dry state and $J = 1$, which would encounter singularity in the calculation of free energy density. When $\lambda_0 = 2$, there is no isotropic state at a temperature higher than the phase transition temperature. Thus UHYPER is not applicable.

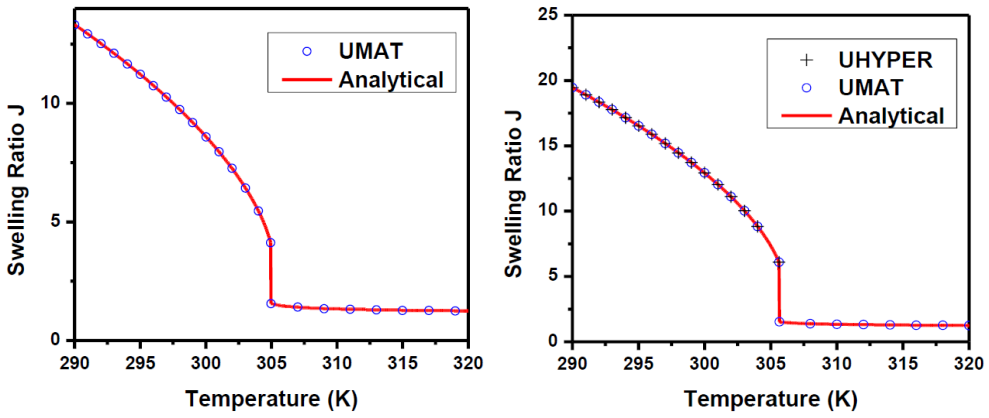

Figure 3-3: Volume of the uniaxial constrained swelling hydrogel as a function of temperature. (a) Fixed stretch in longitudinal direction $\lambda_0 = 1$; (b) Fixed stretch in longitudinal direction $\lambda_0 = 2$. UHYPER is only applicable in the case $\lambda_0 = 2$ and is not applicable at all for the case $\lambda_0 = 1$.

It is obvious that the only non-zero true stress during the uniaxial deformation process is the normal stress in the third direction σ_{33}. In the uniaxial deformation process, Eq. (26) may be written as:

$$\sigma_1 = \sigma_2 = \frac{Nk_BT}{\lambda_0\lambda_1^{\,2}}(\lambda_1^{\,2} - 1) - \Pi \tag{3.39}$$

$$\sigma_3 = \frac{Nk_BT}{\lambda_0\lambda_1^{\,2}}(\lambda_0^{\,2} - 1) - \Pi \tag{3.40}$$

Using condition $\sigma_1 = \sigma_2 = 0$ to eliminate Π , we obtain

$$\sigma_3 = \frac{Nk_BT}{\lambda_0\lambda_1^{\,2}}(\lambda_0^{\,2} - \lambda_1^{\,2}) \tag{3.41}$$

which gives the true stress as a function of temperature T and stretch λ_1. Equation (3.41) could be used to verify the correctness of the stress obtained using our method. Either by using the analytical solution given by equation (3.38), or directly using the numerical obtained from the output of Abaqus, we would be able to get the value for λ_1 at any temperature T, and to substitute these values into equation (3.41) to evaluate stress. Also, we could read the stress at any temperature from the numerical simulation. The stress during the uniaxial swelling process calculated by using equation (3.41) and obtained via our subroutine has been plotted in Figure 3-4. As one can see, they are in good agreement. For convenience, we had normalized the stress by k_BT_0/ν, with $T_0 = 300$ K.

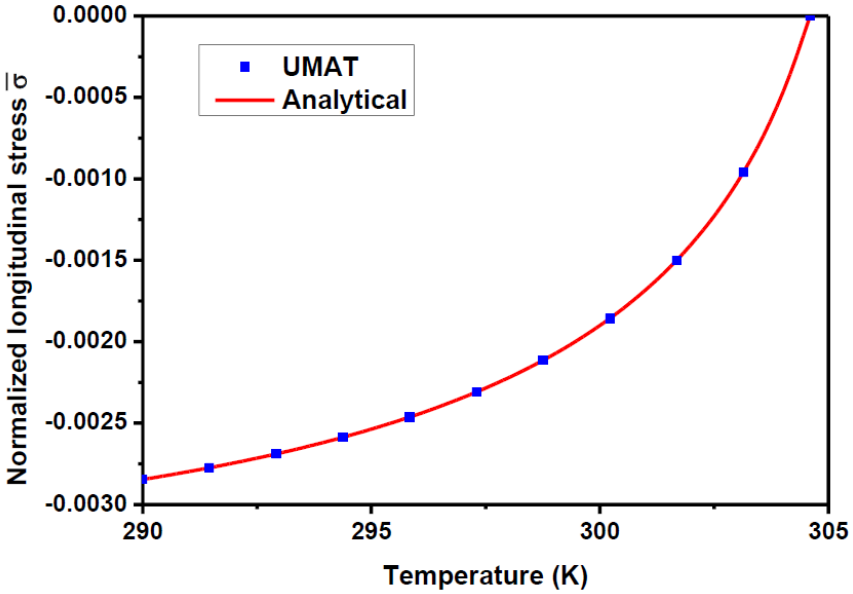

Figure 3-4: Normalized longitudinal stress during uniaxial swelling process. Discrete points represent UMAT results while the solid line represents analytical solution.

3.2. Photo-thermal sensitive hydrogels

In this section, we will investigate the photo-thermal mechanics of deformation of temperature sensitive hydrogels impregnated with light-absorbing nano-particles. The field theory of photo-thermal sensitive gels is developed by incorporating effects of photochemical heating into the thermodynamic theory of neutral and temperature sensitive hydrogels. This is achieved by considering the equilibrium thermodynamics of a swelling gel through a variational approach. The phase transition phenomenon of these gels, and the factors affecting their deformations, will be studied. To facilitate the simulation of large inhomogeneous deformations subjected to geometrical constraints, a finite element model will be developed using a user-defined subroutine in Abaqus, and by modeling the gel as a hyperelastic material. This numerical approach is validated through case studies involving gels undergoing phase coexistence and buckling when exposed to irradiation of varying intensities, and as a micro-valve in microfluidic application.

In this section, we will develop a theory to model the deformation of hydrogels due to photo-thermal effects by building on earlier works on neutral gels (Hong et al., 2009a) and temperature-sensitive gels (Ding et al., 2013). This type of deformation mechanism is made possible through the incorporation of light absorbing NPs into the temperature sensitive polymers.

In what follows, the thermodynamic framework by expressing the stress and chemical potential in terms of the free energy function will be described. We will discuss the phenomenon of phase transition and the effects of adding nano-particles on the material parameters and explore some analytical solutions predicted by the theory. Furthermore, the numerical procedure for simulating the gel will be described. Finally we will investigate some potential applications of the present theory and finite element model, which include phenomena such as coexistent phases within the gel, its buckling during the deswelling process, and its contact with a membrane in microfluidic applications.

3.2.1. Equilibrium swelling theory of photo-thermal sensitive hydrogels

Here we shall describe the mechanism of a hydrogel by considering the change in temperature due to light irradiation, as well as the inhomogeneous large deformation theory for thermally-sensitive hydrogels.

3.2.1.1. *Light irradiation induced temperature change*

Due to the addition of light-absorbing NPs in the gel network, light energy is converted into heat energy and transferred to the polymer through local heat conduction. The use of different NPs will result in different wavelengths required for absorption of irradiation, with copper chlorophyllin absorbing best at 488 nm (Suzuki and Tanaka, 1990), gold-gold sulfide at 1064 nm (Sershen et al., 2000), gold nano-rods at 810 nm (Gorelikov et al., 2004), graphene oxide at 808 nm (Zhu et al., 2012) and iron oxide at 470 nm (Yoon et al., 2012).

Under irradiation, the temperature rise ΔT is proportional to the intensity I_0 and polymer volume fraction ϕ, as shown in the phenomenological equation (3.42) (Richardson et al., 2009; Suzuki and Tanaka, 1990),

$$\Delta T = \alpha I_0 \phi \tag{3.42}$$

where α is the proportionality constant related to the heat capacity of the gel.

3.2.1.2. *Inhomogeneous large deformation of a photo-thermal sensitive gel*

With reference to Figure 3-5, consider a gel subjected to geometrical constraints, with an external weight of P hanging on the gel and kept immersed in a solvent of chemical potential μ^s. Concurrently, a mono-chromatic light is being irradiated onto the gel. Using a thermodynamic approach on the irradiation, the light possesses a non-zero chemical potential

μ^p , produced by photochemical reactions (Haught, 1984; Herrmann and Wurfel, 2005; Kelly, 1981; Ries and McEvoy, 1991; Wurfel, 1982).

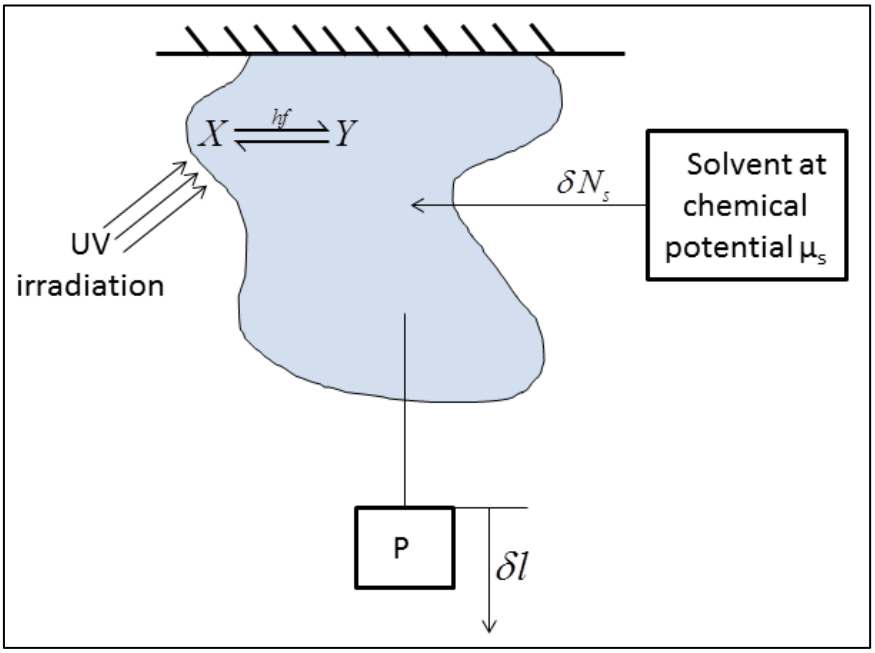

Figure 3-5: A hydrogel domain subjected to external weight P, exposed to an external solvent of fixed chemical potential μ^s, and irradiated with monochromatic light of frequency f.

In equilibrium, the weight is displaced by a distance δl, the chemical potential is maintained by pumping δN^s solvent molecules into the gel and the irradiation causes δN^p photochemical reactions at chemical potential μ^p. The work done on the gel will be equal to the sum of the work done by the external weight $P\delta l$, the chemical potential pump $\mu^s \delta N^s$ and the irradiation $\mu^p \delta N^p$.

Thermodynamically, the change in free energy density of the gel, *W*, is balanced by the work done on the gel

$$\int \delta W dV = \int B_i \delta x_i dV + \int T_i \delta x_i dS + \mu^s \int \delta C^s dV + \mu^p \int \delta C^p dV \qquad (3.43)$$

where C^s and C^p represent the concentration of solvent and photochemical reactions in the reference state respectively.

Assuming that the free energy density in the current state is dependent on the state of deformation, concentration of solvent and photochemical reactions within the gel, i.e. $W = W\left(F_{iK}, C^s, C^p\right)$, a small change in the free energy density can be written as

$$\delta W = \frac{\partial W}{\partial F_{iK}} \delta F_{iK} + \frac{\partial W}{\partial C^s} \delta C^s + \frac{\partial W}{\partial C^p} \delta C^p \tag{3.44}$$

where F_{iK} is the deformation gradient.

Combining equations (3.43) and (3.44), and applying the divergence theorem, the equilibrium equation is re-written as equation (3.45),

$$\int \left[\left(\frac{\partial W}{\partial F_{iK}} - s_{iK} \right) \delta F_{iK} + \left(\frac{\partial W}{\partial C^s} - \mu^s \right) \delta C^s + \left(\frac{\partial W}{\partial C^p} - \mu^p \right) \delta C^p \right] dV = 0 \tag{3.45}$$

where s_{iK} is the nominal stress. This equation holds for arbitrary values of δF_{iK}, δC^s and δC^p, which reduces the conservative form into the differential form

$$\left.\begin{aligned} s_{iK} &= \frac{\partial W}{\partial F_{iK}} \\ \mu^s &= \frac{\partial W}{\partial C^s} \\ \mu^p &= \frac{\partial W}{\partial C^p} \end{aligned}\right\} \tag{3.46}$$

3.2.1.3. *Free energy function*

From the approach of earlier works (Cai and Suo, 2011; Ding et al., 2013; Hong et al., 2009a; Hong et al., 2008), we assume that the free energy density of the gel is the sum of the individual free energies of network stretch and mixing. For a photo-thermal sensitive gel, there is entropic change as photons are absorbed and emitted by the nano-particles. Therefore, although there is dissipation of heat energy, the entropic change will cause a change in the free energy of the gel. With this, we introduce an additional free energy density term due to photochemical reactions W_{pho}, into the free energy density function of a temperature sensitive hydrogel.

$$W\left(\mathbf{F},C^s,C^p,T\right)=W_{net}\left(\mathbf{F}\right)+W_{mix}\left(C^s,T\right)+W_{pho}\left(C^p\right) \tag{3.47}$$

3.2.1.3.1. Free energies of network stretch and mixing

The free energy of network stretch W_{net} and mixing W_{mix} take the same form as the free energies of a temperature sensitive hydrogel, as given in Section 3.1.1.2.

The temperature used in the calculation of the Flory-Huggins interaction parameters is the real temperature of the gel consisting of two parts, given by the equation $T=T_{amb}+\alpha I_0\phi$, where T_{amb} is the ambient temperature and $\alpha I_0\phi$ is the temperature increment given in equation (3.42). In subsequent analyses, all Flory-Huggins interaction parameters will be calculated based on the real temperature, thus implicitly containing the temperature increment due to irradiation.

3.2.1.3.2. Free energy of photochemical reaction

As the nano-particles absorb UV irradiation, molecular excitation occurs, promoting an electron to the next lowest unoccupied orbital, with an energy

jump corresponding to the product of the Planck's constant and the frequency of the UV. The excited particle will decay back into the ground state immediately, releasing the energy harvested during photon absorption.

For gold NPs (and other NP used for the purpose of photo-heating), it has been shown that the quantum yield is of the order of 10^{-6} (Dulkeith et al., 2004), resulting in a near unity conversion of light energy into heat energy (Richardson et al., 2009).

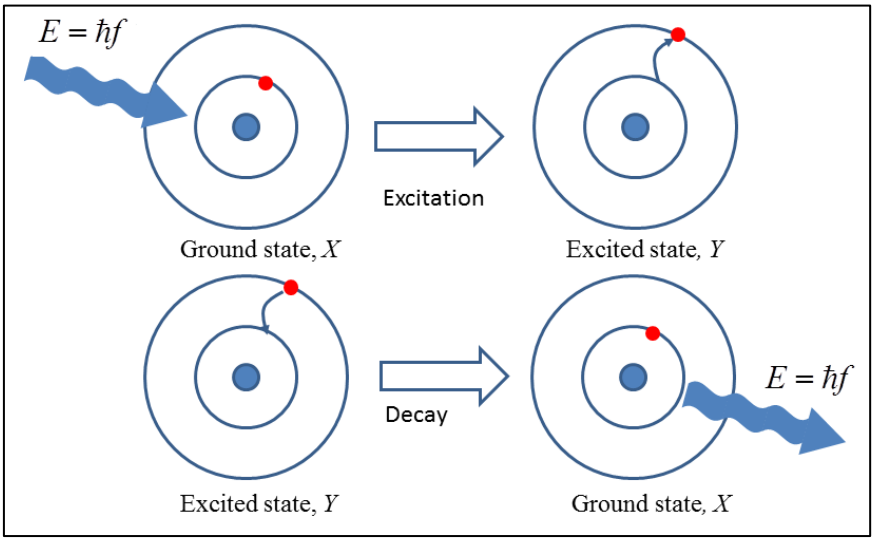

Figure 3-6: Excitation and decay of an atom absorbing a photon

This electronic transition can be represented as a series of two consecutive chemical reactions, with the reactants being the ground-state nano-particle (X) and a photon of relevant frequency $(\hbar f)$, the intermediate product being the excited particle (Y), and the product being the ground-state nano-particle and heat energy. This series of chemical reactions is illustrated in Figure 3-6 and written as equation (3.48).

$$\begin{aligned} X + \hbar f &\rightarrow Y \\ Y &\rightarrow X + heat \end{aligned} \tag{3.48}$$

Under steady state irradiation, *X* and *Y* will have concentrations [*X*] and [*Y*] respectively. The affinity (free energy) associated with one such chemical reaction, *A*, is given by (Parson, 1978)

$$A = \hbar f + kT \ln\left(\frac{[Y]}{[X]}\right) \tag{3.49}$$

where $\hbar f$ corresponds to energy transition of the electron into the excited state and the logarithmic term corresponds to the entropy change associated with the transition.

The free energy density of the entire gel W_{pho} , resulting from photochemical reactions is thus expressed as

$$W_{pho} = C^p \left[hf + kT \ln\left(\frac{C^p}{C^{p,0}}\right)\right] \tag{3.50}$$

where $C^p = [Y]$, $C^{g,0} = [X]$ is taken to be a nominal reference value given that the concentration of excited particles is low $\left(C^p / C^g \sim 10^{-10}\right)$ (Lavergne and Joliot, 2000).

3.2.1.4. *Transformation to a hyperelastic solid*

As discussed in Section 2.1.1.6, the equilibrium equation of a gel can be transformed to assume a hyperelastic form by introducing a new free energy function $\hat{W}$ through a Legendre transformation. For the photo-thermal sensitive hydrogel, we perform the following transformation

$$\hat{W} = W - \mu^s C^s - \mu^p C^p \tag{3.51}$$

where a small change in this free energy density function will yield the following relation

$$\delta\hat{W} = s_{iK}\delta F_{iK} - C^s\delta\mu^s - C^p\delta\mu^p \tag{3.52}$$

Equation (3.52) transforms the equilibrium equation (3.43) into

$$\int \delta\hat{W}dV = \int B_i\delta x_i dV + \int T_i\delta x_i dS \tag{3.53}$$

Equation (3.53) is the equilibrium equation assumed by a hyperelastic solid.

3.2.1.5. *Quantum energy conservation constraint*

As with the neutral and temperature sensitive hydrogels, we assume a molecular incompressibility constraint, given in Section 2.1.1.4.

Whilst the constituents of a temperature sensitive hydrogel undergo temperature changes and experience volumetric changes due to thermal expansion/contraction, we note from the order of magnitude of the coefficients of thermal expansion (see Table 3-1) that the volumetric expansion of individual particles is very small as compared to the volumetric change experienced during phase transition. Therefore, we assume that the effects from thermal expansion are negligible. This practice is also seen in analyses of temperature sensitive gels (Birgersson et al., 2008; Chester and Anand, 2011).

In photochemical reactions, the number of photons and chemical reactions is conserved, as dictated by the Stark-Einstein Equation, or second law of photochemistry (Rohatgi, 2006). The light intensity is proportional to the amount of light energy absorbed. In the irradiation of a material, the spatial distribution of photons within a material follows the radiative transfer equation (Long et al., 2013). However, we assume that at sub-millimeter dimensions, the spatial distribution of photochemical reactions taking place within the gel is evenly distributed. This assumption can be inferred from equation (3.42), as

proportionality to ϕ imply that the gel is not optically thin, and the gel undergoing uniform temperature change implies that there is no spatial distribution of photochemical reactions for gels of sub-millimeter dimensions.

The concentration of photochemical reactions is obtained by considering conservation of energy, where all light energy is transformed into the rise in temperature of the system (Walker, 2009).

The amount of photonic energy released is the sum of energies of all photons undergoing photo-excitation. For a monochromatic light source of uniform frequency, this energy is equal to the product of the energy of a single photon with the number of photo-excited photons

$$E_p = \hbar f \cdot C^p \tag{3.54}$$

where E_0 is a measure of the energy absorbed per unit reference volume, $\hbar$ the Planck constant and f the frequency of irradiation. The product $\hbar f$ measures the amount of energy possessed by a single photon. The amount of thermal energy per unit reference volume generated by the temperature rise is the product of mass, specific heat and temperature change of the system, i.e.

$$E_p = \rho^{gel} c_p^{gel} \Delta T \tag{3.55}$$

Substituting the relations $m^{gel} = \rho^{gel} J$ and $\Delta T = \alpha I_0 / J$ into equation (3.55), the thermal energy can be re-written as

$$E_p = c_v^{gel} \frac{\alpha I_0}{J} \tag{3.56}$$

where $c_v^{gel} = \rho^{gel} c^{gel}$ is the volumetric heat capacity, and J the determinant of the deformation gradient, $J = \det \mathbf{F}$.

The volumetric heat capacity of the gel is taken to be the volume weighted average of the constituents, i.e.

$$c_v^{gel} = \underbrace{\left[f^{Cu} c_v^{Cu} + \left(1 - f^{Cu}\right) c_v^{polymer} \right]}_{c_v^{network}} \phi + c_v^w \left(1 - \phi\right) \tag{3.57}$$

where c_v^{Cu} , $c_v^{polymer}$ and c_v^w are the volumetric heat capacities of copper, polymer and water, respectively. The volumetric heat capacity of the dry network, $c_v^{network}$ is calculated using the rule of mixtures consisting polymer molecules and copper chlorophyllin molecules with volume fractions $\left(1 - f^{Cu}\right)$ and f^{Cu} respectively.

Combining the two equations above, we obtain an expression for C^p in terms of swelling ratio and light intensity

$$C^p = \left[\frac{c_v^w}{J} + \frac{c_v^{network} - c_v^w}{J^2} \right] \frac{\alpha I_0}{\hbar f} \tag{3.58}$$

Substituting free energy functions into equation (3.51), we arrive at

$$\begin{aligned} \hat{W} = {} & \frac{1}{2} N k_B T \left[J^{\frac{2}{3}} \bar{I}_1 - 3 - 2\ln\left(J\right) \right] + \frac{k_B T}{\nu} \left(J - 1\right) \left[\ln\left(\frac{J-1}{J} \right) + \left(\frac{\chi_0}{J} + \frac{\chi_1}{J^2} \right) \right] \\ & - k_B T \frac{\alpha I_0}{\hbar f} \left[\frac{c_v^w}{J} + \frac{c_v^{network} - c_v^w}{J^2} \right] - \mu^s \left(\frac{J-1}{\nu} \right) \end{aligned} \tag{3.59}$$

where $\bar{I}_1$ is the first deviatoric invariant of the deformation gradient. With the free energy density function, we are able to obtain an explicit form of the nominal stress

$$s_{iK} = Nk_B T\left(F_{iK} - H_{iK}\right) + \frac{k_B T}{\nu}\left[\ln\left(\frac{J-1}{J}\right) + \frac{1}{J} + \frac{\chi_0 - \chi_1}{J^2} + \frac{2\chi_1}{J^3}\right] JH_{iK}$$
$$+k_B T \frac{\alpha I_0}{hf}\left[\frac{2\left(c_v^{network} - c_v^w\right)}{J^3} + \frac{c_v^w}{J^2}\right] JH_{iK} - \frac{\mu^s}{\nu} JH_{iK} \tag{3.60}$$

where H_{iK} is the transpose of the inverse of the deformation gradient, $H_{iK}F_{jK} = \delta_{ij}$. To convert the nominal stress into Cauchy stress, we use the following relation $\sigma_{ij} = s_{iK}F_{jK}/\det\mathbf{F}$

The Cauchy stress is thus given by

$$\sigma_{ij} = \frac{Nk_B T}{J}\left(F_{iK}F_{jK} - \delta_{ij}\right) + \frac{k_B T}{\nu}\left[\ln\left(\frac{J-1}{J}\right) + \frac{1}{J} + \frac{\chi_0 - \chi_1}{J^2} + \frac{2\chi_1}{J^3}\right]\delta_{ij}$$
$$+k_B T \frac{\alpha I_0}{\hbar f}\left[\left(c_v^{network} - c_v^w\right)\frac{2}{J^3} + c_v^w\left(\frac{1}{J^2}\right)\right]\delta_{ij} - \frac{\mu^s}{\nu}\delta_{ij} \tag{3.61}$$

3.2.2. Phase transition phenomenon

The phase transition of temperature-sensitive hydrogels is a commonly observed phenomenon, and has been widely studied (Ding et al., 2013; Kondo et al., 1993; Suzuki and Ishii, 1999; Suzuki and Kojima, 1994; Suzuki and Tanaka, 1990; Tanaka, 1978; Wang, 2007). The phase transition temperature is dependent on several factors, including the crosslink density of the polymer network (Harmon et al., 2003a), the chemical potential of the solvent (Pastoor and Rice, 2012), and the intensity of light irradiation. In the present study, we investigate the effects of varying light intensity on the free swelling state of poly(N-isopropylacrylamide) (PNIPAm) using the parameters listed in Table 3-1.

Experimental results have shown that for the same monomer, the addition of chromophores will alter the swelling properties of the gel (Suzuki, 1993).

This implies a change in the Flory-Huggins interaction parameter (Caykara et al., 2006).

We define a new Flory-Huggins interaction parameter by introducing a factor τ to the experimental values obtained for a polymer network without chromophores. Under this definition, we have

$$\begin{aligned} \chi_{0,new} &= \tau\chi_0 = \tau\left(A_0 + B_0 T\right), \\ \chi_{1,new} &= \tau\chi_1 = \tau\left(A_1 + B_1 T\right). \end{aligned} \tag{3.62}$$

Performing a curve fitting process on the experimental results reported, the Flory-Huggins interaction parameters of the gel containing 5% and 8% copper chlorophyllin weere obtained by multiplying the values A_0, B_0, A_1 and B_1 by a factor $\tau = 0.78$ and 0.85, respectively, and the crosslink density corresponds to $N\nu = 0.004$. The change in transition profile is shown in Figure 3-7, which shows a comparison of experimental results with analytical results.

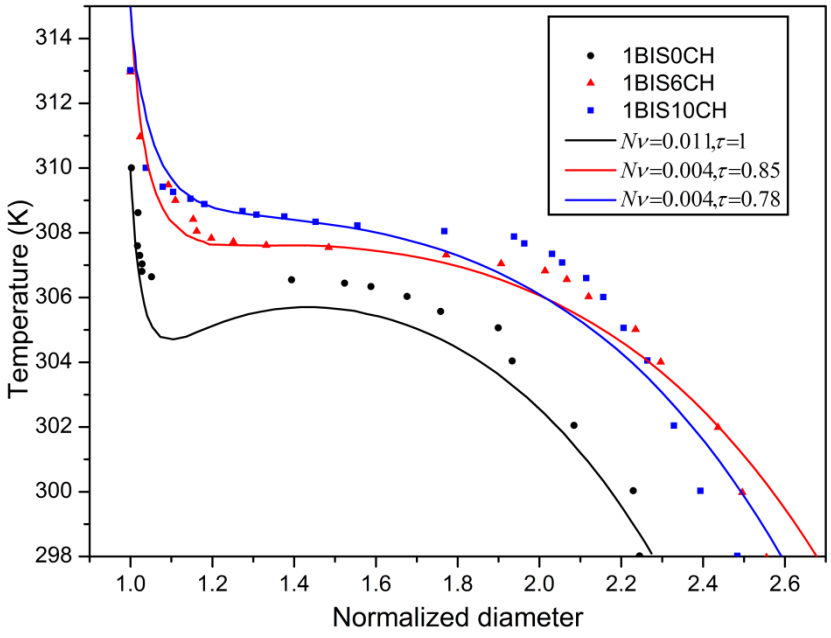

Figure 3-7: Comparison of experimental (Suzuki, 1993) and analytical normalized diameters of a free swelling gel. Naming of experimental data set follows results presented by the reference.

Without any chromophores, the gel undergoes a discontinuous phase transition as temperature is varied; and this is indicated by the two turning points in the curve. The discontinuous phase transition exhibits hysteresis phenomena which will be elaborated subsequently. Upon chromophore addition, it is evident that the two stationary points are not present, indicating that the gel undergoes a continuous phase transition. In addition to stabilizing the phase transition process, the addition of chromophores also increases the phase transition temperature,. This is corroborated by the higher curves Figure 3-7 for higher chromophore concentration.

3.2.3. Some analytical solutions

In the present study, we will investigate the effects of varying light intensity on the free swelling state of poly(N-isopropylacrylamide) (PNIPAm) using the parameters listed in Table 3-1.

Table 3-1: List of material parameters used in analysis

Parameter	Value	Reference
A_0	–12.947	(Afroze et al., 2000)
B_0	0.04496 K^{-1}	(Afroze et al., 2000)
A_1	17.92	(Afroze et al., 2000)
B_1	–0.0569 K^{-1}	(Afroze et al., 2000)
α	0.6 Km^2W^{-1}	(Suzuki and Tanaka, 1990)
f	488 nm	(Suzuki and Tanaka, 1990)
c	2.998×10^8 ms^{-1}	(Serway and Jewett, 2013)
h	6.626×10^{-34} m^2kgs^{-1}	(Barrow, 2002)
ν	10^{-28} m^3	(Hong et al., 2008)
$c_v^{polymer}$	4.18×10^6 $Jm^{-3}K^{-1}$	(Birgersson et al., 2008)
c_v^{w}	2.4×10^7 $Jm^{-3}K^{-1}$	(Birgersson et al., 2008)
c_v^{Cu}	3.443×10^6 $Jm^{-3}K^{-1}$	(Serway and Jewett, 2013)
$\alpha^{(p)}$	77×10^{-6} K^{-1}	(Chester and Anand, 2011)
$\alpha^{(w)}$	67×10^{-6} K^{-1}	(Chester and Anand, 2011)
$\alpha^{(Cu)}$	17×10^{-6} K^{-1}	(Serway and Jewett, 2013)

where $\alpha^{(p)}$, $\alpha^{(w)}$ and $\alpha^{(Cu)}$ are the coefficients of thermal coefficient for the polymer network, water and copper respectively.

3.2.3.1. *Homogeneous free swelling of a cubic gel*

We considered a dry cubic gel without any solvent imbibed in the polymer network, the volume ratio of the gel is unity, $J=1$. This gave rise to a singularity in the free energy function. Therefore, a second reference state of a freely swelling gel with $\nu C^s > 0$ was required, see Figure 3-8. In the free swelling state, there is no stress present ($\sigma_{ij}=0$) and the gel experiences stress free isotropic stretches with $\lambda_1=\lambda_2=\lambda_3$. Taking this free swelling state as the reference, we denote the isotropic stretches as λ_0, occurring at the reference solvent chemical potential μ_0^s and temperature T_0 and exposed to light at intensity I_0. In this configuration, equation (3.60) becomes

$$\frac{\mu_0^s}{k_B T_0}=\frac{N\nu}{\lambda_0^3}\left(\lambda_0^2-1\right)+\ln\left(1-\frac{1}{\lambda_0^3}\right)+\frac{1}{\lambda_0^3}+\frac{\chi_0-\chi_1}{\lambda_0^6}+\frac{2\chi_1}{\lambda_0^9}+\frac{\nu\alpha I_0}{\hbar f}\left[\frac{2\left(c_v^{network}-c_v^w\right)}{\lambda_0^9}+\frac{c_v^w}{\lambda_0^6}\right] \quad . \tag{3.63}$$

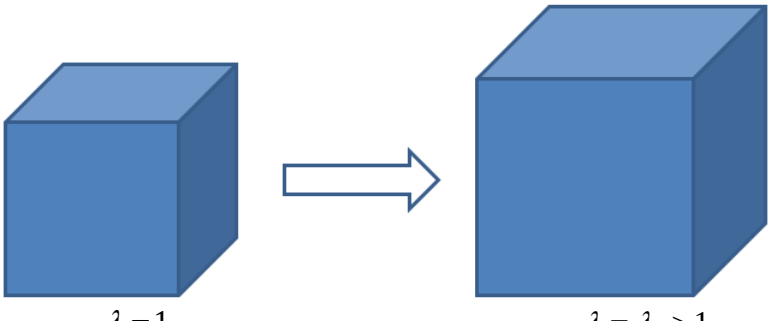

$\lambda=1$ $\qquad$ $\lambda=\lambda_0>1$

(a) $\qquad$ (b)

Figure 3-8: Gel in (a) dry state; and (b) reference state.

This homogeneous state of equilibrium serves as an initial condition during the finite element analysis to circumvent the singularity in the dry state. The variables in equation (3.63) are λ_0 , T_0 , I_0 and μ_0^s . Given any three variables, we can find the fourth using this equation, thus providing the initial condition.

In photo-thermal gels, the primary function of irradiation is to create a temperature change in the temperature sensitive hydrogel. It might not appear obvious that light intensity plays a direct role in the phase transition process but it does, in fact, affect the transition. Experiments by Suzuki and Tanaka (1990) have shown that increasing the light intensity lowers the transition temperature and increases the tendency for the gel to undergo a discontinuous phase transition. Here we first studied the effects of light intensity on the free swelling.

Figure 3-9(a) shows that increasing intensity decreases the phase transition temperature of the gel. In addition, the change in light intensity may trigger a change in the mechanism of the phase transition from a continuous transition into a discontinuous one. When held at a constant temperature, phase transition took place as we varied the intensity of irradiation onto the gel. In Figure 3-9(b), we held temperature constant and varied the light intensity from $0\ \text{mW cm}^{-2}$ to $300\ \text{mW cm}^{-2}$. The curves obtained show that an increase in light intensity decreases the transition temperature and also increases the tendency for the gel to undergo a discontinuous phase transition. These computed result showed similar trends with experimental observations (Suzuki, 1993; Suzuki et al., 1996; Suzuki and Tanaka, 1990).

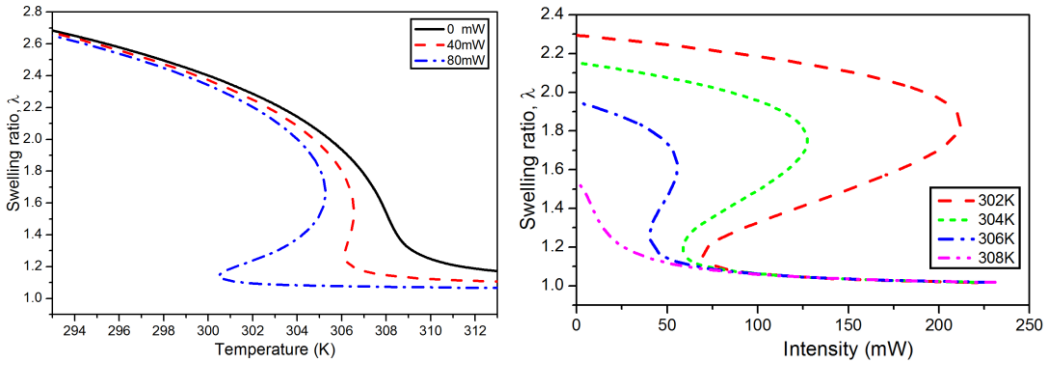

(a) (b)

Figure 3-9: Volumetric phase transition of a gel under (a) constant light intensity but variable temperature, (b) constant temperature but varying light intensity.

3.2.3.2. *Effects of Varying Light Intensity*

In photo-thermal gels, the primary function of irradiation is to create a temperature change in the temperature sensitive hydrogel. It may not appear obvious, but light intensity does, in fact, play a direct role in the phase transition process. Suzuki and Tanaka (1990) have reported experimental observations which show that increasing the light intensity lowers the transition temperature and increases the tendency for the gel to undergo a discontinuous phase transition. Here, we will first study the effects of light intensity on free swelling. To verify that the finite element subroutine developed is numerically correct, we will compare the simulation results with analytical results of free swelling by solving equation (3.63).

The change in transition temperature and the existence of transition intensity suggests that in this photo-thermal deformation process, irradiation does not simply act as a heating agent to initiate temperature sensitive deformation, but also has a second function to alter the phase transition pathway.

3.2.3.3. *Hysteresis*

Depending on values of the various factors discussed in the preceding sections, the swelling-deswelling process of a hydrogel may undergo hysteresis (Suzuki et al., 1996). From the plots presented in Figure 3-10, we see two different types of curves, one that is monotonic, as shown in Figure 3-10(a), and one that possesses stationary points, as shown in Figure 3-10(b). The former monotonic curve represents a smooth transition between the different phases, whereas the latter curve suggests signs of hysteresis during the swelling-deswelling process.

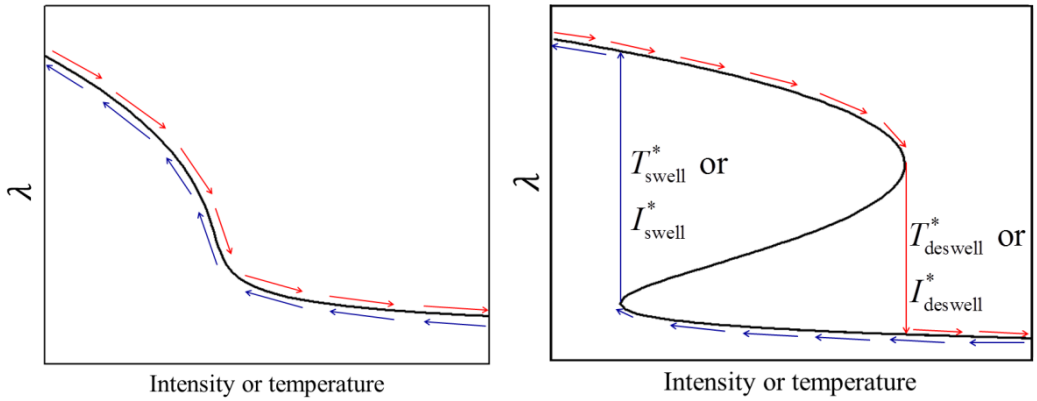

Figure 3-10: (a) Continuous phase transition; (b) Discontinuous phase transition exhibiting hysteresis. The arrows above the curve represent the direction of deswelling and arrows below the curve represent the direction of swelling.

It was demonstrated that deformation caused by one stimulus (light or heat) can be reversed by application of the other stimulus (Suzuki et al., 1996). This property provides useful applications in the area of optical switching where one stimulus can be used to activate the switch, and the other to deactivate the switch.

3.2.3.4. *Internal stress in a constrained gel*

We now consider a gel, initially at a stress-free state of λ_0 , which is constrained on both lateral sides and allowed to deform only in the longitudinal direction. Deformation is triggered by varying light intensity at an isothermal

condition. In the deformed state, the stretches are $\lambda_1 = \lambda_2 = \lambda_0$, whereas λ_3 is a variable. The in-plane stresses are $\sigma_1 = \sigma_2 = \sigma$ while $\sigma_3 = 0$ as the gel is allowed to swell freely in the 3-direction. With these definitions, equation (3.63) becomes

$$0 = \frac{N\nu}{\lambda_0^2 \lambda_3}\left(\lambda_3^2 - 1\right) + \xi \tag{3.64}$$

$$\sigma = \frac{N\nu}{\lambda_0^2 \lambda_3}\left(\lambda_0^2 - 1\right) + \xi \tag{3.65}$$

where ξ represents the shorthand for the long expression given by

$$\xi = \ln\left(1 - \frac{1}{\lambda_0^2\lambda_3}\right) + \frac{1}{\lambda_0^2\lambda_3} + \frac{\chi_0 - \chi_1}{\left(\lambda_0^2\lambda_3\right)^2} + \frac{2\chi_1}{\left(\lambda_0^2\lambda_3\right)^3} + \nu\frac{\alpha I_0}{\hbar f}\left[\frac{2\left(c_v^{network} - c_v^w\right)}{\left(\lambda_0^2\lambda_3\right)^3} + \frac{c_v^w}{\left(\lambda_0^2\lambda_3\right)^2}\right] - \frac{\mu^s}{k_B T}.$$

Equation (3.64) gives the longitudinal stretch while equation (3.65) gives the in-plane stress present in the gel at various light intensities.

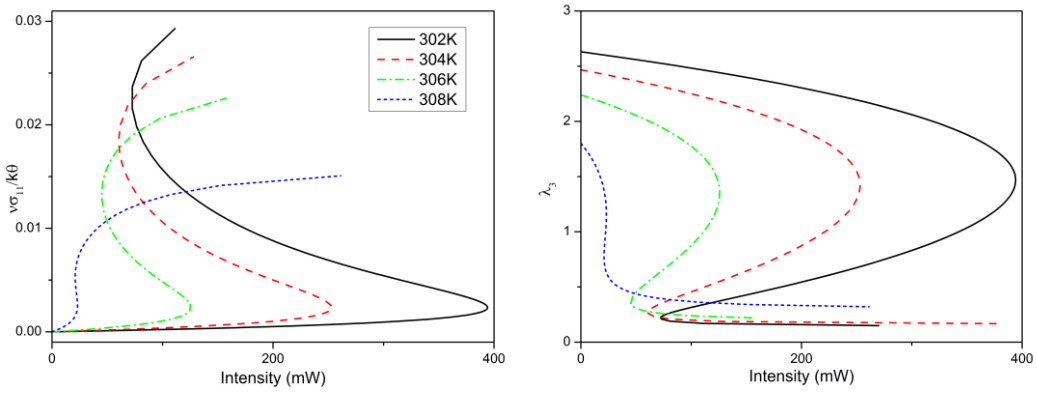

Figure 3-11: A gel in contact with solvent with chemical potential $\mu_0^s = 0$ and maintained at T_0=300K, 302K, 304K, 306K and 308K undergoing uni-axial deformation at various light intensities. The gel experiences (a) an in-plane stress and (b) a longitudinal stretch.

From Figure 3-11, we can see that a photo-thermal gel at fixed deformation experiences a tensile internal stress when exposed to irradiation. As compared to the case of free swelling, the gel deswells more in the case of constrained swelling.

3.2.4. Numerical procedure for equilibrium swelling of photo-thermal sensitive hydrogels

To facilitate the modeling and simulation of gel deformation when subjected to light and temperature changes and constraints, we utilized commercial finite element numerical solver Abaqus. Based on earlier works which implement hydrogel properties as hyperelastic materials (Ding et al., 2013; Hong et al., 2009a; Marcombe et al., 2010), we developed the user-defined subroutine UHYPER to carry out finite element analysis on the gel deformation. The definition of material properties was based on the free energy function derived earlier in equation (3.59) and its respective derivatives with respect to the invariants of the deformation gradient. In this section, we will derive all required expressions for the formulation.

Due to singularity in the dry state, we assumed an initial free swelling condition of

$$\mathbf{F}_0 = \begin{bmatrix} \lambda_0 & 0 & 0 \\ 0 & \lambda_0 & 0 \\ 0 & 0 & \lambda_0 \end{bmatrix} \tag{3.66}$$

Relative to the initial free swelling state, the current deformation of the gel is, as measured by Abaqus, $\mathbf{F}'$. To obtain the actual deformation gradient of the gel, we write $\mathbf{F} = \mathbf{F}'\mathbf{F}_0$.

Therefore, in all subsequent implementation in Abaqus, we write $J = \lambda_0^3 J'$, where J denotes actual swelling ratio and J' denotes swelling ratio used in Abaqus. The non-dimensionalized free energy density is thus re-written as

$$\begin{aligned}\frac{\nu\hat{W}}{k_B T_0} = &\left\{\frac{1}{2}N\nu\left[\lambda_0^2 J'^{\frac{2}{3}}\bar{I}_1 - 3 - 2\ln\left(\lambda_0^3 J'\right)\right] - \nu\frac{\alpha I_0}{\hbar f}\left[\frac{c_v^{network} - c_v^w}{\left(\lambda_0^3 J'\right)^2} + \frac{c_v^w}{\lambda_0^3 J'}\right]\right. \\ &\left. + \left(\lambda_0^3 J' - 1\right)\left[\ln\frac{\lambda_0^3 J' - 1}{\lambda_0^3 J'} + \frac{\chi_0}{\lambda_0^3 J'} + \frac{\chi_1}{\left(\lambda_0^3 J'\right)^2} - \bar{\mu}^s\right]\right\}\frac{T}{T_0}\end{aligned} \tag{3.67}$$

The first, second and third derivatives were given from equations (3.68) to (3.82).

$$\frac{\partial\left(\nu\hat{W}/k_B T_0\right)}{\partial\bar{I}_1} = \left(\frac{1}{2}N\nu\lambda_0^2 J'^{\frac{2}{3}}\right)\frac{T}{T_0} \tag{3.68}$$

$$\frac{\partial\left(\nu\hat{W}/k_B T_0\right)}{\partial\bar{I}_2} = 0 \tag{3.69}$$

$$\begin{aligned}\frac{\partial\left(\nu\hat{W}/k_B T_0\right)}{\partial J'} = &\left\{\frac{1}{3}\left(\lambda_0^2 J'^{-\frac{1}{3}}\bar{I}_1\right) - \frac{N\nu}{J'} + \nu\frac{\alpha I_0}{\hbar f}\left[\frac{2\left(c_v^{network} - c_v^w\right)}{\lambda_0^6 J'^3} + \frac{c_v^w}{\lambda_0^3 J'^2}\right]\right. \\ &\left. + \left[\lambda_0^3\ln\frac{\lambda_0^3 J' - 1}{\lambda_0^3 J'} + \frac{1}{J'} + \frac{\chi_0 - \chi_1}{\lambda_0^3 J'^2} + \frac{2\chi_1}{\lambda_0^6 J'^3}\right] - \bar{\mu}^s\right\}\frac{T}{T_0}\end{aligned} \tag{3.70}$$

$$\frac{\partial^2\left(\nu\hat{W}/k_B T_0\right)}{\partial\bar{I}_1^2} = 0 \tag{3.71}$$

$$\frac{\partial^2\left(\nu\hat{W}/k_B T_0\right)}{\partial\bar{I}_2^2} = 0 \tag{3.72}$$

$$\frac{\partial^2\left(\nu\hat{W}/k_BT_0\right)}{\partial J'^2}=\left[-\frac{1}{9}N\nu\lambda_0^2J'^{-\frac{4}{3}}\bar{I}_1+\frac{N\nu}{J'^2}-\nu\frac{\alpha I_0}{\hbar f}\left(\frac{6\left(c_v^{network}-c_v^w\right)}{\lambda_0^6J'^4}+\frac{2c_v^w}{\lambda_0^3J'^3}\right)\right.$$
$$\left.+\left(\frac{\lambda_0^3}{J'\left(\lambda_0^3J'-1\right)}-\frac{1}{J'^2}-\frac{2\left(\chi_0-\chi_1\right)}{\lambda_0^3J'^3}\frac{6\chi_1}{\lambda_0^6J'^4}\right)\right]\frac{T}{T_0} \tag{3.73}$$

$$\frac{\partial^2\left(\nu\hat{W}/k_BT_0\right)}{\partial\bar{I}_1\partial\bar{I}_2}=0 \tag{3.74}$$

$$\frac{\partial^2\left(\nu\hat{W}/k_BT_0\right)}{\partial\bar{I}_1\partial J'}=\left(\frac{1}{3}N\nu\lambda_0^2J'^{-\frac{1}{3}}\right)\frac{T}{T_0} \tag{3.75}$$

$$\frac{\partial^2\left(\nu\hat{W}/k_BT_0\right)}{\partial\bar{I}_2\partial J'}=0 \tag{3.76}$$

$$\frac{\partial^3\left(\nu\hat{W}/k_BT_0\right)}{\partial\bar{I}_1^2\partial J'}=0 \tag{3.77}$$

$$\frac{\partial^3\left(\nu\hat{W}/k_BT_0\right)}{\partial\bar{I}_2^2\partial J'}=0 \tag{3.78}$$

$$\frac{\partial^3\left(\nu\hat{W}/k_BT_0\right)}{\partial\bar{I}_1\partial\bar{I}_2\partial J'}=0 \tag{3.79}$$

$$\frac{\partial^3\left(\nu\hat{W}/k_BT_0\right)}{\partial\bar{I}_1\partial J'^2}=N\nu\left(-\frac{1}{9}\lambda_0^2J'^{-\frac{4}{3}}\right)\frac{T}{T_0} \tag{3.80}$$

$$\frac{\partial^3\left(\nu\hat{W}/k_BT_0\right)}{\partial\bar{I}_2^2\partial J'}=0 \tag{3.81}$$

$$\frac{\partial^3\left(\nu\hat{W}/k_BT_0\right)}{\partial J'^3}=\left\{\frac{4}{27}N\nu\lambda_0^2J'^{-\frac{7}{3}}\bar{I}_1-2\frac{N\nu}{J'^3}+\nu\frac{\alpha I_0}{\hbar f}\left[\frac{24\left(c^{(p)}-c^{(w)}\right)}{\lambda_0^6J'^5}+\frac{6c^{(w)}}{\lambda_0^3J'^4}\right]\right.$$
$$\left.+\left(-\frac{\lambda_0^3\left(2\lambda_0^3J'-1\right)}{J'^2\left(\lambda_0^3J'-1\right)^2}+\frac{2}{J'^3}+\frac{6\left(\chi_0-\chi_1\right)}{\lambda_0^3J'^4}+\frac{24\chi_1}{\lambda_0^6J'^5}\right)\right\}\frac{T}{T_0} \tag{3.82}$$

For the initial condition of λ_0 , we solve the equation (3.63) at initial temperature T_0 , initial light intensity I_0 and chemical potential μ_0^s .

$$\frac{\mu_0^s}{k_BT_0}=\frac{N\nu}{\lambda_0^3}\left(\lambda_0^2-1\right)+\ln\left(1-\frac{1}{\lambda_0^3}\right)+\frac{1}{\lambda_0^3}+\frac{\chi_0-\chi_1}{\lambda_0^6}+\frac{2\chi_1}{\lambda_0^9}$$
$$+\frac{\nu\alpha I_0}{\hbar f}\left[\left(c_v^{network}-c_v^w\right)\frac{2}{J^3}+c_v^w\left(\frac{1}{J^2}\right)\right] \tag{3.83}$$

Due to limitations of the UHYPER subroutine, only one loading parameter can be applied in the form of a temperature field. Therefore simulations were made by varying one field (temperature, light intensity or chemical potential) and keeping the other two fixed.

The required loading parameter was thus represented by temperature in Abaqus. For example, to simulate effects of change in chemical potential at fixed temperature and intensity, we represent chemical potential as a temperature field, with the fixed values of temperature and intensity as material inputs, together with the crosslink density.

3.2.5. Numerical examples for equilibrium swelling of photo-thermal sensitive hydrogels

Using the finite element model developed in Section 3.2.4, we will investigate some interesting phenomenon and applications of the photo-thermal sensitive hydrogel.

3.2.5.1. *Free swelling of a cube – verification with analytical results*

In this section, we will verify the finite element model through comparison with analytical results developed in Section 3.2.3 before proceeding to conduct simulation for gels of more complex geometries.

To verify that the finite element subroutine developed was numerically correct, we compared the simulation results with analytical results of free swelling by solving equation (3.63). As explained in 3.1.3, it is possible to use a single element to simulate the swelling of the gel due to homogeneity. Therefore no mesh convergence tests were conducted. Figure 3-12 shows a comparison of analytical solutions obtained in Figure 3-9 with FEM results from a cube of $2\times2\times2$ C3D8 elements.

For continuous phase transitions, the finite element analysis is able to fully simulate the entire transition process. In the case of discontinuous phase transition, the simulations conclude when the turning points are reached as the Newton method is not adapted to capture the full resolution of the turning feature. Although Abaqus offers alternatives to overcome stationary points through options such as *RIKS and *BUCKLE, we note that these options are not applicable to gels in the inhomogeneous field theory.

To obtain both portions of the curve shown in Figure 3-12, separate simulations have to be run, with one simulating the shrinking process of low temperature or light intensity to high temperature or light intensity, and anothersimulating from high temperature or light intensity to low temperature or light intensity.

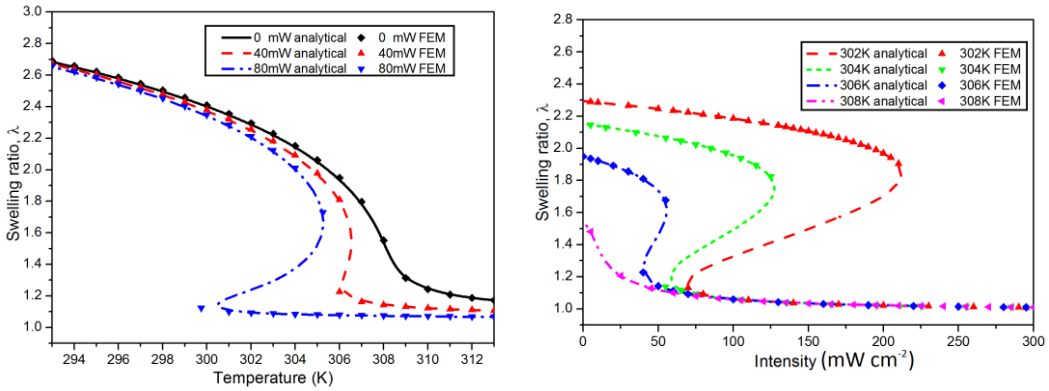

(a) (b)

Figure 3-12: Parametric study of effects of changing light intensity on the phase transition path. The gels of crosslink density $N\nu = 0.01$ are irradiated with light of wavelength 488nm. (a) Light intensity is kept constant while temperature is varied from 293K to 313K; and (b) Temperature of gel is kept constant while light intensity is varied from $0\ \text{mW cm}^{-2}$ to $300\ \text{mW cm}^{-2}$.

3.2.5.2. *Coexistent phases of gel deformation*

During the deformation process of a gel under external constraints, a part of the gel may undergo phase transition while other parts remain in the original phase. This is known as the coexistent phase where the collapsed gel is able to exist with the uncollapsed gel. Although an analytical approach is possible by solving the governing equations (Eshelby, 1956) for temperature sensitive hydrogels (Cai and Suo, 2011), the phenomenon of coexistence within a gel is a complex one and often requires numerical methods to predict the overall self-consistent behavior.

Here we will employ the developed finite element formulation to study this phenomenon. Consider a hydrogel rod immersed in water $\left(\bar{\mu}_0^s = 0\right)$, fixed at both ends and originally unexposed to irradiation. As light is being irradiated on the middle portion of the rod, the exposed portion starts to undergo phase transition. The process takes place under an isothermal condition of 308 K. Due to symmetry, a quarter-model was used. 3125 axisymmetric four-node CAX4

elements were used for the mesh. There were a total of 3276 nodes. Each simulation took about a few minutes to run on 8 cores.

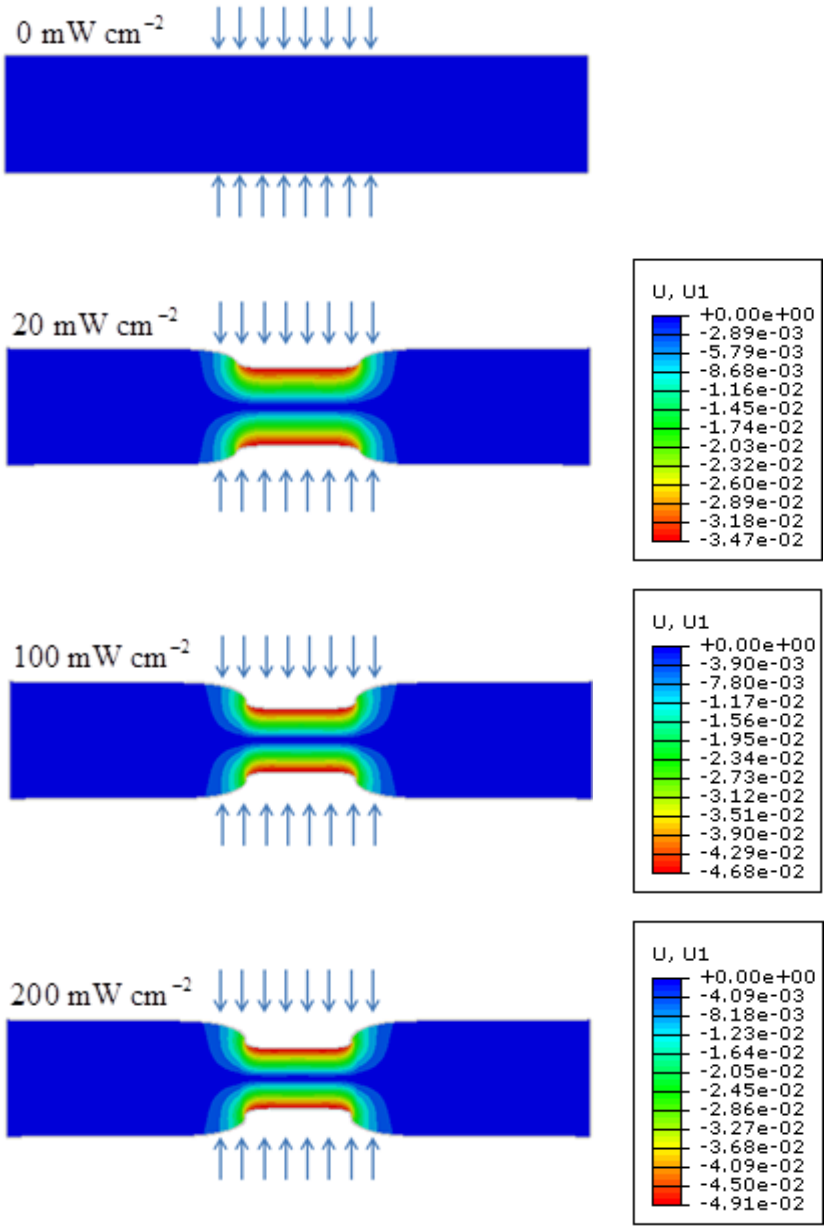

Figure 3-13: Cross-section view of a gel $\left(N\nu = 0.005, \tau = 0.78\right)$ subjected to irradiation of different intensities at 308 K. The contour plots show the deformation in the radial direction.

Figure 3-13 shows the simulation results which successfully captured the state of deformation when the gel was subjected to light with different intensities. Under increasing intensities, the extent of deswelling of the exposed rod increased. As the middle portion shrank, the interface between the two phases experienced tension, which changed the proportion of the radial dimensions of the two phases.

It should be noted, however, that the parameters used in this simulation causes continuous phase transition, thus allowing the simulation to be completed. Certain combinations of parameters will cause discontinuous phase transition and will not allow finite element analysis beyond the instability points.

3.2.5.3. *Application in micro-valves*

The large deformation present during irradiation of light to a photo-thermal gel makes it a useful material as a remotely controlled flow regulator. Without irradiation exposure, the flow passage is blocked by the gel. Upon irradiation, the gel shrinks thus allowing the liquid to flow across the channel. We study the deformation process of such an application using the finite element model presently developed. In this example, we will investigate a hybrid hydrogel-membrane microfluidic valve (He et al., 2012; Moore et al., 2000), where a membrane in contact with a hydrogel is used to control flow across an orifice located directly below center of the gel, see Figure 3-14.

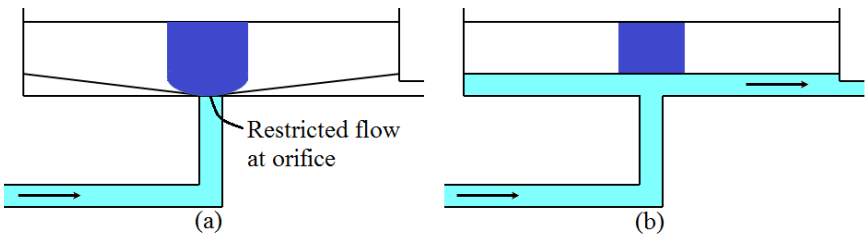

Figure 3-14: (a) Configuration of valve when gel is not being irradiated, gel is swollen and blocks the orifice, restricting flow; (b) Configuration of valve when gel is irradiated, gel deswells and thus allowing flow across orifice.

In this application of the photo-thermal gel, the gel is initially not exposed to irradiation, and the gel is in a swollen state which prevents fluid flow across the orifice. However, as the gel is being exposed to irradiation, the gel shrinks and removes the blockage in the orifice which allows flow. This action of shrinking and swelling is reversible and thus would be a suitable material as a flow control valve. In the valve, a gel originally in the dry state is placed in contact with the membrane. There are no deformations in the membrane. Next, the gel is being exposed to solvent of chemical potential of $\bar{\mu}^s = 0$ to reach the swollen state. This swollen state inhibits flow in the channel. As the gel is being irradiated, shrinkage occurs and unblocks the orifice, thus allowing for flow across the channel.

In the model, axisymmetric CAX4 elements were used. Due to symmetry, only half of the geometry was modeled. Mesh convergence tests were performed and it was determined that 900 elements (961 nodes) and 500 elements (606 nodes) were sufficient. Simulation time was about 3 minutes on 8 cores.

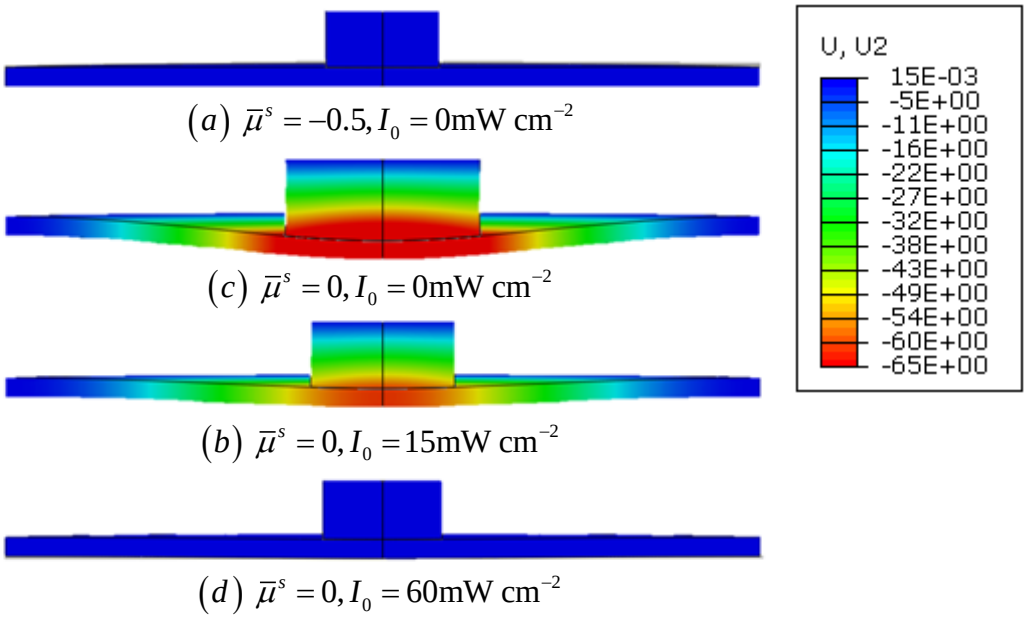

Figure 3-15: Contour plot of the normal displacement of gel with parameters $N\nu = 0.005$ and $T_0 = 308$ K.

Figure 3-15 illustrates the simulation results of the deformation of the gel as it was being irradiated. The capability of presently developed finite element model to capture the gel deformations across various light intensities is clearly evident. Figure 3-15(a) shows the valve being prepared by first setting a dry $\left(\bar{\mu}_0^s = -0.5\right)$ cylindrical gel in contact with the membrane, while Figure 3-15(b) shows the swollen gel at equilibrium with the solvent of chemical potential $\bar{\mu}^s = 0$. The swollen gel causes the membrane to block the opening of the orifice, thus restricting flow. In Figure 3-15(c), the gel deswelled under $15\ \text{mWcm}^{-2}$ irradiation, and in Figure 3-15(d), it deswelled further under $60\ \text{mWcm}^{-2}$ irradiation, and was restored to a strain-free state. Although similar mechanisms have been applied using *pH*-sensitive hydrogels, the slow response mechanism of *pH*-sensitive hydrogels limits their application. Photo-thermal gels would, on the other hand, be a more viable option as a microfluidic valve. In addition, the viability of remotely controlling the valve places photo-thermal gels in greater advantages.

3.3. Magneto-thermal sensitive hydrogels

Although light-sensitive hydrogels satisfy all the checklist of a good gel material, its use is physically limited by the condition of requiring exposure to light, which might not be possible in some applications, such as controllable drug release agents due to the opacity of the human body. Alternatively, hydrogels containing magnetic particles offer a viable solution to this problem as magnetic fields are able to penetrate the human body more strongly than light.

Hyperthermia, or the killing of cancerous tumours using elevated temperatures, has caught the attention of researchers in the biomedical industry. Magnetic hyperthermia refers to the use of heat generated by magnetic nanoparticles (MNPs) exposed to an alternating magnetic field (AMF) to perform hyperthermia (Jordan et al., 1993) is one area with vast potential.

Other than magnetic hyperthermia, the temperature increase in MNPs may be utilized to induce large volumetric changes in temperature sensitive hydrogels, providing possibilities in remotely controlled microfluidics, controlled delivery and hyperthermia (Brazel, 2009; Lai et al., 2007; Satarkar and Hilt, 2008). However, there is a lack of literature describing the theory and mechanics of a magnetically sensitive hydrogel.

Continuing previous works on thermodynamic theories for temperature sensitive and photo-thermal sensitive hydrogels, we will develop a thermodynamic theory to describe the relationship between gel response with temperature and alternating magnetic field.

In what follows, we will build the theoretical framework in terms of thermodynamics of deformation, and subsequently specialize the material to a hydrogel made of poly-n-isopropylacrylamide (PNIPAM) infused with SPIONs. Using the theory developed, we will further discuss some analytical solutions, which include phase transition of gels under free swelling and constrained swelling. In addition, a numerical procedure using finite element as a tool to

predict deformation behaviour of a gel under magnetic and temperature loads will be developed. Finally, we will explore a potential application of magneto-thermal sensitive hydrogels in microfluidic valves with the finite element model.

3.3.1. Equilibrium swelling theory of magneto-thermal sensitive hydrogels

Referring to Figure 3-16, a gel, subjected to geometrical constraints and attached to a body force of B_i and traction of T_i , is maintained at chemical potential μ^s . A wire of alternating current is placed nearby, inducing a magnetic field of B_{mag} in the gel. The work done on the gel by the mechanical load, solvent and magnetic field are $P\delta l$, $\mu^s \delta N^s$ and $B_{mag}\delta M$ respectively.

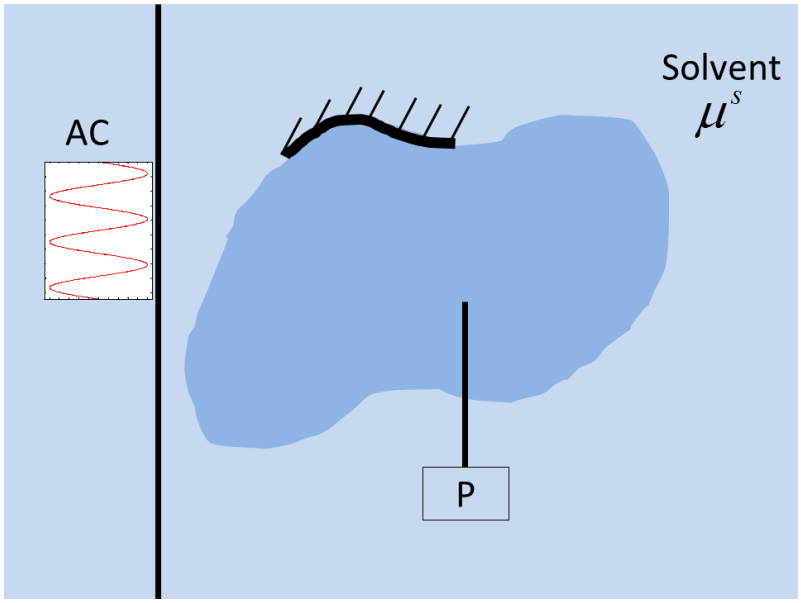

Figure 3-16: External loads on a magnetic gel

These works done on the gel cause a change in the free energy density of the system,

$$\int \delta W dV = \int B_i \delta x_i dV + \int T_i \delta x_i dS + \mu^s \int \delta C^s dV + B_{mag} \int \delta M dV \qquad (3.84)$$

Using the deformation gradient $\left(F_{iK} = \partial x_i / \partial X_K\right)$ as a measure of amount of deformation and invoking the divergence theorem, equation (3.84) is written as

$$\int \delta W dV = \int s_{iK} \delta F_{iK} dV + \mu \int \delta C dV + B_{mag} \int \delta M dV \tag{3.85}$$

Writing the change in free energy density using the chain rule of partial derivatives, we obtain

$$\int \left(\frac{\partial W}{\partial F_{iK}} \delta F_{iK} + \frac{\partial W}{\partial C} \delta C + \frac{\partial W}{\partial M} \delta M \right) dV = \int s_{iK} \delta F_{iK} dV + \mu \int \delta C dV + B_{mag} \int \delta M dV \tag{3.86}$$

under the assumption that the free energy density is a variable dependent on the state of deformation, solvent concentration and magnetization.

For arbitrary values of the integrand, equation (3.86) reduces to the set of three differential equations

$$s_{iK} = \frac{\partial W}{\partial F_{iK}}, \mu = \frac{\partial W}{\partial C^s}, B_{mag} = \frac{\partial W}{\partial M}. \tag{3.87}$$

3.3.1.1. *Free energy function*

Following the works from previous sections, we assume that the total free energy function can be decomposed into a linear sum of the three component densities, we write

$$\begin{aligned} W &= W\left(F_{iK}, C, M\right) \\ &= W_{net}\left(F_{iK}\right) + W_{mix}\left(C\right) + W_{mag}\left(M\right) \end{aligned} \tag{3.88}$$

The free energy of network stretch W_{net} and mixing W_{mix} take the same form as the free energies of a temperature sensitive hydrogel, as given in Section 3.1.1.2.

As the magnetic particles are magnetized, there will be a contribution to the free energy of the gel due to the entropic change in the system. We will assume the simplest case of a paramagnetic system with spin $\frac{1}{2}$ ground state and no orbital angular momentum for this free energy function of. Under this assumption, the free energy of magnetization is written as

$$W_{mag} = -C^m k_B T \left\{ \ln \left[2\cosh\left(\frac{\mu^B B_{mag}}{k_B T} \right) \right] \right\} \tag{3.89}$$

where C^m is the number of magnetic particles per unit reference volume.

3.3.1.2. *Energy conservation constraint*

As with the hydrogels discussed earlier, we assume a molecular incompressibility constraint, given in Section 2.1.1.4.

In addition, we consider conservation of energy during a magnetic hyperthermia process. In a gel with SPIONs, the magnetization is proportional to the magnetic particle concentration and takes the form of a hyperbolic tangent function (Stöhr and Siegmann, 2006), i.e.

$$M = \phi_m C^m \mu^B \tanh\left(\frac{\mu^B B_{mag}}{k_B T} \right) \tag{3.90}$$

Given that the concentration of magnetic particles within the polymer network does not change with swelling, we can write $f_m + f_p = 1$, where f_m is

the volume fraction of magnetic particles with the polymer network and can be regarded as a material parameter.

Combining with equation (3.90), we obtain that magnetization is inversely proportional to the volume swelling ratio, *J*.

$$M = \frac{f_m C^m \mu^B}{J} \tanh\left(\frac{\mu^B B_{mag}}{k_B T} \right) \tag{3.91}$$

We obtain values of C^m by equating temperature rise during magnetic hyperthermia to the total energy of all magnetic dipoles during the magnetization process,

$$C^m \mu^B B_{mag} \tanh\left(\frac{\mu^B B_{mag}}{k_B T} \right) = \rho c \Delta\theta \tag{3.92}$$

Using experimental results from Skumiel et al. (2007), with magnetic field intensity ranging from $H = 500 Am^{-1}$ to $H = 1.75 kAm^{-1}$, temperature rise ranging from $\Delta\theta = 3K$ to $\Delta\theta = 37K$, $\rho = 1480 kgm^{-3}$, $c \approx 2230 Jkg^{-1}K^{-1}$, we obtain an approximate value of $C^m \nu \approx 3\times10^{10}$ for iron (III) oxide $\left(Fe_3O_4\right)$ nanoparticles with volume fraction of $f_m = 0.03$.

3.3.1.3. *Transformation into a hyperelastic solid*

To transform a magneto-thermal sensitive hydrogel into a hyperelastic solid, we introduce a new free energy function $\hat{W}$ by performing the following Legendre transformation

$$\hat{W}\left(F_{iK}, \mu^s, B\right) = W\left(F_{iK}, C^s, M\right) - \mu^s C^s - B_{mag} M \tag{3.93}$$

The non-dimensionalized free energy function of the gel is thus

$$\frac{\hat{W}\nu}{kT_0}=\frac{1}{2}N\nu\frac{T}{T_0}\left(I-3-2\ln J\right)+\frac{T}{T_0}\left[\nu C\ln\left(\frac{\nu C}{1+\nu C}\right)+\frac{\chi\nu C}{1+\nu C}\right]-\frac{\mu^s}{kT_0}\left(J-1\right)$$
$$-N_m\nu\frac{T}{T_0}\ln\left[2\cosh\left(\bar{B}\frac{T_0}{T}\right)\right]-\left[N_m\nu\bar{B}\tanh\left(\bar{B}\frac{T_0}{T}\right)\right]f_m/J \tag{3.94}$$

where $\bar{B}=\mu^B B_{mag}/k_B T$ is the non-dimensionalized magnetic field.

The nominal stress is thus derived to be

$$\frac{s_{ik}\nu}{kT_0}=N\nu\frac{T}{T_0}\left(F_{iK}-H_{iK}\right)+\frac{T}{T_0}\left[\ln\left(\frac{J-1}{J}\right)+\frac{1}{J}+\frac{\chi_0-\chi_1}{J^2}+\frac{2\chi_1}{J^3}\right]JH_{iK}$$
$$-\bar{\mu}^s JH_{iK}+\frac{N_m\nu f_m}{J^2}\bar{B}\tanh\left(\bar{B}\frac{T_0}{T}\right)JH_{iK} \tag{3.95}$$

3.3.2. Some analytical solutions

3.3.2.1. *Homogeneous free swelling*

When undergoing free swelling, there is no stress present in the gel and equation (3.95) reduces to

$$N\nu\frac{T}{T_0}\left(\lambda_0-\frac{1}{\lambda_0}\right)+\lambda_0^2\frac{T}{T_0}\xi-\bar{\mu}^s\lambda_0^2+\frac{N_m\nu f_m}{\lambda_0^4}\bar{B}\tanh\left(\bar{B}\frac{T_0}{T}\right)=0 \tag{3.96}$$

where $\xi=\ln\left(1-\frac{1}{\lambda_0^3}\right)+\frac{1}{\lambda_0^3}+\frac{\chi_0-\chi_1}{\lambda_0^6}+\frac{2\chi_1}{\lambda_0^9}$.

We take the gel to be in chemical equilibrium with water as the solvent, thus $\bar{\mu}^s=0$. Figure 3-17(a) shows plots of λ_0 with temperature at various magnitudes of magnetic field. It is evident that exposure to magnetic field causes a decrease in phase transition temperature of the gel. This causes the phase transition to shift from a continuous transition into a discontinuous one.

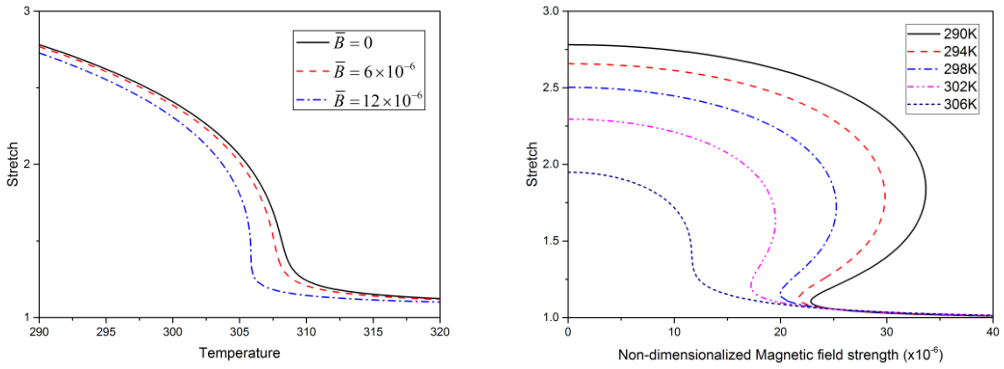

(a) (b)

Figure 3-17: (a) Phase transition of gel held various magnetic fields of regular intervals of $\Delta\bar{B}=6\times10^{-6}$, with the top curve being $\bar{B}=0$. (b) Phase transition of gel held at constant temperatures at 4K intervals ranging from 290K (top curve) to 306K.

When held isothermal under varying magnetic field, we obtain Figure 3-17(b), which suggests that a change in magnetic field alone is sufficient to cause a phase transition in the gel, This allows the gel to be dually controlled: via temperature and magnetic field.

3.3.2.2. *Swelling of a gel constrained laterally*

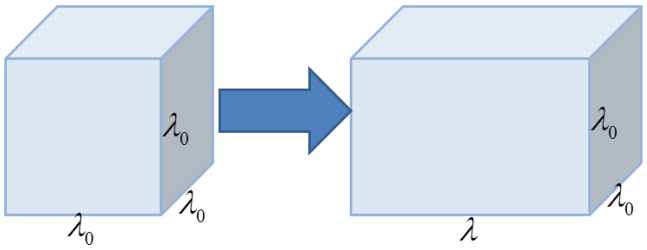

Figure 3-18: An initially isotropic gel cube subjected to constraints on the sides and only swells in 1 direction.

As the gel is constrained in the longitudinal directions, swelling will take place in the longitudinal direction. There will be in-plane stresses while longitudinally it will be stress-free.

$$N\nu\frac{T}{T_0}\left(\lambda-\frac{1}{\lambda}\right)+\lambda_0^2\frac{T}{T_0}\xi_1-\bar{\mu}^s\lambda_0^2+\frac{N_m\nu f_m}{\lambda^2\lambda_0^2}\bar{B}\tanh\left(\bar{B}\frac{T_0}{T}\right)=0 \tag{3.97}$$

$$\frac{s_1\nu}{kT_0}=N\nu\frac{T}{T_0}\left(\lambda_0-\frac{1}{\lambda_0}\right)+\lambda\lambda_0\frac{T}{T_0}\xi_1-\bar{\mu}^s\lambda\lambda_0+\frac{N_m\nu f_m}{\lambda\lambda_0^3}\bar{B}\tanh\left(\bar{B}\frac{T_0}{T}\right) \tag{3.98}$$

where $\xi_1=\ln\left(1-\frac{1}{\lambda\lambda_0^2}\right)+\frac{1}{\lambda\lambda_0^2}+\frac{\chi_0-\chi_1}{\left(\lambda\lambda_0^2\right)^2}+\frac{2\chi_1}{\left(\lambda\lambda_0^2\right)^3}$

The initial state of swelling is determined from equation (3.96) for λ_0 . The values of stretch and in-plane stress are then obtained using equations (3.97) and (3.98). Figure 3-19 shows the longitudinal stretch and in-plane stress of the gel with temperature respectively.

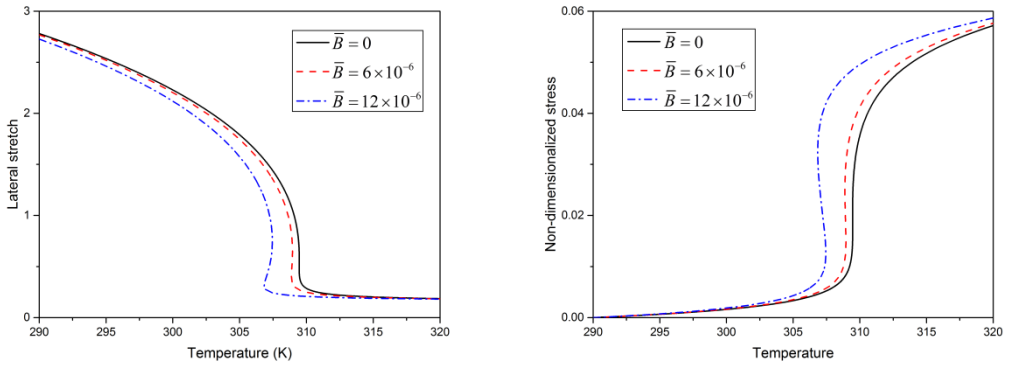

(a) (b)

Figure 3-19: (a) longitudinal stretch and (b) in-plane stress of a laterally constrained hydrogel.

3.3.2.3. *Swelling of a gel constrained longitudinally*

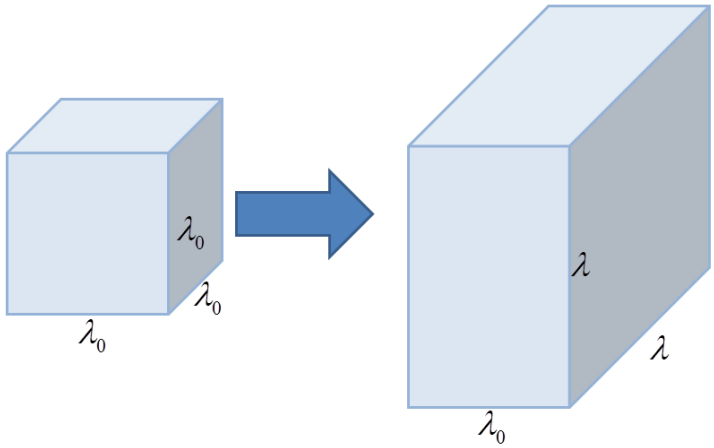

Figure 3-20: An initially isotropic gel cube subjected to constraints on 1 pair of parallel sides and swells in the lateral direction.

Constrained on opposing faces, the gel is free to swell in the lateral directions. Laterally, it will be stress free while there will be stresses induced in the longitudinal direction.

$$N\nu\frac{T}{T_0}\left(\lambda-\frac{1}{\lambda}\right)+\lambda_0\lambda\frac{T}{T_0}\xi_2-\bar{\mu}^s\lambda_0\lambda+\frac{N_m\nu f_m}{\lambda_0\lambda^3}\bar{B}\tanh\left(\bar{B}\frac{T_0}{T}\right)=0 \qquad (3.99)$$

$$\frac{s\nu}{kT_0}=N\nu\frac{T}{T_0}\left(\lambda_0-\frac{1}{\lambda_0}\right)+\lambda^2\frac{T}{T_0}\xi_2-\bar{\mu}^s\lambda^2+\frac{N_m\nu f_m}{\lambda_0^2\lambda^2}\bar{B}\tanh\left(\bar{B}\frac{T_0}{T}\right) \qquad (3.100)$$

where $\xi_2=\ln\left(1-\frac{1}{\lambda_0\lambda^2}\right)+\frac{1}{\lambda_0\lambda^2}+\frac{\chi_0-\chi_1}{\left(\lambda_0\lambda^2\right)^2}+\frac{2\chi_1}{\left(\lambda_0\lambda^2\right)^3}$.

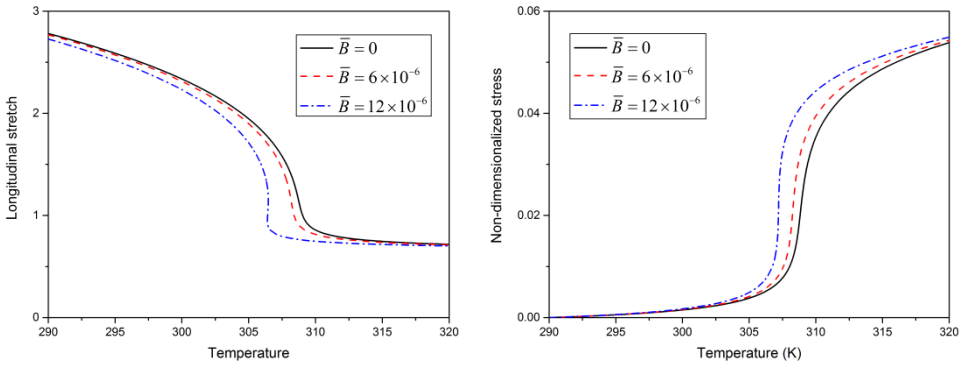

Figure 3-21: (a) in-plane stretch and (b) longitudinal stress of a longitudinally constrained hydrogel.

3.3.3. Numerical procedure for equilibrium swelling of magneto-thermal sensitive hydrogels

In finite element implementation of user-defined materials, commercial finite element software Abaqus is a popular software of choice due to its vast library of subroutines offering wide customizability. For implementation of material properties, Abaqus offers two options: UHYPER and UMAT. The subroutine UHYPER is largely popular with users for the easy implementation.

As a common approach, we implement the material as a hyperelastic model by the definition of the free energy function and its derivatives through the UHYPER subroutine offered by finite element software Abaqus. As the procedure has been documented widely for various types of hydrogels (Ding et al., 2013; Hong et al., 2009a; Marcombe et al., 2010), we did not go through the procedure here, but instead presented all equations required.

The definition of material properties is based on the free energy function derived earlier in equation (3.94) and its respective derivatives with respect to the invariants of the deformation gradient.

Due to singularity in the dry state, we assume an initial free swelling condition of

$$\mathbf{F}_0 = \begin{bmatrix} \lambda_0 & 0 & 0 \\ 0 & \lambda_0 & 0 \\ 0 & 0 & \lambda_0 \end{bmatrix} \tag{3.101}$$

Relative to the initial free swelling state, the current deformation of the gel is, as measured by Abaqus, $\mathbf{F}'$. To obtain the actual deformation gradient of the gel, we write $\mathbf{F} = \mathbf{F}'\mathbf{F}_0$.

Therefore, in all subsequent implementation in Abaqus, we write $J = \lambda_0^3 J'$, where J denotes actual swelling ratio and J' denotes swelling ratio used in Abaqus. The non-dimensionalized free energy density is thus re-written as

$$\begin{aligned} \frac{\nu\hat{W}}{k_B T_0} &= \frac{1}{2} N\nu \left[\lambda_0^2 J'^{\frac{2}{3}} \bar{I}_1 - 3 - 2\ln\left(\lambda_0^3 J'\right) \right] \frac{T}{T_0} \\ &+ \left(\lambda_0^3 J' - 1\right) \left[\ln \frac{\lambda_0^3 J' - 1}{\lambda_0^3 J'} + \frac{\chi_0}{\lambda_0^3 J'} + \frac{\chi_1}{\left(\lambda_0^3 J'\right)^2} - \bar{\mu}^s \right] \frac{T}{T_0} \\ &- N_m \nu \frac{T}{T_0} \ln\left[2\cosh\left(\bar{B} \frac{T_0}{T} \right) \right] - \frac{N_m \nu f_m}{\lambda_0^3 J'} \bar{B} \tanh\left(\bar{B} \frac{T_0}{T} \right) \end{aligned} \tag{3.102}$$

The derivatives of the free energy function are derived to be

$$\frac{\partial\left(\nu\hat{W} / k_B T_0\right)}{\partial \bar{I}_1} = \left(\frac{1}{2} N\nu \lambda_0^2 J'^{\frac{2}{3}} \right) \frac{T}{T_0} \tag{3.103}$$

$$\frac{\partial\left(\nu\hat{W} / k_B T_0\right)}{\partial \bar{I}_2} = 0 \tag{3.104}$$

$$\frac{\partial\left(\nu\hat{W}/k_BT_0\right)}{\partial J'} = N\nu\frac{T}{T_0}\left[\frac{1}{3}\lambda_0^2 J'^{-\frac{1}{3}}\bar{I}_1 - \frac{1}{J'}\right] + \left[\lambda_0^3\ln\frac{\lambda_0^3 J'-1}{\lambda_0^3 J'} + \frac{1}{J'} + \frac{\chi_0-\chi_1}{\lambda_0^3 J'^2} + \frac{2\chi_1}{\lambda_0^6 J'^3} - \bar{\mu}^s\lambda_0^3\right]\frac{T}{T_0} + \frac{N_m\nu f_m}{\lambda_0^3 J'^2}\bar{B}\tanh\left(\bar{B}\frac{T_0}{T}\right) \tag{3.105}$$

$$\frac{\partial^2\left(\nu\hat{W}/k_BT_0\right)}{\partial\bar{I}_1^2} = 0 \tag{3.106}$$

$$\frac{\partial^2\left(\nu\hat{W}/k_BT_0\right)}{\partial\bar{I}_2^2} = 0 \tag{3.107}$$

$$\frac{\partial^2\left(\nu\hat{W}/k_BT_0\right)}{\partial J'^2} = N\nu\frac{T}{T_0}\left(-\frac{1}{9}\lambda_0^2 J'^{-\frac{4}{3}}\bar{I}_1 + \frac{1}{J'^2}\right) + \left(\frac{\lambda_0^3}{J'\left(\lambda_0^3 J'-1\right)} - \frac{1}{J'^2} - \frac{2\left(\chi_0-\chi_1\right)}{\lambda_0^3 J'^3} - \frac{6\chi_1}{\lambda_0^6 J'^4}\right)\frac{T}{T_0} - \frac{2N_m\nu f_m}{\lambda_0^3 J'^3}\bar{B}\tanh\left(\bar{B}\frac{T_0}{T}\right) \tag{3.108}$$

$$\frac{\partial^2\left(\nu\hat{W}/k_BT_0\right)}{\partial\bar{I}_1\partial\bar{I}_2} = 0 \tag{3.109}$$

$$\frac{\partial^2\left(\nu W/k_BT_0\right)}{\partial\bar{I}_1\partial J'} = \left(\frac{1}{3}N\nu\lambda_0^2 J'^{-\frac{1}{3}}\right)\frac{T}{T_0} \tag{3.110}$$

$$\frac{\partial^2\left(\nu W/k_BT_0\right)}{\partial\bar{I}_2\partial J'} = 0 \tag{3.111}$$

$$\frac{\partial^3\left(\nu W / k_B T_0\right)}{\partial \bar{I}_1^2 \partial J'} = 0 \tag{3.112}$$

$$\frac{\partial^3\left(\nu W / k_B T_0\right)}{\partial \bar{I}_2^2 \partial J'} = 0 \tag{3.113}$$

$$\frac{\partial^3\left(\nu W / k_B T_0\right)}{\partial \bar{I}_1 \partial \bar{I}_2 \partial J'} = 0 \tag{3.114}$$

$$\frac{\partial^3\left(\nu W / k_B T_0\right)}{\partial \bar{I}_1 \partial J'^2} = N\nu\left(-\frac{1}{9}\lambda_0^2 J'^{-\frac{4}{3}}\right)\frac{T}{T_0} \tag{3.115}$$

$$\frac{\partial^3\left(\nu W / k_B T_0\right)}{\partial \bar{I}_2^2 \partial J'} = 0 \tag{3.116}$$

$$\begin{aligned}\frac{\partial^3\left(\nu W / k T_0\right)}{\partial J'^3} = N\nu\frac{T}{T_0}&\left(\frac{4}{27}\lambda_0^2 J'^{-\frac{7}{3}}\bar{I}_1 - \frac{2}{J'^3}\right)\\ &+\left(-\frac{\lambda_0^3\left(2\lambda_0^3 J'-1\right)}{J'^2\left(\lambda_0^3 J'-1\right)^2}+\frac{2}{J'^3}+\frac{6\left(\chi_0-\chi_1\right)}{\lambda_0^3 J'^4}+\frac{24\chi_1}{\lambda_0^6 J'^5}\right)\frac{T}{T_0}\\ &+\frac{6N_m\nu f_m}{\lambda_0^3 J'^4}\bar{B}\tanh\left(\bar{B}\frac{T_0}{T}\right)\end{aligned} \tag{3.117}$$

For the initial condition of λ_0 , we solve equation (3.96) at initial temperature T_0 , initial light intensity I_0 and chemical potential μ_0^s .

As with the subroutine developed for the photo-thermal sensitive hydrogel (Section 3.2), this subroutine is limited to one loading parameter at any one time. Therefore simulations were made by varying one field (temperature, magnetic field strength or chemical potential) and keeping the other two fixed.

The required loading parameter was then represented by temperature in Abaqus. For example, to simulate effects of change in chemical potential at fixed temperature and magnetic field strength, we represent chemical potential as a temperature field, with the fixed values of temperature and magnetic field strength as material inputs, together with the crosslink density and initial stretch ratio.

3.3.4. Numerical examples for equilibrium swelling of magneto-thermal sensitive hydrogels

3.3.4.1. *Verification of FE model*

We had verified the numerical results with analytical solutions using the longitudinally constrained cube (presented in Figure 3-21(b)). Figure 3-22 shows the comparison between both sets of results. We can see from the results that FEM is able to correctly predict the swelling ratio of the gel according to theoretical results. As mentioned in Sections 3.1.3 and 3.2.5.1, it is possible to use a single element to simulate the swelling of the gel due to homogeneity.

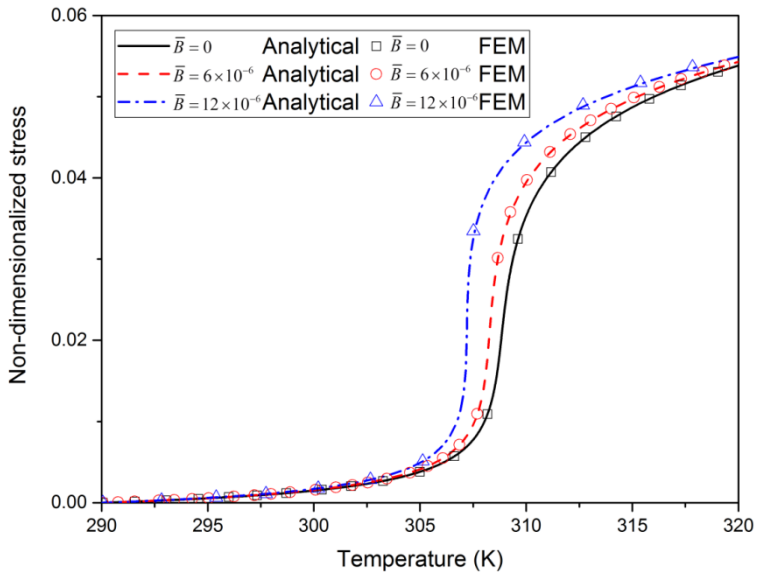

Figure 3-22: Comparison of FEM results (Discrete points) with analytical solution (Solid line)

3.3.4.2. *Applications in microfluidics*

The dependence of the swelling profile on the magnetic field strength proves to be an excellent property for applications in devices which require precise actuation of mechanisms, which may be controlled by the volumetric change of the gel.

We explore a microfluidic valve using a channel consisting of 3 gel pillars. This configuration has been studied extensively (He et al., 2012; Moore et al., 2000). However, contrary to what most studies propose, where the valve is commonly unblocked and swelling of the gel causes flow to be impeded in the valve, we propose the opposite mechanism, which utilizes the magnetic field dependence properties of the gel.

A dry piece of gel (Figure 3-23(a)) was first hydrated, which resulted in a swelling large enough to cause a blockage in the channel (Figure 3-23(c)) This is the operational "OFF" state. In the simulation, 710 CPE4 elements consisting of 803 nodes were used to model the gel, and 80 CPE4 elements consisting of 162 nodes were used to model the wall.

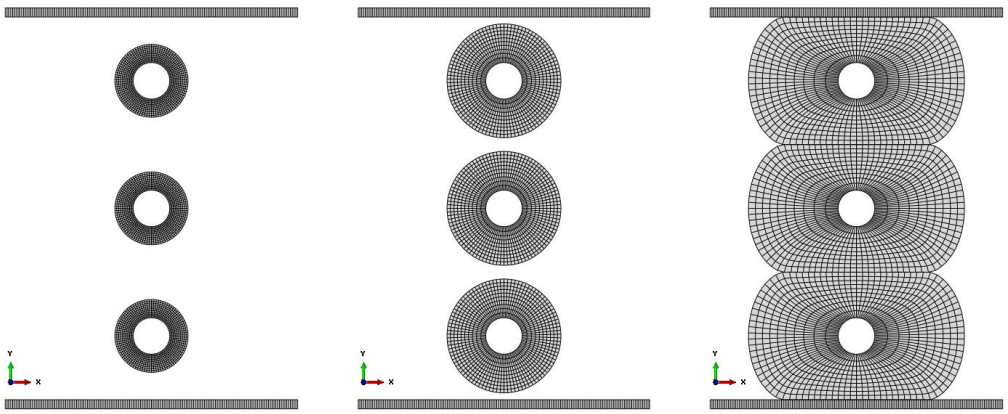

(a) (b) (c)

Figure 3-23: Swelling process of the hydrogel at (a) $\bar{\mu}_0^s = -1$, (b) $\bar{\mu}^s = -0.089$ and (c) $\bar{\mu}^s = 0$.

To switch to the "ON" state, we deswelled the gel by applying a temperature change and magnetic field simultaneously. The temperature change caused large deswelling in the gel and the transition temperature at which the unblocking occurs is controlled by the magnetic field. We measured the size of the opening relative to the hole size in the dry state, i.e. $\frac{l}{l_0}$, where l and l_0 are illustrated in Figure 3-24

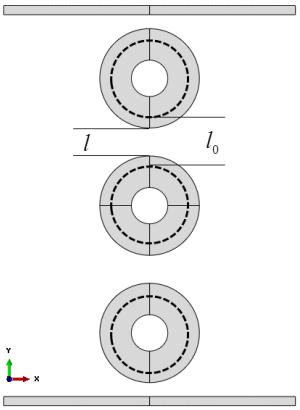

Figure 3-24: Measurement of relative channel opening, dotted line represents initial geometry in the dry state.

As shown in Figure 3-25(b), as the strength of magnetic field is increased, the critical temperature at which the channel starts to occur decreases.

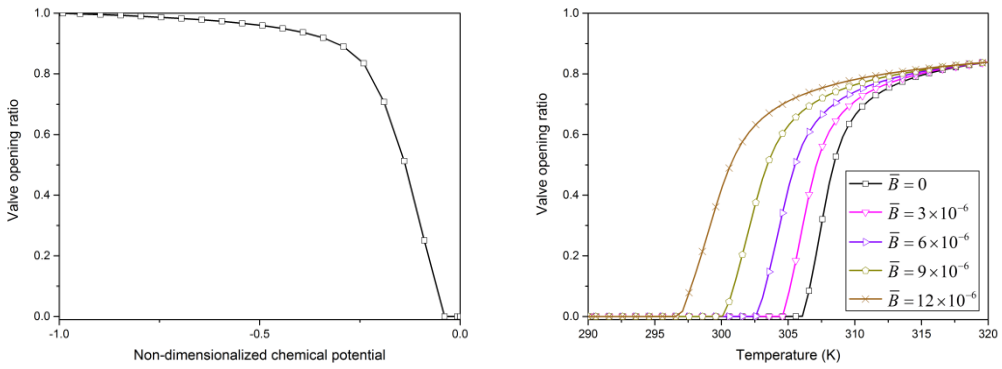

(a) (b)

Figure 3-25: Relative size of channel opening during (a) initial hydration process, (b) switching from "OFF" state to "ON" state.

Using a simple mechanism as proposed, it is possible to decide precisely when the valve opens or closes simply based on the temperature and magnetic field applied.

3.4. Concluding remarks

In this chapter, we have developed equilibrium swelling theories for temperature sensitive, photo-thermal-sensitive and magneto-thermal-sensitive hydrogels. These studies were largely motivated by the phase transition phenomenon that is commonly observed in hydrogels. We had shown that the phase transition of these hydrogels is highly dependent on the material properties and environmental conditions.

The equilibrium theories were developed first in temperature-sensitive hydrogels, and later extended to the dually-sensitive hydrogels based on the same thermodynamic framework. Material parameters used in the analyses were obtained from experimental fittings performed by other researchers. A finite element model for simulating the temperature sensitive hydrogel was developed using UMAT subroutine, by defining the Cauchy stress and the tangent modulus tensor. Numerical examples were presented to compare the difference between implementation using UMAT and UHYPER, and to highlight the advantages of UMAT over UHYPER.

In the thermodynamic theory for photo-thermal sensitive gels, we incorporated effects of photochemical heating into the theory of temperature sensitive hydrogels developed in Section 0. The phase transition of the gel and its dependence on light intensity were studied. The field theory was implemented through the development of a user-defined subroutine UHYPER in a finite element solver by modeling the material as a hyperelastic material. Verification of the finite element formulation and source code was performed by comparison with analytical results for the case of free swelling of a cubic gel. Furthermore, through several examples, we were able to demonstrate that the developed field theory and the finite element formulation can accurately and efficiently predict the deformation of photo-thermal sensitive gels with complex geometries. This was shown through the analyses of deformation of a gel in

coexistent phases, buckling due to the deswelling action and a hybrid hydrogel-membrane light actuated microfluidic valve.

In the theory of magneto-sensitive hydrogels, we incorporated effects of paramagnetic heating into the theory for temperature sensitive hydrogels. The effect of varying magnetic field strength on the phase transition pathway was investigated. In addition, the material properties of the magneto-thermal sensitive hydrogel were implemented in Abaqus using UHYPER. Using this finite element model and utilizing the dependence on magnetic field strength, we proposed a mechanism for microfluidic devices where the opening and closing of the channel may be controlled precisely.

In the numerical simulations performed, we noted that the finite element analysis cannot be completed for cases with discontinuous phase transitions as the solution method was unable to overcome the turning point of the instability.

4. Swelling induced instabilities in hydrogels

When a dry polymer network comes into contact with a solvent, it imbibes the solvent and swells, forming an aggregate known as a hydrogel. Hydrogels may swell to many times their initial volumes, with reports showing a volume change of up to 1,000 times the dry volume. Due to this complex large deformation process, swelling induced instability is a commonly observed phenomenon. The instability of gel deformation causes wrinkling or buckling, which has traditionally been deemed as an undesirable trait in structures. However, there has been significant recent interest in harnessing the instabilities for potential applications, such as gear formation, soft electronics, actuators and tunable adhesion (Kwon et al., 2010; Li et al., 2012a; Rogers et al., 2010; Yang et al., 2010).

The buckling of gels can be broadly classified into two types: bulk buckling and localized surface buckling (DuPont Jr et al., 2010). Many studies had been carried out on the instability mechanisms that a hydrogel experiences during the swelling process. Tanaka et al. (Tanaka et al., 1987) reported that even in the absence of external constraints, a gel may still experience wrinkling during the transient process of swelling. This is due to the differential swelling that occurs between the surface of the gel and the inner layers. The wrinkles that appear are reported to grow with time as solvent molecules diffuse within the gel (Guvendiren et al., 2010a; Peixinho and Mukhopadhyay, 2013). Although abundant literature on the analysis of swelling induced instabilities of gels are available, we note that most of these works involve static analyses, such as that of bi-layer structures (Liu et al., 2011), thin gel structures (Liu et al., 2010; Mora and Boudaoud, 2006; Zhang et al., 2014), functionally graded materials (Wu et al., 2013) and creasing (Hong et al., 2009b).

In this chapter, we investigate this interesting phenomenon of transient wrinkle mode evolution using the finite element and state-space methods. From our simulations and prediction, we find that there is an inverse relation between critical wave number and time, which has earlier been observed in experiments.

4.1. Surface wrinkling in transient swelling

When exposed to an external solvent, a dry polymeric network imbibes the solvent and undergoes large deformation. The resulting aggregate is known as a hydrogel. This swelling process is diffusion driven and thus results in differential swelling during transient swelling. When subjected to external geometrical constraints, such as being rigidly fixed or attached to a compliant substrate, wrinkles have been shown to appear due to mechanical instabilities. In the case of free swelling, there are no external constraints to induce the instabilities accounting for wrinkling patterns. However, during the transient swelling process, the swelling differential between the gel on the exterior and the interior causes compressive stresses and gives rise to mechanical instabilities. It is also observed that the time dependence of the swelling profile causes the wrinkles to evolve with time.

4.1.1. Transient one-dimensional swelling

As a benchmark example, the one-dimensional swelling of a gel blanket attached to a rigid substrate on one side has been investigated extensively (Bouklas and Huang, 2012; Duan et al., 2013). However, in these analyses, there was a common assumption of the non-existence of instabilities. This assumption might not be valid across all cases as the compressive stress induced during swelling will result in the onset of instabilities, as shown in Figure 4-1.

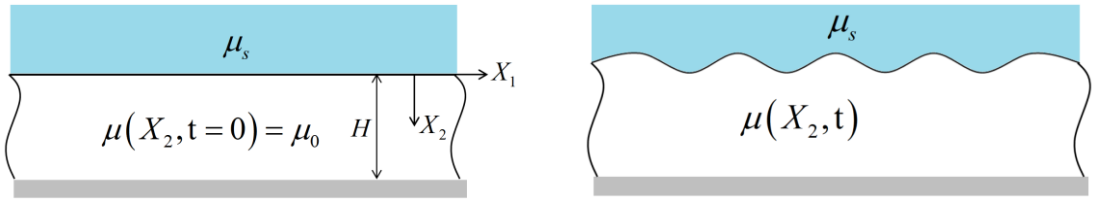

(a) (b)

Figure 4-1: Schematics of a gel exposed to solvent of chemical potential μ_s during (a) initial state of homogeneous swelling at chemical potential of μ_0 , (b) onset of wrinkling at the surface at time *t*.

During the transient state of swelling, the surface of the gel swells faster than the interior of the gel. When this happens, there is a differential in swelling ratios between the surface layer and the layer of gel immediately below the gel surface, resulting in a

compressive stress differential throughout the height of the gel, similar to a functionally graded hydrogel in equilibrium (Wu et al., 2013).

As diffusion progresses, the vertical stress and swelling ratio profiles continually change with time, as shown in Figure 4-2. With an initial homogeneous stretch of $\mathbf{F} = diag\left[\lambda_0, \lambda_0, \lambda_0\right]$, the deformation gradient of the gel at any time is given by $\mathbf{F} = diag\left[\lambda_0, \lambda_0\lambda, \lambda_0\right]$, with λ representing stretch with respect to initial swelling ratio λ_0. This evolution of the profiles implies that the wavelength of the surface wrinkles will also evolve with time.

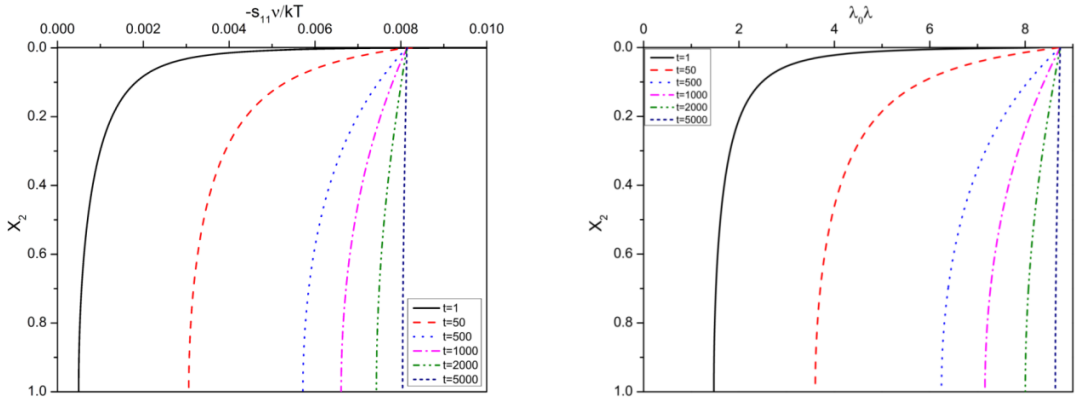

(a) (b)

Figure 4-2: (a) Compressive stresses experienced by a gel with parameters $N\nu = 0.001, \chi = 0.1, \mu_0^s = -1$ swelling under lateral constrains in kinetic analysis, (b) stretch ratio at various times.

Various methods have been developed to solve for the critical conditions of surface wrinkling, such as the finite element method (Lee et al., 2008) and state-space method (Wu et al., 2014). However, these methods were developed for elastic materials rather than gel materials.

4.1.1.1. *Finite element method*

We utilized the subroutine developed in Section 2.1.2 for the simulation of this example. By introducing a perturbation to the mesh, we were able to initiate the onset of surface instabilities in the finite element model. However, it was noted that due to the highly nonlinear feature of the analysis, which resulted in excessive distortion of

elements in the top layer, the finite element model was unable to capture the entire post-buckling analysis. This restricted the simulation of the entire transient evolution of the wrinkles.

To circumvent this problem, we controlled the wavelengths that appeared by using 8 columns elements for each wavelength of the surface wrinkle (Figure 4-3(a)) and imposing periodic multipoint constraints (MPCs) on the surface nodes. Referring to Figure 4-3(b), the MPC were defined as such by setting all vertical displacements of points A (u_A) to be equal, all vertical displacements of points B (u_B) to be equal, all vertical displacements of points C (u_C) to be equal, all vertical displacements of points D having amplitudes equal to the negative of u_B, i.e. $u_B - u_A = u_A - u_D$ and all vertical displacements of points E having amplitudes equal to the negative of u_C, i.e. $u_C - u_A = u_A - u_E$.

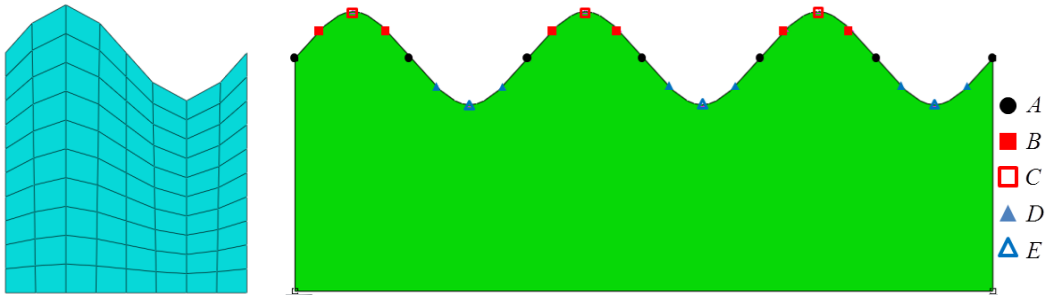

(a) (b)

Figure 4-3: (a) Discretization of a single waveform into 8 elements. (b) Imposition of MPC at surface nodes

Through this MPC imposition, we were able to obtain characteristic times of onset of instability for different wavelengths. The simulation was mesh-independent as the characteristic times showed a trend of convergence for meshes of different refinement. For computational efficiency, graded meshing was used for all simulations, with thickness of the top layer mesh ranging from 0.1% to 5% of gel thickness H, and thickness of bottom-most layer mesh fixed at 20% of H. Figure 4-4 shows three graded meshes of different sizes with top layer mesh thickness of 1%, 0.5% and 0.1%.

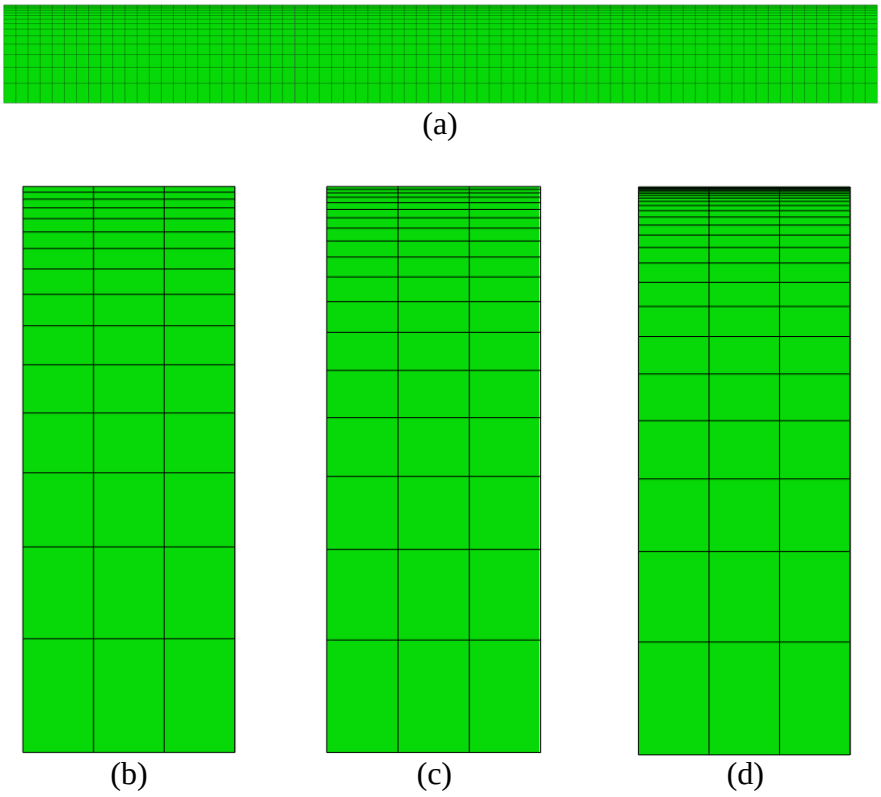

Figure 4-4: (a) Full finite element model of the gel, with thickness 1 and width of 10. (b), (c) and (d) shows different meshes with top layer mesh thickness of 0.01H, 0.005H and 0.001H respectively. Note that meshes (b) to (d) are shortened with width to illustrate the graded mesh used in simulations.

Figure 4-5 shows the time of onset of instability for the case of 10 and 15 waves, with meshes of varying refinement. It can be seen that the predicted times of onset of instability converges as the mesh was gradually refined. Therefore, for all subsequent simulations, we assigned a top layer mesh thickness of 0.001H. Depending on the wavelength, the number of elements in the simulation range from 600 to 20000. The gel was given a fixed boundary condition at the bottom surface and no lateral displacements on the side surfaces. At the top surface, the gel was exposed to a chemical potential of 0 together with MPC discussed earlier.

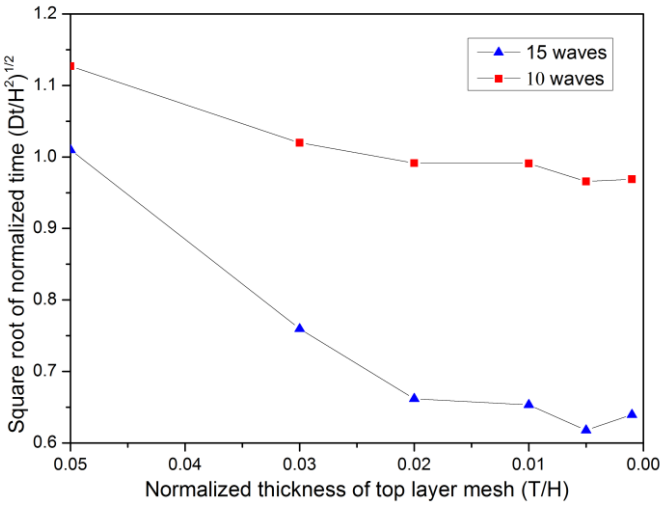

Figure 4-5: Time of onset of wrinkling with increasing refinement of mesh for models with 10 and 15 waves within the width of the gel.

Arranging the wrinkled states according to the size of the wrinkles, we obtained the profiles shown in Figure 4-6. The wave number follows an inverse relationship with square root of time (Figure 4-7(a)). Plotting the wavelengths against the corresponding time of onset of the instabilities, we obtained a linear relationship (Figure 4-7(b)), which had also been observed experimentally (Guvendiren et al., 2010a).

In the limiting case where wavelength is reduced to zero, we predict that the onset of buckling will occur immediately on exposure to solvent. Experimentally, this is observed as a very large number of surface wrinkles appearing during the initial phase of swelling, which coalesces with time to form larger wrinkles, i.e. the number of wrinkles decrease with time (Peixinho and Mukhopadhyay, 2013; Tanaka et al., 1987). It is predicted that the wrinkles of a gel with lower crosslink density grows faster than a highly crosslinked gel.

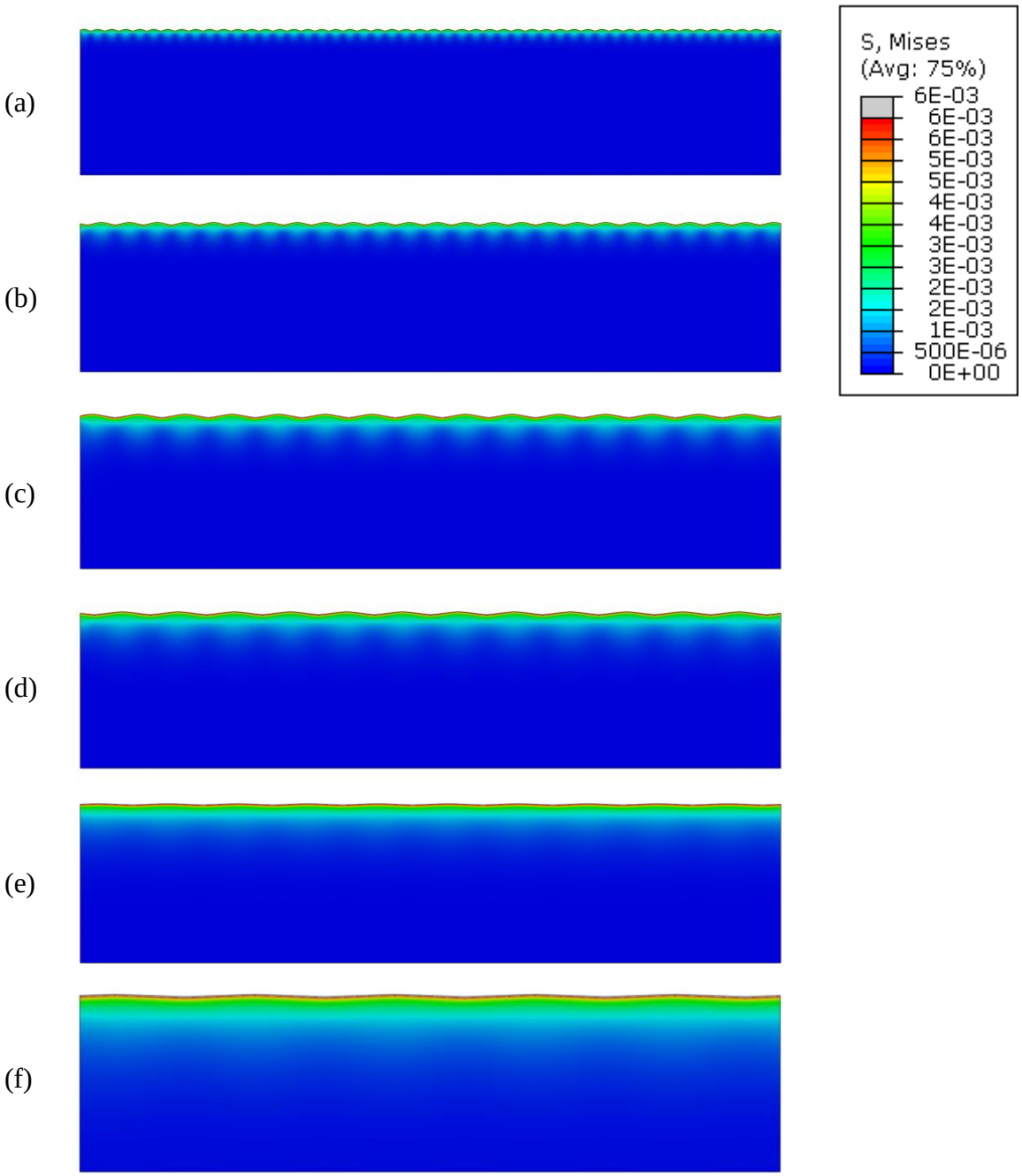

Figure 4-6: Evolution of surface wrinkles of a hydrogel layer. Note that only half of the full length is represented. Number of waves for the full length of the gel decreases from (a) 100, (b) 50, (c) 30, (d) 25, (e) 20 to (f) 10.

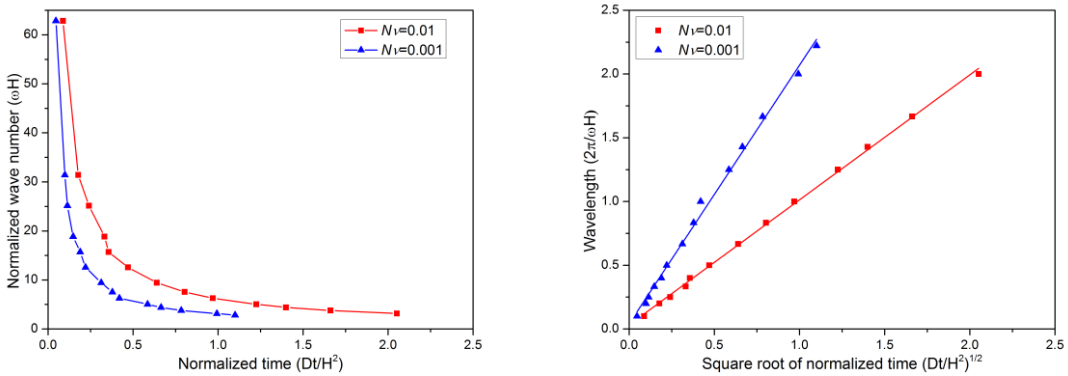

(a) (b)

Figure 4-7: (a) wave number vs time, (b) wavelength vs time for gels of crosslink densities at $N\nu = 0.001$ and $N\nu = 0.01$; Flory-interaction parameter $\chi = 0.1$; and initial chemical potential of $\bar{\mu}_0^s = -1$.

4.1.1.2. *Linear perturbation analysis and state-space solution*

Following the approach of Wu et al. (Wu et al., 2013; Wu et al., 2014), we formulated an eigenvalue problem by performing linear perturbation analysis to the swelling gel. This eigenvalue problem was then solved for the critical wave number using state-space formulation, which was used to solve for the critical conditions for the onset of surface instability of a functionally graded elastic material (Wu et al., 2014).

In what follows, we derive the state equation for the gel at any time *t*. The interested reader may refer to the original reference for the full derivation of the state-space method. First, we divide the gel layer into *n* homogeneous sublayers with equal thickness but different swell states. The deformation gradient of the i^{th} sublayer is $\mathbf{F}_i = diag\left[\lambda_0, \lambda_0\lambda_i, \lambda_0\right]$.

For each sublayer, we consider incremental displacements Δu_i such that the increment in deformation gradient, $\Delta F_{iJ} = \Delta u_{i,k} F_{kJ}$, where

$$\Delta u_{i,k} = \begin{pmatrix} \Delta u_{1,1} & \Delta u_{1,2} & 0 \\ \Delta u_{2,1} & \Delta u_{2,2} & 0 \\ 0 & 0 & 0 \end{pmatrix} \tag{4.1}$$

The deformation gradient after linear perturbation is thus

$$\tilde{\mathbf{F}} = \mathbf{F} + \Delta\mathbf{F} = \begin{pmatrix} \lambda_0\left(1+\Delta u_{1,1}\right) & \lambda_0\lambda\Delta u_{1,2} & 0 \\ \lambda_0\Delta u_{2,1} & \lambda_0\lambda\left(1+\Delta u_{2,2}\right) & 0 \\ 0 & 0 & \lambda_0 \end{pmatrix} \tag{4.2}$$

Retaining the linear terms of increments, the volumetric ratio is approximated by

$$J = \det\tilde{\mathbf{F}} \approx \lambda_0^3\lambda\left(1+\varepsilon\right) \tag{4.3}$$

where $\varepsilon = \Delta u_{1,1} + \Delta u_{2,2}$.

The nominal stress of a hydrogel is given by

$$\frac{\nu s_{iK}}{k_B T} = N\nu\left(F_{iK} - H_{iK}\right) + \left[J\ln\left(\frac{J-1}{J}\right) + 1 + \frac{\chi}{J} - \frac{\mu^s}{k_B T}J\right]H_{iK} \tag{4.4}$$

where $\mathbf{H}$ is the transpose of the inverse of $\mathbf{F}$.

For convenience, we rewrite the nominal stress as

$$\frac{\nu s_{iK}}{k_B T} = N\nu\left(F_{iK} + \xi_1 M_{iK}\right) \tag{4.5}$$

where $\xi_1 = -\frac{1}{J} + \frac{1}{N\nu}\left[\ln\left(\frac{J-1}{J}\right) + \frac{1}{J} + \frac{\chi}{J^2} - \frac{\mu^s}{k_B T}\right]$ and $M_{iJ} = JH_{iJ} = \frac{1}{2}\varepsilon_{ipq}\varepsilon_{Jkl}F_{pk}F_{ql}$.

For the state-space method, we consider the stress increment

$$\Delta\bar{s}_{iK} = N\nu\left(\Delta F_{iK} + \Delta\xi_1 M_{iK} + \xi_1\Delta M_{iK}\right) \tag{4.6}$$

where $\Delta\xi_1 = \xi_2\varepsilon$ and $\xi_2 = \left[\frac{1}{J^2} + \frac{1}{N\nu}\left(\frac{1}{J-1} - \frac{1}{J} - \frac{1}{J^2} - \frac{2\chi}{J^3}\right)\right]\lambda_0^3\lambda$.

The components of incremental stress are derived to be

$$\Delta\bar{s}_{11} = N\nu\left[\left(\lambda_0 + \lambda_0^2\lambda\xi_2\right)\Delta u_{1,1} + \lambda_0^2\lambda\left(\xi_1 + \xi_2\right)\Delta u_{2,2}\right] \tag{4.7}$$

$$\Delta\bar{s}_{12} = N\nu\left[\lambda_0\lambda\Delta u_{1,2} - \lambda_0^2\xi_1\Delta u_{2,1}\right] \tag{4.8}$$

$$\Delta\bar{s}_{21} = N\nu\left[-\lambda_0^2\lambda\xi_1\Delta u_{1,2} + \lambda_0\Delta u_{2,1}\right] \tag{4.9}$$

$$\Delta\bar{s}_{22} = N\nu\left[\lambda_0^2\left(\xi_1+\xi_2\right)\Delta u_{1,1} + \left(\lambda_0\lambda + \xi_2\lambda_0^2\right)\Delta u_{2,2}\right] \tag{4.10}$$

Re-arranging equations (4.8) and (4.10), we obtain expressions for $\Delta u_{1,2}$ and $\Delta u_{2,2}$,

$$\Delta u_{1,2} = \frac{1}{N\nu\lambda_0\lambda}\Delta\bar{s}_{12} + \frac{\lambda_0}{\lambda}\xi_1\Delta u_{2,1} \tag{4.11}$$

$$\Delta u_{2,2} = \frac{1}{N\nu\lambda_0\left(\lambda+\xi_2\lambda_0\right)}\Delta\bar{s}_{22} - \frac{\left(\xi_1+\xi_2\right)\lambda_0}{\lambda+\xi_2\lambda_0}\Delta u_{1,1} \tag{4.12}$$

Taking the derivatives of equations (4.7) and (4.10) with respect to x_1 and substituting equations (4.11) and (4.12) gives

$$\Delta\bar{s}_{11,1} = \left\{N\nu\left[\lambda_0\left(1+\xi_2\lambda_0\lambda\right) - \frac{\lambda_0^3\lambda\left(\xi_1+\xi_2\right)^2}{\lambda+\xi_2\lambda_0}\right]\right\}\Delta u_{1,11} + \left\{\frac{\lambda_0\lambda\left(\xi_1+\xi_2\right)}{\left(\lambda+\xi_2\lambda_0\right)}\right\}\Delta\bar{s}_{22,1} \tag{4.13}$$

$$\Delta\bar{s}_{21,1} = \left\{N\nu\lambda_0\left(1-\lambda_0^2\xi_1^2\right)\right\}\Delta u_{2,11} + \left\{-\lambda_0\xi_1\Delta\bar{s}_{12,1}\right\} \tag{4.14}$$

Substituting into the mechanical equilibrium equation $\Delta s_{iJ,J} = 0$, equations (4.13) and (4.14) become

$$\Delta\bar{s}_{12,2} = \left\{N\nu\left[\frac{\lambda_0^3\lambda\left(\xi_1'+\xi_2'\right)^2}{\lambda+\xi_2\lambda_0} - \lambda_0\left(1+\xi_2'\lambda_0\lambda\right)\right]\right\}\Delta u_{1,11} - \left\{\frac{\lambda_0\lambda\left(\xi_1'+\xi_2\right)}{\left(\lambda+\xi_2\lambda_0\right)}\right\}\Delta\bar{s}_{22,1} \tag{4.15}$$

$$\Delta\bar{s}_{22,2} = \left\{N\nu\lambda_0\left(\lambda_0^2\xi_1^2 - 1\right)\right\}\Delta u_{2,11} + \left\{\lambda_0\xi_1'\right\}\Delta\bar{s}_{12,1} \tag{4.16}$$

Next, we assume that the incremental displacements and stresses take sinusoidal forms, we express

$$\left.\begin{aligned}\Delta u_1 &= U_1(x_2)\sin\omega x_1\\ \Delta u_2 &= U_2(x_2)\cos\omega x_1\\ \Delta s_{12} &= T_1(x_2)\sin\omega x_1\\ \Delta s_{22} &= T_2(x_2)\cos\omega x_1\end{aligned}\right\} \tag{4.17}$$

Substituting equation (4.17) into equations (4.11), (4.12), (4.15) and (4.16) and simplifying,

$$U_1^{'} = -\frac{\xi_1\omega\lambda_0}{\lambda}U_2 + \frac{1}{\lambda_0\lambda N\nu}T_1 \tag{4.18}$$

$$T_2^{'} = -\omega^2 N\nu\lambda_0\left(\lambda_0^2\xi_1^2 - 1\right)U_2 + \xi_1\lambda_0\omega T_1 \tag{4.19}$$

$$U_2^{'} = -\frac{(\xi_1+\xi_2)\lambda_0}{\lambda+\xi_2\lambda_0}\omega U_1 + \frac{1}{N\nu\lambda_0(\lambda+\xi_2\lambda_0)}T_2 \tag{4.20}$$

$$T_1^{'} = \omega^2\lambda_0 N\nu\left[\left(1+\xi_2\lambda_0\lambda\right) - \frac{\lambda_0^2\lambda\left(\xi_1+\xi_2^{'}\right)^2}{\lambda+\xi_2\lambda_0}\right]U_1 + \omega\left(\frac{(\alpha+\xi_2)\lambda_0\lambda}{\lambda+\xi_2\lambda_0}\right)T_2 \tag{4.21}$$

Writing the above equations (4.18) to (4.21) in state-space format gives

$$\frac{d}{dx_2}\begin{bmatrix}U_1\\ T_2\\ U_2\\ T_1\end{bmatrix} = \mathbf{A}\begin{bmatrix}U_1\\ T_2\\ U_2\\ T_1\end{bmatrix} \tag{4.22}$$

where **A** is a 4×4 square matrix as shown below

$$\mathbf{A}=\begin{bmatrix} 0 & 0 & -\dfrac{\xi_1\omega\lambda_0}{\lambda} & \dfrac{1}{N\nu\lambda_0\lambda} \\ 0 & 0 & \omega^2 N\nu\lambda_0\left(1-\lambda_0^2\xi_1^2\right) & \xi_1\lambda_0\omega \\ -\dfrac{\left(\xi_1+\xi_2\right)\lambda_0}{\lambda+\xi_2\lambda_0}\omega & \dfrac{1}{N\nu\lambda_0\left(\lambda+\xi_2\lambda_0\right)} & 0 & 0 \\ \xi_3 & \omega\left(\dfrac{\left(\alpha+\xi_2\right)\lambda_0\lambda}{\lambda+\xi_2\lambda_0}\right) & 0 & 0 \end{bmatrix},$$

$$\xi_3=\omega^2\lambda_0 N\nu\left[\left(1+\xi_2\lambda_0\lambda\right)-\frac{\lambda_0^2\lambda\left(\xi_1+\xi_2^{'}\right)^2}{\lambda+\xi_2\lambda_0}\right],$$

The state equation (4.22) is solved by the exponential matrix operation,

$$\begin{bmatrix} U_1\left(x_{2,n}\right) \\ T_2\left(x_{2,n}\right) \\ U_2\left(x_{2,n}\right) \\ T_1\left(x_{2,n}\right) \end{bmatrix}=e^{\mathbf{A}h}\begin{bmatrix} U_1\left(x_{2,n-1}\right) \\ T_2\left(x_{2,n-1}\right) \\ U_2\left(x_{2,n-1}\right) \\ T_1\left(x_{2,n-1}\right) \end{bmatrix}=\mathbf{D}\begin{bmatrix} U_1\left(x_{2,n-1}\right) \\ T_2\left(x_{2,n-1}\right) \\ U_2\left(x_{2,n-1}\right) \\ T_1\left(x_{2,n-1}\right) \end{bmatrix} \tag{4.23}$$

With *n* sublayers, each sublayer possesses a distinct **A** matrix, $\mathbf{A}_i$, which is dependent on the swelling ratio of the layer, λ_i, taken to be the average value of the two end values of the sublayer. Thus, the state equation for each sublayer can be written as $\mathbf{Q}\left(x_{2,i}\right)=\mathbf{D}_i\left(h_i\right)\mathbf{Q}\left(x_{2,i-1}\right)$. Observing continuity between sublayers, the state equation for the entire gel layer is written as $\mathbf{Q}\left(x_{2,n}\right)=\mathbf{K}\mathbf{Q}\left(x_{2,1}\right)$, where $\mathbf{K}=\prod_{i=1}^{n}\mathbf{D}_i$.

Applying boundary conditions of fixed displacement at the bottom, $U_1\left(x_{2,n}\right)=U_2\left(x_{2,n}\right)=0$, and traction free condition $T_1\left(x_{2,1}\right)=T_2\left(x_{2,1}\right)=0$ at the top, the state equation for the entire gel becomes

$$\begin{bmatrix} 0 \\ T_2\left(x_{2,n}\right) \\ 0 \\ T_1\left(x_{2,n}\right) \end{bmatrix} = \mathbf{K} \begin{bmatrix} U_1\left(x_{2,1}\right) \\ 0 \\ U_2\left(x_{2,1}\right) \\ 0 \end{bmatrix} \tag{4.24}$$

which reduces to

$$\begin{bmatrix} K_{11} & K_{13} \\ K_{31} & K_{33} \end{bmatrix} \begin{pmatrix} U_1\left(x_{2,1}\right) \\ U_2\left(x_{2,1}\right) \end{pmatrix} = 0 \tag{4.25}$$

The critical condition for onset of surface instability is determined when the equation (4.25) gives non-trivial solutions, i.e.

$$\det \begin{bmatrix} K_{11} & K_{13} \\ K_{31} & K_{33} \end{bmatrix} = 0 \tag{4.26}$$

Solution of equation (4.26) yields the critical wave number ω at each time step. Using the swelling ratio profile (Figure 4-2(b)) for each time step, we treat each time step as a quasi-static step and are able to obtain the time dependence of critical wave numbers. In this calculation, it is assumed that the surface wrinkles are of magnitudes small enough to not cause any instability in the diffusion flux such that the stress and swelling profile from 1D calculations are valid.

Unlike the finite element simulations, the results of state-space analysis does not depend on the discretization, i.e. top layer thickness. This is as the state-space method considers all the layers as an entire gel, whereas finite element simulation resembles a bilayer structure. Figure 4-8 shows state-space predictions for gels which are discretized into 50 layers and 1000 equal layers. These predictions do not differ significantly from that obtained from finite element simulations.

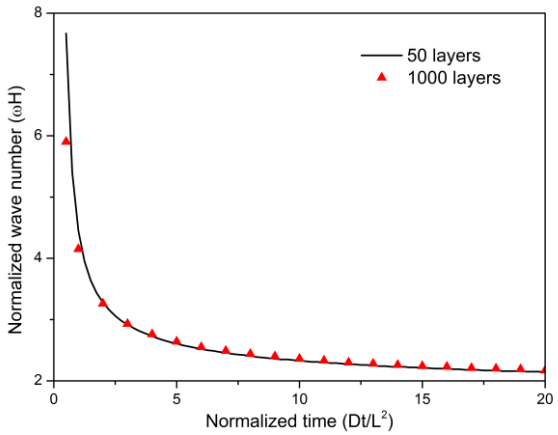

Figure 4-8: Comparison between state-space predictions for different discretization of gel layers.

4.1.2. Comparison between FEM and linear perturbation

Figure 4-9 shows the results obtained from both the finite element and state-space methods. It shows that the state-space method underestimates the critical wave number at all times. This may be due to the strong dependence of linear perturbation analysis on the choice of base state when large deformation is present during the swelling of a gel. Deviations of the state-space model have also been observed in the analysis of elastic materials possessing large strains of more than a few percent (Wu et al., 2014).

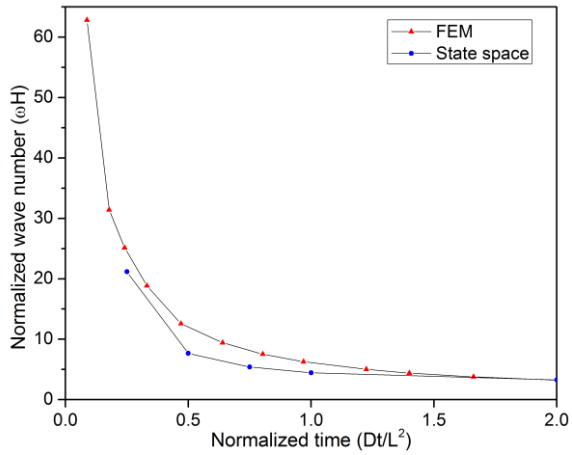

Figure 4-9: Normalized wave number vs time for FEM and state-space methods for $N\nu = 0.01, \chi = .1, \bar{\mu}_0^s = -1$.

While underestimating the critical wave number, the state-space method is proven to be more computationally efficient. This semi-analytical method can provide an

informed estimate for predicting the transient wave evolution with time of a swelling gel.

As a side note, the methods proposed in this work were developed for surface wrinkling of gels. However, they might be extended to the analysis of creasing instability, for example, through the introduction of small defects to initiate the creasing process, as seen from the similar works involving static analysis of creasing (Cao and Hutchinson, 2011; Hohlfeld and Mahadevan, 2011, 2012; Weiss et al., 2013; Wong et al., 2010).

During finite element simulation, the time taken for the onset of surface wrinkles on a swelling gel was characteristic of the wrinkle size. Simulation terminated quickly after reaching the wrinkled state. Although a full post-buckling simulation is not possible, we had shown that through the imposition of periodic multipoint constraints, onset of wrinkling at different times could be initiated. Through this wavelength method, a post-buckling analysis of the evolution of wrinkles could be obtained. For the constrained swelling of a gel blanket, the wavelength of the wrinkles was predicted to follow a linear relation with square root of time, similar to experimental observations. In addition, the state-space method for surface instability was adopted and modified to develop semi-analytical solutions for the critical wave number for surface instabilities of a swelling gel. The trend of decaying critical wave number with time was similar with results obtained from the finite element method. However, the state-space method underestimated the critical wave number as compared with finite element results.

4.2. Buckling of an annular gel ring

The onset of instabilities during the swelling process is an interesting phenomena, and is being studied for possible applications, such as microfluidics, wetting and tunable adhesion (Yang et al., 2010).

Through studies on the buckling behavior of gels (Liu et al., 2010; Liu et al., 2011; Liu et al., 2013; Mora and Boudaoud, 2006), we know that buckling occurs for some geometries, such as a thin film bounded on a substrate and an annulus fixed at the inner wall, see Figure 4-10. These studies assume that chemical potential is homogenous for all stages of swelling This is, however, not reflective of the entire transient swelling process, as it takes time for the solvent molecules to diffuse into the gel. Furthermore, buckling sets in during the transient swelling stage and not the equilibrium homogenous stage.

In this section, we will utilize the kinetic models developed in Chapter 2 to study the transient process of buckling in thin annular gels.

4.2.1. Neutral gel

Upon the onset of buckling, there will be an initial transition between different mode shapes before the gel settles in the equilibrium mode shape and continues to swell in the buckled mode until chemical potential reaches the equilibrium state. This phenomena can be seen in earlier experiments conducted by (Mora and Boudaoud, 2006), where similar gel annuli were immersed in a solution until equilibrium.

In the model shown, 4356 C3D8T elements and 5940 nodes were used. The annulus was fixed at the inner surface and exposed to solvent of chemical potential $\bar{\mu}^s = 0$ on the other surfaces.

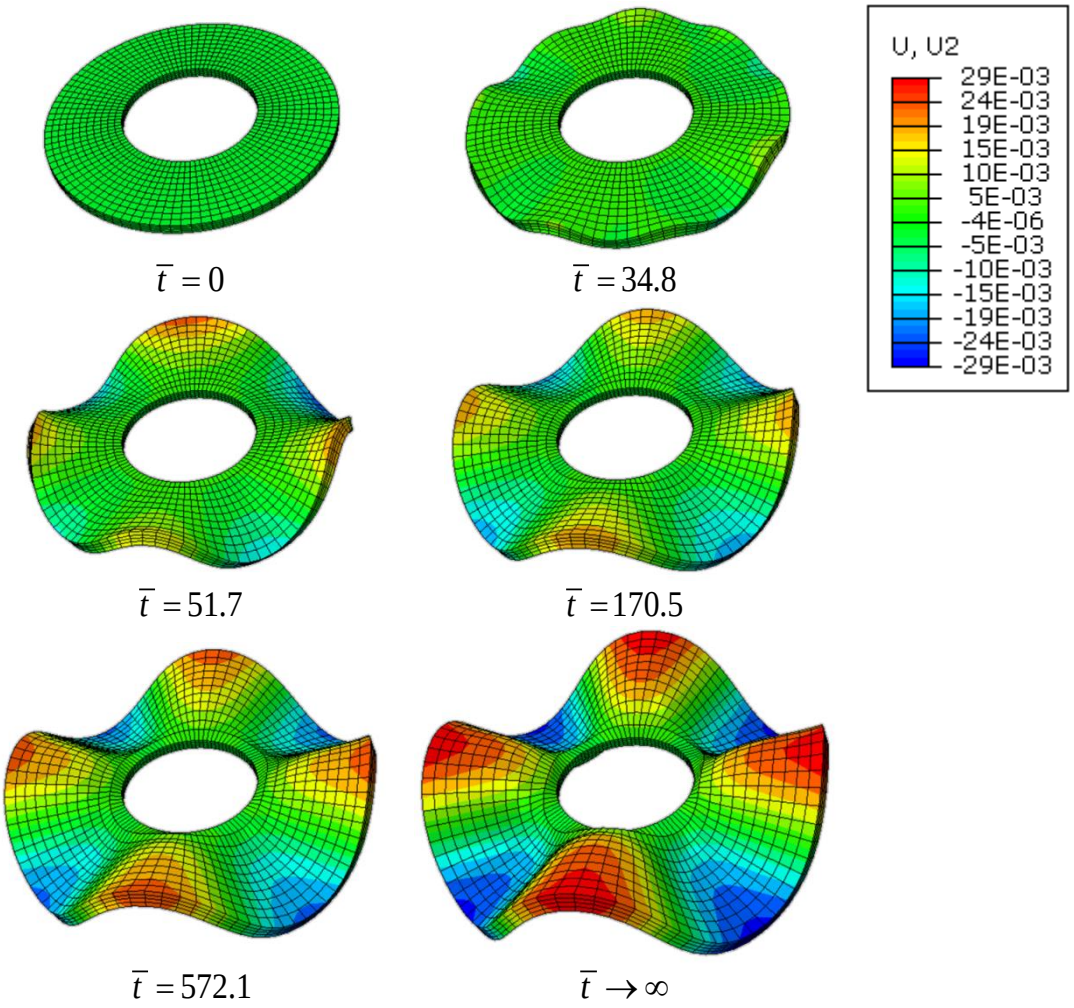

Figure 4-10: Contour plot of y-displacement of an annulus with height 5mm, inner radius 35mm and outer radius 75mm. The inner core of the annulus is fixed and the remaining sides are exposed to external solvent.

Figure 4-11 shows the Mises stress-time curves of one of the peaks (illustrated in inset of Figure 4-11) in the equilibrium mode shape for two simulations performed with different time steps. We can see that the stress at the node experiences a sudden change in magnitude until a minimum, before increasing again. The start of this sudden change indicated the first sign of wrinkling and the minimum point represented the point when the final mode shape was obtained. In the transition between these two points, the variation of stress differed for simulations of different time steps.

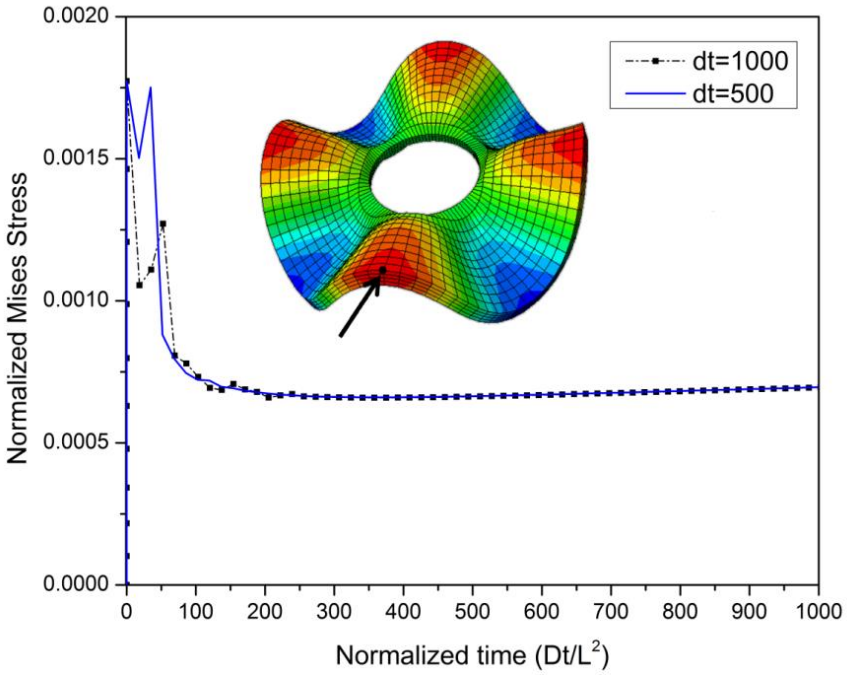

Figure 4-11: Mises stress at the peak of wrinkle for 2 different time steps.

The instability in wrinkle formation of the gel could be observed during the initial phase of wrinkle formation, from the onset of wrinkles to the point when the final mode shape was first obtained. The transitions varied for simulations of different time steps, which reflected the irregularity of wrinkle formation. However, once the final mode shape was obtained, the gel continued to swell in the same mode shape till equilibrium.

4.2.2. Temperature sensitive hydrogel

The patterns arising from the differential swelling of the gels were investigated experimentally and theoretically as a model for the differential growth of living tissues (Liu et al., 2013; Wu et al., 2013). Here we focus on the study of swelling of the annulus gel fixed at the inner wall as an example. It has been generally accepted that buckling pattern depends on the ratio between inner radius and outer radius of the annulus gel (Mora and Boudaoud, 2006). However, transient analysis indicated that there will be transitions between different mode shapes before the gel settle in the equilibrium mode shape. In addition, the buckling patterns will twist after reaching the equilibrium mode shape, as shown in Figure 4-12. To have a better understanding about the swelling process, we plotted the stress and vertical displacement of selected points as shown in Figure 4-13.

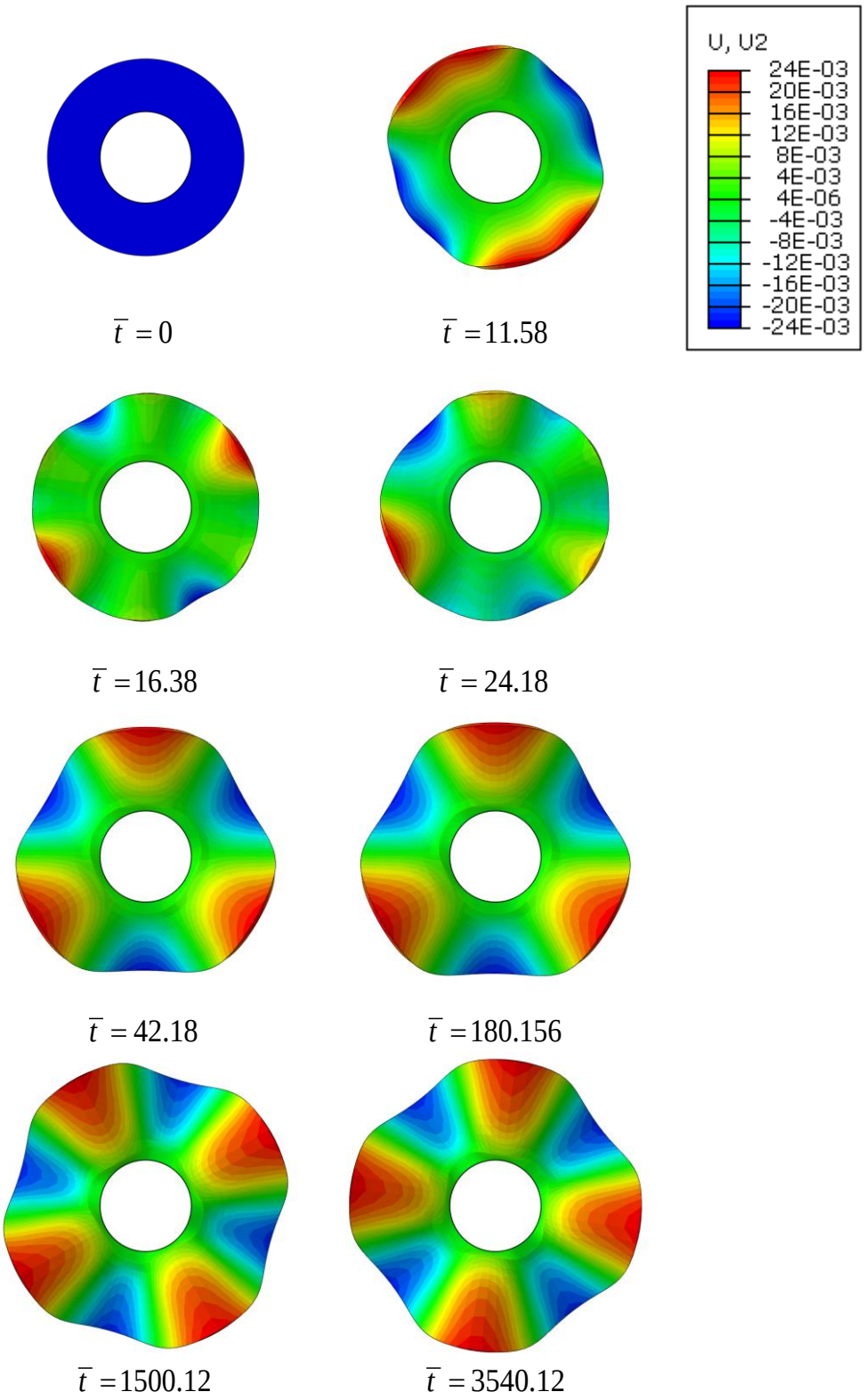

Figure 4-12: Contour

plot of *y*-displacement showing the evolution of wrinkles of an annulus with height 5mm, inner radius 50mm and outer radius 75mm. The transition of buckling

wavelengths from one mode to another can be observed here. The formation of unstable buckling modes causes a travelling wave to propagate around the annulus

It can be observed from Figure 4-13 that mode transitions often happen within the first 50 units of time. In accordance, there are much fluctuations in stress curves and displacement curves as shown in Figure 4-13. After that the annulus will swell under the third mode for about 500 units of time. At about $\bar{t} = 700$, the annulus will turn to the fourth mode and start to rotate at about $\bar{t} = 1500$. This mode transition phenomenon has been observed in earlier simulations conducted using polymeric gels in Section 4.2.1. Though there are mode transitions, the equilibrium mode shape is consistent with the experimental observations (Mora and Boudaoud, 2006) and static simulations (Liu et al., 2013). To our best knowledge, there is no experimental report for the rotational instability of the swelling annulus, but such instability has been predicted numerically (Freund, 2000) and observed experimentally (Holmes et al., 2011) for a swelling disk. Due to the axial symmetry, there are numerous energy favorable orientations for the equilibrium mode shape. Perturbation can lead to re-orientations into other minimum energy states. In our simulations, the dynamics of diffusion and swelling may cause perturbation significant enough to cause a travelling buckle wave to propagate around the annulus.

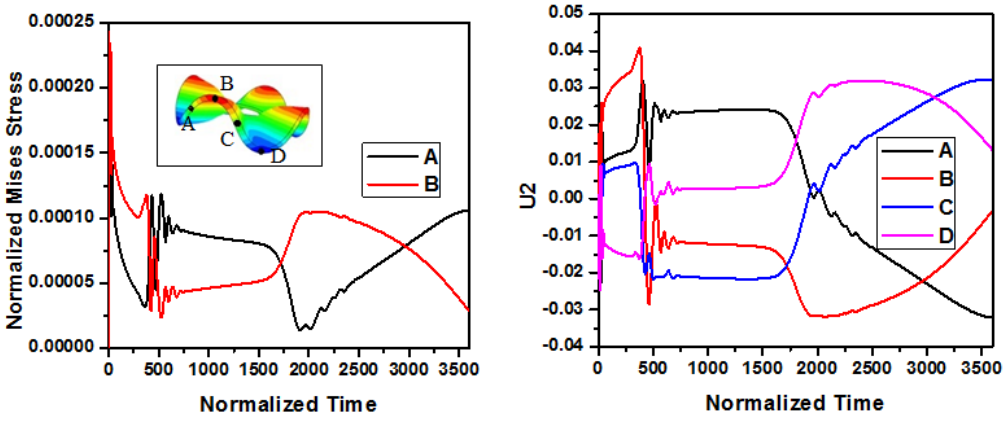

(a) (b)

Figure 4-13: Von-Mises stress (a) and vertical displacement (b) as a function of time of the selected point during the swelling process. Mode transitions happen often within the first 50 unit time at about $\bar{t} = 700$ the annulus turns to the fourth mode and buckle starts to rotate at about $\bar{t} = 1500$.

4.2.3. *pH-sensitive* hydrogel

The onset of instabilities during the swelling of gels is a well-known phenomenon. A better understanding of this phenomenon will allow for more potential applications such as microfluidics, wetting, tunable adhesion and surface topography (Chen and Yang, 2012; Yang et al., 2010). There are many works studying the wrinkling of swelling gels, but these works focus on the equilibrium swelling state and do not take into account the diffusion kinetics within the gel (Liu et al., 2010; Liu et al., 2011).

Similar to the kinetics of a neutral hydrogel, the finite element model developed for *pH*-sensitive gels is also able to simulate cases of swelling induced instabilities, such as wrinkling of thin gel sheets attached to a rigid surface. To demonstrate this instability, we investigated the formation of wrinkles in a thin annular gel, fixed at the inner core.

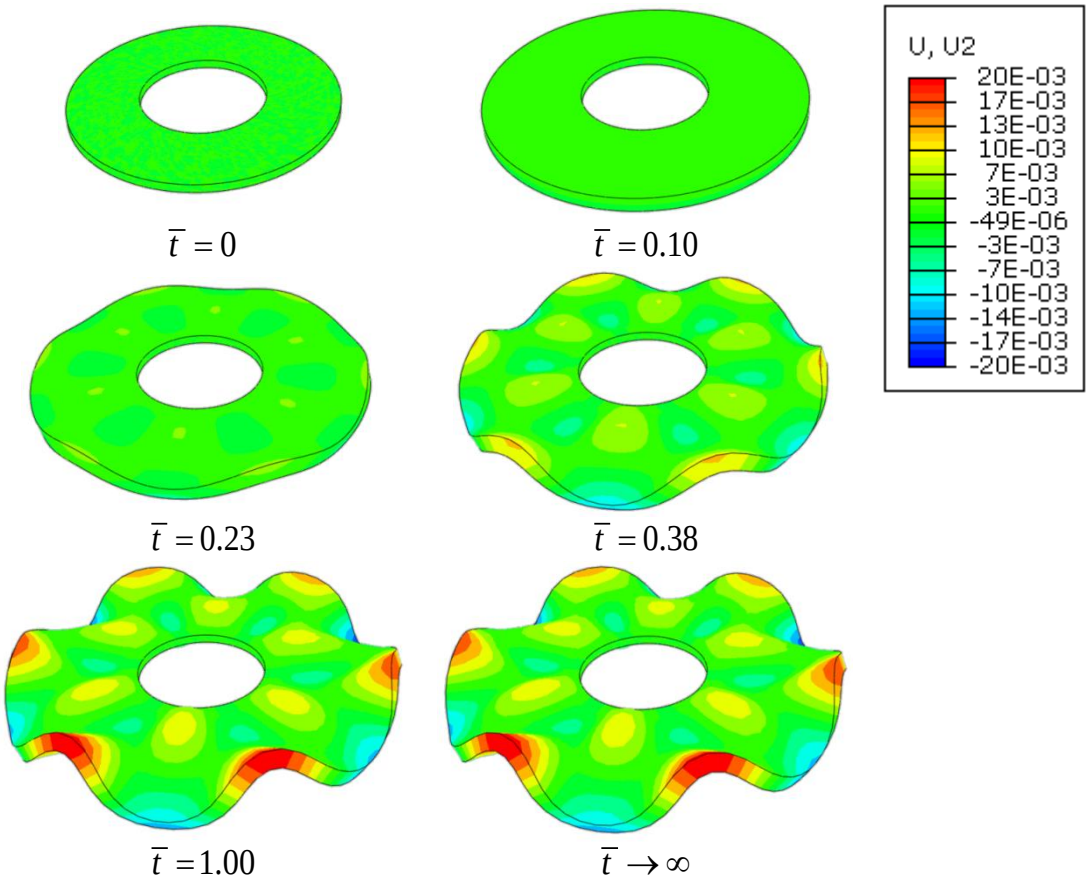

Figure 4-14: Contour plot of normal direction displacement of an annulus, initially in equilibrium at *pH*=3 and height 5mm, inner radius 35mm and outer radius 75mm. The inner core of the annulus is fixed and the remaining sides are exposed to of *pH*=8.

In the simulation, 4356 eight-node brick temperature-displacement elements (C3D8T) were used to mesh the annulus. During the swelling of the annulus, wrinkling does not occur immediately upon exposure to a solvent of higher *pH*-value. Instead, it swells symmetrically and radially until a critical point, where the stress reaches the critical level, before wrinkling to reduce the stress present. The swelling and wrinkling process of the gel is shown in Figure 4-14.

4.3. Buckling control of a gel strip

In the swelling of thin gel structures confined partially, compressive stresses will build up and subsequently cause buckling of gel structures with certain geometries into waves. Examples of such geometries include a thin rectangular strip, a flat annulus and a thin walled ring (Lee et al., 2012; Mora and Boudaoud, 2006). The size of the waves is hugely dependent on the geometry of the gel (Liu et al., 2010; Liu et al., 2011). For circular wavy structures, potential applications such as soft gears have been proposed (Yin et al., 2009; Zhang et al., 2010).

In this section, we explore the buckling and unbuckling of a thin rectangular gel strip confined on one side laterally. It has been shown that the size of the buckled waves is related to the geometry. With a photo-thermal sensitive hydrogel, we note that the dependence on geometry remains, and it is not possible to alter the wave sizes through other forms of stimuli. However, it is possible to switch between the buckled state and the flat strip with application of light. As with the phase transition of a photo-thermal gel, the critical temperature of transition can be altered by changing light intensity.

In this example, we investigated the effects of light intensity on the buckling and unbuckling of a gel strip of dimensions in the ratio $t:B:L=1:2.5:100$ (Figure 4-15a). A total of 6006 C3D8 elements and 9184 nodes were used. Simulation time was about 5 minutes. Boundary conditions included a fixed surface along the long edge and zero normal displacements on the 2 end surfaces. The simulation was divided into three steps, the first being a hydration process where chemical potential of the gel was increased from $\bar{\mu}^s=-0.2$ to $\bar{\mu}^s=0$,the second an imposition of light intensity, and the third an increase in temperature of 20K. Although UHYPER only allows one quantity to be changed at any one time, the steps which required different quantities to be changed was still possible by making use of if-else conditions in the subroutine to switch the material properties between the different variables.

Upon reaching equilibrium with the external solvent, the gel buckled into a wavy pattern (Figure 4-15b), defined as the OFF state. Upon irradiation, the increase in temperature resulted in deswelling. Upon reaching the critical temperature, the waves disappeared, returning the gel into a flat geometry (Figure 4-15c).

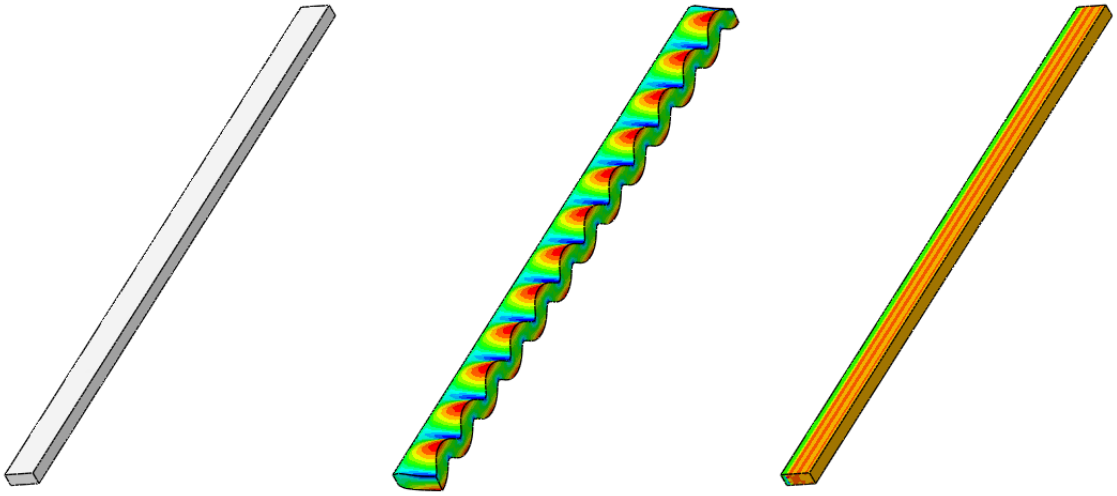

(a) (b) (c)

Figure 4-15: (a) Initial geometry of gel in dry state, (b) gel in hydrated OFF state, (c) gel in irradiated ON state.

From the OFF state, it is possible to toggle to the ON state (flat geometry) and back with application of irradiation. Figure 4-16a shows the maximum longitudinal stress present in the gel as it is hydrated from $\bar{\mu} = -0.2$ to $\bar{\mu} = 0$. Figure 4-16b shows the maximum longitudinal stress in the gel as it is being irradiated from the OFF state with different light intensities.

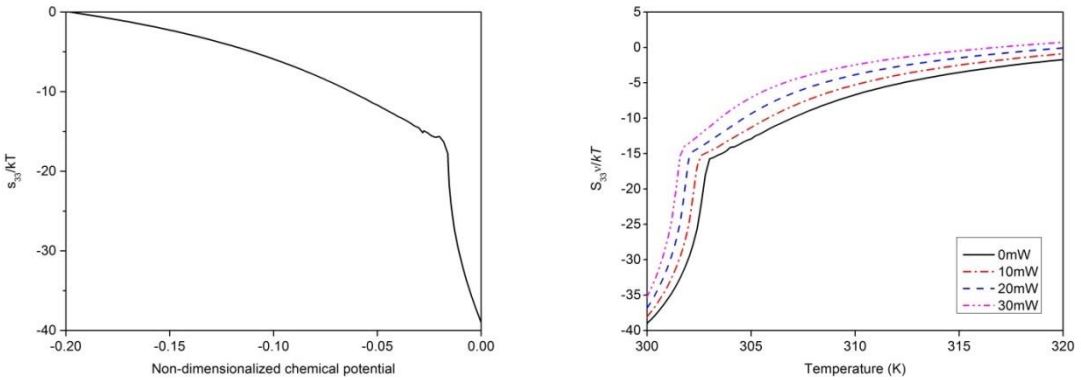

(a) (b)

Figure 4-16: Maximum longitudinal stress in gel as (a) dry gel is hydrated from $\bar{\mu} = -0.2$ to $\bar{\mu} = 0$, (b) buckled gel is irradiated with varying light intensities across a temperature range.

Due to the difference in light intensity, we can see that for the same temperature rise in the gel, the critical transition where the buckled structure returns to a flat geometry is affected. This observation may be useful for active controlling purposes, as the buckled states can be toggled on and off by simply varying the light intensity.

4.4. Pattern transformation in a periodic array

In an extensive gel film fixed at the bottom and having periodic array of holes, as shown in Figure 4-17, swelling of the gel causes instabilities in the form of rotation of unit cells to form slits with periodic patterns, such as alternating slits which are perpendicular to each other.

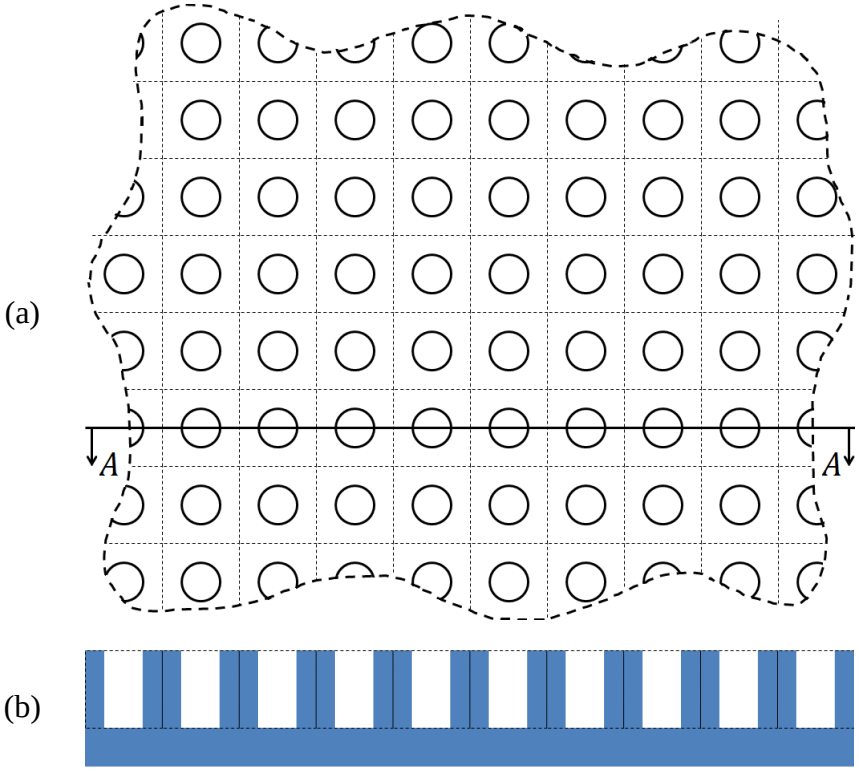

Figure 4-17: (a) Top view of the gel layer with periodic square array of holes, (b) cross section view of section A-A

Owing to the several attractive mechanical (Hu et al., 2014) and acoustic applications (Wang et al., 2014; Wang et al., 2013b), many researchers have tried to explain the behavior using the thermodynamic model of gel (Ding et al., 2013; Hong et al., 2009a; Okumura et al., 2014).

4.4.1. Equilibrium study in a photo-thermal sensitive hydrogel

In the finite element model, the simplest repeating unit consists of a square with a circle in the middle. However, this repeating unit does not allow for appearance of alternating slits. Thus,we make use of $m \times n$ repeating units to form the unit cell for

simulation, upon which we apply periodic boundary conditions, where displacements of opposite sides are equal. Imposition of periodic boundary condition is done by using the *EQUATION option. For computational efficiency, we will make use of plane stress elements (CPS4) to perform two-dimensional analysis on the pattern formation in the gel structure.

4.4.1.1. *Effects of light intensity on bifurcation process*

In studying the effects of light intensity, we turn our focus to a square repeating unit. As reported by (Okumura et al., 2015; Okumura et al., 2014), for a gel with a square array of holes, a minimum of 2×2 repeating units are required to form the unit cell, as shown in Figure 4-18. The four corners of the unit cell were fixed and the sides of the unit cell were subjected to periodic boundary conditions. A total of 3040 CPS4 elements and 3265 nodes were used in the model. Simulation time was about 10 minutes on 8 cores.

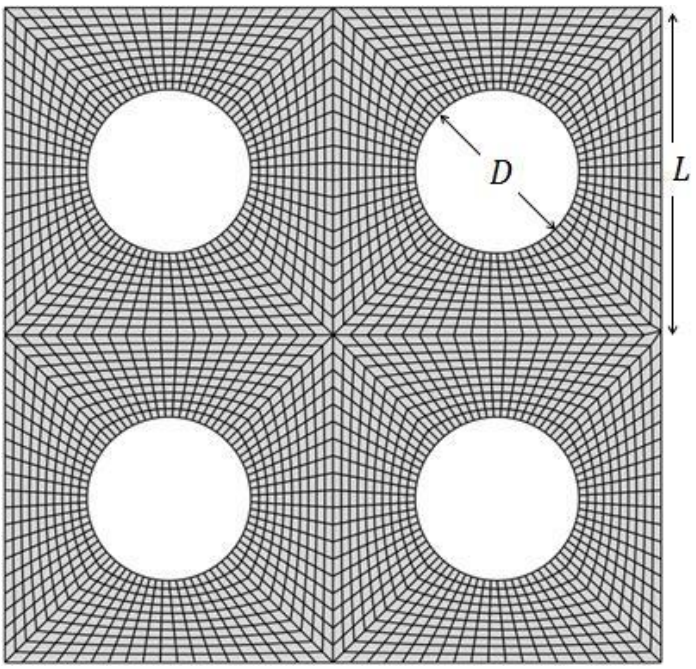

Figure 4-18: Mesh of unit cell of 2×2 repeating units of length *L=1.5* and diameter *D=0.75*.

We first subjected a gel of initial chemical potential of $\bar{\mu} = -0.2$ in the stress free state to a final chemical potential of $\bar{\mu} = 0$. As swelling occurred, the holes remained circular in the initial period. However, across a critical chemical potential, bifurcation

set in and we were able to observe rotation in the middle of the four holes, as indicated in the diagram. Due to this rotation, the holes transit into alternating slits, as shown in Figure 4-19.

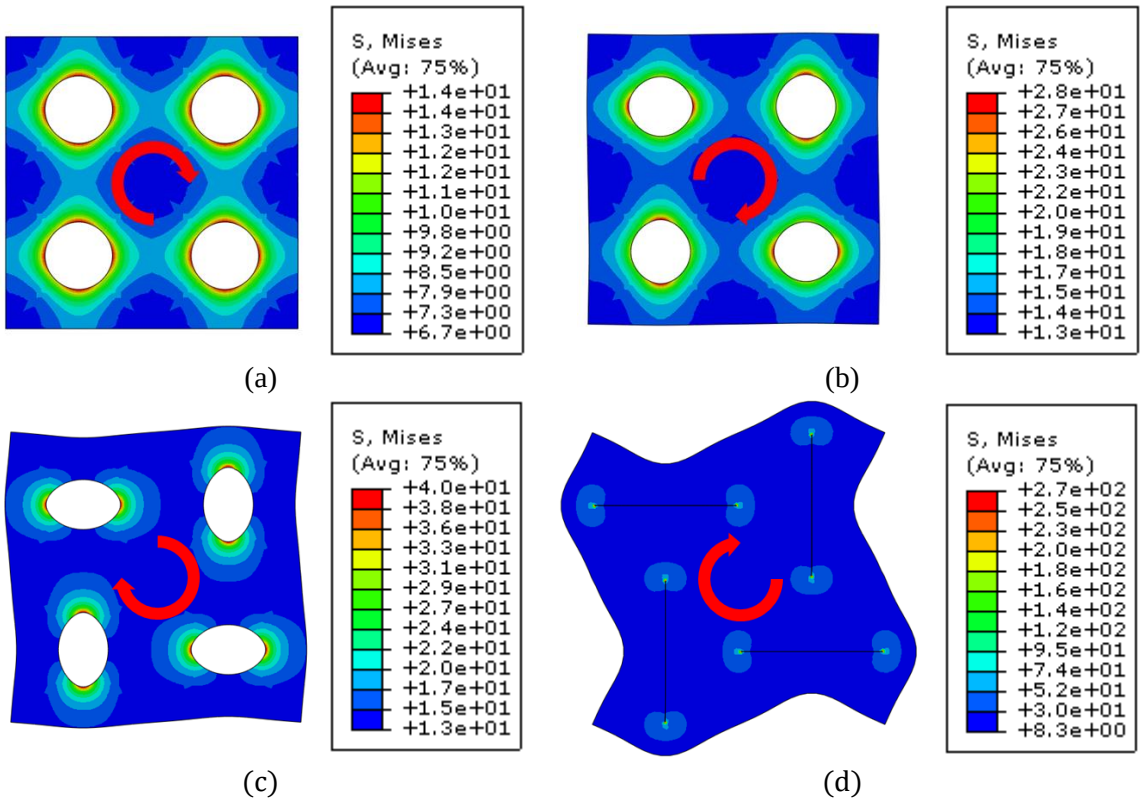

Figure 4-19: Transition of holes into slits at chemical potentials at (a) $\bar{\mu} = -0.1$, (b) $\bar{\mu} = -0.053$, (c) $\bar{\mu} = -0.052$ and (d) $\bar{\mu} = 0$. The red arrows indicate direction of rotation of the middle of the unit cell. Contours show the non-dimensionalized Mises stress.

To quantify the amount of deviation from the original circular geometry, we calculated the eccentricity of the slit, given by $e = \sqrt{1-(a/b)^2}$, with a and b being the semi-minor and semi-major axes. Under this definition, $e = 0$ when the hole is a perfect circle, and becomes $e = 1$ as the elongation of this hole propagates.

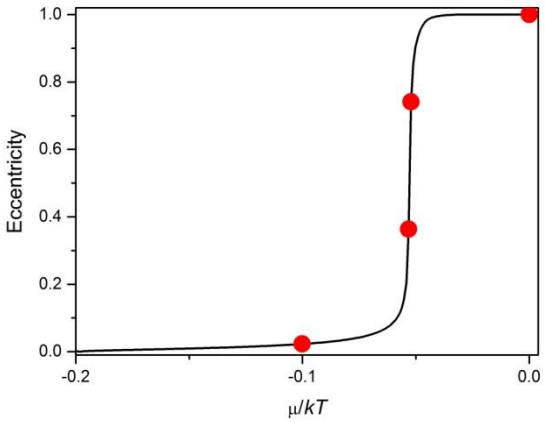

Figure 4-20: Change in eccentricity of the gel structure as chemical potential is changed from $\bar{\mu} = -0.2$ to $\bar{\mu} = 0$. The four discrete points correspond to swelling states illustrated in Figure 4-19.

In this example, we propose an optical switch which utilizes the ON-OFF geometry of the slits. We first hydrated a dry gel which was in a square array (Figure 4-21a). This hydration resulted in swelling, and eventually bifurcation into the arrangement with alternating slits (Figure 4-21b), which we set as the normal OFF state. When we applied an irradiation, the gel gained temperature and underwent deswelling. This deswelling action allowed the gel to return to circular arrangement (Figure 4-21c) (OFF state).

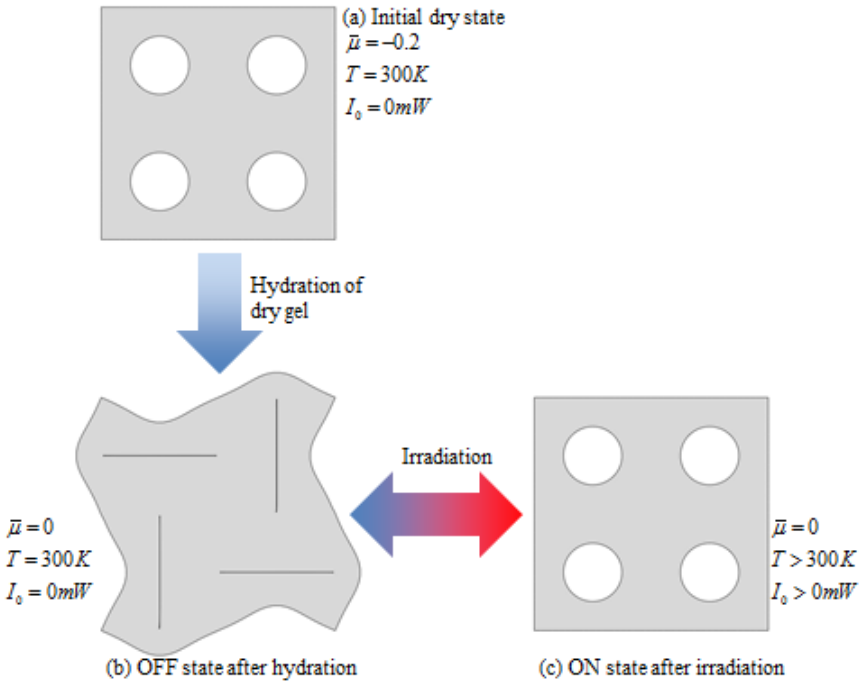

Figure 4-21: Geometry of (a) initial dry state, (b) swollen state with no irradiation, (c) gel returns to circular geometry under irradiation.

In this swollen state, we subjected the gel to irradiation of different intensities. This resulted in a temperature change in the gel, causing the gel to deswell and undo the effects of bifurcation, returning the geometry of the slits into circles. Figure 4-22 shows the eccentricities of gels which were exposed to different levels of light intensity. There is a clear distinction of the critical transition temperatures as light intensity is increased.

Plotting this relationship between light intensity and the critical temperature (Figure 4-23), we obtained a linear relationship between critical temperature and light intensity. The clear distinction of critical temperatures of bifurcation indicates potential applications in areas of optical switching or microfluidics, as the opening and closing of the holes can be precisely controlled with different light intensities.

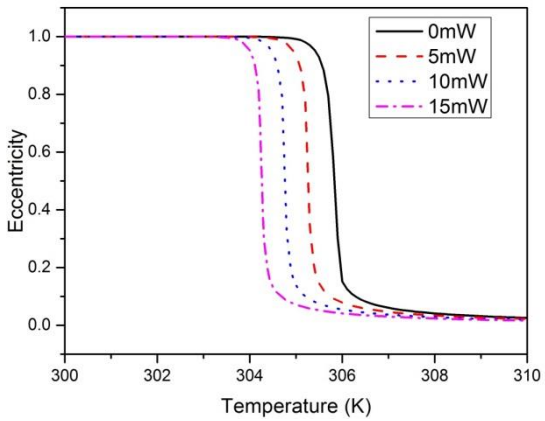

Figure 4-22: Dependence of eccentricity with temperature at various light intensities.

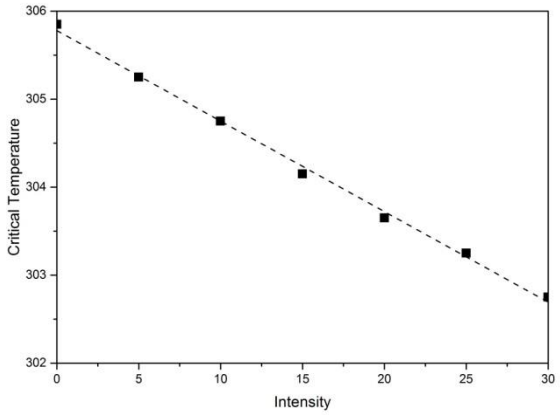

Figure 4-23: Dependence of critical temperature of bifurcation on light intensity.

4.4.1.3. *Bifurcation of gel layer with staggered array of holes*

In a square array of holes, bifurcation causes spontaneous transition into mutually perpendicular ellipses, which eventually close up into slits upon eventual swelling. This mutually perpendicular arrangement of slits, however, is dependent on the obliquity of the repeating unit. In addition to the square repeating unit, we will now consider rhombic repeating units slanted at 60° and 45° to the horizontal, as shown in Figure 7.

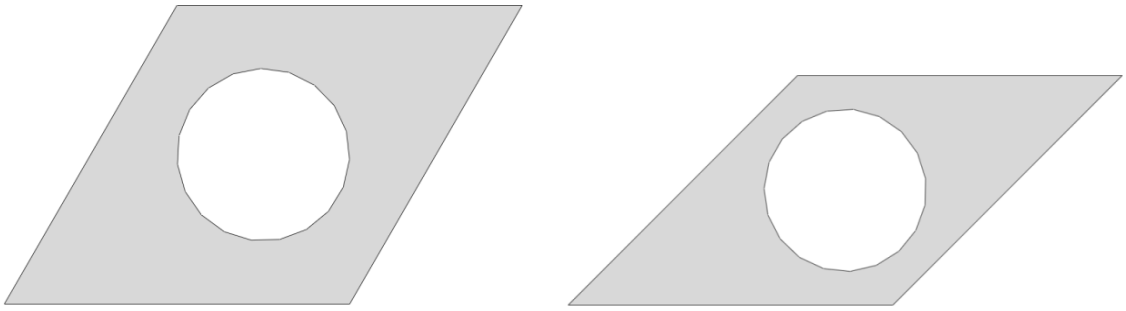

(a) (b)

Figure 4-24: Rhombic repeating unit slanted at (a) 60°, and (b) 45°.

In initial simulations, unit cells of different configurations of repeating units ($m \times n$) were used and unfavorable results were obtained. This was due to the incorrect configuration of repeating units, thus rendering the simulations unable to obtain the periodic patterns. These configurations were obtained by studying the pattern formation in finite sized unit cells of 10×10 repeating units, without any periodic boundary conditions applied. Eventually, 4×4 and 2×1 repeating units were required to form the unit cells for the cases of 60° and 45°obliquity respectively. The 60° model consisted of 4984 elements and 5429 nodes while the 45° model consisted of 742 elements and 836 nodes. Figure 4-25 shows the mesh of both models. The time taken for simulation of both models were less than an hour.

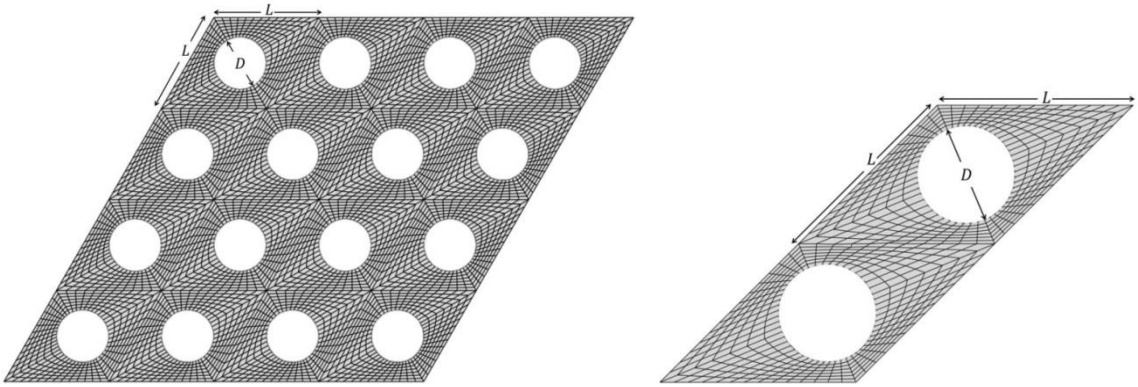

(a) (b)

Figure 4-25: Mesh of unit cell consisting of 4×4 and 2×1 repeating units for repeating units slanted at (a) 60° and (b). The lengths of each side of the repeating unit are 1.5 and diameters are 0.75.

Figure 4-26 shows the deformed geometries for the unit cell at 290K for both obliquities. It is clearly seen that for different arrangements of the holes, we obtained different bifurcation patterns, and the size of openings after bifurcation were also different. For a clearer picture of the extended gel structure, we repeated the unit cells in Figure 4-27. This may be used as a design parameter for the control of end state sizes of pores required for different applications.

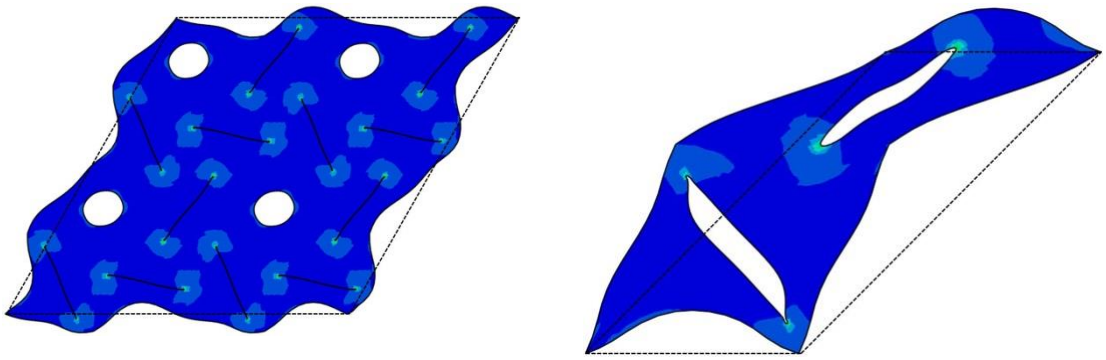

(a) (b)

Figure 4-26: Deformed unit cell at the end of simulation for (a) 60°, and (b) 45°. Dotted lines denote the original geometry of the unit cell.

(a)

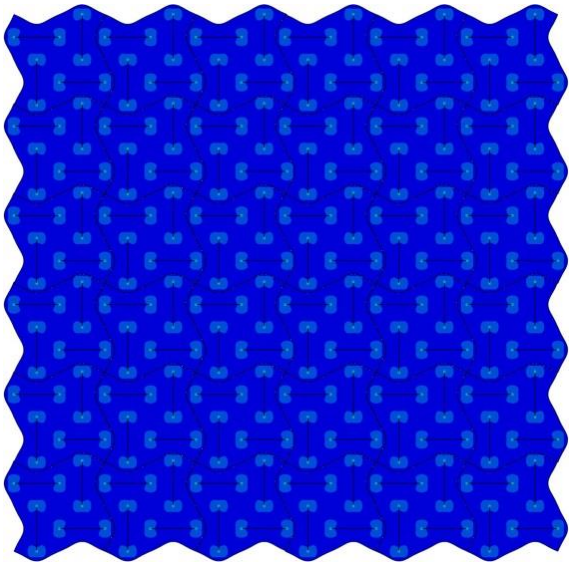

(b)

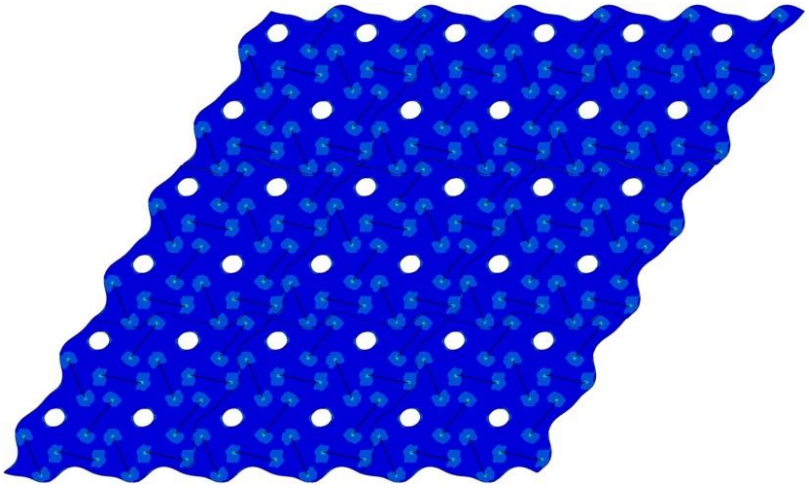

(c)

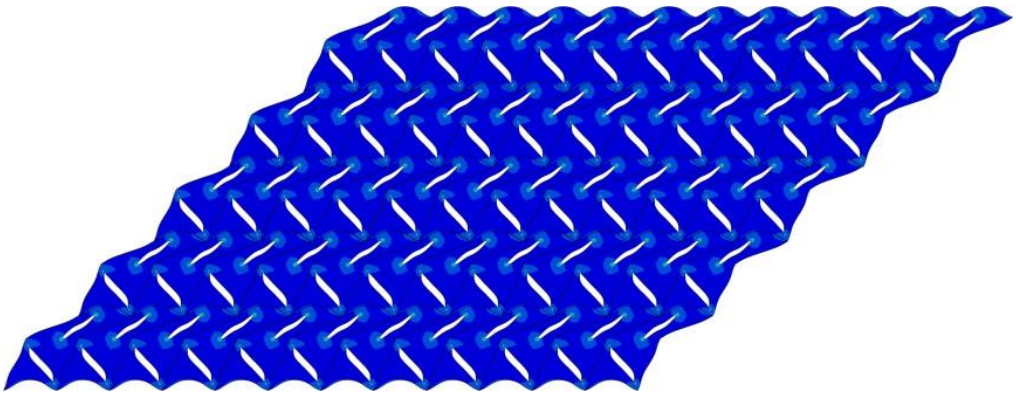

Figure 4-27: Bifurcation pattern of gel layers with 12×12 repeating units for (a) square array, (b) rhombic array slanted at 60°, and (c) rhombic array slanted at 45°.

4.5. Concluding remarks

In this chapter, we had explored the interesting phenomenon of swelling induced instabilities using finite element simulation, including surface wrinkling in transient swelling, buckling of thin annular structures, pattern transformation in periodic arrays and creasing of gel structures controllable by appropriate position of protrusions in the substrate.

In the study of transient surface wrinkling, due to the continual evolution of stress profile in the vertical direction, the wavelength of surface wrinkles constantly evolve with time. It was observed from the FE analysis that the wavelength of surface wrinkles that appear is proportional to the square root of the time it takes for the gel to swell and buckle to that particular state. In addition to finite element simulation, we have proposed a state-space method to predict the wave number of the surface wrinkles at different times of swelling. Both finite element method and state-space method predict a decaying trend of wave numbers with increasing time, similar to experimental observations.

In the simulation of the buckling of thin annular rings, we had shown that during the initial phase of swelling, the gel transitions in between different mode shapes before settling into the equilibrium mode shape, determined by initial geometry rather than the rate of swelling. The buckling of thin annular rings is due to compressive stresses being generated in the tangential direction of the ring, causing buckled waves to appear circumferentially. In addition, the phenomenon of wave rotation when the gel settles in the equilibrium mode shape was also observed.

In gel films with periodic holes arranged orderly, our simulation results showed that there would be pattern transformation into different types of slit arrangements, depending on the lattice of the holes. A square lattice would give rise to alternating perpendicular slits. A lattice slanted at 60° would give rise to a structure that does not close up completely as six slits surround a hole. A lattice slanted at 45° would give rise to rows of slits alternated at slants of 45° and -45°.

Making use of the dependence on geometry rather than material properties, we had shown that it is possible to come up with actuating devices which can be precisely

controlled by the irradiation of light. This concept has been shown for the cases of a flat gel strip which buckles into wavy patterns, and for a gel film with periodic hole array. For both cases, it is clearly seen that a change in light intensity affects the critical temperature where the instabilities disappear. Thus it is possible to have devices which can be actuated at different temperatures based on light intensity.

5. Conclusion

This thesis had investigated several aspects of the mechanical behavior of hydrogels. Through a thorough literature review of many works related to hydrogels, the scope of the thesis was sculpted to study the swelling kinetics, response to environmental stimuli and the instabilities that are associated with the deformation of hydrogels under various conditions. Several finite element simulation models, created using commercial finite element software Abaqus, had been developed for the various materials studied in this thesis.

Firstly, in the study of swelling kinetics, the work covered in this thesis had led to development of finite element models to simulate the transient swelling response of three types of hydrogels, namely the neutral hydrogel, temperature-sensitive hydrogel and *pH*-sensitive hydrogel. The models developed were based on a central idea of utilizing the similarities between governing equations of kinetic laws and heat transfer laws. Due to this similarity, when the chemical potential of the gel was represented as temperature in Abaqus, simulation of swelling kinetics could be easily performed by using coupled temperature-displacement elements, which was readily available in the Abaqus element library. Material properties were defined with three subroutines used concurrently, namely UHYPER, USDFLD and HETVAL. This procedure significantly reduced the effort required to define the entire constitutive model via more lengthy subroutines, such as the user-defined elements (UEL), as the need to discretize constitutive equations had been eliminated. In addition, the subroutine allowed for more flexibility in the choice of element types, for example 2D or 3D elements, without additional effort in customizing the subroutine for the different element types.

Secondly, the mechanics and behaviors of environmentally sensitive hydrogels were investigated. Constitutive models, based on continuum thermodynamics, were developed for temperature-sensitive, photo-thermal-sensitive and magneto-thermal-sensitive hydrogels to study various phenomena associated with these materials. Primarily, the models studied the phase transition phenomenon and the factors affecting it. Finite element models were developed and implemented using two different subroutines, UMAT and UHYPER, each with its own advantages and disadvantages over the other.

Thirdly, this thesis studied various instabilities associated with the deformation of hydrogels. The finite element models developed in Chapters 2 and 3 were utilized in this study for surface wrinkling in transient swelling, buckling of thin gel structures, pattern transformation and creasing commonly observed in gels. In addition, a state-space method was developed as a semi-analytical approach to predict the wave numbers at different times of a transient swelling.

6. Future work

Many issues related to the mechanics of hydrogel behaviors remain open and is worthy of investment of more time for in-depth investigation. We list below, some plausible future directions in the research of the mechanical behaviors of hydrogels.

Firstly, the kinetic models developed in this thesis studied the long time range diffusion mechanism of solvent molecules and ions. One possible extension will be the addition of short time range effects, such as visco-elastic effects.

Secondly, the finite element models developed are only capable of handling one loading parameter at any one time. Therefore, in order to better simulate the actual behaviors of gels, more robust subroutines which can handle multiple loading parameters simultaneously will be useful to study the effects of various stimuli on the gel.

Thirdly, a unified formulation to incorporate the effects of various stimuli may provide researchers with the tools required to study multi-stimuli-responsive hydrogels rather than singly or dually responsive gels. This, together with the previous point, may be implemented hand-in-hand as multi-stimuli-responsive gels are investigated.

Fourthly, the study of mechanics and phase transition phenomenon in this thesis is limited to the equilibrium swelling state with homogenous dispersion of stimuli-induced chemical reactions within the gel, such as photo-chemical reactions. In reality, the distribution of such chemical reactions in gels are never homogeneous, therefore, models can be developed to incorporate this inhomogeneity.

Finally, it was noted that the finite element models are unable to overcome turning points and unstable points. In the simulation of discontinuous phase transition, the methods were unable to simulate full transition of the gel. In the simulation of instabilities, the methods were unable to overcome unstable points to obtain post-buckling behavior of the gels. Therefore, much work lie in the area of developing sufficiently robust models to overcome these points for the exhibition of the full range of mechanical behaviors of gels.

7. References

Achilleos, E.C., Prud'homme, R.K., Christodoulou, K.N., Gee, K.R., Kevrekidis, I.G., 2000. Dynamic deformation visualization in swelling of polymer gels. Chemical Engineering Science 55, 3335-3340.

Afroze, F., Nies, E., Berghmans, H., 2000. Phase transitions in the system poly(N-isopropylacrylamide)/water and swelling behaviour of the corresponding networks. Journal of Molecular Structure 554, 55-68.

Aguilar, M.R., Elvira, C., Gallardo, A., Roman, J.S., 2007. Smart Polymers and Their Applications as Biomaterials, Topics in Tissue Engineering.

Anand, L., 1996. A constitutive model for compressible elastomeric solids. Computational Mechanics 18, 339-355.

Arruda, E.M., Boyce, M.C., 1993. A three-dimensional constitutive model for the large stretch behavior of rubber elastic materials. Journal of the Mechanics and Physics of Solids 41, 389-412.

Bae, Y.H., Okano, T., Kim, S.W., 1989. Insulin permeation through thermo-sensitive hydrogels. Journal of Controlled Release 9, 271-279.

Baek, S., Pence, T.J., 2011. Inhomogeneous deformation of elastomer gels in equilibrium under saturated and unsaturated conditions. Journal of the Mechanics and Physics of Solids 59, 561-582.

Baek, S., Srinivasa, A.R., 2004. Diffusion of a fluid through an elastic solid undergoing large deformation. International Journal of Non-Linear Mechanics 39, 201-218.

Baldi, A., Yuandong, G., Loftness, P.E., Siegel, R.A., Ziaie, B., 2002. A hydrogel-actuated smart microvalve with a porous diffusion barrier back-plate for active flow control, Micro Electro Mechanical Systems, 2002. The Fifteenth IEEE International Conference on, pp. 105-108.

Barros, W., de Azevedo, E.N., Engelsberg, M., 2012. Surface pattern formation in a swelling gel. Soft Matter 8, 8511-8516.

Barrow, J.D., 2002. The Constants of Nature: From Alpha to Omega - The Numbers that Encode the Deepest Secrets of the Universe. Pantheon Books.

Bashir, R., Hilt, J.Z., Elibol, O., Gupta, A., Peppas, N.a., 2002. Micromechanical cantilever as an ultrasensitive pH microsensor. Applied Physics Letters 81, 3091-3091.

Bassik, N., Abebe, B.T., Laflin, K.E., Gracias, D.H., 2010. Photolithographically patterned smart hydrogel based bilayer actuators. Polymer 51, 6093-6098.

Bassil, M., Davenas, J., El Tahchi, M., 2008. Electrochemical properties and actuation mechanisms of polyacrylamide hydrogel for artificial muscle application. Sensors and Actuators B: Chemical 134, 496-501.

Bassil, M., Ibrahim, M., El Tahchi, M., 2011. Artificial muscular microfibers: hydrogel with high speed tunable electroactivity. Soft Matter 7, 4833-4838.

Ben Amar, M., Ciarletta, P., 2010. Swelling instability of surface-attached gels as a model of soft tissue growth under geometric constraints. Journal of the Mechanics and Physics of Solids 58, 935-954.

Bergman, T.L., Incropera, F.P., Lavine, A.S., DeWitt, D.P., 2011. Fundamentals of Heat and Mass Transfer, 6th ed. John Wiley & Sons, Inc.

Bird, R.B., Stewart, W.E., Lightfoot, E.N., 2007. Transport Phenomena. John Wiley and Sons.

Birgersson, E., Li, H., Wu, S., 2008. Transient analysis of temperature-sensitive neutral hydrogels. Journal of the Mechanics and Physics of Solids 56, 444-466.
Bouklas, N., Huang, R., 2012. Swelling kinetics of polymer gels: comparison of linear and nonlinear theories. Soft Matter.
Boyce, M.C., Arruda, E.M., 2001. Swelling and Mechanical Stretching of Elastomeric Materials. Mathematics and Mechanics of Solids 6, 641-659.
Brannon-Peppas, L., Peppas, N.A., 1991. Equilibrium swelling behavior of pH-sensitive hydrogels. Chemical Engineering Science 46, 715-722.
Brazel, C.S., 2009. Magnetothermally-responsive Nanomaterials: Combining Magnetic Nanostructures and Thermally-Sensitive Polymers for Triggered Drug Release. Pharmaceutical Research 26, 644-656.
Breid, D., Crosby, A.J., 2011. Effect of stress state on wrinkle morphology. Soft Matter 7, 4490-4496.
Cai, S., Breid, D., Crosby, A.J., Suo, Z., Hutchinson, J.W., 2011. Periodic patterns and energy states of buckled films on compliant substrates. Journal of the Mechanics and Physics of Solids 59, 1094-1114.
Cai, S., Suo, Z., 2011. Mechanics and chemical thermodynamics of phase transition in temperature-sensitive hydrogels. Journal of the Mechanics and Physics of Solids 59, 2259-2278.
Cai, S., Suo, Z., 2012. Equations of state for ideal elastomeric gels. EPL (Europhysics Letters) 97, 34009.
Calderer, M.C., Chabaud, B., Lyu, S., Zhang, H., 2008. Modeling approaches to the dynamics of hydrogel swelling. Journal of Computational and Theoretical Nanoscience 7, 766-779.
Cao, Y., Hutchinson, J.W., 2011. From wrinkles to creases in elastomers: the instability and imperfection-sensitivity of wrinkling. Proceedings of the Royal Society A: Mathematical, Physical and Engineering Science.
Cao, Y., Hutchinson, J.W., 2012. Wrinkling Phenomena in Neo-Hookean Film/Substrate Bilayers. Journal of Applied Mechanics 79, 031019.
Cao, Y., Jiang, Y., Li, B., Feng, X., 2012. Biomechanical modeling of surface wrinkling of soft tissues with growth-dependent mechanical properties. Acta Mechanica Solida Sinica 25, 483-492.
Caykara, T., Kiper, S., Demirel, G., 2006. Network parameters and volume phase transition behavior of poly(N-isopropylacrylamide) hydrogels. Journal of Applied Polymer Science 101, 1756-1762.
Chatterjee, A., Yu, Q., Moore, J., Aluru, N., 2003. Mathematical Modeling and Simulation of Dissolvable Hydrogels. Journal of Aerospace Engineering 16, 55-55.
Chen, C.-M., Yang, S., 2012. Wrinkling instabilities in polymer films and their applications. Polymer International 61, 1041-1047.
Chen, J., Li, H., Lam, K.Y., 2005. Transient simulation for kinetic responsive behaviors of electric-sensitive hydrogels subject to applied electric field. Materials Science and Engineering: C 25, 710-712.
Chen, X., Yin, J., 2010. Buckling patterns of thin films on curved compliant substrates with applications to morphogenesis and three-dimensional micro-fabrication. Soft Matter 6, 5667-5680.
Chester, S.A., 2011. Mechanics of amorphous polymers and polymer gels. Massachusetts Institute of Technology, Cambridge, Massachusetts.

Chester, S.A., 2012. A constitutive model for coupled fluid permeation and large viscoelastic deformation in polymeric gels. Soft Matter 8, 8223-8233.
Chester, S.A., Anand, L., 2010. A coupled theory of fluid permeation and large deformations for elastomeric materials. Journal of the Mechanics and Physics of Solids 58, 1879-1906.
Chester, S.A., Anand, L., 2011. A thermo-mechanically coupled theory for fluid permeation in elastomeric materials: Application to thermally responsive gels. Journal of the Mechanics and Physics of Solids 59, 1978-2006.
Chester, S.A., Di Leo, C.V., Anand, L., 2014. A finite element implementation of a coupled diffusion-deformation theory for elastomeric gels. International Journal of Solids and Structures.
Chu, C., 2003. Biodegradable Hydrogels as Drug Controlled Release Vehicles, Tissue Engineering And Novel Delivery Systems. CRC Press.
Chu, Y., Varanasi, P.P., McGlade, M.J., Varanasi, S., 1995. pH-induced swelling kinetics of polyelectrolyte hydrogels. Journal of Applied Polymer Science 58, 2161-2176.
Colombo, I., Grassi, M., Fermeglia, M., Lapasin, R., Pricl, S., 1996. Modeling phase transitions and sorption desorption kinetics in thermo-sensitive gels for controlled drug delivery systems. Fluid Phase Equilibria 116, 148-161.
De, S.K., Aluru, N.R., 2004. A chemo-electro-mechanical mathematical model for simulation of pH sensitive hydrogels. Mechanics of Materials 36, 395-410.
De, S.K., Aluru, N.R., Johnson, B., Crone, W.C., Beebe, D.J., Moore, J., 2002. Equilibrium swelling and kinetics of pH-responsive hydrogels: models, experiments, and simulations. Microelectromechanical Systems, Journal of 11, 544-555.
Deligkaris, K., Tadele, T.S., Olthuis, W., van den Berg, A., 2010. Hydrogel-based devices for biomedical applications. Sensors and Actuators B: Chemical 147, 765-774.
Dervaux, J., Ben Amar, M., 2011. Buckling condensation in constrained growth. Journal of the Mechanics and Physics of Solids 59, 538-560.
Ding, Z., Liu, Z.S., Hu, J., Swaddiwudhipong, S., Yang, Z., 2013. Inhomogeneous large deformation study of temperature-sensitive hydrogel. International Journal of Solids and Structures 50, 2610-2619.
Doi, M., 2009. Gel Dynamics. Journal of the Physical Society of Japan 78, 052001-052001.
Doi, M., Onuki, A., 1992. Dynamic coupling between stress and composition in polymer solution and blends. J. Phys. II (Paris) 2, 1631-1656.
Duan, Z., Zhang, J., An, Y., Jiang, H., 2013. Simulation of the Transient Behavior of Gels Based on an Analogy Between Diffusion and Heat Transfer. Journal of Applied Mechanics 80, 041017-041017.
Duda, F.P., Souza, A.C., Fried, E., 2010. A theory for species migration in a finitely strained solid with application to polymer network swelling. Journal of the Mechanics and Physics of Solids 58, 515-529.
Dulkeith, E., Niedereichholz, T., Klar, T.A., Feldmann, J., von Plessen, G., Gittins, D.I., Mayya, K.S., Caruso, F., 2004. Plasmon emission in photoexcited gold nanoparticles. Physical Review B 70, 205424-205424.

DuPont Jr, S.J., Cates, R.S., Stroot, P.G., Toomey, R., 2010. Swelling-induced instabilities in microscale, surface-confined poly(N-isopropylacryamide) hydrogels. Soft Matter 6, 3876-3882.

Durning, C.J., Morman, K.N.J., 1993. Nonlinear swelling of polymer gels. The Journal of Chemical Physics 98, 4275-4293.

Elvira, C., Abraham, G., Gallardo, A., Roman, J.S., Román, J.S., 2004. Smart Biodegradable Hydrogels with Applications in Drug Delivery and Tissue Engineering. CRC Press.

Erman, B., Flory, P.J., 1986. Critical phenomena and transitions in swollen polymer networks and in linear macromolecules. Macromolecules 19, 2342-2353.

Eshelby, J.D., 1956. The Continuum Theory of Lattice Defects, in: Physics, F.S., David Turnbull, B.T.S.S. (Eds.). Academic Press, pp. 79-144.

Feynman, R.P., Leighton, R.B., Sands, M., 1963. The Feynman Lectures on Physics.

Flory, P.J., 1942. Thermodynamics of High Polymer Solutions. The Journal of Chemical Physics 10, 51-61.

Flory, P.J., 1953. Principles of Polymer Chemistry. Cornell University Press, Ithaca.

Flory, P.J., Rehner, J., 1943. Statistical Mechanics of Cross-Linked Polymer Networks I. Rubberlike Elasticity. The Journal of Chemical Physics 11, 512-512.

Fogle, C., Rowat, A.C., Levine, A.J., Rudnick, J., 2013. Shape transitions in soft spheres regulated by elasticity. Physical Review E 88, 052404.

Freund, L.B., 2000. Substrate curvature due to thin film mismatch strain in the nonlinear deformation range. Journal of the Mechanics and Physics of Solids 48, 1159-1174.

Gorelikov, I., Field, L.M., Kumacheva, E., 2004. Hybrid Microgels Photoresponsive in the Near-Infrared Spectral Range. Journal of the American Chemical Society 126, 15938-15939.

Grassi, M., Hong Yuk, S., Hang Cho, S., 1999. Modelling of solute transport across a temperature-sensitive polymer membrane. Journal of Membrane Science 152, 241-249.

Gupta, P., Vermani, K., Garg, S., 2002. Hydrogels: from controlled release to pH-responsive drug delivery. Drug Discovery Today 7, 569-579.

Guvendiren, M., Burdick, J.A., Yang, S., 2010a. Kinetic study of swelling-induced surface pattern formation and ordering in hydrogel films with depth-wise crosslinking gradient. Soft Matter 6, 2044-2049.

Guvendiren, M., Burdick, J.A., Yang, S., 2010b. Solvent induced transition from wrinkles to creases in thin film gels with depth-wise crosslinking gradients. Soft Matter 6, 5795-5801.

Guvendiren, M., Yang, S., Burdick, J.A., 2009. Swelling-Induced Surface Patterns in Hydrogels with Gradient Crosslinking Density. Advanced Functional Materials 19, 3038-3045.

Harmon, M.E., Kuckling, D., Pareek, P., Frank, C.W., 2003a. Photo-cross-linkable PNIPAAm Copolymers. 4. Effects of Copolymerization and cross-linking on the volume-phase transition in constrained hydrogel layers. Langmuir2 19, 10947-10956.

Harmon, M.E., Tang, M., Frank, C.W., 2003b. A microfluidic actuator based on thermoresponsive hydrogels. Polymer 44, 4547-4556.

Hassan, M.M., Durning, C.J., 1999. Effects of polymer molecular weight and temperature on case II transport. Journal of Polymer Science Part B: Polymer Physics 37, 3159-3171.

Haught, A.F., 1984. Physics Considerations of Solar Energy Conversion. Journal of Solar Energy Engineering 106, 3-15.
He, T., Li, M., Zhou, J., 2012. Modeling deformation and contacts of pH sensitive hydrogels for microfluidic flow control. Soft Matter 8, 3083-3089.
Helfferich, F., Plesset, M.S., 1958. Ion Exchange Kinetics. A Nonlinear Diffusion Problem. The Journal of Chemical Physics 28, 418-424.
Herrmann, F., Wurfel, P., 2005. Light with nonzero chemical potential. American Journal of Physics 73, 717-721.
Hino, T., Prausnitz, J.M., 1998. Molecular thermodynamics for volume-change transitions in temperature-sensitive polymer gels. Polymer 39, 3279-3283.
Hoffmann, J., Plötner, M., Kuckling, D., Fischer, W.-J., 1999. Photopatterning of thermally sensitive hydrogels useful for microactuators. Sensors and Actuators A: Physical 77, 139-144.
Hohlfeld, E., Mahadevan, L., 2011. Unfolding the Sulcus. Physical Review Letters 106, 105702.
Hohlfeld, E., Mahadevan, L., 2012. Scale and Nature of Sulcification Patterns. Physical Review Letters 109, 025701.
Holmes, D.P., Roche, M., Sinha, T., Stone, H.A., 2011. Bending and twisting of soft materials by non-homogenous swelling. Soft Matter 7, 5188-5193.
Hong, W., Liu, Z.S., Suo, Z., 2009a. Inhomogeneous swelling of a gel in equilibrium with a solvent and mechanical load. International Journal of Solids and Structures 46, 3282-3289.
Hong, W., Zhao, X., Suo, Z., 2009b. Formation of creases on the surfaces of elastomers and gels. Applied Physics Letters 95, 111901-111901.
Hong, W., Zhao, X., Suo, Z., 2010. Large deformation and electrochemistry of polyelectrolyte gels. Journal of the Mechanics and Physics of Solids 58, 558-577.
Hong, W., Zhao, X., Zhou, J., Suo, Z., 2008. A theory of coupled diffusion and large deformation in polymeric gels. Journal of the Mechanics and Physics of Solids 56, 1779-1793.
Hu, J.Y., He, Y.H., Lei, J.C., Liu, Z.S., Swaddiwudhipong, S., 2014. Mechanical behavior of composite gel periodic structures with the pattern transformation. Structural Engineering and Mechanics 50, 605-616.
Hu, Z., Chen, Y., Wang, C., Zheng, Y., Li, Y., 1998. Polymer gels with engineered environmentally responsive surface patterns. Nature 393, 149-152.
Huang, R., Suo, Z., 2002a. Instability of a compressed elastic film on a viscous layer. International Journal of Solids and Structures 39, 1791-1802.
Huang, R., Suo, Z., 2002b. Wrinkling of a compressed elastic film on a viscous layer. Journal of Applied Physics 91, 1135-1142.
Huang, Z., Hong, W., Suo, Z., 2004. Evolution of wrinkles in hard films on soft substrates. Physical Review E 70, 30601-30601.
Huggins, M.L., 1941. Solutions of Long Chain Compounds. The Journal of Chemical Physics 9, 440-440.
Huggins, M.L., 1964. A Revised Theory of High Polymer Solutions. Journal of the American Chemical Society 86, 3535-3540.
Huglin, M.R., 1989. Hydrogels in medicine and pharmacy. British Polymer Journal 21, 184-184.
Jeong, B., Gutowska, A., 2002. Lessons from nature: stimuli-responsive polymers and their biomedical applications. Trends Biotechnol. 20, 305-311.

Jeong, S.H., Fu, Y., Park, K., 2005. Hydrogels for Oral Administration. Informa Healthcare, pp. 195-214.
Jeong, S.H., Huh, K.M., Park, K., 2006. Hydrogel Drug Delivery Systems. CRC Press.
Ji, S., Ding, J., 2001. A Macroscopic Helix Formation Induced by the Shrinking of a Cylindrical Polymeric Hydrogel. Polym J 33, 701-703.
Ji, S., Ding, J., 2002. The Wetting Process of a Dry Polymeric Hydrogel. Polym J 34, 267-270.
Jia, F., Ben Amar, M., 2013. Theoretical analysis of growth or swelling wrinkles on constrained soft slabs. Soft Matter 9, 8216-8226.
Jin, L., Cai, S., Suo, Z., 2011. Creases in soft tissues generated by growth. EPL (Europhysics Letters) 95, 64002.
Jin, L., Chen, D., Hayward, R.C., Suo, Z., 2014. Creases on the interface between two soft materials. Soft Matter 10, 303-311.
Johnson, B.D., Beebe, D.J., Crone, W.C., 2004. Effects of swelling on the mechanical properties of a pH-sensitive hydrogel for use in microfluidic devices. Materials Science and Engineering: C 24, 575-581.
Jordan, A., Wust, P., Fähling, H., John, W., Hinz, A., Felix, R., 1993. Inductive heating of ferrimagnetic particles and magnetic fluids: physical evaluation of their potential for hyperthermia. International Journal of Hyperthermia 9, 51-68.
Kakac, M., Yener, Y., 1985. Heat Conduction, 2 ed. John Wiley.
Kang, M.K., Huang, R., 2010a. Effect of surface tension on swell-induced surface instability of substrate-confined hydrogel layers. Soft Matter 6, 5736-5742.
Kang, M.K., Huang, R., 2010b. Swell-induced surface instability of confined hydrogel layers on substrates. Journal of the Mechanics and Physics of Solids 58, 1582-1598.
Kang, M.K., Huang, R., 2010c. A Variational Approach and Finite Element Implementation for Swelling of Polymeric Hydrogels Under Geometric Constraints. Journal of Applied Mechanics 77, 61004-61012.
Kelly, P., 2008. Solid Mechanics Part III, 4 ed.
Kelly, R.E., 1981. Thermodynamics of blackbody radiation. American Journal of Physics 49, 714-719.
Kenkare, N.R., Hall, C.K., Khan, S.A., 2000. Theory and simulation of the swelling of polymer gels. The Journal of Chemical Physics 113, 404-418.
Kim, J., Yoon, J., Hayward, R.C., 2010. Dynamic display of biomolecular patterns through an elastic creasing instability of stimuli-responsive hydrogels. Nat Mater 9, 159-164.
Kim, P., Zarzar, L.D., He, X., Grinthal, A., Aizenberg, J., 2011. Hydrogel-actuated integrated responsive systems (HAIRS): Moving towards adaptive materials. Current Opinion in Solid State and Materials Science 15, 236-245.
Kishida, A., Ikada, Y., 2001. Hydrogels for Biomedical and Pharmaceutical Applications. CRC Press.
Kojima, H., Tanaka, F., Scherzinger, C., Richtering, W., 2013. Temperature dependent phase behavior of PNIPAM microgels in mixed water/methanol solvents. Journal of Polymer Science Part B: Polymer Physics 51, 1100-1111.
Komura, S., Tamura, K., Kato, T., 2005. Buckling of spherical shells adhering onto a rigid substrate. Eur Phys J E Soft Matter 18, 343-358.
Kondo, O., Suzuki, A., Shimazaki, T., 1993. Volume Phase Transition in Polymer Gels Induced by Uniaxial Stress. Journal of Intelligent Material Systems and Structures 4, 279-282.

Kwon, G.H., Choi, Y.Y., Park, J.Y., Woo, D.H., Lee, K.B., Kim, J.H., Lee, S.-H., 2010. Electrically-driven hydrogel actuators in microfluidic channels: fabrication, characterization, and biological application. Lab on a Chip 10, 1604-1610.

Lai, F., Li, H., 2010. Transient modeling for kinetic swelling/deswelling of the ionic-strength-sensitive hydrogel. Eur. Phys. J. E 31, 269-274.

Lai, F., Li, H., 2011. Transient modeling of the reversible response of the hydrogel to the change in the ionic strength of solutions. Mechanics of Materials 43, 287-298.

Lai, J.J., Hoffman, J.M., Ebara, M., Hoffman, A.S., Estournès, C., Wattiaux, A., Stayton, P.S., 2007. Dual Magnetic-/Temperature-Responsive Nanoparticles for Microfluidic Separations and Assays. Langmuir 23, 7385-7391.

Lam, K.Y., Li, H., Ng, T.Y., Luo, R., 2006. Modeling and simulation of the deformation of multi-state hydrogels subjected to electrical stimuli. Engineering Analysis with Boundary Elements 30, 1011-1017.

Lavergne, J., Joliot, P., 2000. Thermodynamics of the excited states of photosynthesis, in: Cramer, W.A. (Ed.). Biophysical Society.

Lee, D., Triantafyllidis, N., Barber, J.R., Thouless, M.D., 2008. Surface instability of an elastic half space with material properties varying with depth. Journal of the Mechanics and Physics of Solids 56, 858-868.

Lee, H., Zhang, J., Jiang, H., Fang, N.X., 2012. Prescribed Pattern Transformation in Swelling Gel Tubes by Elastic Instability. Physical Review Letters 108, 214304-214304.

Li, B., Cao, Y.-P., Feng, X.-Q., Gao, H., 2011a. Surface wrinkling of mucosa induced by volumetric growth: Theory, simulation and experiment. Journal of the Mechanics and Physics of Solids 59, 758-774.

Li, B., Cao, Y.-P., Feng, X.-Q., Gao, H., 2012a. Mechanics of morphological instabilities and surface wrinkling in soft materials: a review. Soft Matter 8, 5728-5745.

Li, B., Jia, F., Cao, Y.-P., Feng, X.-Q., Gao, H., 2011b. Surface Wrinkling Patterns on a Core-Shell Soft Sphere. Physical Review Letters 106, 234301-234301.

Li, H., 2009. Kinetics of smart hydrogels responding to electric field: A transient deformation analysis. International Journal of Solids and Structures 46, 1326-1333.

Li, H., Chen, J., Lam, K.Y., 2003. Multiphysical modeling and meshless simulation of electric-sensitive hydrogels. Journal of Polymer Science Part B: Polymer Physics.

Li, H., Chen, J., Lam, K.Y., 2006. A Transient Simulation to Predict the Kinetic Behavior of Hydrogels Responsive to Electric Stimulus. Biomacromolecules 7, 1951-1959.

Li, H., Chen, J., Lam, K.Y., 2007a. Transient simulation of kinetics of electric-sensitive hydrogels. Biosensors and Bioelectronics 22, 1633-1641.

Li, H., Lai, F., 2011. Transient analysis of the effect of the initial fixed charge density on the kinetic characteristics of the ionic-strength-sensitive hydrogel by a multi-effect-coupling model. Anal Bioanal Chem 399, 1233-1243.

Li, H., Luo, R., Birgersson, E., Lam, K.Y., 2007b. Modeling of multiphase smart hydrogels responding to pH and electric voltage coupled stimuli. Journal of Applied Physics 101.

Li, H., Luo, R., Lam, K.Y., 2007c. Modeling and simulation of deformation of hydrogels responding to electric stimulus. Journal of biomechanics 40, 1091-1098.

Li, H., Luo, R., Lam, K.Y., 2007d. Modeling of ionic transport in electric-stimulus-responsive hydrogels. Journal of Membrane Science 289, 284-296.

Li, H., Mulay, S.S., 2011. 2D simulation of the deformation of pH-sensitive hydrogel by novel strong-form meshless random differential quadrature method. Computational Mechanics 48, 729-753.
Li, H., Ng, T.Y., Yew, Y.K., Lam, K.Y., 2005a. Modeling and Simulation of the Swelling Behavior of pH-Stimulus-Responsive Hydrogels. Biomacromolecules 6, 109-120.
Li, H., Wang, X., Yan, G., Lam, K.Y., Cheng, S., Zou, T., Zhuo, R., 2005b. A novel multiphysic model for simulation of swelling equilibrium of ionized thermal-stimulus responsive hydrogels. Chemical Physics 309, 201-208.
Li, H., Wang, Z., Wang, X., Lam, K.Y., 2005c. Simulation of the influences of bathing solution and crosslink density on the swelling equilibrium of ionic thermo-sensitive hydrogels. Biophysical Chemistry 118, 57-68.
Li, H., Yew, Y.K., 2009. Simulation of soft smart hydrogels responsive to pH stimulus: Ionic strength effect and case studies. Materials Science and Engineering: C 29, 2261-2269.
Li, H., Yew, Y.K., Lam, K.Y., Ng, T.Y., 2004a. Numerical simulation of pH-stimuli responsive hydrogel in buffer solutions. Colloids and Surfaces A: Physicochemical and Engineering Aspects 249, 149-154.
Li, H., Yew, Y.K., Ng, T.Y., 2009. Modeling for analysis of the effect of Young's modulus on soft active hydrogels subject to pH stimulus. Smart Materials and Structures 18, 045010.
Li, H., Yew, Y.K., Ng, T.Y., Lam, K.Y., 2005d. Meshless steady-state analysis of chemo-electro-mechanical coupling behavior of pH-sensitive hydrogel in buffered solution. Journal of Electroanalytical Chemistry 580, 161-172.
Li, H., Yuan, Z., Lam, K.Y., Lee, H.P., Chen, J., Hanes, J., Fu, J., 2004b. Model development and numerical simulation of electric-stimulus-responsive hydrogels subject to an externally applied electric field. Biosensors and Bioelectronics 19, 1097-1107.
Li, J., Hu, Y., Vlassak, J.J., Suo, Z., 2012b. Experimental determination of equations of state for ideal elastomeric gels. Soft Matter.
Li, K., Ding, K., Cai, S., 2013a. Diffusion-induced wrinkling instability in a circular poroelastic plate. Applied Physics Letters 102, 1-4.
Li, M., Jin, C., Zhou, J., 2013b. Finite element implementation of poroelasticity theory for swelling dynamics of hydrogels. Theoretical and Applied Mechanics Letters 3, -.
Li, M., Kong, J., 2007. Smart Hydrogels, Smart Polymers. CRC Press, pp. 247-268.
Li, Y., Tanaka, T., 1990. Kinetics of swelling and shrinking of gels. The Journal of Chemical Physics 92, 1365-1365.
Liu, T.-Y.T.-Y., Hu, S.-H., Liu, D.-M., Chen, S.-Y., 2006. Magnetic-Sensitive Behavior of Intelligent Ferrogels for Controlled Release of Drug. Langmuir 22, 5974-5978.
Liu, Z.S., Hong, W., Suo, Z., Swaddiwudhipong, S., Zhang, Y., 2010. Modeling and simulation of buckling of polymeric membrane thin film gel. Computational Materials Science 49, S60-S64.
Liu, Z.S., Swaddiwudhipong, S., Cui, F.S., Hong, W., Suo, Z., Zhang, Y.W., 2011. Analytical Solutions of Polymeric Gel Structures Under Buckling and Wrinkle. International Journal of Applied Mechanics 03, 235-235.
Liu, Z.S., Swaddiwudhipong, S., Hong, W., 2013. Pattern formation in plants via instability theory of hydrogels. Soft Matter 9, 577-587.

Long, R., Qi, H.J., Dunn, M.L., 2013. Thermodynamics and mechanics of photochemcially reacting polymers. Journal of the Mechanics and Physics of Solids 61, 2212-2239.
Lopez-Pamies, O., 2010. A new -based hyperelastic model for rubber elastic materials. Comptes Rendus Mécanique 338, 3-11.
Lucantonio, A., Nardinocchi, P., Teresi, L., 2013. Transient analysis of swelling-induced large deformations in polymer gels. Journal of the Mechanics and Physics of Solids 61, 205-218.
Luo, R., Li, H., Lam, K.Y., 2007. Coupled chemo-electro-mechanical simulation for smart hydrogels that are responsive to an external electric field. Smart Materials and Structures 16, 1185.
Luo, R., Li, H., Lam, K.Y., 2008. Modeling and analysis of pH-electric-stimuli-responsive hydrogels. Journal of Biomaterials Science, Polymer Edition 19, 1597-1610.
Marckmann, G., Verron, E., 2006. Comparison of Hyperelastic Models for Rubber-Like Materials. Rubber Chemistry and Technology 79, 835-858.
Marcombe, R., Cai, S., Hong, W., Zhao, X., Lapusta, Y., Suo, Z., 2010. A theory of constrained swelling of a pH-sensitive hydrogel. Soft Matter 6, 784-784.
Matsuo, E.S., Tanaka, T., 1992. Patterns in shrinking gels. Nature 358, 482-485.
Meng, H., Hu, J., 2010. A Brief Review of Stimulus-active Polymers Responsive to Thermal, Light, Magnetic, Electric, and Water/Solvent Stimuli. Journal of Intelligent Material Systems and Structures 21, 859-885.
Mirfakhrai, T., Madden, J.D.W., Baughman, R.H., 2007. Polymer artificial muscles. Materials Today 10, 30-38.
Mooney, M., 1940. A Theory of Large Elastic Deformation. Journal of Applied Physics 11, 582-592.
Moore, J.S., Bauer, J.M., Yu, Q., Liu, R.H., Devadoss, C., Jo, B.-h., Beebe, D.J., 2000. Functional hydrogel structures for autonomous flow control inside microfluidic channels. Nature 404, 588-590.
Mora, T., Boudaoud, A., 2006. Buckling of swelling gels. The European physical journal. E, Soft matter 20, 119-124.
Mullin, T., Deschanel, S., Bertoldi, K., Boyce, M.C., 2007. Pattern Transformation Triggered by Deformation. Physical Review Letters 99, 084301.
Ng, T.Y., Li, H., Yew, Y.K., 2010. Computational analysis of smart soft hydrogels subjected to pH-electrical coupled stimuli: Effects of initial geometry. International Journal of Solids and Structures 47, 614-623.
Oguz, O., 2007. Macroporous Hydrogels from Smart Polymers, Smart Polymers. CRC Press, pp. 269-297.
Oh, K.S., Oh, J.S., Choi, H.S., Bae, Y.C., 1998. Effect of Cross-Linking Density on Swelling Behavior of NIPA Gel Particles. Macromolecules 31, 7328-7335.
Ohzono, T., Shimomura, M., 2004. Ordering of microwrinkle patterns by compressive strain. Physical Review B 69, 132202.
Okajima, T., Harada, I., Nishio, K., Hirotsu, S., 2002. Kinetics of volume phase transition in poly(N-isopropylacrylamide) gels. The Journal of Chemical Physics 116, 9068-9077.
Okumura, D., Inagaki, T., Ohno, N., 2015. Effect of prestrains on swelling-induced buckling patterns in gel films with a square lattice of holes. International Journal of Solids and Structures 58, 288-300.

Okumura, D., Kuwayama, T., Ohno, N., 2014. Effect of geometrical imperfections on swelling-induced buckling patterns in gel films with a square lattice of holes. International Journal of Solids and Structures 51, 154-163.
Oliveira, É.D., Silva, A.F.S., Freitas, R.F.S., 2004. Contributions to the thermodynamics of polymer hydrogel systems. Polymer 45, 1287-1293.
Parson, W.W., 1978. Thermodynamics of the Primary reactions of Photosynthesis. Photochemistry and Photobiology 28, 389-393.
Pastoor, K.J., Rice, C.V., 2012. Anion effects on the phase transition of N-isopropylacrylamide hydrogels. Journal of Polymer Science Part A: Polymer Chemistry 50, 1374-1382.
Peixinho, J., Mukhopadhyay, S., 2013. Diffusion-mechanical instability of a spherical gel. rencontre du non-lin´eaire, 116-119.
Peters, A., Candau, S.J., 1986. Kinetics of swelling of polyacrylamide gels. Macromolecules 19, 1952-1955.
Peters, A., Candau, S.J., 1988. Kinetics of swelling of spherical and cylindrical gels. Macromolecules 21, 2278-2282.
Pritchard, R.H., Terentjev, E.M., 2013. Swelling and de-swelling of gels under external elastic deformation. Polymer 54, 6954-6960.
Prokop, A.F., Vaezy, S., Noble, M.L., Kaczkowski, P.J., Martin, R.W., Crum, L.A., Polyacrylamide gel as an acoustic coupling medium for focused ultrasound therapy. Ultrasound in Medicine and Biology 29, 1351-1358.
Qiu, Y., Park, K., 2001. Environment-sensitive hydrogels for drug delivery. Advanced drug delivery reviews 53, 321-339.
Quesada-Perez, M., Ramos, J., Forcada, J., Martin-Molina, A., 2012. Computer simulations of thermo-sensitive microgels: Quantitative comparison with experimental swelling data. The Journal of Chemical Physics 136, 244903-244909.
Reyssat, E., Mahadevan, L., 2011. How wet paper curls. EPL 93.
Richardson, H.H., Carlson, M.T., Tandler, P.J., Hernandez, P., Govorov, A.O., 2009. Experimental and Theoretical Studies of Light-to-Heat Conversion and Collective Heating Effects in Metal Nanoparticle Solutions. Nano Letters 9, 1139-1146.
Richter, A., Paschew, G., Klatt, S., Lienig, J., Arndt, K.-F., Adler, H.-J.P., 2008. Review on Hydrogel-based pH Sensors and Microsensors. Sensors 8, 561-581.
Ricka, J., Tanaka, T., 1984. Swelling of ionic gels: quantitative performance of the Donnan theory. Macromolecules 17, 2916-2921.
Ries, H., McEvoy, A.J., 1991. Chemical potential and temperature of light. Journal of Photochemistry and Photobiology A: Chemistry 59, 11-18.
Rivlin, R.S., Saunders, D.W., 1951. Large Elastic Deformations of Isotropic Materials. VII. Experiments on the Deformation of Rubber.
Rogers, J.A., Someya, T., Huang, Y., 2010. Materials and Mechanics for Stretchable Electronics. Science 327, 1603-1607.
Rohatgi, K.K., 2006. Fundamentals of Photochemistry. New Age International Publishers, New Delhi.
Satarkar, N.S., Hilt, J.Z., 2008. Magnetic hydrogel nanocomposites for remote controlled pulsatile drug release. Journal of Controlled Release 130, 246-251.
Satarkar, N.S., Zhang, W., Eitel, R.E., Hilt, J.Z., 2009. Magnetic hydrogel nanocomposites as remote controlled microfluidic valves. Lab on a chip 9, 1773-1779.

Schwaiger, F., Köhler, W., 2013. Photothermal Deformation of a Transient Polymer Network. Macromolecules 46, 1673-1677.
Sershen, S.R., Westcott, S.L., Halas, N.J., West, J.L., 2000. Temperature-sensitive polymer – nanoshell composites for photothermally modulated drug delivery. Journal of Biomedical Materials Research 51, 293-298.
Serway, R.A., Jewett, J.W., 2013. Physics for Scientists and Engineers, 8 ed. Brooks/Cole Cengage Learning.
Sheppard Jr, N.F., Lesho, M.J., McNally, P., Shaun Francomacaro, A., 1995. Microfabricated conductimetric pH sensor. Sensors and Actuators B: Chemical 28, 95-102.
Shimizu, S., Seyama, T., Sekine, R., Kurita, K., 2003. Effect of added organic solvent on interaction parameters of poly(N-isopropylacrylamide) in aqueous solution. Journal of Applied Crystallography 36, 694-697.
Shirota, H., Endo, N., Horie, K., 1998. Volume phase transition of polymer gel in water and heavy water. Chemical Physics 238, 487-494.
Siepmann, J., Kranz, H., Bodmeier, R., Peppas, N.A., 1999. HPMC-Matrices for Controlled Drug Delivery: A New Model Combining Diffusion, Swelling, and Dissolution Mechanisms and Predicting the Release Kinetics. Pharmaceutical Research 16, 1748-1756.
Silva Nykanen, V.P., Nykanen, A., Puska, M.A., Silva, G.G., Ruokolainen, J., 2011. Dual-responsive and super absorbing thermally cross-linked hydrogel based on methacrylate substituted polyphosphazene. Soft Matter 7, 4414-4424.
Simulia, 2010. Abaqus Theory Manual, 6.10 ed. Dassault Systemes.
Skumiel, A., Labowski, M., Gojzewski, H., 2007. The heating effect of the magnetic fluid APG-832 in an alternating magnetic field. Molecular and Quantum Acoustics 28, 229-239.
Stöhr, J., Siegmann, H.C., 2006. Magnetism: From Fundamentals to Nanoscale Dynamics. Springer Berlin / Heidelberg.
Sugiura, S., Sumaru, K., Ohi, K., Hiroki, K., Takagi, T., Kanamori, T., 2007. Photoresponsive polymer gel microvalves controlled by local light irradiation. Sensors and Actuators A: Physical 140, 176-184.
Sultan, E., Boudaoud, A., 2008. The Buckling of a Swollen Thin Gel Layer Bound to a Compliant Substrate. Journal of Applied Mechanics 75, 051002-051002.
Suzuki, A., 1993. Phase transition in gels of sub-millimeter size induced by interaction with stimuli, in: Dušek, K. (Ed.). Springer Berlin Heidelberg, pp. 199-240.
Suzuki, A., Ishii, T., 1999. Phase coexistence of neutral polymer gels under mechanical constraint. The Journal of Chemical Physics 110, 2289-2296.
Suzuki, A., Ishii, T., Maruyama, Y., 1996. Optical switching in polymer gels. Journal of Applied Physics1 80, 131-136.
Suzuki, A., Kojima, S., 1994. Phase transition in constrained polymer gel. The Journal of Chemical Physics 101, 10003-10007.
Suzuki, A., Tanaka, T., 1990. Phase transition in polymer gels induced by visible light. Nature 346, 345-347.
Tamai, Y., Tanaka, H., Nakanishi, K., 1996. Molecular Dynamics Study of Water in Hydrogels. Molecular Simulation 16, 359-374.
Tanaka, H., Tomita, H., Takasu, A., Hayashi, T., Nishi, T., 1992. Morphological and kinetic evolution of surface patterns in gels during the swelling process: Evidence of dynamic pattern ordering. Physical Review Letters 68, 2794-2797.

Tanaka, T., 1978. Collapse of Gels and the Critical Endpoint. Physical Review Letters 40, 820-823.
Tanaka, T., Fillmore, D.J., 1979. Kinetics of swelling of gels. The Journal of Chemical Physics 70, 1214-1214.
Tanaka, T., Hocker, L.O., Benedek, G.B., 1973. Spectrum of light scattered from a viscoelastic gel. The Journal of Chemical Physics 59, 5151-5151.
Tanaka, T., Sun, S.-T., Hirokawa, Y., Katayama, S., Kucera, J., Hirose, Y., Amiya, T., 1987. Mechanical instability of gels at the phase transition. Nature 325, 796-798.
Tokita, M., Miyamoto, K., Komai, T., 2000. Polymer network dynamics in shrinking patterns of gels. The Journal of Chemical Physics 113, 1647-1650.
Trujillo, V., Kim, J., Hayward, R.C., 2008. Creasing instability of surface-attached hydrogels. Soft Matter 4, 564-569.
Valanis, K.C., Landel, R.F., 1967. The Strain-Energy Function of a Hyperelastic Material in Terms of the Extension Ratios. Journal of Applied Physics 38, 2997-3002.
van der Linden, H.J., Herber, S., Olthuis, W., Bergveld, P., 2003. Stimulus-sensitive hydrogels and their applications in chemical (micro)analysis. Analyst 128, 325-331.
Wagner, W., Pruß, A., 2002. The IAPWS Formulation 1995 for the Thermodynamic Properties of Ordinary Water Substance for General and Scientific Use. Journal of Physical and Chemical Reference Data 31, 387-535.
Walker, J.S., 2009. Physics, Fourth ed. Prentice Hall.
Wallmersperger, T., Keller, K., Kröplin, B., Günther, M., Gerlach, G., 2011a. Chemo-electro-mechanical modeling of pH-sensitive hydrogels, pp. 79761O-79761O-79769.
Wallmersperger, T., Keller, K., Kröplin, B., Günther, M., Gerlach, G., 2011b. Modeling and simulation of pH-sensitive hydrogels. Colloid Polym Sci 289, 535-544.
Wang, E., Desai, M.S., Lee, S.-W., 2013a. Light-Controlled Graphene-Elastin Composite Hydrogel Actuators. Nano Letters 13, 2826-2830.
Wang, P., Casadei, F., Shan, S., Weaver, J.C., Bertoldi, K., 2014. Harnessing Buckling to Design Tunable Locally Resonant Acoustic Metamaterials. Physical Review Letters 113, 014301.
Wang, P., Shim, J., Bertoldi, K., 2013b. Effects of geometric and material nonlinearities on tunable band gaps and low-frequency directionality of phononic crystals. Physical Review B 88, 014304.
Wang, X., 2007. Modeling the nonlinear large deformation kinetics of volume phase transition for the neutral thermosensitive hydrogels. The Journal of Chemical Physics 127, 1-8.
Wang, X., Hong, W., 2012. A visco-poroelastic theory for polymeric gels. 1-23.
Weiss, F., Cai, S., Hu, Y., Kyoo Kang, M., Huang, R., Suo, Z., 2013. Creases and wrinkles on the surface of a swollen gel. Journal of Applied Physics 114, 1-9.
Wichterle, O., Lim, D., 1960. Hydrophilic Gels for Biological Use. Nature 185, 117-118.
Wong, W.H., Guo, T.F., Zhang, Y.W., Cheng, L., 2010. Surface instability maps for soft materials. Soft Matter 6, 5743-5750.
Wu, Z., Bouklas, N., Huang, R., 2013. Swell-induced surface instability of hydrogel layers with material properties varying in thickness direction. International Journal of Solids and Structures 50, 578-587.

Wu, Z., Meng, J., Liu, Y., Li, H., Huang, R., 2014. A State Space Method for Surface Instability of Elastic Layers With Material Properties Varying in Thickness Direction. Journal of Applied Mechanics 81, 10.
Wurfel, P., 1982. The chemical potential of radiation. Journal of Physics C: Solid State PhysicsEmail alert RSS feed 15, 3967-3985.
Xiao, Z., Li, M., Zhou, J., 2012. Surface instability of a swollen cylinder hydrogel. Acta Mechanica Solida Sinica 25, 550-556.
Yamaue, T., Doi, M., 2004a. Swelling dynamics of constrained thin-plate gels under an external force. Physical Review E 70, 11401-11401.
Yamaue, T., Doi, M., 2004b. Theory of one-dimensional swelling dynamics of polymer gels under mechanical constraint. Physical review. E, Statistical, nonlinear, and soft matter physics 69, 041402.
Yamaue, T., Doi, M., 2005. The stress diffusion coupling in the swelling dynamics of cylindrical gels. The Journal of Chemical Physics 122, 84703-84706.
Yan, H., Jin, B., Gao, S., Chen, L., 2014. Equilibrium swelling and electrochemistry of polyampholytic pH-sensitive hydrogel. International Journal of Solids and Structures 51, 4149-4156.
Yang, S., Khare, K., Lin, P.-C., 2010. Harnessing Surface Wrinkle Patterns in Soft Matter. Advanced Functional Materials 20, 2550-2564.
Yin, J., Bar-Kochba, E., Chen, X., 2009. Mechanical self-assembly fabrication of gears. Soft Matter 5, 3469-3474.
Yin, J., Cao, Z., Li, C., Sheinman, I., Chen, X., 2008. Stress-driven buckling patterns in spheroidal core/shell structures. Proceedings of the National Academy of Sciences 105, 19132-19135.
Yoon, J., Bian, P., Kim, J., McCarthy, T.J., Hayward, R.C., 2012. Local Switching of Chemical Patterns through Light-Triggered Unfolding of Creased Hydrogel Surfaces. Angewandte Chemie International Edition 51, 7146-7149.
Yoon, J., Cai, S., Suo, Z., Hayward, R.C., 2010. Poroelastic swelling kinetics of thin hydrogel layers: comparison of theory and experiment. Soft Matter 6, 6004-6012.
Zhang, J., Zhao, X., Suo, Z., Jiang, H., 2009. A finite element method for transient analysis of concurrent large deformation and mass transport in gels. Journal of Applied Physics 105, 93522-93529.
Zhang, X.X., Guo, T.F., Zhang, Y.W., 2010. Formation of gears through buckling multilayered film–hydrogel structures. Thin Solid Films 518, 6048-6051.
Zhang, Y., Chen, L., Swaddiwudhipong, S., Liu, Z.S., 2014. Buckling Deformation of Annular Plates Describing Natural Forms. International Journal of Structural Stability and Dynamics 14, 1350054-1350054.
Zhang, Y., Ji, H.F., Snow, D., Sterling, R., Brown, G.M., 2004. A pH Sensor Based on a Microcantilever Coated with Intelligent Hydrogel. Instrumentation Science & Technology 32, 361-369.
Zhang, Y., Liu, Z.S., Swaddiwudhipong, S., Miao, H., Ding, Z., Yang, Z., 2012. pH-Sensitive Hydrogel for Micro-Fluidic Valve. Journal of Functional Biomaterials 3, 464-479.
Zhang, Y., Matsumoto, E.A., Peter, A., Lin, P.-C., Kamien, R.D., Yang, S., 2008. One-Step Nanoscale Assembly of Complex Structures via Harnessing of an Elastic Instability. Nano Letters 8, 1192-1196.
Zhao, X., Hong, W., Suo, Z., 2008. Inhomogeneous and anisotropic equilibrium state of a swollen hydrogel containing a hard core. Applied Physics Letters 92, -.

Zhu, C.-H., Lu, Y., Peng, J., Chen, J.-F., Yu, S.-H., 2012. Photothermally Sensitive Poly(N-isopropylacrylamide)/Graphene Oxide Nanocomposite Hydrogels as Remote Light-Controlled Liquid Microvalves. Advanced Functional Materials 22, 4017-4022.

Zhuang, Y., Chen, L., Zhu, Z., Yang, H., 2000. Preparation and separation function of N-isopropylacrylamide copolymer hydrogels. Polymers for Advanced Technologies 11, 192-197.

List of publications related to thesis

Research outcomes arising from this thesis have been published and presented in various journals and conferences, as listed below in reverse chronological order.

Journal publications

1) Ding, Z., Toh, W., Hu, J, Liu, Z.S., Ng, T.Y., 2016. A simplified coupled thermo-mechanical model for the transient analysis of temperature-sensitive hydrogels. Mechanics of Materials 97, 212-227.

2) Toh, W., Ding, Z., Ng, T.Y., Liu, Z.S., 2016. Light intensity controlled wrinkling patterns in photo-thermal sensitive hydrogels. Multiscale and Multiphysics Mechanics 01(01), 87-99.

3) Liu, Z, Toh, W., Ng, T.Y., 2015. Advances in Mechanics of Soft Materials - A review of deformation behavior of hydrogel. International Journal of Applied Mechanics 07, 1530001

4) Toh, W., Ding, Z., Yong Ng, T., Liu, Z., 2015. Wrinkling of a Polymeric Gel During Transient Swelling. Journal of Applied Mechanics 82, 061004-061004.

5) Toh, W., Ng, T.Y., Hu, J., Liu, Z., 2014. Mechanics of inhomogeneous large deformation of photo-thermal sensitive hydrogels. International Journal of Solids and Structures 51, 4440-4451.

6) Toh, W., Ng, T.Y., Liu, Z.S., Hu, J.Y., 2014. The deformation kinetics of pH-sensitive hydrogels. Polymer International 63, 1578-1583.

7) Toh, W., Liu, Z.S., Ng, T.Y., Hong, W., 2013. Inhomogeneous large deformation kinetics of polymeric gels. International Journal of Applied Mechanics 05, 1350001-1350001.

8) Toh, W., Liu, Z.S., Ng, T.Y., 2013. Non-Linear Large Deformation Kinetics of Polymeric Gel. Key Engineering Materials 535-536, 338-341.

Conference papers

1) Toh, W., Liu, Z.S., Ng, T.Y., 2015. Light intensity controlled wrinkling patterns in photo-thermal sensitive hydrogels. *Oral presentation at the ASME 2015 Applied Mechanics and Materials Conference (McMAT 2015), Seattle,* USA.

2) Toh, W., Liu, Z.S., Ng, T.Y., 2014. Modeling and simulation of the phase transition phenomenon in photo-thermal sensitive hydrogels, *Poster presentation at the International Symposium on Frontiers in Applied Mechanics (ISFAM 2014),* Singapore. *Awarded Best Poster Prize.*

3) Toh, W., Liu, Z.S., Ng, T.Y., 2014. Surface Wrinkling of a Polymeric Gel During Transient Swelling, *Oral presentation at the 5th International Conference on Computational Methods (ICCM 2014), Cambridge,* UK

4) Toh, W., Liu, Z.S., Ng, T.Y., 2013. The Deformation Kinetics of pH-sensitive hydrogels, *Oral presentation at the 7th International Conference on Materials for Advanced Technologies (ICMAT 2013),* Singapore

5) Toh, W., Liu, Z.S., Ng, T.Y., 2012. Non-Linear Large Deformation Kinetics of Polymeric Gel, *Oral presentation at the 11th Asia-Pacific Conference on Engineering Plasticity and its Applications* (AEPA2012), Singapore.

Appendix

In the following finite element formulation for swelling kinetics of a gel, we adopt the formulation procedure developed by Zhang et al. (2009).

In the gel, local equilibrium is satisfied. The state of mechanical equilibrium is represented by the equation

$$\frac{\partial s_{iK}}{\partial X_K} + B_i = 0 \tag{A.1}$$

in the volume of the gel, and

$$s_{iK} N_K = T_i \tag{A.2}$$

on the surface of the gel.

In addition, the number of solvent molecules within the gel is conserved, and this follows the equation

$$\frac{\partial C}{\partial t} + \frac{\partial J_K}{\partial X_K} = 0 \tag{A.3}$$

We multiply equations (A.1) and (A.2) with weight (or test) functions $\mathbf{w}^{(1)}$ (or $w_i^{(1)}$ in tensor form) and $w^{(2)}$ respectively, then integrate over the volume and apply the divergence theorem to obtain

$$\int \frac{\partial \hat{W}}{\partial F_{iK}} \frac{\partial w_i^{(1)}}{\partial X_K} dV = \int B_i w_i^{(1)} dV + \int T_i w_i^{(1)} dA \tag{A.4}$$

$$\int \left(\frac{\partial^2 \hat{W}}{\partial \mu \partial F_{jL}} \frac{\partial F_{jL}}{\partial t} + \frac{\partial^2 \hat{W}}{\partial \mu^2} \frac{\partial \mu}{\partial t} \right) w^{(2)} dV - \int M_{KL} \frac{\partial \mu}{\partial X_L} \frac{\partial w^{(2)}}{\partial X_K} dV = 0 \tag{A.5}$$

where M_{KL} is the mobility tensor of the solvent molecules within the gel.

Next, we discretize the equations using the shape function φ_a (for the a^{th} node in element) and writing displacement and chemical potential of the gel using the shape function, i.e.

$$x_i - X_i = \varphi_a u_{ai} \tag{A.6}$$

$$\mu = \varphi_a \mu_a \tag{A.7}$$

Substituting equations (A.6), equation (A.4) is transformed into

$$\int \frac{\partial \hat{W}}{\partial F_{iK}} \frac{\partial \varphi_j}{\partial X_K} dV = \int B_i \varphi_j dV + \int T_i \varphi_j dA \tag{A.8}$$

Differentiating with respect to time, we obtain

$$\frac{du_{bj}}{dt} \int \frac{\partial^2 \hat{W}}{\partial F_{iK} \partial F_{jL}} \frac{\partial \varphi_a}{\partial X_K} \frac{\partial \varphi_b}{\partial X_L} dV + \frac{d\mu_b}{dt} \int \frac{\partial^2 \hat{W}}{\partial F_{iK} \partial \mu} \frac{\partial \varphi_a}{\partial X_K} \varphi_b dV = \int \frac{dB_i}{dt} \varphi_a dV + \frac{dT_i}{dt} \varphi_a dA \tag{A.9}$$

Applying the same procedures to equation (A.5), we obtain

$$\frac{du_{bj}}{dt} \int \frac{\partial^2 \hat{W}}{\partial \mu \partial F_{jL}} \frac{\partial \varphi_b}{\partial X_L} \varphi_a dV + \frac{d\mu_b}{dt} \int \frac{\partial^2 \hat{W}}{\partial \mu^2} \varphi_b \varphi_a dV - \mu_b \int M_{KL} \frac{\partial \varphi_b}{\partial X_L} \frac{\partial \varphi_a}{\partial X_K} dV = 0 \tag{A.10}$$

Equations (A.9) and (A.10) may be written in matrix form as

$$\mathbf{R} \frac{d\mathbf{q}}{dt} + \mathbf{K}\mathbf{q} = \mathbf{P} \tag{A.11}$$

where

$$\mathbf{R} = \begin{pmatrix} \int \frac{\partial^2 W}{\partial F_{iK} \partial F_{jL}} \frac{\partial \varphi_a}{\partial X_K} \frac{\partial \varphi_b}{\partial X_L} dV & \int \frac{\partial^2 W}{\partial F_{iK} \partial \mu} \frac{\partial \varphi_a}{\partial X_K} \varphi_b dV \\ \int \frac{\partial^2 W}{\partial \mu \partial F_{jL}} \frac{\partial \varphi_b}{\partial X_L} \varphi_a dV & \int \frac{\partial^2 W}{\partial \mu^2} \varphi_b \varphi_a dV \end{pmatrix},$$

$$\mathbf{q} = \begin{pmatrix} u_{bj} \\ \mu_b \end{pmatrix},$$

$$\mathbf{K} = \begin{pmatrix} 0 & \int M_{KL} \frac{\partial \varphi_b}{\partial X_L} \frac{\partial \varphi_a}{\partial X_K} dV \end{pmatrix} \text{ and}$$

$$\mathbf{P} = \begin{pmatrix} \int \frac{dB_i}{dt} \varphi_a dV + \frac{dT_i}{dt} \varphi_a dA \\ 0 \end{pmatrix}.$$

We discretize the equation in time using an implicit method, where the increment in the generalized nodal variable $\Delta\mathbf{q}$ at current time $t + \Delta t$ is obtained by solving

$$\mathbf{A}^{t+\Delta t} \Delta\mathbf{q} = \mathbf{Y}^{t+\Delta t} \tag{A.12}$$

here $\mathbf{A}^{t+\Delta t} = \frac{\mathbf{R}^{t+\Delta t}}{\Delta t} + \mathbf{K}^{t+\Delta t}$, $\mathbf{Y}^{t+\Delta t} = \mathbf{P}^{t+\Delta t} - \mathbf{R}^t \frac{d\mathbf{q}^t}{dt} - \mathbf{K}^t \mathbf{q}^t$.

In solving equation (A.12), several methods have been proposed. These methods include using a direct solver which requires $\mathbf{A}$ to be positive definite; and an iterative solver, which does not require $\mathbf{A}$ to be positive definite. In using both methods, the equation

$$\mathbf{A}^* = \mathbf{A} + \alpha \mathbf{I} \tag{A.13}$$

may be employed to overcome convergence or instability issues which may arise.